Mechanical Behaviour of Unsaturated Highly Expansive Clays

by

Radhey Shyam Sharma

Keble College

A thesis submitted for the degree of
Doctor of Philosophy

at the

University of Oxford

Trinity Term, 1998

Abstract

Mechanical Behaviour of Unsaturated Highly Expansive Clays

A thesis submitted to the University of Oxford for the degree of Doctor of Philosophy

Radhey Shyam Sharma, Keble College, Oxford

Trinity Term, 1998

This thesis concerns the mechanical behaviour of unsaturated highly expansive clays. Given the high cost of damage to buildings, structures and roads caused by unexpected ground movements associated with unsaturated highly expansive clays and the increasing use of compacted expansive clays for engineered barriers for environmental protection and other purposes, it was considered important to investigate the behaviour of these materials.

Previous researchers had reported the occurrence of substantial irreversible components of either wetting-induced swelling or drying-induced shrinkage during cycles of wetting and drying performed on unsaturated highly expansive clays containing active clay minerals such as montmorillonite. This form of irreversible behaviour cannot be represented by existing elasto-plastic models for unsaturated non-expansive clays. It had therefore been suggested that the behaviour of unsaturated highly expansive clays was fundamentally different to that of unsaturated non-expansive clays, and that the constitutive models developed for unsaturated non-expansive clays were inappropriate.

The behaviour of an unsaturated highly expansive compacted bentonite/kaolin mix under isotropic stress states has been studied in a programme of controlled-suction tests incorporating isotropic loading and unloading at constant suction and cycles of wetting and drying (variation of suction) performed either under constant load or at constant volume. A smaller series of tests was also performed on unsaturated compacted samples of non-expansive pure kaolin.

Either net shrinkage or net swelling occurred over a wetting/drying cycle for samples of the same soil, depending upon the compaction pressure. Irreversible shrinkage or swelling occurred during subsequent wetting/drying cycles, not just during the first cycle. Net shrinkage during a wetting/drying cycle was sometimes accompanied by a distinct change of stiffness (a yield point) during the appropriate drying path, but at other times was not. Yield points were never observed during both drying and wetting stages of a cycle. Net shrinkage or swelling during a wetting/drying cycle was always accompanied by a substantial net change of degree of saturation S_r during the cycle (termed hydraulic hysteresis). Experimental evidence showed that there is no fundamental difference between the mechanical behaviours of unsaturated highly expansive soils and unsaturated non-expansive soils

The experimental results suggested that unified modelling for both unsaturated highly expansive soils and unsaturated non-expansive soils is desirable. A new constitutive modelling framework is therefore proposed. In the modelling framework new forms of stress variables, with conjugate strain increment parameters, are used for the first time. Results from theoretical analysis of the influence of suction on inter-particle forces are used in developing the modelling framework. The influence of hydraulic hysteresis on stress-strain behaviour is included in the framework, which has been developed in such a way that the otherwise difficult, transition between saturated and unsaturated conditions can be modeled in a relatively straightforward fashion. In the new modelling framework, both net shrinkage and net swelling during wetting/drying cycles, can be explained.

Acknowledgements

I am indebted to my supervisors Professor Simon Wheeler and Professor Guy Houlsby, who provided immense help and encouragement. The research project was conceived by Professor Simon Wheeler. With Professor Wheeler's move to Glasgow University (one year into the research), to take up the Cormack Chair, I had the privilege of additional invaluable supervision from Professor Houlsby.

Professor Wheeler provided crucial guidance and assistance during the performance of laboratory-based research and both supervisors were influential in the subsequent interpretation and modelling. In particular, Professor Houlsby suggested the use of the new stress variables and conjugate strain parameters and then Professor Wheeler provided numerous suggestions in developing the new constitutive modelling framework. Finally, Professor Houlsby kindly permitted use of his *GPLOT* program for analysing and plotting the experimental results.

Dr V Sivakumar provided valuable assistance in the use of the experimental equipment and was always available for discussion, even after his move from Oxford.

I am grateful to Mr Robert Sawala who devoted such care and attention to the fabrication of various pieces of equipment for the modification of drainage arrangements in the apparatus.

I would also like to thank other members of the Civil Engineering Group at Oxford for advice and discussion, which created such a stimulating environment for research.

The project was funded by a research grant from the Engineering and Physical Sciences Research Council (*EPSRC*). Personal financial support from the Radhakrishnan Memorial Trust, in the final stage of the work, is also gratefully acknowledged.

Special mention is needed for the contribution of my parents, brother (Professor R P Sharma) and *Bhabhi* (Saroj) for their help and support throughout my career. I was fortunate to have encouragement and support from several other family members and many friends.

Finally, I must thank my wife (Raj), who provided tremendous help with a cheerful smile. I wish to dedicate this thesis to my son Navneet and daughter Sonu, for their surprisingly deep understanding (at such a young age) of the need for Raj and me to be away from them.

To my son Navneet and daughter Sonu

Table of Contents

Notation

a	elastic stiffness parameter for change in stress variable s^*
a, b, c	calibration constants
a_1, b_1, c_1, d_1	parameters for defining state surface in terms of voids ratio
a_2, b_2, c_2, d_2	parameters for defining state surface in terms degree of saturation
a, b, c, d, e, f	labels indicating start and finish of test stages
CF_B, CF_A	calibration factors
C_m, C_t	compression indices for state surface in terms of voids ratio
c'	cohesion intercept
D	dielectric constant
D_m, D_t	compression indices for state surface in terms degree of saturation
d	distance between diffuse double layers
d_u	distance between unit layers
E	surface charge density
e	unit electronic charge
e	voids ratio
f_A	attractive force per unit area
f_E	external force per unit area
f_R	repulsive force per unit area
$f_1(s), f_2(s)$	functions of suction
G	shear stiffness
G_s	specific gravity
g	acceleration due to gravity
$1/K$	$=\left(DkT/8\pi n_0 e^2 v^2\right)^{1/2}$ thickness of diffuse double layer
k	parameter describing the increase in cohesion with suction
k	constant used in non-linear variation of suction with time
k	Boltzmann constant
L	length of a clay platelet
L	length or width of unit layer
M	slope of the critical state line in $q : p''$ plot.
$M(s)$	slope of critical state hyper-line in $q : p''$ plane in the model of Wheeler and Sivakumar (1995)
$N(0)$	value of $N(s)$ at zero suction

$N(s)$	intercept of normal compression line, for suction s, in v : ln $(p'' p_{at})$ plot
N_{sat}	intercept of normal compression line, for S_r =1, in v : ln p^* plot
ΔN_s	additional normal inter-particle force due to suction in meniscus water
n	concentration of cations at the mid-plane between the unit layers
n	porosity
n_0	concentration of cations in the bulk solution
p	pressure
p	mean total stress
p_c	reference pressure in the model of Alonso *et al* (1990)
p'	$(= p - u_w)$ mean effective stress
p''	$= \frac{1}{3}(\sigma_1 + 2\sigma_3) - u_a = p - u_a$ mean net stress
p_c''	value of mean net stress during initial equalisation
p_0''	isotropic yield value of mean net stress p''
p^*	$= p - S_r u_w - (1 - S_r) u_a$ stress variable
p_{0sat}^*	yield value of p^* for saturated soil (S_r = 1)
$p_0''(0)$	yield value of mean net stress p'' at zero suction
dp''	increment of mean net stress
dp^*	increment of p^*
p_{at}	atmospheric pressure
p_{os}	component of pore water pressure at the mid-plane between unit layers arising from osmotic effects
q	deviator stress
R	radius of idealised spherical soil particle
R	universal gas constant
R_H	relative humidity
r	radius
r	parameter defining the variation of soil stiffness as a function of suction
r_1, r_2	principal radii of curvature of air-water interface
r_d	radius of curvature of air-water interface during drying process
r_w	radius of curvature of air-water interface during wetting process
S	specific surface area
s	$(= u_a - u_w)$ suction
ds	increment of suction

ds/dt	rate of variation of suction during a test stage
s^*	$= n(u_a - u_w) = ns$ stress variable
ds^*	increment of s^*
s_{ae}	air entry value of suction
s^*_{ae}	air entry value of s^*
s_e	value of suction during initial equalisation
s_i	initial suction produced by compaction process
s_{i0}	initial suction at $t = 0$ in a test stage
S_r	degree of saturation
dS_r	increment of degree of saturation
T	absolute temperature
T	surface tension
t	thickness of a clay platelet or unit layer
t	time into a test stage
u	$= 8\tanh^{-1}\left(\exp(-kd)\tanh(z/4)\right)$ a parameter used in defining diffuse double layer
u_a	pore air pressure
u_w	pore water pressure
u_w	pore water pressure in the bulk liquid
u_{wd}	pore water pressure at the mid-plane between unit layers
V	volume of water in burette
V_0	volume of sample at the start of a test stage
V_s	volume of solids within sample
V_{w0}	volume of water in the sample at the start of a test stage
ΔV	change in volume of sample
ΔV_w	amount of water inflow into sample
v	$(= 1 + e)$ specific volume
dv^e	elastic increment of specific volume
dv^p	plastic increment of specific volume
v_w	$(= 1 + eS_r = 1 + wG_s)$ specific water volume
w	water content
X_A, X_B	output voltage corresponding to points A and B
x	distance from clay surface
y	$(= ze\psi/kT)$ normalised value of electrical potential

z	$(= \upsilon e \psi_0 / kT)$ normalised value of electrical potential at clay surface
$\Gamma(s)$	intercept of critical state hyper-line in v : ln $(p'' p_{at})$ plane in the model of Wheeler and Sivakumar (1995)
α	Hamaker constant
α	wetting angle
β	parameter defining the variation of soil stiffness as a function of suction
χ	a parameter, which is function of S_r
ε_1, ε_3	axial and radial strains
$d\varepsilon_d$	$(= -d(v - v_w)/v)$ strain variable
$d\varepsilon_{vm}^e$	elastic volumetric strain increment of microfabric
$d\varepsilon_{vM}^p$	plastic volumetric strain increment of macrofabric
$d\varepsilon_w$	$(= -dv_w / v)$ strain variable
ε_p	volumetric strain
$d\varepsilon_p$	increment of volumetric strain
$d\varepsilon_p^e$	elastic increment of volumetric strain
$d\varepsilon_p^p$	plastic increment of volumetric strain
ε_q	shear strain
$d\varepsilon_q$	increment of shear strain
$d\varepsilon_q^e$	elastic increment of shear strain
$d\varepsilon_q^p$	plastic increment of shear strain
ϕ'	angle of friction
ϕ^b	angle of friction with respect to suction
κ	elastic stiffness parameter for change in mean net stress p''
κ_s	elastic stiffness parameter for change in suction s
$\lambda(0)$	value of $\lambda(s)$ at $s = 0$
$\lambda(s)$	slope of normal compression line, for suction s, in v : ln $(p'' p_{at})$ plot
λ_{sat}	slope of normal compression line, for $S_r = 1$, in v : ln p^* plot
$\mu(s)$	intercept of critical state hyper-line in q : p'' plane in the model of Wheeler and Sivakumar (1995)
θ	$(= S_r e/(1+e) = wG_s/(1+e))$ volumetric water content
σ	total stress
$\Delta\sigma$	additional normal inter-particle stress due to suction in meniscus water

$\Delta\sigma_{limit}$ maximum value of $\Delta\sigma$

σ_1, σ_3 axial and radial total stresses

$\sigma - u_a$ net stress

$\sigma_v - u_a$ vertical net stress

$\sigma - u_w$ stress variable

σ' effective stress

σ^* $= \sigma - S_r u_w - (1 - S_r) u_a$ stress parameter

τ shear strength

v cation valence

ω a parameter with values varying from zero to unity

ξ ($= Kx$) a parameter used in defining the diffuse double layer

ψ electrical potential

ψ_0 electrical potential at clay surface

$\psi(s)$ slope of critical state hyper-line in v : ln ($p''p_{at}$) plane in the model of Wheeler and Sivakumar (1995)

CHAPTER 1

INTRODUCTION

In saturated soils the void spaces contain a single liquid (typically water), whereas in unsaturated soils the voids are filled with a mixture of a liquid and a gas (typically water and air). Unsaturated conditions prevail in arid and semi-arid parts of the world. Significant de-saturation of soils is, however, possible even in temperate climates during dry-spells. The occurrence of saturated and unsaturated soil conditions in any geographical region is a direct function of dynamic environmental factors such as rainfall and evapo-transpiration. In fact soils in most parts of the world undergo cycles of wetting and drying. In addition to occurrence of unsaturated conditions above the ground water table, unsaturated soils are widely encountered in the form of compacted fills, and soils with biogenic activity on and offshore.

1.1 Unsaturated Highly Expansive Clays

Most soils can either swell or "collapse" (compress) on wetting, depending upon the applied stress level and the stress history, and therefore rigid divisions into swelling and collapsing soils can be misleading. When swelling on wetting occurs, the magnitude of swelling can, however, vary greatly between different soils, with some highly plastic clays having the potential for much larger magnitudes of swelling than other soils. These clays are referred to as highly expansive clays.

McKeen (1992) proposed a classification system for expansive soils. According to this classification, soils which swell less than 1.8% on wetting are considered as non-expansive soils, those which swell 1.8 to 5.3% are moderately expansive soils, those which swell 5.3 to 10% are highly expansive and finally soils which swell more than 10% are considered as special cases of highly expansive soils. It is, however, important to point out that such classifications are very tentative, and can be used only for very limited purposes, because the amount of swelling of a soil is a function of the stress and suction histories of the soil.

The high degree of swelling in expansive clays is mainly due to the presence of active clay minerals, such as montmorillonite. In these soils important physico-chemical interactions occur in the vicinity of the active clay minerals. A proper understanding of these interactions can explain some of the observed features of soil behaviour. This helps in constructing a conceptual picture of the swelling and shrinkage processes.

An understanding of the mechanical behaviour of unsaturated expansive soils is required in the design and construction of a wide range of buildings, light structures, embankments, and roads. The annual cost of damage to buildings, structures, and roads caused by expansive soils is estimated at £150 million in the UK, $1000 million in the USA, and many billions of pounds worldwide (Gourley *et al* (1993)). Unsaturated expansive clays are however used for beneficial purposes also. Containment of contaminants is an integral part of environmental protection strategy, and unsaturated expansive clays are extensively used for engineered clay barriers, and as buffer materials for radioactive waste disposal. Another important application of unsaturated soils, including unsaturated highly expansive soils, is in the area of contaminant transport through unsaturated layers of ground (called the *vadose* zone in the literature on geo-environmental engineering), see, for example, Domenico and Schwartz (1998).

1.2 Constitutive Modelling of Unsaturated Soils

The importance of unsaturated soils in geotechnical engineering has long been recognised, and efforts have been made to model their mechanical behaviour. Only recently, however, have unified elasto-plastic constitutive models for unsaturated soils been proposed, using the overall framework of critical state concepts. Alonso *et al* (1990) were the first to present such an elasto-plastic model for unsaturated clays, in which volume changes and shear strength were linked in a single framework. A central feature of the model is that both wetting-induced swelling and wetting-induced plastic compression (referred to as "collapse" compression in the literature on unsaturated soils) is represented in a consistent fashion. Wheeler and Sivakumar (1995) reported results from an experimental investigation of compacted kaolin. These results provided support for the main features of the model proposed by Alonso *et al* (1990) and they suggested a number of refinements.

The elasto-plastic models of Alonso *et al* (1990) and Wheeler and Sivakumar (1995) were developed for non-expansive and moderately expansive clays, and were thought to be inappropriate for unsaturated highly expansive clays. Chu and Mou (1973) reported test results from wetting and drying cycles performed on a highly expansive clay which showed a large irreversible component of swelling on first wetting. Subsequently, Alonso *et al* (1995) reported cyclic wetting/drying test results for another highly expansive clay, which showed an irreversible component of shrinkage during each drying stage. Neither of these patterns of behaviour, which were the dominant features in the tests, could be represented by the existing elasto-plastic models (which assume that both wetting-induced swelling and drying-induced shrinkage are

elastic processes). In the light of these experimental observations, Gens and Alonso (1992) and Alonso *et al* (1994) proposed an extended form of elasto-plastic model for highly expansive unsaturated clays. The model was based on an assumption of two levels of soil fabric (an unsaturated macrofabric and a saturated microfabric within individual clay packets), with coupling between the mechanical behaviour of the two levels. The extended model required complex concepts and mechanisms in order to represent, even at a qualitative level, the forms of behaviour reported by Chu and Mou (1973) and Alonso *et al* (1995). There were few data to validate the proposed modelling framework, and these were only from oedometer tests, with no measurement of horizontal stress, so that the stress state was not fully known.

1.3 Aims of Research

Given the high cost of damage to civil engineering structures caused by unexpected ground movements associated with unsaturated highly expansive clays, and the increasing use of compacted expansive clays for engineered barriers for environmental protection and other purposes, it was considered important to investigate further the behaviour of these materials. With this background, the aims of this research were:

1. To carry out experimental work under appropriate stress condition to generate a database that could be used for validating or disproving the modelling framework proposed by Gens and Alonso (1992) and Alonso *et al* (1994).
2. If the existing modelling framework were shown to be invalid, to develop an alternative framework.

1.4 Outline of Thesis

Chapter 1 gives an introduction to this study. In Chapter 2, the mechanical behaviour of unsaturated non-expansive soils is reviewed and an analysis of the influence of suction on inter-particle forces is given.

Chapter 3 starts with a review of micro-level features of soil behaviour, in order to develop a conceptual model for swelling and compression behaviour of highly expansive soils, and then constitutive modelling of unsaturated highly expansive soils is discussed.

The experimental apparatus employed in the testing programme is presented in Chapter 4. In Chapter 5, material selection and characterisation are discussed, together with the experimental procedure used in the test programme.

The results from the main experimental tests are presented in Chapter 6. The discussion of results and a proposal for an alternative constitutive framework for modelling the behaviour of unsaturated highly expansive clays are taken up in Chapter 7.

The main findings of this study and consideration of possible future work are presented in Chapter 8.

CHAPTER 2

UNSATURATED NON-EXPANSIVE SOILS

There are three requisites for developing constitutive models for unsaturated highly expansive soils. Firstly, an understanding of current models for unsaturated non-expansive soils is required. Secondly, the factors contributing to the expansivity of the clays need detailed examination, and the additional features likely to be required of constitutive models for highly expansive unsaturated soils can then be identified. Thirdly, experimental data should be generated to examine the concepts emerging from the first two steps. A review of the main features of the mechanical behaviour of unsaturated non-expansive soils is, therefore, presented in this chapter, prior to moving on to the special features of highly expansive soils in the next chapter.

2.1 Pore Pressure and Suction in Unsaturated Soils

Unsaturated soils are three phase materials, containing soil particles, water, and air. The presence of air along with water in the soil voids gives rise to two types of pore pressures: pore air pressure u_a and pore water pressure u_w. The pore air pressure is generally higher than the pore water pressure because of surface tension effects.

To illustrate the effects of surface tension, Figure 2.1 shows two idealised spherical soil particles and a section of curved meniscus forming an interface between pore air and pore water. The interface is concave on the air side in accordance with the wetting phenomenon of water in contact with a solid boundary (the soil particles). Whenever a liquid comes in contact with a solid surface, an angle is formed between the surfaces of solid and liquid. This angle between the surfaces of solid and liquid, at the contact point, is known as the wetting angle and is represented in Figure 2.1 by α. If α is zero, the liquid is known as a perfect wetting liquid. Conversely, if the wetting angle α is greater than zero the wetting is said to be imperfect. The wetting angle of a liquid gives an indication of the wetting characteristics of a solid-liquid interface and it varies for different liquids. For water, the wetting angle α is considerably less than 90^0, and typically approaching zero (Price (1985)). This low value of wetting angle can generally only be achieved if the air-water interface is concave on the air side (see Figure 2.1). With the meniscus concave on the air side, a simple equilibrium calculation shows that the pore air pressure u_a is greater than the pore water pressure u_w by an amount given by:

$$u_a - u_w = T\left(\frac{1}{r_1} + \frac{1}{r_2}\right) \qquad (2.1)$$

where T is the surface tension and r_1 and r_2 are the two principal radii of curvature of the interface (both measured on the air side of the interface).

In an unsaturated soil with a continuous air phase, the pore air pressure u_a in the field is typically equal to atmospheric pressure, and the pore water pressure u_w is then negative, relative to atmospheric pressure, according to Equation 2.1.

Soil suction was first defined by Schofield (1935) as "pressure deficiency" in the pore liquid within a saturated or an unsaturated soil. Due to this pressure deficiency, an unsaturated soil absorbs more water, if additional water is made available at atmospheric pressure. If defined in this way, suction can be divided into two components: matrix and osmotic. The matrix component, which can be thought of as the physical negative value of the pore water pressure, is due to the surface tension effects, and the osmotic component results from the dissolved ionic concentration in the pore liquid.

The roles of both components of total suction i.e. matrix and osmotic (along with an appropriate gravitational term) are equally important in flow processes in unsaturated soils. In contrast, for the mechanical behaviour the influence of the osmotic effects is difficult to identify, and the relevant variable is usually taken as the matrix suction, on the assumption that the ionic concentration of the pore fluid remains unchanged (Alonso *et al* (1987) and Fredlund and Rahardjo (1993)). The influence of chemical changes in the pore liquid on the mechanical behaviour of saturated clays, with active clay minerals such as montmorillonite, is however significant and well recognised (see Section 3.3.4). As a direct corollary, it should be expected that the response of an unsaturated soil containing clay minerals such as montmorillonite will also be influenced by changes in the chemistry of pore liquid. This means the assumption of no change in pore liquid chemistry can have quite important implications and should not be overlooked. The aim of this research was to study the response of an unsaturated clay due to mechanical changes only and no chemical parameter was therefore included. This had implications in selecting experimental techniques (see Section 4.1).

Matrix suction is generally defined as the difference between pore air pressure and pore water pressure. This means that Equation 2.1, gives matrix suction as a function of the two principal radii of curvature, r_1 and r_2, of the air-water interface. In this thesis the term suction is used to refer to matrix suction.

2.2 Forms of Pore Water in Unsaturated Soils

Each individual void in an unsaturated soil is either water-filled or air-filled. This can be explained by considering the shape of the voids in an element of soil. The voids are random in shape, but generally with entrances in the form of necks (sections of minimum cross-sectional dimension within a void). If one of these necks is idealised as a tube of equivalent radius r, the cross-sectional dimension everywhere else within the void is more than the neck diameter $2r$. For a hemispherical section of air-water interface filling a tube of radius r, assuming a contact angle α of zero, Equation 2.1 becomes:

$$u_a - u_w = \frac{2T}{r} \tag{2.2}$$

According to Equation 2.2, the matrix suction $u_a - u_w$ is inversely proportional to the radius of the tube. In other words, if for a value of suction air can enter the neck of a void, it will fill the remaining void portion also as the applied value of suction is already higher than the suction values corresponding to the cross section anywhere else within the void. This means, a void is likely to be either water-filled or air-filled rather than being partly filled with water and partly with air. Likewise a number of voids with varying neck radii can be considered in an element of soil. In a drying process, voids will empty of water and fill with air progressively from voids with larger sized necks to those with smaller necks.

The pore water in an unsaturated soil can be categorised into three forms: adsorbed water, bulk water, and meniscus water, as suggested by Wheeler and Karube (1996). The adsorbed water is tightly bound to the soil particles and acts as an integral part of the particles. Bulk water occurs in the completely flooded void spaces. The meniscus water occurs at contacts of soil particles, which are not covered by the bulk water, in ring-shaped lenses of water. The bulk and meniscus forms of pore water are schematically shown in Figure 2.2.

The fundamental influences of pore water pressure and pore air pressure on the behaviour of an unsaturated soil depend on the relative amounts of water in bulk and meniscus forms. The pore water pressure in the bulk water influences the soil behaviour in a similar way as the pore water pressure in saturated soils, except that the pore water pressure acts only within the portion of total void volume that is flooded with bulk water. It is useful to consider an unsaturated soil with continuous bulk water filling a proportion S_r (where S_r is the degree of saturation) and continuous air filling the remaining proportion 1- S_r of voids, but no meniscus water. For such a soil, by analogy with saturated soil behaviour, it would perhaps be possible to use a stress variable of the form given below to describe the soil behaviour:

$$\sigma^* = \sigma - S_r u_w - (1 - S_r) u_a \quad (2.3)$$

In contrast, the influence of meniscus water on the response of soil is qualitatively different (see Sections 2.3 and 2.9) and needs to be accounted for separately in the constitutive models (see Section 7.3).

Unsaturated soils with very high degrees of saturation, wherein the air occurs in the form of occluded bubbles, can be considered in two separate categories. Firstly, if the sizes of air bubbles are much smaller than the average size of soil particles, the soil obeys the same effective stress law as a saturated soil and can be modelled relatively easily as the sole effect of the air bubbles is to change the compressibility of the pore fluid, as suggested by Sparks (1963) and Wheeler (1988). In contrast, if the size of the air bubbles is much larger than the soil particles, as is generally the case in offshore gassy soils, a different approach is needed for modelling the soil behaviour, because the gas bubbles now form large cavities within the soil fabric. A conceptual model for such soils was proposed by Wheeler (1986 and 1988) and this category of unsaturated soils is not discussed here any further as these soils are not the focus of this research. This project concentrates on unsaturated compacted clays, where the pore water can occur in bulk and meniscus forms

2.3 Early Attempts to Use a Single Effective Stress Expression

The success of the principle of effective stress in explaining the mechanical behaviour of saturated soils led early researchers to search for an equivalent effective stress principle for unsaturated soils. It would be helpful to first note the basic concept behind "effective stress". Terzaghi (1936) defined effective stress by saying that *".... all the measurable effects of a change in stress, such as compression, distortion and a change in shearing resistance are exclusively due to changes in the effective stress"*. For saturated or dry soils the excess of total stress over the pore pressure fits this definition.

Many researchers, including Bishop (1959), Aitchison (1961), and Jennings (1961) proposed modified forms of effective stress equation for unsaturated soils to incorporate both pore air pressure u_a and pore water pressure u_w. Bishop (1959) suggested the following effective stress expression for unsaturated soils:

$$\sigma' = \sigma - \chi u_w - (1 - \chi) u_a \quad (2.4)$$

where σ' is the effective stress, σ is the total stress, and χ is a parameter which is a function of the degree of saturation S_r. The parameter χ varies from 0 to 1, being 0 for dry soil and 1 for saturated soil. If χ is equal to S_r then Bishop's proposed effective stress from Equation 2.4 is

identical to the stress σ^* introduced in Equation 2.3. Bishop's proposed effective stress equation received widespread support at a conference, held in 1960 in London, on Pore Pressure and Suction in Soils (British National Society of the International Society of Soil Mechanics and Foundation Engineering, 1961).

To check the validity of Equation 2.4, Jennings and Burland (1962) analysed data obtained from oedometer and triaxial inundation tests conducted on three different unsaturated soils (silt, silty clay and sand). They showed that the volume reduction (known as "collapse compression") sometimes observed during wetting could not be accounted for on the basis of the modified effective stress relation given by Equation 2.4.

According to equation 2.4, effective stress always decreases on wetting under constant total stress from an unsaturated state (with $u_a = 0$, $u_w < 0$, and a positive value of χ) to a saturated state (with $u_w = 0$, and $\chi = 1$). As the effective stress decreases, an increase in the volume of the soil should be observed in accordance with the tenets of the effective stress principle. However, the experimental evidence often shows additional compression on wetting (collapse) and this is exactly opposite to predictions based on the effective stress principle. The general pattern of volumetric behaviour of an unsaturated soil is illustrated in Figure 2.3. A sample which is wetted at a low value of applied total stress σ swells as represented by AA' in Figure 2.3. In contrast, if the sample is wetted at a higher value of applied stress, compression BB' occurs.

It is generally accepted that the single effective stress approach, for unsaturated soils, does not work (see, for example, Jennings and Burland (1962), Matyas and Radhakrishna (1968), Fredlund and Morgenstern (1977), Alonso *et al* (1987), and Wheeler and Karube (1996)). This is because suction within meniscus water acts in a qualitatively different way on the soil skeleton to external stress applied to the boundary of a soil element and pore pressures within bulk water or pore air, whereas in the effective stress approach the various stresses are all combined together. The different modes of action of external stress and suction within meniscus water can be illustrated, as noted by Wheeler and Karube (1996), by considering an idealised case of two spherical soil particles, as shown in Figure 2.4. Pore air pressure u_a is taken at atmospheric pressure and then the water in the meniscus is under negative pressure. Application of even an isotropic external total stress σ to the boundary of a soil element containing many soil particles will give rise to normal and tangential forces at the particle contacts, whereas application of suction within the meniscus water produces only normal forces at the particle contacts

influenced by meniscus water. If the external stress is increased sufficiently, the corresponding increase in tangential forces at the particle contacts can result in slippage of particles, which in turn manifests as yielding and plastic deformation of the soil. This tendency for slippage at the particle contacts, due to an increase of external stress, can be counteracted by the increased normal force resulting from the application of suction within the meniscus water. The implications of this additional inter-particle normal force due to suction within the meniscus water can be visualised as:

- An increase in shear strength of the soil due to additional normal force at the frictional particle contacts. In this respect the effect of increasing suction within meniscus water is like increasing effective stress in a saturated soil.
- In terms of elastic volumetric strains, the increased inter-particle normal force caused by suction within meniscus water causes elastic compression and distortion of the individual soil particles and hence elastic compression of the soil. This is again like an increase of effective stress in saturated soils.
- In terms of plastic strains, increased suction within the meniscus water tends to prevent slippage and hence plastic deformation. This is like a reduction of effective stress in saturated soils.

Clearly an increase in suction within meniscus water has some effects (on shear strength and elastic volumetric strains) that are like an increase of effective stress in saturated soils, and other effects (on plastic strains) that are like a decrease in effective stress. This conflict means that it is impossible to represent all the effects of suction within a single effective stress parameter.

2.4 Selection of Stress State Parameters

It was recognised in the early 1960s that the mechanical behaviour, especially the volumetric response, of an unsaturated soil cannot be described in terms of a single stress state parameter, but an additional stress parameter is required. Several researchers including Bishop and Blight (1963) and Burland (1964) suggested the use of two independent stress variables. Matyas and Radhakrishna (1968) adopted the "net stress" $\sigma - u_a$ and the matrix suction $u_a - u_w$ as the independent stress variables to describe the mechanical behaviour of unsaturated soils.

Fredlund and Morgenstern (1977) argued, on the basis of equilibrium analysis and experimental results, that any two of the three stress parameters $\sigma - u_a$, $\sigma - u_w$, and $u_a - u_w$ would be sufficient to describe fully the stress state of an unsaturated soil. The first two of these stress parameters $\sigma - u_a$ and $\sigma - u_w$ are tensor quantities, whilst the third parameter $u_a - u_w$ is a scalar quantity. It is therefore sensible to select either $\sigma - u_a$ and $u_a - u_w$ or $\sigma - u_w$ and

$u_a - u_w$ as the appropriate stress variables, because use of the two tensor variables $\sigma - u_a$ and $\sigma - u_w$ would lead to unnecessary complexity and redundant information. The combination of "net stress" $\sigma - u_a$ and matrix suction $u_a - u_w$ is usually selected, because u_a is commonly zero (relative to atmospheric pressure) in the field, and the net stress and the matrix suction then simplify to the total stress and the negative pore water pressure respectively. In addition, the pore water pressure in an unsaturated soil is generally negative, which is often difficult to measure accurately. This means an element of uncertainty will be involved in only one stress variable if $\sigma - u_a$ and $u_a - u_w$ are selected, whereas the uncertainty will affect both the variables if $\sigma - u_w$ and $u_a - u_w$ are adopted.

Considerable research has been done using the net stress $\sigma - u_a$ and the suction $u_a - u_w$ as the two variables, but other alternative sets of stress variables have been proposed by a number of researchers, including Kohgo *et al* (1993 *a* and *b*), Modaressi and Abou-Bekr (1994), Jommi and Di Prisco (1994) and Bolzon *et al* (1996). The search for alternative stress variables seems to be prompted by an objective to adopt stress variables with stronger physical significance than the set of net stress $\sigma - u_a$ and suction $u_a - u_w$. To achieve it, a stress variable is quite commonly selected in such way that it defines uniquely the variation of shear strength of an unsaturated soil. For a full description of the remaining aspects of mechanical behaviour, such as, volumetric response and yielding, suction or some function of suction is adopted as another stress variable. The general form of the proposed variables is: $\sigma - u_a + f_1(s)$ and $f_2(s)$, with $f_1(s)$ and $f_2(s)$ being functions of suction. A comprehensive summary of stress variables used by various researchers is given by Gens (1996) and critical evaluation is presented by Wheeler and Karube (1996). It is important to note that the use of alternative stress variables should be justified by either:

- describing additional important aspects of unsaturated soil behaviour that cannot be represented by using the net stress $\sigma - u_a$ and the suction $u_a - u_w$ as the two stress variables;

or

- resulting in simpler constitutive relationships between stresses and strains than can be achieved with models described in terms of net stress $\sigma - u_a$ and suction $u_a - u_w$.

The potential advantages in using the alternative stress variables should be substantial rather than merely resulting in another way of expressing the existing constitutive models. This is because the alternative stress variables are generally more complex than the net stress $\sigma - u_a$ and the suction $u_a - u_w$ and working in terms of the alternative variables can pose new

problems. One example of such potential problems is representation of stress paths. Wetting and drying paths under constant applied loading or isotropic loading and unloading paths at constant suction are simple stress paths in terms of net stress $\sigma - u_a$ and suction $u_a - u_w$ (with one or the other variable being held constant), whereas these stress paths can become complicated and difficult to define in terms of the alternative stress variables. This in turn can lead to two potential problems. Firstly, devising simple experimental tests to measure soil parameters can be difficult. Secondly, it can be difficult for a user of the model to "think" in terms of the alternative stress variables. It is, however, important to note that these arguments are cautionary only, and the issue of selecting stress variables should not be considered as settled, because there are important aspects of unsaturated soil behaviour that it has, so far, not been possible to describe by the models formulated in terms of the net stress $\sigma - u_a$ and the suction $u_a - u_w$. These points are discussed further in Sections 2.10.3 and 7.2.

If net stress $\sigma - u_a$ (a tensor variable) and suction $u_a - u_w$ (a scalar variable) are selected as appropriate stress variables, the appropriate stress variables to use for the special conditions of the triaxial test ($\sigma_2 = \sigma_3$) are given by Matyas and Radhakrishna (1968) as the mean value of net stress $p - u_a$, the deviator value of net stress q and matrix suction s, and can be defined as follows:

$$p - u_a = \frac{1}{3}(\sigma_1 + 2\sigma_3) - u_a \tag{2.5}$$

$$q = (\sigma_1 - u_a) - (\sigma_3 - u_a) = \sigma_1 - \sigma_3 \tag{2.6}$$

$$s = (u_a - u_w) \tag{2.7}$$

where σ_1 and σ_3 are the axial total stress and radial total stress respectively.

2.5 Work Conjugate Strain Parameters

For saturated soils, the state of deformation can be fully defined, within the special case of a triaxial test ($\varepsilon_2 = \varepsilon_3$), by the volumetric strain ε_p and shear strain ε_q, defined by:

$$\varepsilon_p = \varepsilon_1 + 2\varepsilon_3 \tag{2.8}$$

$$\varepsilon_q = \frac{2}{3}(\varepsilon_1 - \varepsilon_3) \tag{2.9}$$

where ε_1 and ε_3 are the axial and radial strains respectively.

For a saturated soil the volumetric strain ε_p and shear strain ε_q are work conjugate with the mean effective stress p' and deviator stress q in that the increment of work input per unit volume of soil dW is given by:

$$dW = p'd\varepsilon_p + qd\varepsilon_q \tag{2.10}$$

An increment of volumetric strain $d\varepsilon_p$ can be related to the change of specific volume v:

$$d\varepsilon_p = -\frac{dv}{v} \tag{2.11}$$

where the specific volume v is the volume of soil (soil particles and voids) containing unit volume of soil particles, related to the void ratio e by:

$$v = 1 + e \tag{2.12}$$

For saturated soils, the volumetric state is uniquely defined by the value of v.

For an unsaturated soil an additional volumetric parameter is required, in addition to v, in order to specify fully the relative volumes of soil particles, pore air and pore water. This additional volumetric parameter could be selected as the degree of saturation S_r, the water content w or specific water volume v_w, introduced by Wheeler (1991) and defined as the volume of solid particles and water within a body of soil containing unit volume of soil particles:

$$v_w = 1 + eS_r = 1 + wG_s \tag{2.13}$$

From Equation 2.13, it is clear that the specific water volume v_w tends to specific volume v as the degree of saturation S_r approaches unity.

Houlsby (1997) presented a comprehensive theoretical analysis of the work input to an unsaturated granular material. This analysis shows that, as stated by Wheeler and Sivakumar (1995), if $p - u_a$, q, and $u_a - u_w$ are selected as the stress variables, the work input equation can be written as:

$$dW = (p - u_a)d\varepsilon_p + qd\varepsilon_q + (u_a - u_w)d\varepsilon_w \tag{2.14}$$

where the strain variable $d\varepsilon_w$ is defined by:

$$d\varepsilon_w = -\frac{dv_w}{v} \tag{2.15}$$

Alternatively, if $p - u_w$, q, and $u_a - u_w$ are selected as stress state variables, Equation 2.14 can be re-arranged to:

$$dW = (p - u_w)d\varepsilon_p + qd\varepsilon_q + (u_a - u_w)d\varepsilon_a \tag{2.16}$$

where the strain variable $d\varepsilon_a$ is defined by:

$$d\varepsilon_v = \frac{d(v - v_w)}{v} \tag{2.17}$$

Houlsby (1997) also shows that Equation 2.14 can be re-arranged to:

$$dW = \left(p - S_r u_w - (1 - S_r)u_a\right)d\varepsilon_p + q d\varepsilon_q - n(u_a - u_w)dS_r \tag{2.18}$$

where n is the porosity.

Equation 2.18 indicates that an alternative choice of stress state variables would be $\left(p - S_r u_w - (1 - S_r)u_a\right)$ [corresponding to the form of stress variable presented in Equation 2.3], q, and $n(u_a - u_w)$. The corresponding conjugate strain parameters are then volumetric strain ε_p, shear strain ε_q, and the decrease of degree of saturation. Other forms of re-arrangement of Equation 2.14 are also possible. It is clear that in terms of a valid work input equation, various possible combinations of stress state variables are acceptable, and each combination of stress state variables has a different set of conjugate strain parameters.

2.6 Soil-Water Characteristic Curve

A curve of matrix suction $u_a - u_w$ versus volumetric water content θ (defined as the volume of water present in unit volume of soil) is widely used in Soil Science and is known as the soil-water characteristic curve or the water retention curve. The degree of saturation S_r or gravimetric water content w are often used in place of volumetric water content θ to define the soil-water characteristic curve. Relationship between volumetric water content θ, degree of saturation S_r and gravimetric water content w can be written as:

$$\theta(1 + e) = S_r e = wG_s \tag{2.19}$$

where G_s is the specific gravity of the soil particles. In Soil Science the soil is generally assumed to be incompressible (e = constant), so the variations of θ, S_r or w all provide equivalent information.

Considerable work has been done in Soil Science on various aspects of the soil-water characteristic curve (see, for example, Mualem (1974)). It is however important to note that in Soil Science the main focus of research pertaining to the soil-water characteristic curve has been for modelling the inflow or outflow of water to or from unsaturated soils, rather than the mechanical behaviour, and it is generally assumed that the applied net stresses are negligible ($p - u_a = q = 0$) and the soil is incompressible (e = constant). Clearly these assumptions are not appropriate within geotechnical engineering.

Fredlund and Xing (1994), using concepts from Soil Science work, proposed an empirical expression for the drying portion of the soil-water characteristic curve. The expression in its present form is incomplete and needs inclusion of the wetting process and the effects of soil deformation.

Many authors, including Croney (1952), have reported the hysteretic nature of the soil-water characteristic curve, which is shown schematically in Figure 2.5. This "hydraulic hysteresis" gives rise to different degrees of saturation in the wetting and the drying paths at a given value of suction, as illustrated schematically in Figure 2.5. A dramatic effect of the hysteretic relationship is in the transition between saturated and unsaturated conditions. It is well known that a saturated soil can sustain a significant value of suction applied to the boundary, which is known as the air entry value, without any drop in the degree of saturation below unity (see, for example, Bishop *et al* (1975)). In contrast, the degree of saturation can remain significantly below unity on reducing the applied suction to zero (see, for example, Sivakumar (1993)).

The primary wetting and drying curves shown in Figure 2.5 correspond to wetting from a dry state and drying from a fully saturated condition respectively. If wetting or drying commences from any other point and follows a previous drying or wetting stage respectively, the new wetting and drying curves lie within the region enclosed by the bounding primary wetting and drying curves. Childs (1969) termed these new wetting and drying curves as "scanning curves" (see Figure 2.6). In cycles of wetting and drying performed over a constant range of suction the response of the soil should gradually approach a stable closed hysteresis loop in the $S_r : u_a - u_w$ plot (see Figure 2.7). For cycles performed over a given suction range, the form of the final stable hysteresis loop should be independent of whether the first cycle starts on a wetting curve or a drying curve (compare Figures 2.7 (i) and 2.7 (ii)).

The reason for hydraulic hysteresis is illustrated in Figure 2.8 in which emptying and flooding of a void with water is considered. In Figure 2.8 (i), the void is about to empty of water at point *A* during a drying path (see Figure 2.5) when the menisci are at the narrow entry points to the void. This means the radius of curvature r_d is small and therefore according to Equation 2.2, the corresponding matrix suction will be high. In Figure 2.8 (ii), the void is empty of water. In subsequent wetting the same void is about to be flooded with water (see Figure 2.8 (iii)) at point *B* on a wetting path (see Figure 2.5). Two sections of menisci are about to coalesce at locations well inside the narrowest entry points. This means the radius of curvature r_w in Figure 2.8 (iii) is greater than the radius r_d in Figure 2.8 (i) and hence the matrix suction is correspondingly lower

during wetting than the corresponding point A during drying. Differences in the contact angles during the wetting and drying processes also contributes to hydraulic hysteresis (see, for example, Dineen (1997)). Fredlund and Rahardjo (1993) suggested that the entrapped air in the soil might also cause hysteresis.

For two points at the same value of suction (such as A and C in Figure 2.5) the degree of saturation on a drying path would be much higher than on a wetting path, and hence the proportions of bulk water and meniscus water would be different in the two cases. Since pore water pressure within meniscus water acts on the soil skeleton in a different way to the pore water pressure within bulk water, as described in Section 2.2, samples at A and C would be expected to have different mechanical properties i.e. hydraulic hysteresis affects the mechanical behaviour of an unsaturated soil. The effects of hydraulic hysteresis are not incorporated into existing constitutive models, mainly to avoid complexity in the models.

2.7 Volumetric Behaviour

Matyas and Radhakrishna (1968) were amongst the first researchers to use the net stress $\sigma - u_a$ and the matrix suction $u_a - u_w$ as two independent stress variables in their work. They used mean net stress $p - u_a$, deviator stress q and matrix suction s, as defined in Equations 2.5 to 2.7, as the three stress parameters for triaxial test conditions. Matyas and Radhakrishna (1968) conducted compression tests on a mixture of flint powder (80%) and kaolin (20%). The tests, conducted in a triaxial cell, involved either isotropic compression or anisotropic K_0 compression. Test results were presented in the form of three dimensional "state surfaces" relating the void ratio e and the degree of saturation S_r to the mean net stress $p - u_a$ (or the vertical net stress $\sigma_v - u_a$ for the K_0 tests) and the suction $u_a - u_w$. These three-dimensional state surfaces are shown schematically in Figure 2.9.

It is interesting to note that the state surface for the void ratio e is warped, and, therefore, capable of representing wetting-induced swelling at the low values of mean net stress and wetting-induced collapse compression at high values of mean net stress. The state surface for void ratio e for a given soil was found to be unique only for stress paths involving wetting (reduction of s) or loading (increase of mean net stress $p - u_a$ or vertical net stress $\sigma_v - u_a$) and for other stress paths involving drying or unloading the state surface was not found to be completely unique. Similar conclusions were reached for the state surface for the degree of saturation S_r.

Fredlund (1979) suggested the following mathematical expressions for the state surfaces for void ratio e and water content w:

$$e = e_0 - C_t \log(\sigma - u_a) - C_m \log(u_a - u_w) \quad (2.20)$$

$$w = w_0 - D_t \log(\sigma - u_a) - D_m \log(u_a - u_w) \quad (2.21)$$

Equation 2.20 represents a planar surface in e : $\log(\sigma - u_a)$: $\log(u_a - u_w)$ space. This means it cannot explicitly account for both wetting-induced swelling and wetting-induced collapse. As Fredlund (1979) suggested, these effects can, however, be incorporated if the compression indices C_t and C_m are functions of stress state.

Lloret and Alonso (1985) proposed relations for the state surfaces for the void ratio e and the degree of saturation S_r, as follows:

$$e = a_1 + b_1 \log(\sigma - u_a) + c_1 \log(u_a - u_w) + d_1 \log(\sigma - u_a)\log(u_a - u_w) \quad (2.22)$$

$$S_r = a_2 - (1 - \exp(-b_2(u_a - u_w)))(c_2 + d_2(\sigma - u_a)) \quad (2.23)$$

where a_1, b_1, c_1, d_1, a_2, b_2, c_2, and d_2 were soil constants. Equation 2.22 represents a warped state surface for the void ratio, enabling both wetting-induced swelling and wetting-induced collapse to be represented. Clearly Equations 2.22 and 2.23 can sensibly apply only to a limited range of stresses.

Volume change relations based on the state surface approach tend to assume uniqueness of the state surface linking the void ratio e to the mean or vertical net stress and the suction. The uniqueness of the state surface is, however, limited to virgin loading conditions involving increase of the net stress or decrease of the suction (wetting). Stress paths involving unloading or drying follow swelling surfaces. These swelling surfaces lie below the unique virgin loading surface and are analogous to swelling lines for saturated soils. Matyas and Radhakrishna (1968) were the first to report this type of behaviour. Ho *et al* (1992) also acknowledged it by suggesting different values of the compression indices for loading and unloading paths in Equations 2.20 and 2.21.

2.8 Shear Behaviour

Fredlund *et al* (1978) proposed that the shear strength of an unsaturated soil was a function of the two independent stress variables: the component of mean net stress normal to the shearing plane $\sigma - u_a$ and the matrix suction $u_a - u_w$. They suggested the following expression for shear strength:

$$\tau = c' + (\sigma - u_a)\tan\phi' + (u_a - u_w)\tan\phi^b \quad (2.24)$$

where c' and ϕ' are the cohesion intercept and angle of friction, respectively, for saturated conditions and ϕ^b is the angle of friction with respect to suction $u_a - u_w$. Gulathi and Satija (1981) further examined the shear strength behaviour of unsaturated soils. They conducted triaxial shear tests at constant water content and in fully drained conditions on Dhanauri clay and their results were reported to be consistent with Equation 2.24.

Fredlund *et al* (1978) and Gulhati and Satija (1981) represented the increase of shear strength with suction by a linear function given by Equation 2.24. However, shear box tests conducted by Escario and Saez (1986) on various unsaturated soils provided experimental evidence for a non-linear increase of shear strength with suction. Subsequent experimental evidence for non-linearity of the increase of shear strength with suction was provided by Gan *et al* (1988), Escario and Juca (1989) and many other researchers. Non-linearity of the shear strength with suction is now well established, as is evident from numerous research papers published on this topic in the First International Conference on Unsaturated Soils held in September, 1995 in Paris (see, for example, Wheeler and Karube (1996)).

Gan *et al* (1988) provided experimental evidence that, for suctions less than the air entry value of a soil, the value of friction angle with respect to suction ϕ^b is equal to ϕ' and then ϕ^b decreases as the suction increases. This means for suctions less than the air entry value of a soil, the shear strength Equation 2.24 can, as required, be written as:

$$\tau = c' + (\sigma - u_a)\tan\phi' + (u_a - u_w)\tan\phi' = c' + (\sigma - u_w)\tan\phi' \qquad (2.25)$$

Over the full range of suction, Equation 2.24 can be replaced by:

$$\tau = c' + (\sigma - u_a)\tan\phi' + f(u_a - u_w) \qquad (2.26)$$

where $f(u_a - u_w)$ is a nonlinear function of suction. A graph of $f(u_a - u_w)$ against $(u_a - u_w)$ would have a slope equal to ϕ' for suctions less than the air entry value, with the slope then decreasing for higher values of suction.

Escario and Juca (1989) showed that at very high values of suction the shear strength began to fall slightly with increasing suction, suggesting that the function $f(u_a - u_w)$ in Equation 2.26 was reducing. Data presented by Gan and Fredlund (1996), support the suggestion of Escario and Juca (1989). If this suggestion is extended to a dry granular soil in which the contacts of soil particles have dried out, the function $f(u_a - u_w)$ would be expected to tend to zero as suction tends to infinity, in order to give the required shear strength expression of

$$\tau = c' + (\sigma - u_a)\tan\phi' \qquad (2.27)$$

Fredlund *et al* (1995) and Vanapalli *et al* (1996) suggested a method in which the term $f(u_a - u_w)$ in the shear strength expression of Equation 2.26 can be predicted from a soil water characteristic curve relating matrix suction $u_a - u_w$ and the degree of saturation S_r. This proposal has the advantage that determination of parameters for unsaturated shear strength will become straightforward and practising engineers can use unsaturated shear strength in design and analysis without having to carry out complex and specialised soil tests.

Research on the shear stiffness G of unsaturated soil is not as extensive as work on the shear strength. Consequently, effects of suction on the shear stiffness G are not well established. There are, however, some indications that the shear stiffness G increases with increasing suction. Richards (1978) suggested a power law relationship between small strain shear stiffness and suction. Marinho *et al* (1995) reported data that suggests that the small strain shear stiffness initially increases with suction and after reaching a maximum begins to fall. This suggests that the variation of shear stiffness with suction could be similar to the variation of shear strength with suction.

2.9 Influence of Suction on Inter-particle Forces

As pointed out in Section 2.2, pore water in unsaturated soils can occur in the form of either bulk water or meniscus water. The pore water pressure in bulk water influences the soil behaviour in a similar way as the pore water pressure in saturated soils. In contrast, pore water pressure within meniscus water affects inter-particle forces in a qualitatively different way, as described in Section 2.2.

In this section, this influence of suction within meniscus water on inter-particle forces will be analysed and examined in some detail. For this purpose, two idealised types of particle contacts are considered: contact of spherical particles and contact of platy particles. Haines (1925) and Fisher (1926) presented detailed analyses for spherical particles. These analyses are re-formulated here in such a way that a comparison can be made with a new analysis for a contact of platy particles, presented in Section 2.9.2.

2.9.1 Contact of spherical particles

A contact between two idealised spherical particles of equal radius R is schematically illustrated in Figure 2.10. Meniscus water collects at the particle contact forming an annular ring with double curvature represented by radii r_1 and r_2. A contact angle of zero (full wetting) is

assumed where the air-water interface is in contact with each of the soil particles. The water inside the ring is at a pressure u_w and the air outside the ring is at a pressure u_a. An expression for matrix suction $u_a - u_w$ in terms of radii r_1 and r_2 can be written as:

$$u_a - u_w = T\left(\frac{1}{r_1} - \frac{1}{r_2}\right) \tag{2.28}$$

where T is surface tension.

Equation 2.28 is similar to Equation 2.1 except that the radii r_1 and r_2 are measured on the opposite sides of the meniscus in Figure 2.10 and hence the radius r_2 is negative. For the single ring of meniscus water shown in Figure 2.10, it is possible at large values of r_2/R (r_2 greater than $2R/3$, see below) to have r_1 greater than r_2, and hence, to have a negative value of matrix suction. In practice, however, within the pores of a soil, such large values of r_2/R are unlikely, because each soil particle is contacted by many other soil particles, and coalescence of water rings around the different inter-particle contact points would occur well before r_2/R reached the critical value of 2/3.

An expression for r_1 in terms of R and r_2 can be developed from simple geometrical considerations, as:

$$r_1 = \frac{r_2^2}{2(R - r_2)} \tag{2.29}$$

In deriving Equation 2.29, it has been assumed that the cross-section of the water ring has a circular profile (of radius r_1). Fisher (1926) has presented a refined analysis, taking account of the true non-circular shape of the ring cross-section, but the results are very similar to those for the circular assumption.

Combining Equations 2.28 and 2.29 to eliminate r_1, gives:

$$u_a - u_w = \frac{T}{R}\left[\frac{2 - 3\left(\frac{r_2}{R}\right)}{\left(\frac{r_2}{R}\right)^2}\right] \tag{2.30}$$

This expression shows that the matrix suction is a function of the particle size R and the ratio r_2/R only, and it can be used to estimate the values of suction corresponding to different particle sizes and ratio r_2/R. Inspection of Equation 2.30 shows that the matrix suction reduces to zero at $r_2/R = 2/3$, when the radii r_1 and r_2 become equal (see Equation 2.29).

Figure 2.11 shows $u_a - u_w$ plotted against r_2/R for different values of R, calculated from Equation 2.30 and using a value of 73×10^{-3} N/m for T (corresponding to an air-water interface at 20^0C, see Fredlund and Rahardjo (1993)). Inspection of Figure 2.11 shows that for particles with a radius R of 1 mm a suction of 10 kPa occurs with r_2/R = 0.110 and suctions of 100 kPa or 1000 kPa are attainable only at very low values of r_2/R = 0.037 and 0.012 respectively. In contrast, for much smaller particles with radius R of 1 μm suctions of 10 kPa, 100 kPa and 1000 kPa occur at r_2/R values of 0.647, 0.535, and 0.287 respectively.

The presence of water in the ring-shaped menisci at the particle contact gives rise to an additional inter-particle normal force ΔN_s, which can be determined by considering equilibrium of the particles in Figure 2.10. For equilibrium analysis, forces acting on a body consisting of the upper particle and the upper half of the water ring (above a horizontal plane A-A passing through the contact point) are considered. If the forces acting on the upper particle in the absence of the water ring (with the pore air pressure u_a acting throughout the entire void space) are in equilibrium, then the additional forces produced by the presence of the water ring (containing water at pressure u_w) can be calculated by considering equilibrium of only the additional forces. These additional forces acting on the defined body are:

1. A downward force due to the fact that over a circular area of radius r_2 the air pressure u_a has been replaced by a lower pore water pressure u_w.
2. A downward force caused by the surface tension T acting round the perimeter of same circular area of radius r_2.
3. A balancing upward force ΔN_s representing an increase in the normal reaction at the inter-particle contact.

The resulting mathematical expression is as follows:

$$\Delta N_s = (u_a - u_w)\pi r_2^2 + 2T\pi r_2 \qquad (2.31)$$

Elimination of $u_a - u_w$ between Equations 2.28 and 2.31, gives:

$$\Delta N_s = \pi T\left(\frac{r_2}{r_1}\right)(r_1 + r_2) \qquad (2.32)$$

Substitution for r_1 from Equation 2.29 into Equation 2.32, gives:

$$\Delta N_s = \pi TR\left(2 - \frac{r_2}{R}\right) \qquad (2.33)$$

Assuming that the increase in inter-particle force ΔN_s can be expressed as an averaged increase of stress $\Delta\sigma$ over a square region of area $4R^2$, an expression for the stress increase $\Delta\sigma$ can be written as:

$$\Delta\sigma = \frac{\pi T}{4R}\left(2 - \frac{r_2}{R}\right) \qquad (2.34)$$

Inspection of Equation 2.34 shows that the additional component of inter-particle stress $\Delta\sigma$ arising from the presence of meniscus water at inter-particle contacts increases from $\pi T/3R$ at zero suction (when $r_2/R = 2.3$) to a limiting value $\pi T/2R$ as suction tends to infinity (when r_2/R tends to zero). Values of suction corresponding to intermediate values of $\Delta\sigma$ can be calculated by using Equation 2.34 to calculate the values of r_2/R and then inserting this in Equation 2.30. Results of how $\Delta\sigma$ varies with $u_a - u_w$ can be plotted in non-dimensional form, $R\Delta\sigma/T$ against $R(u_a - u_w)/T$, as shown in Figure 2.12.

Figure 2.13 shows the limiting value of $\Delta\sigma$, reached as suction tends to infinity, plotted against particle radius R, with a value of $73\text{x}10^{-3}$ N/m assumed for surface tension T. It is clear that the maximum value of $\Delta\sigma$ that can be achieved is very small for millimetre-sized particles ($\Delta\sigma_{Limit}$ = 0.115 kPa for R = 1 mm), and likely to be insignificant compared with the inter-particle stresses caused by externally applied loads. In contrast, much larger values of $\Delta\sigma$ can be achieved for micron-sized particles ($\Delta\sigma_{Limit}$ = 115 kPa for R = 1 μm), and this additional component of inter-particle normal stress may be very significant in comparison with inter-particle stresses caused by external loading.

2.9.2 Contact of platy particles

The purpose of analysing a contact between platy particles is that the shape of a clay platelet cannot be described as approximately spherical. Contacts between different clay platelets are random, but to keep the analysis simple an edge-to-face contact is analysed. An idealised edge-to-face contact of two platelets of length L and thickness t is shown in Figure 2.14.

The expression for matrix suction for this case is as follows:

$$u_a - u_w = \frac{T}{r} \qquad (2.35)$$

where r is the radius of the cylindrical section of meniscus. Assuming that the platelet thickness t is much less than its length L, the meniscus radius r can take values between zero and $L/2$ (see Figure 2.14). Equation 2.35 can be re-written as:

$$u_a - u_w = \frac{T}{L\left(\frac{r}{L}\right)} \tag{2.36}$$

For comparison with the spherical particle contact, values of $u_a - u_w$ calculated from Equation 2.36 are plotted against r/L, for different values of platelet dimension L in Figure 2.15. It is evident, from this figure, that for clay platelets with a size of L = 1 μm, the value of suction must be at least 146 kPa (corresponding to r/L = 0.5) and suction of 1 MPa requires r/L = 0.073.

Equilibrium analysis for a contact of two square platelets (of plan dimensions L and thickness t) is carried out on similar lines as for the spherical particle in the previous section, and the symbols have the same meaning unless specifically mentioned. Ignoring the end effects (equivalent to assuming that t and r are much smaller than L), the following expression for ΔN_s is obtained from equilibrium considerations:

$$\Delta N_s = 2TL \tag{2.37}$$

Expressing this force as an averaged inter-particle stress $\Delta\sigma$ acting over and area of L^2, gives:

$$\Delta\sigma = \frac{2T}{L} \tag{2.38}$$

Note that (given the assumption that r and t are much less than L) $\Delta\sigma$ is independent of r/L and is a function only of the platelet dimension L. For a clay platelet with L = 1 μm, the value of $\Delta\sigma$ predicted by Equation 2.38 is 146 kPa. This is likely to be very significant in comparison with inter-particle stresses arising from external loading.

2.9.3 Important results

1. For millimetre-sized spherical particles (sand grains or packets of clay containing many platelets), the meniscus water configuration shown in Figure 2.10 can occur at any suction, but this requires very low values of r_2/R, if suctions greater than, say, 10 kPa are to be achieved. In consequence, whatever the value of suction, the contribution of this suction in meniscus water to inter-particle contact stresses is likely to be less than 1 kPa for such large particles.
2. For micron-sized clay platelets, the meniscus water configuration shown in Figure 2.14 can occur only for suctions in excess of about 100 kPa. For these conditions, the contribution of suction in meniscus water to inter-particle stresses is largely dependent on platelet size (and independent of suction value), with a contribution in excess of 100 kPa possible for clay-sized platelets.

3. Given that meniscus water around individual clay platelet contacts can occur only at suctions above about 100 kPa, and that meniscus water around contacts between millimetre-sized spherical particles can never contribute substantially to inter-particle stresses, within the range of suction from zero to 100 kPa the most significant effect of suction within meniscus water on inter-particle stresses arises from water around contacts between silt-sized bodies (either individual silt particles or silt-sized aggregation of clay platelets).

2.10 Elasto-plastic Constitutive Modelling

Generalised elasto-plastic models, incorporating both volumetric and shear behaviour, are well established for saturated soils. In recent years, this type of approach has been extended to unsaturated soils. In describing these models, the symbol p'' will be used for mean net stress $p - u_a$ and the symbol s for matrix suction $u_a - u_w$ (in the interest of convenience).

2.10.1 The model of Alonso *et al* (1990)

Alonso *et al* (1987) were among the first researchers to propose an integrated framework incorporating both volumetric and shear behaviour of unsaturated soil. This proposed framework was based on the theory of elasto-plasticity and was initially presented in a qualitative way, rather than with full mathematical development.

A fully developed mathematical formulation, in the form of a critical state type model for non-expansive unsaturated soils was presented by Alonso *et al* (1990). This model is formulated in terms of four state variables, namely: mean net stress p''; deviator stress q; matrix suction s; and specific volume v, with p'', q and s defined, for the conditions of triaxial test, by Equations 2.5 to 2.7 and v defined by Equation 2.12.

The model of Alonso *et al* (1990) is based on the concept of a yield surface in $q : p'' : s$ space. Elastic behaviour occurs within the yield surface, and on reaching the yield surface the onset of plastic volumetric and shear strains occurs. The elastic variation of specific volume was proposed as:

$$dv^e = -\kappa\left(\frac{dp''}{p''}\right) - \kappa_s\left(\frac{ds}{s + p_{at}}\right) \qquad (2.39)$$

where κ and κ_s are elastic constants and p_{at} is atmospheric pressure. Inclusion of atmospheric pressure in the Equation 2.39 was essentially arbitrary and was to keep the predicted elastic changes of v finite as the suction tended to zero.

For isotropic loading to virgin states, plastic strains occur and the soil state lies on a normal compression line for the particular value of suction defined by:

$$v = N(s) - \lambda(s)\ln\left(\frac{p''}{p_c}\right) \qquad (2.40)$$

where $N(s)$ is the value of specific volume on the normal compression line at a reference stress p_c (an additional soil constant, defined later) and $\lambda(s)$ is the compression index for changes in mean net stress for virgin states of the soil. $N(s)$ and $\lambda(s)$ both vary with suction. Alonso *et al* (1990) suggested the following expression for the variation of $\lambda(s)$ with suction:

$$\lambda(s) = \lambda(0)((1-r)\exp(-\beta s) + r) \qquad (2.41)$$

$\lambda(0)$ is the compression index at zero suction (saturated conditions), r (which takes a value between 0 and 1) is the ratio of the asymptotic value of $\lambda(s)$ at very high suction to the value $\lambda(0)$ at zero suction and β defines the rate at which the compression index reduces towards the asymptotic value with increasing suction. The equivalent expression for $N(s)$ showing its variation with suction is defined later by Equation 2.43.

For isotropic stress states, the intersection of the yield surface with the $q = 0$ plane gives a yield curve, termed the "loading collapse" *LC* yield curve by Alonso *et al* (1990). Mathematically the shape of the *LC* yield curve is given in the model of Alonso *et al* (1990) by:

$$\frac{p_0''}{p_c} = \left(\frac{p_0''(0)}{p_c}\right)^{\frac{\lambda(0)-\kappa}{\lambda(s)-\kappa}} \qquad (2.42)$$

p_0'' is the yield value of mean net stress under isotropic loading at a particular suction s, and $p_0''(0)$ is the value of p_0'' at zero suction (saturated conditions). The *LC* yield curve becomes more inclined as it expands, as shown in Figure 2.16.

Inspection of Equation 2.42 shows that the model of Alonso *et al* (1990) assumes the *LC* yield curve to be a vertical straight line at $p_0''(0) = p_c$ and this provides a definition for the soil constant p_c. This assumption in the model, that there is a particular stress p_c at which the yield curve takes the form of a straight vertical line, which has not been validated experimentally, controls the subsequent development of the yield curve shape as it expands. One consequence of the assumption is that the variation of the intercept $N(s)$ in Equation 2.40 with suction s is given by:

$$N(s) = N(0) - \kappa_s \ln\left(\frac{s + p_{at}}{p_{at}}\right) \qquad (2.43)$$

where $N(0)$ is the value of the intercept at zero suction (saturated conditions).

In Figure 2.17, the *LC* yield curve is shown schematically and four stress paths *ABC*, *DEF*, *GH*, and *JK* are included to illustrate the performance of the model in a qualitative way. *ABC* is a stress path followed under isotropic loading at zero suction and *DEF* is similar isotropic loading, but at a constant value of suction that is higher than zero. The yield stress p_0'' in test *DEF* is greater than the yield stress $p_0''(0)$ in the saturated test *ABC*, consistent with the expectation that suction within meniscus water increases the stability of inter-particle contacts (by increasing the inter-particle normal forces) and therefore delays the onset of yield. Stress paths *GH* and *JK* in Figure 2.17 represent wetting (reduction of suction at constant value of mean net stress). At low values of mean net stress, a wetting stress path remains within the elastic region (stress path *GH*) and only elastic swelling occurs when suction is reduced. Stress path *JK* represents suction reduction (wetting) at a high value of mean net stress, exhibiting elastic swelling in the first portion *JJ*, whereas wetting further (beyond point *J*) results in plastic compression (collapse). The model is therefore capable of representing both wetting-induced swelling and wetting-induced collapse. Once the stress state reaches the *LC* yield curve, a further increase of mean net stress or reduction of suction leads to expansion of the yield curve as shown by portions *BC*, *EF* and *JK* of stress paths *ABC*, *DEF* and *JK* respectively. The corresponding plastic reduction of v is assumed to be dependent solely on the degree of expansion of the yield curve, which can be represented by the increase of $p_0''(0)$, irrespective of the stress path followed to produce this expansion, so that:

$$dv^p = -(\lambda(0) - \kappa)\frac{dp_0''(0)}{p_0''(0)} \qquad (2.44)$$

This means that collapse compression on wetting at high value of mean net stress p'' is modelled as the same process as plastic compression that occurs on isotropic loading beyond the preconsolidation pressure.

Alonso *et al* (1990) considered the Modified Cam-Clay model as a limiting condition corresponding to the saturated case. Consequently, extension of the model to anisotropic stress states resulted in elliptical yield curves in the $q : p''$ plane for each value of suction, as shown in Figure 2.18. They assumed a linear increase of shear strength with suction, though non-linearity of shear strength with suction is well established (see Section 2.8). An expression for deviator stress q at critical states was therefore proposed as:

$$q = Mp'' + Mks \qquad (2.45)$$

where M is the critical state stress ratio for saturated conditions and k is an additional soil constant defining the rate of increase of critical state shear strength with suction. A linear

variation of shear strength with suction, as described by Equation 2.45, was considered by Alonso *et al* (1990) as a reasonable first approximation for unsaturated soil modelling, especially in view of the main objective of keeping the model simple. It should be noted that the Equation 2.45 is equivalent to Equation 2.24 (with $c' = 0$), which was used by Fredlund *et al* (1978) for defining the shear strength as a linear function of the suction.

Taking into account the assumptions proposed by Alonso *et al* (1990) and noting that they assumed elliptical yield curves of fixed aspect ratio, the specific volume v at critical states predicted by their model, although not reported explicitly by Alonso *et al* (1990), is given by:

$$v = N(s) - (\lambda(s) - \kappa)\ln\left(2 + \frac{ks}{p''}\right) - \lambda(s)\ln\left(\frac{p''}{p_c}\right) \qquad (2.46)$$

Figure 2.19 shows the form of critical state line predicted by Equation 2.46. The critical state line for a given value of suction is curved in the v:ln p'' plane. At values of p'' much higher than the suction s the curve becomes asymptotic to a straight line with slope λ(s) lying a distance $(\lambda(s) - \kappa)\ln 2$ below the corresponding normal compression line for the same value of suction.

Alonso *et al* (1990) proposed a non-associated flow rule (to provide a good match to the K_0 value for saturated soil) which tended to an associated flow rule at critical states. Ten soil constants (κ, κ_s, G, $N(0)$, $\lambda(0)$, β, r, p_c, M, k) are required in the model and the current soil state is defined by the values of p'', q, s, and v or by the values of p'', q, s, and $p_0''(0)$.

2.10.2 Subsequent validation and refinement

Experimental data presented by Wheeler and Sivakumar (1995), Maâtouk *et al* (1995) and Cui and Delage (1996) supported the main features of the model proposed by Alonso *et al* (1990). However, aspects of the experimental data suggested minor modifications to the original model, and Wheeler and Sivakumar (1995), for example, proposed a revised model.

Wheeler and Sivakumar (1995) presented experimental data obtained from controlled-suction triaxial tests on speswhite kaolin that indicated the existence of a unique normal compression line for each value of suction of the form:

$$v = N(s) - \lambda(s)\ln\left(\frac{p''}{p_{at}}\right) \qquad (2.47)$$

where p_{at} is atmospheric pressure and the intercept N(s) and slope λ(s) are functions of suction. Equation 2.47 is same as Equation 2.40 except that Wheeler and Sivakumar (1995) used p_{at} to

avoid introducing an additional soil constant p_c. The slope $\lambda(s)$ was found to vary with increasing suction, as shown schematically in Figure 2.20 (c). Alonso *et al* (1990) however proposed that $\lambda(s)$ decreased with increasing suction (see Equation 2.41), as shown in Figure 2.20 (a), which implies that wetting-induced collapse increases indefinitely with increasing mean net stress p''. A limit to the maximum value of wetting-induced collapse is nonetheless reported by researchers such as Yudhbir (1982). Subsequently Josa *et al* (1992) incorporated this aspect in their model, which includes the modified forms of normal compression lines shown schematically in Figure 2.20 (b). In this modified form the normal compression lines initially diverge with increasing mean net stress and then converge. The data reported by Wheeler and Sivakumar (1995) relate to a limited range of stresses which, for this compacted kaolin, presumably corresponds to stresses above that where the maximum collapse occurs.

Wheeler and Sivakumar (1995) showed that the form of normal compression lines in the $v : p''$ plane is inextricably linked with the development of the shape of the LC yield curve in the $s : p''$ plane as the curve expands. This implies that defining either the normal compression lines for different values of suction or the changing shape of the yield curve as it expands is sufficient for developing these aspects of an elasto-plastic model. Wheeler and Sivakumar (1995) used the former approach, whereas Josa *et al* (1992) used the latter approach. Alonso *et al* (1990) used a mixed approach wherein they made an assumption for the shape of yield curve at a particular reference pressure p_c and another assumption for the variation of the slope $\lambda(s)$ of the normal compression line as given by Equation 2.41, but they made no explicit assumption for the variation of the intercept $N(s)$. Wheeler and Sivakumar (1995) argued in favour of treating $N(s)$ and $\lambda(s)$, and the variation of these with suction, as experimentally measured soil "constants", because the locations and slopes of the normal compression lines for different values of suction can be experimentally ascertained with greater ease than can the changing shape of the LC yield curve as it expands.

Derivation of the equation for the LC yield curve from the normal compression lines can be illustrated by considering stress path ABC in Figure 2.21. It should be noted that points A and C lie on the same yield curve at different values of suction (Figure 2.21 (a)), and that each lies on the normal compression line for the appropriate value of suction in Figure 2.21 (b). The change of specific volume in following stress path ABC can be estimated in two ways. Firstly by considering the stress path ABC in Figure 2.21 (a), the change of specific volume in going from A to C can be calculated in terms of the elastic swelling indices κ and κ_s, as:

$$\Delta v = -\kappa_s \ln\left(\frac{s + p_{at}}{p_{at}}\right) - \kappa \ln\left(\frac{p_0''}{p_0''(0)}\right) \tag{2.48}$$

Alternatively, using Figure 2.21 (b), the change of specific volume for stress path ABC can be calculated in terms of $N(0)$, $\lambda(0)$, $\lambda(s)$, and $N(s)$ as:

$$\Delta v = N(s) - \lambda(s)\ln\left(\frac{p_0''}{p_{at}}\right) - N(0) + \lambda(0)\ln\left(\frac{p_0''(0)}{p_{at}}\right) \tag{2.49}$$

By eliminating Δv between Equations 2.48 and 2.49, Wheeler and Sivakumar (1995) derived the following Equation for the LC yield curve:

$$(\lambda(s) - \kappa)\ln\left(\frac{p_0''}{p_{at}}\right) = (\lambda(0) - \kappa)\ln\left(\frac{p_0''(0)}{p_{at}}\right) + N(s) - N(0) + \kappa_s \ln\left(\frac{s + p_{at}}{p_{at}}\right) \tag{2.50}$$

Equation 2.50 gives the values of p_0'' for different values of s for any given value of $p_0''(0)$; thus defining the shape of the LC yield curve and how this shape changes as the curve expands. If it is assumed that there exists a reference stress p_c at which the LC yield curve is a straight vertical line in the $s : p''$ plot, Equation 2.50 reduces to Equation 2.42 which was the LC yield curve equation suggested by Alonso *et al* (1990).

The existence of unique critical state relationships, for compacted kaolin, was verified by Wheeler and Sivakumar (1995) and relations for deviator stress and specific volume of the following form were proposed:

$$q = M(s)p'' + \mu(s) \tag{2.51}$$

$$v = \Gamma(s) - \psi(s)\ln\left(\frac{p''}{p_{at}}\right) \tag{2.52}$$

where $M(s)$, $\mu(s)$, $\Gamma(s)$, and $\psi(s)$ were all functions of suction. The function $\mu(s)$ increases at a non-linear rate with suction, so that Equation 2.51 represents a non-linear increase of strength with suction. This is an improvement over the linear increase of shear strength with suction given by Equation 2.45. Alonso *et al* (1990) assumed that constant suction cross-sections of the yield surface were elliptical in shape and of constant aspect ratio (see Figure 2.18). This had the result that the critical state line for a given value of suction s was predicted to take the form given by Equation 2.46 in the $v : \ln p''$ plane. Wheeler and Sivakumar (1995) found that the experimental data for the critical state values of v for compacted kaolin were very different to the predictions of Equation 2.46 and they therefore introduced freedom for the aspect ratio of the elliptical yield curve to vary with suction in such a way as to fit the empirical critical state line expression of Equation 2.52. These modifications enabled Wheeler and Sivakumar (1995) to achieve excellent agreement between the predicted and measured test paths (in $q : p'' : v$ space)

for the samples of compacted kaolin. They used an associated flow rule for predicting stress-strain curves during shearing that showed reasonable agreement with the measured stress-strain curves.

The model proposed by Wheeler and Sivakumar (1995) includes three elastic constants (κ, κ_s and G) and six parameters that vary with suction ($N(s)$, $\lambda(s)$, $M(s)$, $\mu(s)$, $\psi(s)$, *and* $\Gamma(s)$).

2.10.3 Current status of the elasto-plastic models

There is now general consensus in favour of using two independent stress variables rather than adopting a single stress variable for describing the behaviour of unsaturated soils. Whilst the net stress $\sigma - u_a$ and the matrix suction $u_a - u_w$ are commonly chosen as the two variables, other alternative choices have also been suggested by various researchers (see, for example, Kohgo *et al* (1993 *a* and *b*), Modaressi and Abou-Bekr (1994), Jommi and Di Prisco (1994) and Bolzon *et al* (1996)). This is mainly to try to have simpler stress-strain relationships and a better transition between unsaturated and saturated stages of the suction history of a soil than can achieved by using the net stress $\sigma - u_a$ and the matrix suction $u_a - u_w$. Moreover, choice of stress variables is now being linked with the work conjugate strain parameters (Houlsby (1997)).

Constitutive models for saturated soils, such as Modified Cam Clay, are formulated in terms of specific volume v, mean effective stress p', and deviatoric stress q. By direct analogy to the saturated soil models, constitutive models for unsaturated soils can be formulated in terms of specific volume v, specific water volume v_w, mean net stress p'', suction s, and deviatoric stress q. Most of the unsaturated soil models developed so far are limited to $v : p'' : s : q$ space and do not explicitly provide predictions of the variation of specific water volume v_w (or degree of saturation S_r). This means the current models are incomplete. One consequence of this is that these models cannot be used to predict unsaturated soil behaviour during undrained loading or within coupled flow-deformation analysis, where knowledge of the variation of the water content w or the degree of saturation S_r is essential. Wheeler (1996) put forward a method of incorporating specific water volume v_w (and hence w or S_r) in a consistent fashion within an elasto-plastic model, but this approach is still unsatisfactory, because it does not incorporate hydraulic hysteresis in the variation of degree of saturation (as described in Section 2.6)

The experimental evidence presented by Maâtouk *et al* (1995), Cui and Delage (1996), Zakaria (1994), and Zakaria *et al* (1995) suggests that the shape of the yield surface is a function of stress history of the soil: constant suction yield curves in $q : p''$ space being roughly symmetrical about

the mean net stress p'' axis for soils with an isotropic stress history, but roughly inclined about the K_0 line for soils with a one-dimensional stress history. This means that there is evidence for kinematic rather than isotropic hardening (which until now has been assumed in all the elasto-plastic models for unsaturated soils). This non-isotropic evolution of yield surface, as a function of strain history, also occurs for saturated soils, but is not included in conventional models such as Modified Cam Clay. To include this feature into saturated soil models, authors such as Whittle and Kavvadas (1994), Houlsby and Sharma (1997), and Wheeler (1997) suggested models, which could perhaps be extended to unsaturated soils.

For saturated soils, the transition from elastic to plastic straining is more gradual than predicted by classical single yield surface models and this also occurs for unsaturated soils (see, for example, Zakaria (1994)). This aspect of unsaturated soil behaviour could be modelled by two main approaches developed for saturated soils: multiple yield surface plasticity, originally formulated by Iwan (1967) and Mroz (1967) and applied to soils first by Prevost (1978) with subsequent refinements by Al-Tabbaa and Wood (1989), and Atkinson and Stallebrass (1991); and bounding surface plasticity, as proposed by Dafalias and Popov (1975), Krieg (1975), Bardet (1990) and Whittle and Kavvadas (1994). In fact, the best approach for modelling this aspect of soil behaviour is not yet settled and is still a topic of intense research for saturated soils. It is therefore likely to take more time for these types of features to be incorporated into elasto-plastic models for unsaturated soils.

Whilst the existing elasto-plastic models are incomplete in some respects, implementation of the models into numerical formulations such as finite element and finite difference methods has begun. Nesnas (1995) implemented the Alonso *et al* (1990) model into the finite element programme *CRISP* and carried out drained analysis of a footing. Several other authors, including Gatmiri *et al* (1995), Gens *et al* (1995), Ramesh (1996) and Alonso *et al* (1998) have also reported numerical implementation of unsaturated elasto-plastic models.

CHAPTER 3

UNSATURATED HIGHLY EXPANSIVE CLAYS

Most soils can either swell or collapse on wetting, depending upon the applied stress level and the stress history, and therefore rigid divisions into swelling and collapsing soils can be misleading. When swelling on wetting occurs, the magnitude of swelling can however vary greatly between different soils, with highly plastic clays having the potential for much larger magnitudes of swelling than other soils. These clays are referred to as highly expansive clays.

The high degree of swelling is mainly due to the presence of active clay minerals, such as montmorillonite. In these soils important physico-chemical interactions occur in the vicinity of the active clay minerals. Proper understanding of these interactions can explain some of the observed features of soil behaviour. This helps in constructing a conceptual picture of the swelling and shrinkage processes. In this chapter, therefore, some fundamental aspects of expansive clay behaviour at a micro-level (such as salient features of unit layers, cation exchange, and clay expansion theories) are first briefly reviewed, then a conceptual model for soil fabric is outlined and finally features of constitutive modelling are critically examined.

3.1 Unit Layers

A unit layer is a basic repeating structural element of a clay mineral. At the molecular level, clays are made up of two basic structural units: silica tetrahedra and alumina or magnesium octahedra. These units are shown schematically in Figure 3.1. Silica tetrahedra are interconnected in such a way that the bases of the tetrahedra are all in the same plane, and all the tips point in same direction. This leads to a silica sheet of 4.63 $\mathring{A}$ thickness (Grim (1968)). Alumina or magnesium octahedra combine together giving a sheet thickness of 5.05 $\mathring{A}$ (Grim (1968)).

In kaolinite, a representative non-expansive clay mineral, a unit layer is formed by combination of a silica sheet and an octahedral sheet, whereas in highly expansive clays (such as montmorillonite) a unit layer is formed by an octahedral sheet sandwiched between two silica sheets. Inter-sheet bonding within both kaolinite and montmorillonite unit layers is of the primary valence type, which is very strong, making the sheets inseparable. Unit layers of kaolinite and montmorillonite are shown schematically in Figure 3.2.

3.1.1 Nature of electrical charge on unit layers

Prior to looking into the nature of electrical charge on the surface of a unit layer, it is appropriate to consider the shape and dimensions of typical unit layers. Unit layers are very thin with similar length and width. Edges of the unit layers are seldom straight and the unit layers can be visualised as thin flakes. The length and width are of the order of 1 or 2 μm and the thickness is about 10 Å. This gives a ratio of the length or width to the thickness of a unit layer of the order of 2000:1.

Unit layers are not electrically neutral, but carry unbalanced electrical charge on the surfaces and edges. Possible sources of unbalanced electrical charge are:

1. In any unit layer positively charged ions are generally within the interior of the layer, whereas the oxygen or hydroxyl ions on the surfaces of the unit layer are negatively charged. This spatial distribution of the positive and negative charges results in a net negative charge on the surface of a unit layer.
2. Partial replacement of Si^{4+} by Al^{3+} in a tetrahedral sheet or of Al^{3+} by Mg^{2+} in an octahedral sheet (a process known as isomorphous substitution) results in a net negative charge on the unit layers.
3. At the edges of unit layers, tetrahedral silica sheets and octahedral sheets are disrupted, and primary bonds are broken. This leads to the hypothesis of positively charged edges of unit layers. Experimental evidence reported by Thiessen (1942) supports this hypothesis.

In this way, a unit layer can be conceptualised as a flake carrying negative charge on the surfaces and positive charge in the interior and on the edges. This is shown schematically in Figure 3.3.

3.1.2 Stacking and bonding of unit layers in a platelet

A typical clay platelet, of either non-expansive clay mineral such as kaolinite or highly expansive clay mineral such as montmorillonite, can contain up to 20 unit layers stacked one over the other. If there are 20 unit layers in a platelet, the ratio of the length or width to the thickness of the platelet becomes, typically, 100:1. The bonding between unit layers is, however, qualitatively different in the two clay mineral types. In kaolinite, the bonding of unit layers is by both hydrogen bonds and van der Waals forces. This type of bond is sufficiently strong to prevent swelling between unit layers in kaolinite. In contrast, the bonding of unit layers in montmorillonite is by cations (which are attached to the surfaces of unit layers to balance the electrical charge deficiencies) or by van der Waals forces. This type of bond is weak, and

therefore, separation of the unit layers or swelling can occur when a polar liquid like water is available.

It is, therefore, reasonable to say that the main source of additional swelling in a highly expansive clay, containing a significant percentage of active clay minerals such as montmorillonite, is due to separation of unit layers of the active clay mineral. The nature of this swelling and re-compression is examined in more detail in Section 3.3.

3.2 Cation Exchange in Clays

Isomorphous substitution, in which lower positive valence elements replace the existing higher positive valence elements in clay crystals, results in a net negative charge on clay crystals. This negative charge attracts cations (positive ions) towards the surface of the clay. These cations, attached to the clay surface, are termed exchangeable cations as they can be exchanged with other cations. In clay materials the common type of exchangeable cations are H^+, K^+, NH_4^+, Na^+, Ca^{2+}, and Mg^{2+}. The replaceabilty of one type of cation by another type depends upon many factors including valence and ion size. Cations can be arranged in order of ascending replacing capability as follows:

$Na^+ < Li^+ < K^+ < NH_4^+ < Mg^{2+} < Ca^{2+} < Ba^{2+} < Cu^{2+} < Al^{3+} < Fe^{3+} < Th^{4+}$

Details of exchange reactions for montmorillonite are given by several authors, including Sposito *et al* (1983), Levy *et al* (1983), Rytwo *et al* (1995), and Rytwo *et al* (1996).

The total amount of exchangeable cations is called cation exchange capacity CEC. Cation exchange capacity of a clay is affected by particle size, grinding, temperature, and the exchange reaction environment. CEC is used in the calculation of the surface charge on a clay platelet by the following relationship:

$$E = -\frac{CEC}{S} \tag{3.1}$$

where CEC is in C/g and S is the specific surface area in m^2/g, and E is surface charge density in C/m^2.

An estimate of electrical charge on the clay surface, which is related to cation exchange capacity as given in Equation 3.1, is essential in describing ionic distribution around a unit layer. Moreover, the amount of wetting-induced swelling is strongly influenced by the type of exchangeable cation. Development of a particular type of soil fabric is also influenced by the type of cations. Flocculation and deflocculation of clay suspensions are important inter-platelet interactions influencing fabric type, with the former being promoted by monovalent cations,

such as sodium, and the latter being observed in the presence of di- and tri-valent cations (see, for example, Mitchell (1993)).

3.3 Theories of Clay Expansion

The basic mechanism of clay expansion and compression has attracted the attention of several researchers who have proposed a number of theories to explain the phenomenon. One such theory is diffuse double layer theory, proposed by Gouy (1910) and Chapman (1913), and also known as the Gouy-Chapman theory. It was further refined by Stern (1924) to describe the ionic distribution in the immediate vicinity of the surface of a unit layer. This theory has frequently been used to provide a microscopic explanation for the volume change behaviour of clays.

Clay surfaces, dry or wet, carry an unbalanced negative charge, which attracts cations (positive ions). These cations become strongly attached to a dry clay surface. In addition to cations required for the electrical neutrality of the clay surface, there are generally some salt precipitates comprising a combination of cations (positive) and anions (negative). On addition of water, these ions go into solution. De-sorption of cations from the clay surface leads to a higher concentration of cations near the clay surface than the concentration of cations farther away, which makes the cations have a tendency to diffuse farther away. This diffusing tendency is, however, opposed by the attractive force between the cations and the negative particle surface. The net result of these opposing trends is an ion distribution in the vicinity of the clay particle as shown in Figure 3.4. This system of distributed charge, along with the charged surface, is termed the diffuse double layer (*DDL*). The two charged surfaces (the negative charge of the clay surface and the distributed positive charge of the attached cations) are spatially separated and the cations occur in a diffused cluster, hence the name diffuse double layer.

Assuming that the ions in the diffuse double layer are point charges and do not interact with each other, that the distribution of charge on the particle surface is uniform, and that the clay particles are in a parallel arrangement, the distribution of electrical potential ψ (which is defined as the work done to bring a positive unit charge from a reference state to the specified position in the electrical field) within the *DDL* is given by the Poisson-Boltzmann Equation:

$$\frac{d^2\psi}{dx^2} = \frac{8\pi n_0 \upsilon e}{D} \sinh\left(\frac{\upsilon e \psi}{kT}\right) \tag{3.2}$$

where ψ is electrical potential at a distance x from the clay surface, n_0 is the bulk solution electrolyte concentration, υ is cation valence, e is unit electronic charge, D is the dielectric constant, k is the Boltzmann constant, and T is the absolute temperature.

Solutions for Equation 3.2 are generally given in terms of dimensionless quantities and are listed by many authors, such as van Olphan (1977) and Mitchell (1993). The normalised value y of electrical potential at a general distance x from the clay surface is a function of z (the normalised value of electrical potential at the clay surface) and ξ (the normalised distance from the clay surface):

$$y = f(z, \xi) \tag{3.3}$$

The parameters y, z and ξ are given by:

$$y = \frac{\upsilon e \psi}{kT} \tag{3.4}$$

$$z = \frac{\upsilon e \psi_0}{kT} \tag{3.5}$$

where ψ_0 is the value of ψ at $x = 0$.

$$\xi = Kx \tag{3.6}$$

$$\text{where } K^2 = \frac{8\pi n_0 e^2 \upsilon^2}{DkT}. \tag{3.7}$$

$1/K$ is termed the thickness of the diffuse double layer. The quantity z can be related to the surface charge density E, which can be calculated using Equation 3.1, by the following relationship:

$$z = 2\sinh^{-1}\left(E\left(\frac{\pi}{2n_0 DkT}\right)^{\frac{1}{2}}\right) \tag{3.8}$$

The *DDL* is therefore fully defined mathematically by Equations 3.3 to 3.8. Electrical potential at the clay surface ψ_0 is given by Equation 3.5 and 3.8, and the distribution of ψ as a function of distance x from the clay surface can be calculated from Equations 3.3 to 3.7. This potential decays approximately exponentially with distance from the clay surface to a value of potential for the bulk fluid, as shown in Figure 3.5.

3.3.1 Interaction of diffuse double layers

The diffuse double layer can develop for individual unit layers as well as clay platelets. The diffuse double layers of neighbouring unit layers or clay platelets interact, resulting in a net repulsive force between the unit layers or platelets. The repulsive force per unit area f_R between two parallel double layers separated by a distance d is given by Equations 3.9 and 3.10, as follows:

$$f_R = 2n_0 kT(\cosh u - 1) \tag{3.9}$$

where u is a function given by:

$$u = 8\tanh^{-1}\left[\exp(-kd)\tanh\left(\frac{z}{4}\right)\right] \tag{3.10}$$

Equation 3.8 can be used to calculate z for a given value of surface charge density E. Hence for given values of n_0, T, d, D, and E (and given the value of Boltzmann constant k), Equations 3.8 and 3.10 can be combined with Equation 3.9 to give value of repulsive force per unit area f_R.

Attractive molecular forces, however, develop between two double layers if they approach extremely close to each other. The motion of electrons around the nucleus of different atoms and molecules in the system give rise to fluctuating dipoles having opposite electrical charge at their ends. The oppositely charged ends of different fluctuating dipoles attract each other. London (1937) developed a theory for attractive force between two molecules. Casimir and Polder (1948) extended this theory to a case of two parallel layers. The attractive forces are commonly termed as the London-van der Waals forces. An expression for this attractive force per unit area is:

$$f_A = \frac{\alpha}{24\pi}\left[\frac{1}{d^3} + \frac{1}{(d+t)^3} - \frac{1}{\left(d+\left(\frac{t}{2}\right)\right)^3}\right] \tag{3.11}$$

where α is the Hamaker constant, d is the distance between the double layers and t is the thickness of the unit layers or the clay platelets.

It should be noted that whilst the repulsive force f_R depends upon the distance between the parallel double layers (see Equations 3.9 and 3.10), the attractive force f_A depends upon the thickness of the clay platelets as well as the distance between the double layers (see Equation 3.11). Inspection of Equation 3.11 shows that the attractive force f_A decreases as the thickness of the platelet increases (more unit layers stacked one over the other). The repulsive force f_R, however, remains the same irrespective of the thickness. This limits the number of unit layers that would tend to stack together in a platelet, whereas if the attractive force did not decrease with increasing thickness of the platelet, there would be no limit to the maximum possible number of unit layers in a platelet. Different clay platelets will, however, have different numbers of unit layers (up to the maximum value), because of the element of randomness in the process of unit layers approaching each other. This includes the possibility of clay platelets consisting of a single independent unit layer.

For equilibrium of a clay system (comprising independent unit layers, clay platelets and water) the external force f_E should be in balance with the net internal force $f_R - f_A$. For a given distance d between the unit layers the repulsive force f_R can be calculated by using Equations 3.9, 3.10 and 3.8 and the internal force f_A can be estimated from Equation 3.11. This means that by calculating the net internal force $f_R - f_A$ corresponding to various values of distance d between the unit layers, a value of d (and hence volume of the clay system) can be deduced that would be equal to the external force f_E (which is known). If the external force is increased, the net internal force $f_R - f_A$ should also increase which can happen only when the increase in f_R is more than the increase in f_A. Inspection of Equations 3.9, 3.10, and 3.11 shows that f_R increases exponentially with decreasing d and f_A is approximately inversely proportional to d^3, suggesting that there will be net increase in $f_R - f_A$ with decreasing d (hence compression of the clay). Conversely, with decrease in external force swelling will occur.

The advantage of the *DDL* theory is that the effects of factors such as cation valence, dielectric constant, electrolyte concentration, and temperature on the double layer thickness can readily be determined. Successful applications of *DDL* theory, in predicting the volume change behaviour of saturated clays, are reported by several investigators, including Bolt (1956), Olsen and Mesri (1970), Callaghan and Ottewill (1974), van Olphen (1977), Sridharan and Jayadeva (1982), Madsen and Müller-Vonmoos (1985), Stepkewska (1990), Yong and Mohamed (1992), Mitchell (1993), Shang *et al* (1994), and Gleason *et al* (1997). Komine and Ogata (1994, 1996) have recently reported application of *DDL* theory for predicting the volumetric behaviour of unsaturated clays.

Shortcomings of the *DDL* theory mainly arise due to the simplifying assumptions, which are used in its derivation. These assumptions are: that the ions in the diffuse double layer are point charges and do not interact with each other, that the distribution of charge on the particle surface is uniform, and that the clay particles are in a parallel arrangement. Some researchers proposed alternative theories for clay swelling such as mixture theory (Hueckel (1992)) and regular solution theory (Graber and Mingelgrin (1994)). Nevertheless, the limitations of the *DDL* theory are mainly for very dense soils where development of the diffuse double layer is hindered.

3.3.2 Concept of osmotic pressure

One approach to estimate the swelling of a clay system (comprising unit layers, clay platelets and water) is by analysing the equilibrium condition between the external forces and internal forces $f_R - f_A$ acting on the system, as described in the previous section. Alternatively, the concept

of osmotic pressure can be used to estimate the swelling of clay. The concept of osmotic pressure can also be used as an aid to get insight into the physics of the swelling process.

The existence of a gradient in the concentration of dissolved ions between two regions of a liquid, and separation of the regions by a semi-permeable membrane are two essential pre-requisites for osmotic pressure difference to occur. A semi-permeable membrane permits flow of the solvent but not of the solute. The attractive force, between the negatively charged surface of a unit layer and the attached cations, prevents the diffusion of the cations away from the surface. This creates the effect of a semi-permeable membrane. Whenever diffuse double layers of two unit layers overlap, a dissolved ion concentration gradient occurs between the liquid within the diffuse double layer region and the bulk liquid. This concentration gradient causes the water to flow from the bulk water into the *DDL* region. As water flows into the *DDL* region, the pore water pressure in the *DDL* region increases with respect to the pore water pressure in the bulk water, resulting in a pore water pressure gradient tending to induce flow in the opposite direction to that caused by the concentration gradient. The inflow of water continues until a balance is reached between the two gradients. With the additional pore water pressure within the *DDL* region, equilibrium must be reached between the various forces acting on a unit layer. Bolt (1956) was the first to use the concept of osmotic pressure to calculate swelling of a clay system.

3.3.3 Saturated clay

Interaction of diffuse double layers of two unit layers for the fully saturated case is schematically shown in Figure 3.6, where σ is the external stress applied on the unit layers, u_{wd} and n are the pore water pressure and concentration of cations respectively at the mid-plane between the unit layers, u_w and n_0 are the pore water pressure and the cation concentration respectively in the bulk liquid and d_u is the distance between the unit layers. Under equilibrium conditions of cation concentration and pore water pressure gradients:

$$u_{wd} = u_w - p_{os} \tag{3.12}$$

where p_{os} is the component of pore water pressure at the mid-plane due to the concentration difference $n - n_0$.

Considering the equilibrium of forces acting on unit area of the upper unit layer in Figure 3.6 and the section of the *DDL* extending down to the mid-plane, the following expression is obtained:

$$\sigma = u_{wd} \tag{3.13}$$

In deriving Equation 3.13, it has been assumed that there is no net electrostatic force on the body. This is possible only because the body considered covers the region extending from the mid-plane of the unit layer to the mid-plane of the inter-unit layer region. Equation 3.13 can be rearranged and combined with Equation 3.12 to give:

$$\sigma - u_w = \sigma' - p_{os} \qquad (3.14)$$

Equation 3.14 can be used to illustrate the effects of increasing effective stress $\sigma - u_w$ on the volumetric response of a clay system. For example, if $\sigma - u_w$ is externally increased, according to Equation 3.14 the component of mid-plane pore water pressure due to the osmotic effect p_{os} should increase. For no change in the ionic concentration of the bulk liquid n_0, the increase in p_{os} is possible only if the ionic concentration n in the *DDL* is increased, which can be achieved by reduction in the distance d_u between the unit layers. This reduction in the separation of the unit layers results in the overall compression of the clay system. Conversely, if $\sigma - u_w$ is decreased the clay system will swell. Swelling or compression (increase or decrease of d_u respectively) thus occurs as a function of effective stress σ'. Several researchers, such as Bolt (1956), Olsen and Mesri (1970), van Olphen (1977), and Mitchell (1993), have reported this function of the form shown schematically in Figure 3.7.

3.3.4 Effect of pore fluid chemistry

Changes in the chemistry of the pore fluid can occur in many ways. Changes in ionic concentration of the pore fluid and valency of the ions in the pore fluid are, however, two important chemical changes that are known to affect significantly the volumetric response of a clay (see, for example, Olson and Mesri (1970), Morgenstern and Balasubramonian (1980), and Di Maio (1996)). These two changes can occur simultaneously, but for simplifying the discussion they are considered to occur separately.

The effect of changes in ionic concentration of the pore fluid can be illustrated by considering a clay system (comprising independent unit layers, clay platelets and water) in which forces acting on the system prior to the change in ionic concentration are in equilibrium. The external total stress applied to the system is kept constant and only the ionic concentration n_0 of the bulk pore fluid is increased. With the increase in n_0 and no instantaneous change in ionic concentration n in the *DDL*, there is initially a decrease in osmotic pressure difference p_{os}. This results in a flow of water out of the *DDL* region into the bulk water. The flow of water out of *DDL* means the distance d_u between the unit layers decreases and hence the clay system will compress. Likewise if the ionic concentration n_0 in the bulk water is reduced the clay system will swell.

The effect of changes in valence of the ions in the pore fluid can be illustrated with the help of Equation 3.7. According to Equation 3.7, the *DDL* thickness $1/K$ is inversely proportional to the valence of the cations. This means that if higher valence cations are available in the pore liquid for exchange reaction the *DDL* thickness will decrease and compression will occur. Conversely, if there are only lower valence cations in the pore liquid, the *DDL* thickness will increase, leading to swelling.

3.3.5 Effect of unsaturated condition

It is important to understand, at least qualitatively, how unsaturated conditions within a clay system will affect the behaviour at unit layer level. The water from the region between unit layers cannot be squeezed out completely unless an excessively high value of suction is applied (Equation 2.2 gives a value of suction of the order of 10^5 kPa by taking the half distance between the two unit layers of 10 $\mathring{A}$, and a value of 73 $\times 10^{-3}$ N/m for surface tension T), whereas in general geotechnical applications suction is unlikely to be more than a few thousand kPa. Under unsaturated conditions, the regions between unit layers within a platelet (intra-platelet spaces) therefore remain water-filled, whereas the larger inter-platelet and inter-packet spaces (which are usually referred to as voids) can be either water-filled or air-filled. Two unit layers bounded by air-filled voids are shown in Figure 3.8, together with the menisci forming the boundary between water in the intra-platelet space between the unit layers and the air in the surrounding voids. The unit layers, shown in Figure 3.8, are considered square in plan with length and width equal to L, and out of the total perimeter, of length $4L$, a length $4\omega L$ is bounded by water-filled voids (at pressure u_w) and length of $4(1-\omega)L$ is bounded by air-filled voids (at pressure u_a). The parameter ω therefore varies between zero (all surrounding voids dry) to 1 (all surrounding voids saturated). The equilibrium of forces gives:

$$\sigma L^2 = u_{wd} L^2 - 4(1-\omega) LT \tag{3.14}$$

where T is the surface tension at the air-water interface. Equation 3.14 can be re-arranged as:

$$\sigma = u_{wd} - \frac{4T(1-\omega)}{L} \tag{3.15}$$

Substituting for u_{wd} from Equation 3.12 into Equation 3.15 and re-arranging gives:

$$p_{os} = \sigma - u_w + \frac{4T(1-\omega)}{L} \tag{3.16}$$

Equation 3.16 can be re-written as:

$$p_{os} = \sigma - u_a + (u_a - u_w) + \frac{4T(1-\omega)}{L} \tag{3.17}$$

The effect of unsaturated conditions on a system of two unit layers can be explored by inspection of Equations 3.16 and 3.17. If wetting occurs at a constant value of $\sigma - u_a$, inspection of Equation 3.17 shows that p_{os} reduces for two reasons: firstly, the reduction of suction $u_a - u_w$ during wetting and, and secondly, the reduction in the surface tension term $4T(1-\omega)/L$, as ω rises as more of the surrounding voids become water-filled (this surface tension term falls to zero on reaching fully saturated condition, with $\omega = 1$). This reduction of p_{os} is produced by an inflow of water from the surrounding voids to the spaces between the unit layers (leading to reduction in the ionic concentration n in the *DDL* region), which causes an increase in the distance d_u between unit layers and hence swelling of the clay. The reduction in the term $4T(1-\omega)/L$ can be highly significant. A change from $\omega = 0$ (all surrounding voids dry) to $\omega = 1$ (all surrounding voids water-filled) would produce a reduction of 292 kPa in this term for platelets with $L = 1$ μm.

3.4 Conceptual Model of Fabric

The arrangement of clay platelets and larger packets of soil is termed fabric. This fabric has a strong influence on the mechanical behaviour of soils, as reported by a number of researchers, including Seed and Chan (1959), Barden and Sides (1970), and Anandarajah *et al* (1996). The effects of fabric on the behaviour of unsaturated speswhite kaolin were observed in recent research carried out at Oxford University (Sivakumar and Wheeler (in press)). Interactions at unit layer and platelet levels, a key feature in expansive clays containing active clay minerals, exert a profound influence on the development of a particular type of fabric. This suggests that the role of fabric is likely to be of even greater significance for these clays than for unsaturated non-expansive soils. A conceptual model for the fabric of unsaturated clays is therefore proposed here, prior to examining aspects of constitutive modelling.

Lambe (1958) proposed a conceptual model for the fabric of clays. With the advent of scanning electron microscopy *SEM* and mercury porosimetry techniques, significant information about the fabric of soils became available. *SEM* and porosimetry studies are now widely used for description of fabric of various different types of soils, see for example, Aylmore and Quirk (1959, 1960), Diamond (1970), Collins and McGown (1974). Most fabric studies pertain to saturated soils, but a few researchers, such as Pusch (1982), Delage and Lefebvre (1984), and Lapierre *et al* (1990) reported data for compacted fine-grained soils. These studies are soil specific. A trend, however, emerges. On the dry side of optimum moisture content, compacted fine-grained soils tend to develop a bimodal distribution of pore sizes. Such a distribution of pore sizes is confirmed by Atabek *et al* (1991) and Wan *et al* (1995) also. In contrast, on the wet

side of optimum, soils tend to have a massive fabric with a unimodal rather than bimodal, distribution of pore sizes. This information, along with the nature of the dual electrical charge on unit layers, is used to develop a conceptual model of fabric for unsaturated clays compacted dry of optimum.

The model is described at different scales with the help of sketches in Figure 3.9. Three levels of fabric can be identified, corresponding to three different sizes of fluid-filled spaces within the soil: intra-platelet spaces between individual unit layers; small voids (hereafter referred to as "microvoids") between individual clay platelets within a larger floc or packet of soil; and large voids (hereafter referred to as "macrovoids") between these larger flocs or packets. It is the last two categories of voids that form the bimodal pore size distribution identified in porosimetry studies. An important point to be noted about this model is that three levels of fabric are clearly identified and they all play a role in the swelling and shrinkage of expansive clays.

In active clay minerals, such as montmorillonite, separation of some unit layers occurs in the presence of water and individual unit layers can therefore exist alongside the platelets. The "microvoids" therefore exist between platelets or between platelets and independent unit layers. The clay platelets aggregate in a random structure leading to a three dimensional floc or packet of soil. Edge-to-face contact of clay platelets might be expected, on the basis of negatively charged surfaces and positively charged edges of a platelet, but micrographs reported by, for example, Smart and Tovey (1981), show hardly any edge-to-face contact between clay platelets and the contacts are actually rather random.

Equation 2.2 can be used to explore the feasibility of unsaturated conditions occurring within each of the three levels of the fabric. A platelet containing several unit layers can be treated as a saturated material because it requires an extremely high level of suction (of the order of 10^5 kPa) to squeeze out water from the intra-platelet spaces. Air can enter the "microvoids" (which are of the order of micron size) at about a suction of 100 kPa and hence the voids between the platelets can become unsaturated. The "macrovoids", which are much bigger than the "microvoids" can be unsaturated even at very low values of suction. This means that for the values of suction of practical interest the intra-platelet spaces will remain saturated, but both the microvoids and the macrovoids can become unsaturated.

Gens and Alonso (1992) lumped the intra-platelet spaces and the "microvoids" between platelets together as microfabric and therefore considered only two levels of fabric. They further assumed

that what they termed as the microfabric (comprising intra-platelet spaces and the "microvoids" between platelets) is fully saturated. As described above, it now however seems likely that, whereas intra-platelet spaces will remain saturated for suction values of practical interest, "microvoids" between platelets will often be unsaturated. This means that the microfabric, comprising both the inter-platelet spaces and the "microvoids" between platelets, cannot be assumed to be saturated.

For compacted soils, the fabric is strongly influenced by the energy used in the compaction process. The three levels of fabric discussed above occur for soils compacted on the dry side of optimum moisture content under stresses used in general geotechnical applications. It may however be that for very highly compacted soils, such as the soils proposed for radioactive waste disposal, the large macrovoids between flocs or clay packets disappear and only two levels of soil fabric can then be identified (intra-platelet spaces and "microvoids" between platelets). For such a soil the hypothesis of Gens and Alonso (1992), of a saturated microfabric and an unsaturated macrofabric, is perhaps appropriate (with the microfabric now representing only intra-platelet spaces and the macrofabric representing the voids between platelets).

3.5 Previous Experimental Data on Volume Change Behaviour

The volume change behaviour of unsaturated highly expansive clays has been studied by several authors. A brief review of such studies is given in this section, prior to moving on to constitutive modelling. Attempts to develop an elasto-plastic constitutive framework for unsaturated highly expansive soils have started only recently, but much of the existing experimental data is difficult to interpret in terms of constitutive models, because the tests were often carried out in an oedometer, in which the stress state is not fully known. Some useful patterns of the behaviour of these soils can nonetheless be identified from these studies.

3.5.1 Patterns of behaviour of unsaturated non-expansive and highly expansive soils

Firstly there are some common patterns of behaviour of unsaturated non-expansive and highly expansive clays, which are:

- Swelling strain is a function of factors such as applied stress, initial water content or suction, and initial dry density or void ratio. The amount of swelling strain decreases with the intensity of the applied stress and evidence for this has been reported by many authors including Kassif *et al* (1973), Escario and Saez (1973), and Brackley (1975). Results reported by Richards *et al* (1984); and Justo *et al* (1984) suggest that the total amount of swelling increases with the increase in initial value of the suction. Moreover, the relationship

between swelling strain and suction reduction is non-linear, with the rate of swelling increasing as suction is reduced.

- Whilst the swelling strain depends upon the factors mentioned above, the swelling pressure (the amount of external stress required to prevent change in volume of soil during wetting) is mainly controlled by the initial dry density or the void ratio of the soil. Support for this trend is provided by the data reported by Brackley (1973) and Chen (1973). Gens and Alonso (1992) suggest that the maximum swelling pressure increases slightly with an increase in the initial value of the suction.
- Finally, the fabric of the soil influences its behaviour. For example, a soil with open fabric subjected to high stress can exhibit collapse in the final stages of a wetting path. The results reported by Escario and Saez (1973) support this feature. Similarly, in a swell test, Brackley (1975) reported that swelling pressure reaches a maximum and then decreases as the wetting path approaches to a fully saturated state.

All of these features of the volume change behaviour of non-expansive and highly expansive unsaturated clays can be explained in terms of the elasto-plastic constitutive models for non-expansive unsaturated soils described in Section 2.10 (see, for example, Alonso *et al* (1987)).

Having considered the similarities between the behaviour of non-expansive and highly expansive unsaturated soils, it is important to highlight the reported differences in behaviour.

1. The first obvious difference is that the magnitudes of volumetric strains during wetting and drying paths are much greater in highly expansive clays than in non-expansive clays. This quantitative difference, though important, is not a serious problem in itself from the point of view of developing constitutive models, because it simply requires scaling up of the appropriate soil constants within the constitutive models.
2. The fundamental difference between unsaturated non-expansive and highly expansive clays is reported in the nature of wetting-induced swelling and drying-induced shrinkage. Whilst wetting-induced swelling and drying-induced shrinkage are reported to be largely reversible (elastic) for non-expansive clays, these volume changes are often reported to be irreversible (plastic) in highly expansive clays. Chu and Mou (1973) and Pousada (1984) presented results for cyclic wetting and drying tests, which showed irreversible swelling on wetting paths. Data from the work of Chu and Mou (1973) are shown in Figure 3.10. It is evident from these results that plastic volumetric swelling occurs in the first wetting, and the behaviour then remains approximately reversible during the subsequent wetting and drying paths. In contrast, results reported by Alonso *et al* (1995) showed irreversible shrinkage on drying paths. These results are shown in Figure 3.11. From the above studies, it is clear that

irreversible wetting-induced swelling and drying-induced shrinkage occur in highly expansive clays. It is however unclear whether both can occur in the same soil (in samples with different stress states or stress histories) or whether the contrasting behaviour reported by Chu and Mou (1973) and Alonso *et al* (1995) represents a distinction between different types of highly expansive unsaturated clays. In contrast, in constitutive models for non-expansive unsaturated clays presented in Section 2.10, wetting-induced swelling and drying-induced shrinkage are both treated as elastic processes, and only wetting-induced collapse is treated as a plastic (irreversible) process.

3.5.2 Limitations of the past experimental research

There are three main limitations of the past experimental research on highly expansive soils:

1. Most of the experimental work has been carried out using the oedometer apparatus, with no measurement of the lateral confining stress. This means that the stress state of the soil sample is not fully known. Consequently, it is difficult to interpret these data within the framework of any constitutive model. Probably, the main reason that there are few data corresponding to isotropic or triaxial conditions is the requirement of very long test times, because the drainage path length for samples used in isotropic or triaxial tests is generally much greater than the drainage path length for oedometer samples.
2. Another drawback with the data reported in the literature is that the tests are seldom conducted under controlled suction. Often the tests have been carried out simply by inundating the sample, without controlling or measuring the suction. This means that the volumetric behaviour cannot be deduced as a continuous function of suction on wetting and drying paths. Interestingly, even for non-expansive unsaturated soils, there are hardly any data for wetting/drying cycles under controlled suction conditions.
3. Often only the overall volume change is measured, without corresponding measurements of the water inflow to the sample. This leads to major gaps in the available data, because parameters such as the degree of saturation S_r are not known on a stress path.

Finally, it is important to note that there are some concepts reported in the literature for highly expansive soils which should be treated with caution. For example, attempts have been made to define empirical terms such as swell potential and swell pressure, which have resulted in confusion rather than contributing to the development of constitutive models, because such parameters, instead of being unique to a soil, are functions of stress and suction history of a soil.

3.6 Constitutive Modelling

The elasto-plastic models for non-expansive unsaturated soils, described in Section 2.10, are not constructed to account for the irreversible component of wetting-induced swelling and drying-induced shrinkage observed for highly expansive soils. These models treat volume changes that occur in wetting and drying paths inside the *LC* yield curve as elastic (reversible) processes.

3.6.1 Approach to modelling

A step-wise approach was suggested by Gens and Alonso (1992) in developing constitutive models for unsaturated expansive clays. The proposed steps were as follows:

1. A model for unsaturated non-expansive soils should first be developed. Currently available elasto-plastic models for these soils were reviewed in Sections 2.10.1 and 2.10.2, with some of the limitations and shortcomings of these models when applied to non-expansive soils discussed in Section 2.10.3.
2. The particular features of behaviour of highly expansive soils that are not taken into account in the models discussed in Section 2.10, should be identified. These features are outlined briefly in Section 3.5.
3. An understanding of the behaviour of clay minerals (that are mainly responsible for the high degree of swelling) should be achieved. Significant work is reported by various authors for saturated highly expansive clays and the main features of this work have been examined in Section 3.3.
4. The final step is integration of the first three features in a consistent manner. Gens and Alonso (1992) suggested a method for this, which is examined in the following section.

3.6.2 Proposed framework of Gens and Alonso (1992)

Recognising the vital role played by physico-chemical interactions occurring at micro-level in expansive clays, Gens and Alonso (1992) modified the original elasto-plastic model that was proposed for unsaturated soils by Alonso *et al* (1990). The modified model is based on the postulation of two levels of soil fabric: a saturated microfabric consisting of intra-platelet spaces and microvoids between platelets, and an unsaturated macrofabric, consisting of the macrovoids between floes or clay packets. The physico-chemical interactions influenced by the active clay minerals occur within the microfabric.

On the basis of two levels of soil fabric, extension of the existing unsaturated elasto-plastic models to highly expansive soils by Gens and Alonso (1992) involved three key elements. These elements were: description of the soil behaviour at the macrofabric level; defining the behaviour of the microfabric; and defining the coupling mechanism between the micro and macrofabrics.

Gens and Alonso (1992) considered the macrofabric as unsaturated and suggested that the existing elasto-plastic model of Alonso *et al* (1990), described in Section 2.10.1, could adequately represent its behaviour.

Gens and Alonso (1992) argued that the microfabric will remain saturated, and therefore, the conventional effective stress principle of saturated soil will remain valid for the microfabric. As noted in Section 3.4, this assumption now appears somewhat inappropriate, because, although the intra-platelet spaces are likely to remain saturated, the microvoids between platelets may well be unsaturated. This means that the assumption adopted by Gens and Alonso (1992) would, strictly, be valid only if the microfabric were restricted to the intra-platelet spaces.

Gens and Alonso (1992) assumed that volume changes at the microfabric level remain reversible and are not affected by strains of the macrofabric. They suggested that volume changes at the microfabric level are a function of the local value of mean effective stress (mean total stress minus pore water pressure) within this material that they assume to be saturated. On the assumption that the local value of mean total stress within a saturated clay packet is identical to the externally applied mean total stress p (applied at a continuum level), the volume change within the microfabric is therefore a function of p - u_w. This can be expressed in terms of the stress variable p'' (mean net stress) and s (matrix suction) used within the elasto-plastic models described in Section 2.10:

$$p - u_w = p - u_a + (u_a - u_w) = p'' + s \tag{3.18}$$

This means that if $p'' + s$ is held constant there should be no volume change of the saturated microfabric. In the $s : p''$ plane this corresponds to a straight line inclined at 45^0, as shown in Figure 3.12. Gens and Alonso (1992) refer to this as a neutral line. Compression and swelling of the material within the microfabric correspond to increasing and decreasing respectively the value of $p''+s$, as shown in Figure 3.12. They, therefore, suggested that the saturated microfabric should obey the conventional effective stress law for saturated soil and that the volumetric strains of the microfabric should depend upon the sum of mean net stress and suction. Using this concept, Alonso *et al* (1994) proposed that the total elastic variation of specific volume v could be calculated as:

$$dv^e = -\frac{\kappa dp''}{p''} - \frac{\kappa_s ds}{s + p_{at}} - f(p'' + s)d(p'' + s) \tag{3.19}$$

In Equation 3.19 the first two terms represent volume changes occurring at macrofabric level (given by the existing models described in Section 2.10) and the last term, $f(p'' + s)d(p'' + s)$,

represents change in specific volume of the microfabric due to changes in the value of $p'' + s$. Alonso *et al* (1994) suggested an exponential relationship between the microfabric volumetric strain and the stress $p'' + s$ for the form of this final term in Equation 3.19.

The coupling mechanism between the micro- and macro-levels of soil fabric proposed by Gens and Alonso (1992) is such that the micro level volume changes can cause volume changes in the macrofabric, but not vice versa. They argued that swelling of the microfabric (individual clay packets) beyond a certain limiting value will tend to prise open the unsaturated macrofabric. To represent this effect they proposed a Suction Decrease *SD* yield curve inclined at 45^0 in the $s : p''$ plane (see Figure 3.13). The significance of the *SD* yield curve lies in the fact that when the *SD* yield curve is pushed downwards during a reduction of $p'' + s$, a coupled inward movement of the loading collapse *LC* curve occurs, representing irreversible (plastic) swelling of the macrofabric. The *SD* curve is therefore not a standard yield curve, in that the hardening relationship is not linked directly to the movement of the *SD* curve itself but to the coupled movement of the *LC* curve.

Gens and Alonso (1992) proposed a coupling relationship between the plastic swelling of the macrofabric $d\varepsilon_{vM}^{p}$ produced by a given elastic swelling of the microfabric $d\varepsilon_{vm}^{e}$ as a function of the stress ratio p''/p_0''. This is schematically shown in Figure 3.14. Inspection of Figure 3.14 shows that the ratio of $d\varepsilon_{vM}^{p}/d\varepsilon_{vm}^{e}$ decreases as the fabric of the soil becomes more open, which is represented by an increasing value of p''/p_0''. Experimental data presented by Alonso *et al* (1994) suggests that the coupling ratio $d\varepsilon_{vM}^{p}/d\varepsilon_{vm}^{e}$ can become negative at high value of p''/p_0''. This means elastic swelling of the microfabric can produce strain-hardening expansion of the *LC* yield curve, by compression of the macrovoids between packets, which is feasible for a very open fabric in which the swelling of microfabric can fill up part of the large inter-packet voids.

Alonso *et al* (1994) proposed a counterpart of the *SD* yield curve, which is reached when a limiting value of microfabric shrinkage occurs on increasing of $p'' + s$. This was named the Suction Increase *SI* yield curve, as shown in Figure 3.13, inclined at 45^0 in the $s : p''$ plane. It should be noted that Alonso *et al* (1987) and Alonso *et al* (1990) proposed a horizontal *SI* yield curve, which is now replaced by the inclined *SI* curve shown in Figure 3.13. The model proposed by Alonso *et al* (1994) has the potential to represent the continuing plastic strains observed in wetting and drying cycles in expansive soils, (see, for example, Figure 3.11), with a

suitable choice of coupling between the *SI* and *SD* yield curves. For example, if the movement of *SD* and *SI* yield curves is cross-coupled, so that pushing the *SD* curve downwards by decreasing $p'' + s$ also drags down the *SI* curve (see Figure 3.13), then continuing plastic strains during wetting and drying cycles can be predicted.

An important shortcoming of the models proposed by Gens and Alonso (1992) and Alonso *et al* (1994) is that these are constructed assuming a saturated microfabric, which comprises intra-platelet spaces and microvoids between platelets. It has been shown in Section 3.4 that the microvoids between the platelets can become unsaturated, and, therefore, to assume that these pores are saturated may not be appropriate. This leads to a fundamental shortcoming of the proposed model, which is based on the hypothesis that the behaviour of the microfabric can be represented by the conventional effective stress law for saturated soil, and hence $p'' + s$ is the only stress variable of relevance to volume changes of the microfabric. This hypothesis can be accepted only for very dense clay in which the macrovoids between clay packets have been completely removed by high compaction stresses and the microfabric of the soil then comprises only the intra-platelet spaces. Another limitation of the proposed model is that it is still highly tentative and qualitative in nature requiring validation and refinement in order to be of practical use. In particular, it could prove very difficult, in practice, to measure the appropriate parameters coupling microfabric and macrofabric strains.

3.7 Objectives of Research Project

The elasto-plastic models for highly expansive soils proposed by Gens and Alonso (1992) and Alonso *et al* (1994) are very tentative, as there are few experimental data with which to validate the models. Moreover, there are a number of features that need detailed examination. There is little direct evidence for the existence of the *SD* and *SI* yield curves and also whether these are inclined at 45^0 in the $s : p''$ plane. The proposed form of coupling between the *SD* and *SI* yield curves and the *LC* yield curve is also not yet supported by direct experimental evidence. To examine these aspects of behaviour, objectives for this research were:

1. To confirm the occurrence of irreversible swelling on wetting and/or irreversible shrinkage on drying.
2. To examine whether this irreversibility is best modelled by *SD* and *SI* curves. If so, what are the shapes of these curves in the $s : p''$ plane.
3. To check whether the irreversibility occurs only during the first cycle of wetting and drying or also during subsequent cycles, as irreversibility in subsequent cycles would require

movement of the *SD* yield curve even when not in contact with it and similarly for the *SI* curve.

4. To explore the influence of soil fabric on the irreversibility in volumetric behaviour. Also to examine whether the irreversibility is unique to unsaturated highly expansive clays or also occurs in unsaturated non-expansive clays.
5. To check for any evidence of coupled movement of the *LC* yield curve with the movement of the *SD* and *SI* curves.
6. One aspect of 5 was to find out if there is a unique normal compression line for each value of suction or the location of the normal compression line for each value of suction is dependent on wetting and drying history.
7. To explore whether the soil behaviour could be modelled more easily within an alternative framework, perhaps involving alternative stress parameters instead of p'' and s (with corresponding changes in strain parameters).
8. If time permitted, to extend this work to triaxial stress conditions, to examine the role of q. Unfortunately constraints of time (with each test taking about 8 weeks) meant that it was not possible to tackle this objective, and the experimental work was therefore subsequently restricted to isotropic stress conditions.

To achieve objectives 1 to 3, wetting and drying cycles under isotropic stress conditions were planned, with typical stress paths shown in Figure 3.15. Wetting and drying paths were expected to provide suitable evidence for or against the occurrence of irreversible volumetric changes, and by carrying out the tests at different values of mean net stress p'', exploration of the shape of the *SD* and *SI* curves was planned. To examine the coupling relationship between the *SD* and *SI* yield curves and the *LC* curve, pairs of tests of the form shown in Figure 3.16 were envisaged. In the first test (see Figure 3.16 (*a*)) a constant suction loading path (increase of p'') would be used to identify a point on the *LC* yield curve. In the second test, on an identical sample, the loading path would be preceded by a wetting/drying cycle, to see whether this had any influence on the position of the *LC* yield curve (as predicted in the constitutive model proposals of Gens and Alonso (1992) and Alonso *et al* (1994)).

CHAPTER 4

EXPERIMENTAL APPARATUS AND CALIBRATION TECHNIQUES

To achieve the objectives set out in Section 3.7, selection of a suitable testing strategy was of critical importance. Obviously this had implications for the choice of experimental equipment. This chapter starts with a review of methods and techniques required for laboratory testing of unsaturated soils. The presentation concentrates on triaxial testing rather than other types of tests, such as shear box and oedometer, although some of the information is also relevant to other test types. Subsequently, salient features of the equipment used are presented, together with details of the calibration exercises that were carried out.

4.1 Methods of Applying Suction

In unsaturated soils the pore water pressure u_w in the field is generally negative relative to atmospheric pressure. Reproduction of these conditions in the laboratory is likely to result in the formation of air bubbles in the pore water pressure control or measurement system, due to exsolution of dissolved air. As the absolute value of pore water pressure falls towards zero, the capacity of the water to hold dissolved air also falls to zero. The dynamic process of bubble nucleation and rapid growth is referred to as cavitation. Marinho and Chandler (1995) discussed the physics of cavitation within soils and its influence on suction-measuring systems.

The measurement of negative pore water pressure is very difficult, due to the potential problem of cavitation, and this in turn leads to uncertainty in the value of suction. To avoid this problem special techniques of controlling or measuring suction are used in laboratory testing of unsaturated soils. An ideal method of applying suction should be such that:

- Values of suction appropriate to the soil being tested can be achieved (this typically implies suction less than 100 kPa for coarse grained soils, but substantially higher suctions for fine-grained soils).
- Controlled variation of suction is feasible.
- Measurement of suction is easy and reliable.
- Field conditions can be simulated in the testing.
- No extra unknown variables are introduced by the method itself.

In attempting to achieve the above requirements, three different methods of applying suction have been used for testing of unsaturated soils: axis translation, osmotic technique, and humidity control using salt solutions. The salient features of these techniques are briefly discussed below.

4.1.1 Axis translation technique

The basic principle of the axis translation technique is to elevate the total stress, the pore air pressure and the pore water pressure by equal amounts so that the pore water pressure is raised to a positive value (relative to atmospheric pressure) and it can then be controlled or measured. The matrix suction $u_a - u_w$ remains the same as long as the pore air pressure u_a and pore water pressures u_w are increased by equal amounts. Likewise the net stress $\sigma - u_a$ remains unchanged provided the total stress σ and the pore air pressure u_a are increased by equal amounts.

The axis translation technique is by far the most common method used in geotechnical engineering for applying controlled values of suction to a soil sample. This technique was first developed by Hilf (1956). Subsequently several researchers, including Matyas and Radhakrishna (1968), Escario and Saez (1986), and Wheeler and Sivakumar (1995) have reported successful use of the axis translation technique. Both pore water pressure and pore air pressure are controlled and measured independently in the axis translation technique. This in turn enables controlled variation of suction. Moreover, the measurement of suction does not require any special transducer to be used. Since no chemical is used in the process of applying suction, there is no risk of change in chemistry of the pore fluid.

One disadvantage of the axis translation technique is that by elevating the pore water pressure from a negative to a positive value, the possibility of cavitation is prevented not only in the measuring system but also within the soil pores. This implies that any influence of cavitation of the pore water, which may be an important phenomenon under in-situ stress conditions, is not accounted for in the laboratory tests using the axis translation technique. Cavitation cannot, however, occur even in the field if the pore air exists in continuous form rather than in the form of occluded air bubbles (see, for example, Bocking and Fredlund (1980)). Even with occluded air, cavitation is unlikely to occur if there is significant presence of air bubbles in the soil. This is due to the fact that it is much easier for dissolved air to come out of solution into existing bubbles than to nucleate new bubbles, because a new bubble nucleus is very small and therefore at a much higher pressure than existing larger bubbles. This means that the cavitation phenomenon is likely to be of importance only when a soil is de-saturating from a saturated state or a nearly saturated state.

Another limitation of the axis translation technique pertains to the maximum value of suction that can be applied, because of practical limitations on the value of total stress. The suction is applied by increasing pore air pressure with respect to pore water pressure (which is greater than or equal to atmospheric pressure) and the cell pressure σ_3 is elevated with respect to pore air pressure to apply a net stress. This means in the axis translation technique, with the pore water at a positive pressure, the cell pressure is always greater than the sum of suction $u_a - u_w$ and net stress $\sigma_3 - u_a$. The maximum value of suction that can be achieved in the axis translation apparatus therefore depends upon the highest value of cell pressure that can be applied and the value of mean net stress for a test. For example, with the equipment used by Sivakumar (1993) a maximum cell pressure of 600 kPa could be applied, and pore water pressure needed to be maintained at a value of at least 50 kPa, for proper functioning of the stepper motor-controlled regulators, and therefore the maximum suction was typically about 400 kPa (with a mean net stress of 150 kPa). Obviously higher values of suction would require a suitable high pressure cell.

4.1.2 Osmotic technique

The osmotic technique of applying suction involves use of an aqueous solution (such as Polyethyelne Glycol (*PEG*)) separated from the soil sample by a semi-permeable membrane. The semi-permeable membrane is permeable to small molecules (such as water) but not to larger molecules (such as *PEG*). The concentration of dissolved ions in the prepared solution is different from the concentration in the soil water. This leads to a concentration gradient across the membrane. The concentration gradient causes water to flow from the lower concentration side to the higher concentration side, but this in turn gives rise to lower hydrostatic pressure in the soil water. The flow of water continues until equilibrium is established between the concentration imbalance and the imbalance of pressure head, and therefore, matrix suction equal to the difference of the osmotic suction of the chemical solution and the soil water is applied to the soil sample.

The most commonly used chemical for preparation of the chemical solution is Polyethylene Glycol (*PEG*), primarily because of its large molecular size. The desired value of suction can be applied by using different concentrations of *PEG*. For two molecular weights of *PEG*, i.e. 6000 and 20000, William and Shaykewich (1969) presented relationships between suction and *PEG* concentration. These relationships can be used for initial estimation of suction corresponding to

various concentrations of *PEG*, but independent calibration is needed, as test conditions might vary from the conditions for which William and Shaykewich (1969) presented the relationships.

The osmotic technique was first developed by biologists (see Lagerwerff *et al* (1961)) and it was subsequently used by soil scientists such as Zur (1966). Kassiff and Ben Shalom (1971) were the first researchers to use the technique in geotechnical engineering. Subsequently, it has been used by Komornik *et al* (1980), the research group led by Delage in Paris (Delage *et al* (1987) and Cui and Delage (1996)), and Dineen and Burland (1995).

Cui and Delage (1996) used the osmotic technique in triaxial testing of silt samples. They applied suction at the top and bottom of the sample by circulating *PEG* solution in a closed loop. The exchange of water from the sample was into the *PEG* solution via semi-permeable membranes and the change in the volume of water within the sample was measured by monitoring the volume of the *PEG* solution. Temperature fluctuations could change the volume of the *PEG* solution and hence Cui and Delage (1996) kept the *PEG* reservoir within a water bath to hold the temperature constant within an accuracy of $\pm 0.1^{0}$C.

Dineen and Burland (1995) have reported improvements in the osmotic technique of applying suction. To measure water volume change of the sample, they measured the mass of water exchanged between the soil sample and the *PEG* solution rather than directly measuring the volume of exchanged water. This was achieved by placing the *PEG* reservoir on an electronic balance, which was logged by a computer for continuous measurements. By monitoring mass rather than volume, they did not have to control the temperature of the measuring system, as mass remains unaffected by the variations in temperature. Another important improvement achieved by Dineen and Burland (1995) was in the drainage arrangement beneath the soil sample. They used a nylon mesh beneath the semi-permeable membrane for circulation of *PEG* solution underneath the sample.

The main advantage cited in favour of the osmotic technique is that the possibility of cavitation within the soil pores is not excluded because the pore water pressure within the soil is maintained at its negative value. A second advantage is that high values of suction can be applied without the use of very high cell pressures.

There are still limitations in the osmotic technique when used in experimental work aimed at developing elasto-plastic models, in which controlled variation of suction is needed. The

technique in its current form cannot be used for varying suction in a continuous manner, because in the existing technology, suction changes are applied in steps by exchanging containers of *PEG* solutions with different concentrations. This means that features such as yield points would be harder to identify than with a continuous variation of suction, as can be employed with the axis translation technique.

Another concern about the osmotic technique is possible migration of soil salts dissolved in the soil water from the soil sample to the *PEG* solution and the impact of this change in soil water chemistry on the soil properties. Moreover, smaller molecules of *PEG* can also pass through the semi-permeable membrane. These problems have been reported by Delage *et al* (in press) and Dineen and Burland (1995). The behaviour of highly expansive clays is likely to be influenced more by these inadvertent chemical changes than other soils. Here, it would be worth mentioning that the osmotic technique of applying suction is still not in common use in geotechnical engineering and it seems that more experience is desirable in its use.

4.1.3 Humidity control with salt solutions

The humidity control method of applying suction is based on Kelvin's Law, which gives suction $u_a - u_w$ as a function of the relative humidity R_H of the air in contact with the pore water:

$$u_a - u_w = \frac{RT}{Mg}\ln(R_H) \qquad (4.1)$$

Where R is the universal gas constant; T is absolute temperature; M is the molecular mass of water; and g is the acceleration due to gravity.

The suction can be controlled by controlling the relative humidity R_H, which in turn can be achieved by having a sealed volume of air in contact with a saturated salt solution. Different salt solutions can be used for this purpose. A list of appropriate salt solutions with corresponding relative humidity and the suction values is given in Table 4.1. An important point to be noted from this table is that with this method very high values of suction can be applied.

The humidity control method of applying suction was first developed by soil scientists, and recently its use in geotechnical testing has been reported by Al Mukhtar *et al* (1993).

The relative humidity method has all the advantages that are described above in Section 4.1.2 for the osmotic method with an additional advantage that this method can be used to apply very high values of suction (in excess of 1000 MPa). The main limitations of the method are: that only

fixed values of suction can be applied and variation of suction is even more inflexible than the osmotic technique; and equilibration of suction within the soil is often very slow, because water transfer is by diffusion of water vapour through the soil pores.

4.1.4 Selection of method of applying suction

For this research programme the ability to identify yield points with a reasonable degree of confidence during wetting/drying paths and loading paths was an essential requirement. Wetting and drying paths involve variation of suction. With the axis translation technique an almost continuous variation of suction (with a precision of 1kPa) can readily be achieved, whereas with the osmotic or humidity control techniques control over variation of suction to such a level of precision is difficult. The step changes of suction in the osmotic technique are generally much larger than 1 kPa as precise control of *PEG* solution concentration is not easy to achieve. With the humidity control technique, only fixed values of suction corresponding to different salts are possible. The implication of this is that in loading at a constant value of suction identification of yield point should be equally possible with any of the three methods of suction control, but in wetting and drying paths the axis translation technique would have significant advantages. The axis translation technique was therefore selected as the method of suction for this research programme. Another reason, which weighed in favour of the axis translation technique was the nature of soil that was tested in this research. The volumetric behaviour of saturated highly expansive clays is well known to be affected by the changes in pore fluid chemistry (see, for example, Bolt (1956)). With the use of the osmotic technique there was a risk of unintentional changes in the pore fluid chemistry, which in turn could have influenced the response of the unsaturated expansive clay.

4.2 Measurement of Volume Change

The volume of an unsaturated soil sample can change due to compression or expansion of the air phase as well as drainage of water. This means, for example, an undrained (constant water content) triaxial test on an unsaturated soil is no longer a constant volume test. There are two main implications of this:

- Unlike saturated soils, the volume change of an unsaturated soil sample in the triaxial apparatus cannot be measured simply by recording the inflow or outflow of water from the sample.
- To know the volumes of all the three phases in an unsaturated soil, separate measurements of overall volume change of the sample as well as the changes in volume of water in the sample are required, assuming that the volume of the soil solids remains unchanged.

Whilst the measurement of the overall volume change of a soil sample is used to calculate the variation of specific volume v of the sample, combination of the measurement of the sample volume change with measurement of the inflow of water to the sample can be used to calculate the variation of degree of saturation S_r. The details of the step-wise procedure followed in calculating these parameters for this research are given in Section 5.7.

4.2.1 Sample volume change measurement

The changes in the volume of an unsaturated soil sample in a triaxial test can be measured in two ways:

1. By measuring the effect of sample volume change on the surrounding cell fluid. This method gives the change in volume of the whole sample.
2. By measuring local values of axial and radial strain, sample volume change can be calculated. This method gives the volume change of a central portion of the sample, rather than of the whole sample.

Bishop and Donald (1961) developed a special triaxial cell for measuring overall volume change of an unsaturated soil sample (see Figure 4.1), based on method 1 above. This cell consisted of two jackets made out of acrylic. The inner jacket was partially filled with mercury, to a level above the top of the sample. The outer cell and the upper part of the inner jacket were filled with water, and at the top of the cell there was direct connection between the inner and outer cells. The sample volume change was measured by monitoring the movement of the mercury surface using a cathetometer. The outer cell was needed to apply equal pressure on the inner and outer surfaces of the inner jacket so that the inner cell volume did not change with variations in cell pressure.

Wheeler (1986) developed a new double-walled triaxial cell, which was similar in principle to the cell developed by Bishop and Donald (1961), but Wheeler achieved significant improvements. A view of Wheeler's triaxial cell is shown in Figure 4.2. The triaxial cell consisted of inner and outer acrylic cells so that equal pressures could be applied on the inner and outer surfaces of the inner cell. Instead of mercury, water was used as the cell fluid and the inner cell was sealed from the outer cell in such way that the inflow of water to the inner cell could be used for measuring the changes in sample volume. This facilitated the automatic logging of sample volume changes. Wheeler's design therefore:

- Avoided the use of mercury as the cell fluid and hence the safety and working were improved.

- Facilitated automatic logging of sample volume change, which was a major step forward as using a cathetrometer was not only cumbersome, but it was very sensitive to disturbance and was not suitable for long duration tests.

As indicated above, the volume change of unsaturated samples could also be measured by monitoring axial and radial strains of the sample (see, for example, Zakaria (1994) and Maâtouk *et al* (1995)). Axial and radial strains can be measured locally on the sample by using inclinometer gauges (Jardine *et al* (1984)), strain gauges (Sharma (1984)), LVDTs (Costa Filho (1985)), Hall effect transducers (Clayton and Khatrush (1986)), proximity transducers (Hird and Yung (1989)) or local deformation transducers based on strain-gauged flexible metal strips (Goto *et al* (1991)).

For measuring sample volume change, the double-walled cell technique was selected in this project. The reasons for choosing double-walled cells over internal axial and radial strain measurement technique were:

1. Internal measurements of axial and radial strains provide measurement of the volume change of a central portion of the sample, whereas volume changes for the whole sample were needed if these measurements were to be combined with water inflow to the sample, in order to calculate the variation of degree of saturation. The double-walled cell technique gave the volume change of the whole sample and therefore was better-suited to calculation of the variation of degree of saturation.
2. Techniques for internal axial and radial strain measurement are not well-suited to the measurement of large strains, because they have been specifically developed for measurement of strains less than 1%. Many of the devices have a measurement range of only a few percent strain, and even those devices with larger range become increasingly unreliable at large strains, because of non-uniformity of sample straining. Large volumetric strains (up to 20%) were anticipated in testing of the highly expansive soils, and the internal strain measurement techniques were therefore considered inappropriate for this project.
3. The double-walled triaxial cells were already available and in the previous research of Wheeler (1986), Sham (1989), and Sivakumar (1993) had been shown to work satisfactorily.

4.2.2 Water volume change measurement

The change of volume of water within the sample can be measured by recording the inflow or outflow of water from the sample. The measurement is straightforward, but to avoid entry of air

into the water drainage line special filter arrangements are required. Details of these filters and the techniques involved in using the filters are discussed in Section 4.3.5.

4.3 Experimental Apparatus

The experimental apparatus was inherited from Sivakumar (1993). The main changes that were made for this research were: arrangements for filling the inner and outer cells with water (see Section 4.3.2); water drainage from both top and bottom of the sample (see Section 4.4); and modifications to the control and logging software (see Sections 4.3.8 and 5.6)

4.3.1 General layout

The general layout of the experimental apparatus used in this research is shown in Figure 4.3. An important feature of the apparatus was the double-walled isotropic cell which, along with one volume change unit, was used for sample volume change measurement. A second volume change unit was used for measuring the inflow or outflow of water to the sample.

The pore air pressure u_a, pore water pressure u_w, and cell pressure σ_3 were measured by three pressure transducers and all three pressures were controlled through independent stepper motors by a computerised control and logging system.

Three independent sets of triaxial apparatus, referred to as Systems *A*, *B* and *C* for identification purposes, were inherited from Sivakumar (1993). General views of Systems *A* and *B* are shown in Figures 4.4 and 4.5 respectively and the two systems were broadly similar to each other, though they differed in some points of detail. System *C* (see Figure 4.6) was significantly different, in that it was an adaptation of a Bishop and Wesley hydraulic triaxial cell (rather than the conventional triaxial cells of Systems *A* and *B*).

The maximum suction that could be achieved in these sets of apparatus (which were based on the axis translation technique) was about 400 kPa. This limitation was due to the arrangement of cell pressure with respect to pore air and water pressures in the axis translation technique. The suction is applied by increasing pore air pressure with respect to pore water pressure (which is greater than or equal to atmospheric pressure) and the cell pressure is elevated with respect to pore air pressure to apply a net stress. This means that in the axis translation technique the cell pressure σ_3 is always greater than the sum of the required values of net stress $\sigma_3 - u_a$ and suction $u_a - u_w$. Since the maximum value of cell pressure that could be applied was 550 kPa (due to the operating range of the compressor providing the pressure source), and pore water

pressure needed to be maintained at a value of at least 50 kPa for proper functioning of the stepper motor-controlled regulators, the maximum suction that could be achieved was typically about 400 kPa (assuming a net stress $\sigma_3 - u_a$ of at least 100 kPa).

4.3.2 Double-walled cells

The double-walled cells were acrylic cylinders with fibreglass reinforcing bands in Systems *A* and *B*. In System *C* the reinforcing bands were not used, but the wall thickness of the acrylic cylinders was 15 mm instead of 5 mm as used in the other two systems. The main purpose of having double-walled construction was to prevent or reduce the volume change of the inner cell by applying equal pressures on the inner and outer surfaces of the inner cell. It should be noted that, without an outer cell, calibration for cell volume change due to differential pressure across the inner and outer surfaces of the inner cell would have been complex and difficult due to creep and hysteresis of the acrylic. The cell pressure was applied through the volume change device to the inner cell, whereas the pressure to the outer cell was applied via a simple air-water interface (see Figure 4.3). Wheeler (1986) noted that there could be slight time lag in applying cell pressure in the outer and inner cells and this could result in error in volume change measurement without using reinforcement bands or thick-walled cells.

An alternative to using acrylic cells would have been a metal cell. The metal cell would have had some potential advantages. Firstly, a metal cell, such as stainless steel, would have been much stiffer than acrylic and would be expected to be elastic within the operating range of pressures, thus avoiding the difficulties of creep and hysteresis present with acrylic and so avoiding the need for double-walled construction. Secondly, a metal cell would not have suffered from the problem of water absorption that occurred with an acrylic cell (see Section 4.5.4 below). The metal cell would, however, not have been transparent. Consequently, it would not have been possible to see any entrapped air. This would have meant less confidence in the results. For this reason, it was decided to use the acrylic doubled-walled cells that were already available.

In using the double-walled cell system for sample volume change measurement, it was essential to prevent any entrapment of air within the inner cell during filling with water. Wheeler (1986) and Sivakumar (1993) achieved this by placing the top plate on the inner cell while the whole apparatus was within a large tank of de-aired water. This method was, however, very time-consuming and it was therefore decided to re-design the top plate of the cell, so that the inner cell could be filled with water from the bottom, with air vented through a hole in the top plate. The re-designed top plate was fabricated in a very simple form, suitable only for isotropic testing

of the soil. Similar arrangement of air vent holes can be used for shearing tests also, if the rolling diaphragm seal used by Wheeler (1986) and Sivakumar (1993) around the axial loading ram (which tended to trap air when the cell was filled with water from below) is replaced with a simple o-ring seal.

4.3.3 Transducers

For each set of apparatus, two volume change measurement transducers and three pressure transducers were used. A brief summary of the salient features of these transducers is given in the following sections.

4.3.3.1 Volume change measurement devices

Each set of apparatus included two volume change devices: one for measuring the flow of water into or out of the inner cell (and hence the change of sample volume), the other for measuring the flow of water into or out of the soil sample. Two different types of volume change devices were used: burette type devices in System *A* and Imperial College type devices in Systems *B* and *C*.

Each of the two devices in System *A* consisted of a burette with a differential pressure transducer, as shown in Figure 4.7. The device, which was developed by Sivakumar (1993), operates on the principle that the movement of the water column in the inner tube of the burette is detected by the attached differential pressure transducer (Pradhan *et al* (1986) and Araruna *et al* (1995)).

The burette had a double-walled construction with two tubes so that:

1. The outer tube could be filled partially with water to provide a reference pressure for the differential pressure transducer.
2. There was no differential pressure across the walls of the inner tube of the burette.

The high-pressure terminal of the differential pressure transducer was connected to the bottom end of the inner tube of the burette, whilst the low-pressure terminal was connected to the base of the outer tube. To avoid rapid evaporation of water and to minimise the diffusion of air into water, thin layers of paraffin oil were floated on the surface of water in the inner and outer tubes. A differential pressure of 2 kPa was the maximum capacity of these transducers, although the line pressure on the transducers could go up to 2000 kPa. The differential pressure of 2 kPa corresponded to a column of water 20 cm high in the inner tube. The cross-sectional area of the inner tube was 1.75 cm^2, and therefore, with the differential pressure transducers a volume

change up to about 35 cm^3 could be measured. The tendency of the water to stick to the burette wall and the influence of changes in the shape of meniscus required special care in its use (see Sivakumar (1993)). The problem of water sticking to the burette wall was minimised by keeping the burette walls clean of any dirt or grease.

Initially when System *A* was developed, Sivakumar (1993) was not confident about the performance of Imperial College type volume change measurement devices in testing of unsaturated soils (because of worries regarding entrapment of air inside the devices). He therefore used the burette type devices for System *A*, but he subsequently found that there were no problems in using the Imperial College devices. Moreover, the Imperial College volume change measurement devices are commercially available and are cheaper than the burette type devices. The Imperial College volume change measurement devices were therefore used by Sivakumar for Systems *B* and *C*. A general view of the Imperial College volume change measurement device is shown in Figure 4.8. It consists of a cylinder, piston, rolling diaphragms, and a displacement transducer. Any flow of water into or out of the cylinder causes movement of the piston, which is detected by the attached displacement transducer. All the Imperial College volume change measurement devices were of 50 cm^3 capacity except the one used for sample volume change measurement in System *C*, which was of 100 cm^3 capacity. The larger capacity for sample volume change measurement in System *C* was not essential for the isotropic loading tests performed in this research. This would have, however, been required if shear testing had been performed, because of the larger volume of water displaced from the cell by movement of the large diameter hydraulic ram providing the axial loading. Imperial College volume change measurement devices have been used successfully by many researchers, including Sivakumar (1993). The weight of the piston, friction at the rolling diaphragms, some uncertainty in de-airing, and difficulty in its use at zero pressure are, however, the main aspects which need care in using the Imperial College type device.

4.3.3.2 Pressure transducers

Diaphragm type pressure transducers were used for measuring pore air pressure u_a, pore water pressure u_w, and cell pressure σ_3. The range for each pressure transducer was 0 to 700 kPa.

4.3.4 Pressure control

Pressure to all the three Systems (*A*, *B*, and *C*) was supplied by a centralised air compressor, which ensured a minimum pressure of 550 kPa. For each system three stepper motor-controlled regulators were used to control the pore air pressure u_a, pore water pressure u_w, and cell pressure

σ_3. The maximum capacity of each regulator was 700 kPa with each step of the motor corresponding to approximately 0.42 kPa. The stepper motors could be controlled manually or automatically through the logging and control programme.

With the initial configuration of the apparatus, inherited from Sivakumar (1993) and used for the first 3 tests, the pore air pressure u_a was applied at the top of the sample, and pore water pressure u_w was applied at the bottom of the sample (see Figure 4.9). Modifications to these drainage connections were made for subsequent tests (see Section 4.4 below). Since both the pore air pressure and the pore water pressure could be controlled independently, a specified value of suction could be maintained or suction could be increased or decreased at a specified rate, according to the requirement of a test.

4.3.5 Filter arrangements

A dry porous filter was used at the top of the sample for applying the pore air pressure u_a. A conventional 50 mm diameter filter with an air entry value of less than 5 kPa was used for this purpose. The filter had to be cleaned using an ultrasonic bath after each test to prevent progressive clogging with fine particles of soil.

With the axis translation technique, the pore air pressure u_a within the sample is always higher than the pore water pressure u_w applied via the water drainage line to the base of the sample. This difference in the two pressures would have caused the air from the unsaturated soil sample to flow into the water drainage line unless prevented by special means. This was achieved by the use of a water-saturated ceramic filter, with a high air entry value, for the water pressure connection at the base of the sample. Bishop (1961) listed the following characteristics for high air entry filters to be used for this purpose:

1. The filter should be strong enough to withstand the mechanical stresses applied during testing.
2. The specified air entry value should be achieved, if possible with a uniform pore size distribution.
3. Ideally the permeability of the filter should be higher than that of the soil being tested.
4. The filter needs to be fully saturated to achieve the specified air entry value.

These requirements can be achieved by a ceramic filter with an air entry value more than the maximum suction $u_a - u_w$ applied in a test. The air entry value is inversely proportional to the pore size of the filter, because this controls the radii of curvature of the air-water menisci at the

filter boundary, as air is just about to enter. The air entry value can, therefore, be increased by reducing the pore size of the ceramic filter during manufacturing. Ceramic filters with air entry values up to 1500 kPa are commonly available. As the air entry value of a filter increases, the permeability of the filter is likely to decrease, because of the reduction in pore size. The air entry value is governed by the maximum pore size, but if there are numerous pores much smaller in size than the maximum pore size, the permeability will be low without any commensurate increase in the air entry value. This suggests that the pore size of the ceramic filter should be as uniform as possible. In some cases, permeability of the ceramic filter could become a limiting factor in controlling the time required for testing, rather than the permeability of the soil. It is therefore advisable to select a ceramic filter with an air entry value only slightly greater than the maximum suction to be applied within a given series of tests.

A chart giving values of air entry, permeability and average pore size is given in the catalogue of Soilmoisture Equipment Corp. Ltd (USA). For this research, ceramic filters with an air entry value of 500 kPa were selected, as a maximum suction of 400 kPa was envisaged for the test programme. The high air entry filter was placed in an assembly for using it in tests. The assembly, shown schematically in Figure 4.10, contained a high air entry filter on top of a low air entry filter, with both the filters glued within an acrylic annulus having 30 mm and 50 mm internal and external diameters respectively. The glue thickness between the annulus and the filters was 0.5 mm and the diameter of the high air entry filter was therefore 29 mm. The purpose of the low air entry filter in this arrangement was to avoid constricted flow through the high air entry filter, which Sivakumar (1993) noted and suggested was due to the limited portion of the bottom surface of the ceramic in contact with the drainage groove underneath it. The use of low air entry filter allowed drainage through the whole lower surface of the high air entry ceramic filter.

To achieve the specified air entry value of the ceramic filter, it was essential that the filter be fully saturated with water prior to testing. Since these filters are commonly used in the testing of unsaturated soils, a general procedure for filter saturation has evolved (see, for example, Fredlund and Rahardjo (1993) and Sivakumar (1993)). The steps involved in the saturation process are listed below:

1. The filter assembly was mounted on the pedestal of a conventional triaxial cell.
2. The drainage line through the pedestal was flushed with freshly de-aired water to remove any trapped air.

3. The cell was assembled and filled with freshly de-aired water and pressurised to 550 kPa through an air-water interface. The cell pressure was maintained for two days.
4. The drainage line connecting to the base of the filter was opened to the atmospheric pressure on the third day and, with the cell pressure still held at 550 kPa, water was allowed to drain freely through the filter for one day.
5. On the fourth day the cell pressure line was closed, whilst leaving open the drainage line from the base of the filter. This resulted in a gradual reduction of cell pressure as water continued to flow through the filter. Once the cell pressure had reduced to about 25 kPa, the cell was emptied and then re-filled with freshly de-aired water. The cell was then pressurised again to about 550 kPa with the drainage line open to atmospheric pressure for one further day.
6. The cell pressure was reduced gradually, as described in step 5, and then the filter was ready for use in a test.
7. Steps 3 to 5 were repeated at least twice for new filters.

The air entry value of each new filter was confirmed at greater than 450 kPa. This was done by mounting the saturated filter on the pedestal of the de-airing cell, with the cell filled with air. The air pressure of 450 kPa was applied in the cell (to the top surface of the ceramic filter), while connecting the water-filled drainage line (below the filter) to a volume change measurement device at atmospheric pressure. Flow of water was monitored for two days and if there was no flow out into the measuring System, the filter could be used in a test. In fact, water flowed into the cell, at a rate of about 0.05 cm^3/day representing evaporation from the top surface of the filter.

4.3.6 Fuse wire technique

In spite of fully saturating the high air entry filter according to the procedure described in Section 4.3.5, desaturation of the filter was possible during setting up a test because of the following:

- The ceramic filter could slightly dry out if was left exposed to atmosphere for significant time. This was prevented by leaving a small amount of water on the surface of the ceramic filter, which was removed just before placing the sample. Moreover setting-up time was kept to the minimum possible (about 30 minutes).
- If the soil sample was directly mounted on to the ceramic filter before starting a test, direct contact with the sample, which contained pore water at a high value of negative pressure after compaction, would induce large negative water pressure within the ceramic filter and the drainage line beneath. This could lead to cavitation in the system, leading to subsequent

air leakage through the ceramic filter. It was therefore essential to prevent direct contact between the soil sample and the high air entry filter until the cell pressure was applied and a small positive value of back pressure was applied to the water drainage connection beneath the filter.

The problem of desaturation arising due to direct contact between the ceramic filter and the unsaturated soil sample has been noted by previous researchers. A special technique, known as the "fuse wire technique", was developed by Maswoswe (1985) to prevent this problem and was subsequently used by Sivakumar (1993). Two lengths of thin metal fuse wire, bent into semi-circles, were placed on to the acrylic annulus containing the ceramic filter and then the soil sample was placed on top of these wires. These wires prevented direct contact between the ceramic filter and the soil sample until a cell pressure of about 35 kPa was applied. The fuse wires then embedded into the body of the soil sample leading to direct contact between the ceramic filter and the sample during a test. In this research wires of 0.30 mm diameter were used for this purpose. Another set of similar wires was used on the interface between the top of the soil sample and the ceramic filter for the top face drainage in the double drainage arrangement, which is described in Section 4.4. A correction, corresponding to the extra volume due to embedment of the fuse wires, was made to the sample volume measurement. It was assumed that the initial space created by the fuse wires between the sample and the ceramic filters at top and bottom of the sample was completely air-filled.

4.3.7 Flushing System

In spite of the use of the high air entry ceramic filter for prevention of bulk air flow into the water drainage line, the possibility of air leakage into the water drainage line still existed due to diffusion of dissolved air through the water in the filter. Fredlund (1975) noted this and devised a flushing arrangement so that air could be flushed from the drainage line beneath the filter into an inverted burette, and the measured volume of water flow into the sample corrected accordingly. Nageswaran (1983) also observed that any diffused air could cause error in the measurement of pore water pressure.

Sivakumar (1993) used a flushing device (see Figure 4.11) based on the technique described by Fredlund (1975), but he rarely recorded the presence of a measurable quantity of diffused air in the water drainage line. In this research flushing was carried out using the system shown in Figure 4.11. Water was sent from one air water interface through the flushing grooves adjacent to the ceramic filters and finally to another air-water interface, which was kept at a slightly lower

elevation than the first interface. By using a four-way valve, as shown in Figure 4.11, the flow direction was reversed, so that any remaining air bubbles could be removed. Again there was, however, no evidence of any diffused air.

4.3.8 Logging and control

Logging and control software, written in Quick Basic, was developed for the test programme of Sivakumar (1993). The software was developed specifically to suit the requirements of controlled-suction triaxial testing of unsaturated soils. From the operational point of view, the software had two parts: one for conducting isotropic tests and the other for shearing tests.

The main feature of the isotropic loading part of the software was that the cell pressure, pore air pressure, and pore water pressure could each be increased or decreased at a pre-set rate to achieve a given final target pressure. For each stage of a test (equalisation, wetting, drying, loading, etc), target pressures and rate of increase or decrease were specified and inserted in the software prior to running the given stage. The required accuracy of pressure control was also inserted in the software before running a stage and then the control loop of the software maintained the pressures at the instantaneous target values within this accuracy. The pressure accuracy was defined as 0.5 kPa for all tests.

The software, along with the stepper motors, could be used for varying independently the pore air pressure, pore water pressure and cell pressure. Therefore any specified isotropic stress path could be followed. The data corresponding to the various transducer channels (pore air pressure, pore water pressure, cell pressure, and the two volume change devices) could be logged at any specified logging interval. The data could also be copied to a floppy disc whilst the test was in progress. This enabled analysis of the data without disturbing or stopping a test.

Two new features were added to the control and logging software. Firstly, the capability to vary pore air pressure and pore water pressure or cell pressure at a non-linear rate with time (rather than just a constant rate) was incorporated. The reasons for this development are explained in Section 5.6. Secondly, capability for constant volume wetting and drying under isotropic conditions was incorporated (see Section 5.6).

4.3.9 Temperature control

Large fluctuations in room temperature were undesirable, because the double-walled cell was used for sample volume change measurement. Without temperature control, the volume of the

cell and water within it would have changed with variations in temperature. This in turn would obviously have resulted in error in the sample volume change measurement. A temperature control unit installed in the laboratory kept the room temperature at 20^0C with a variation of $\pm 0.5^0$C.

4.4 Development of Double Drainage System

In the initial configuration, all three Systems (*A*, *B*, and *C*) had control or measurement of pore water pressure at the bottom of the sample and control of pore air pressure at the top of the sample (see Figure 4.9). This is the conventional layout used with the axis translation technique by researchers including Hilf (1956), Bishop and Donald (1961), Matyas and Radhakrishna (1968), Fredlund and Rahardjo (1993), and Sivakumar (1993). With water drainage from only one face, the test duration for unsaturated clays becomes exceedingly long; worse than for saturated clays because the water permeability drops markedly as the degree of saturation falls. For example the tests of Sivakumar (1993) on unsaturated kaolin (a relatively free-draining clay) had an average duration of about 4 weeks (each test involved three stages: wetting, isotropic consolidation and shearing). For unsaturated expansive clays tested in this programme the problem was exacerbated by the fact that expansive clays are typically of much lower permeability than kaolin.

The obvious solution for this problem was to design a drainage arrangement with water drainage from both top and bottom of the sample, theoretically reducing the drainage time by a factor of four, provided that the permeability of the high air entry filters was significantly greater than that of the soil.

Maâtouk *et al* (1995) reported a new arrangement with water draining from both faces of the sample and pore air pressure applied through a diffuser mounted at the mid height of the sample. They, however, did not use the doubled-walled cell for sample volume change measurement and instead used local strain measurement transducers. The drainage arrangement of Maâtouk *et al* (1995) was not adopted, because the accuracy of measurement of sample volume change with the double-walled cell method could have been adversely affected because:

- The diffuser could have changed in volume with variation in cell pressure. This would have needed at least one additional calibration, which might well have been non-linear and non-elastic in nature.
- With the diffuser inside the rubber membrane, the removal of entrapped air within the rubber membrane during setting up of the sample would not have been easy to achieve.

With the intention to shorten the duration of a given test and avoid the sources of potential error in the measurement of sample volume change, a new design was undertaken with the objective of achieving:

- Control of pore water pressure at both top and bottom of the sample.
- Control of pore air pressure at the top of the sample.

The general layout of new double drainage design is shown schematically in Figure 4.12. Two water drainage connections for the top face and two for the bottom face were required to provide the capability of flushing any diffused air from the water drainage lines (see Section 4.3.7). The connections for the bottom face were through the cell base and the pedestal, whereas the connections to the top face were made through the cell base and then via flexible nylon tubes from the cell base to the top cap. The single air drainage connection to the top face was made in a similar way, through the cell base and then via a flexible nylon tube to the top cap.

4.4.1 Top cap filter assembly

The top cap filter assembly is shown schematically in Figure 4.13. The top cap filter assembly was similar in principle to the filter assembly used for water drainage from the bottom, with an additional facility for applying air back pressure alongside the water back pressure to the top of the sample. To accommodate the facility for applying air pressure within the 50 mm diameter top surface of the sample without reducing the diameter of the high air entry ceramic filter posed practical problems. The top cap filter assembly had two parts: low air entry filter and an assembly containing the high air entry filter.

Since air permeability of the soils is much higher than the water permeability, it was decided to use only a part of the top face of the soil sample to apply air pressure and to use the remaining area for water drainage. To achieve this, an annular-shaped low air entry filter (with outer and inner diameters 50 mm and 34 mm respectively) rather than the full disc of 50 mm diameter was used. This annulus was a tight fit on to the acrylic mounting ring assembly containing the high air entry filter. The annular low air entry filter for pore air pressure control was kept separate from the acrylic mounting ring containing the high air entry filter, so that the high air entry filter could be water-saturated without the annular-shaped low air entry filter, which had to be maintained in a dry state. This arrangement also facilitated independent cleaning of the annular low air entry filter in an ultrasonic bath. This cleaning would not have been feasible if the low air entry filter was permanently fixed to the acrylic ring containing the high air entry filter, because the glued seal of the high air entry filter within the acrylic mounting ring could have been

adversely affected in the ultrasonic bath. The annular-shaped low air entry filter was sleeved on to the acrylic mounting ring at the time of setting up a sample for a test. The air pressure was applied through a single hole, with a circular groove in the lower face of the acrylic mounting ring (see Figure 4.13) to allow circulation of air over the entire circumference of the low air entry filter. There was no risk of water entering the low air entry filter and the connected air line, because the pore air pressure u_a was always higher than the pore water pressure u_w.

The top cap filter assembly consisted of a high air entry filter on which a low air entry filter was placed and then both the filters were glued into the acrylic mounting ring as shown in Figure 4.13. The low air entry filter was 19 mm in diameter and the high air entry filter was of 28 mm diameter. To fit these filters, the acrylic mounting ring had a shoulder 4 mm wide, on which the ceramic filter rested. This shoulder reduced the risk of leakage of air through the glue, because it was easier to achieve a good quality glued seal on this shoulder than on the vertical outer cylindrical surface of the high air entry filter.

4.4.2 Testing of double drainage arrangement

Initial testing of the double drainage arrangement with System *B* indicated that there were leaks in the system. There were various possible sources of leakage:

1. Leakage of air through the glue between the high air entry filter and the acrylic mounting ring.
2. Leakage of air from the air pressure line to the water drainage line through the o-ring seal which separated these two lines.
3. Leakage of cell water into the air line through the connections of the air line into the base of the cell and/or to the top cap. This water could have passed through the low air entry filter and then to the sample before finally coming out into the water drainage line through the high air entry filter.
4. Leakage of cell water to the water drainage line through the connection in the base of the cell and/or the connections of the flexible tube to the top cap.

The source of leakage was tracked down by a process of elimination.

In the initial tests, relatively large amounts of air were noticed in the water drainage line from the top face of the sample. The large amount of air suggested that:

- Either air from the soil sample leaked into the water drainage line through the glue between the high air entry filter and the acrylic ring containing this filter.

- Or air could have leaked from the air pressure line to the water drainage line through the o-ring seal that separated the two lines.

This major leak was finally confirmed through the o-ring seal and was prevented by changing the o-ring design at the interface between the top cap and the filter assembly (see Figure 4.14). By making the o-ring groove wider and shallower a successful seal was achieved. Use of a small amount of silicon grease was also found helpful in prevention of this leakage.

In a subsequent test, a small amount of air was found in the bottom face drainage line. This leak could have been either due to wear and tear of the high air entry filter and/or the presence of very high initial suctions, caused by compaction of the highly expansive clay inducing a negative pressure in the water contained in the high air entry filter (this could have caused cavitation in the high air entry ceramic filter and this subsequently could have resulted in leakage of air from the soil sample into the water drainage line). By using a set of fresh filters the leakage was prevented. Confirmation that the cause of leakage was not associated specifically with the high suctions came from successful completion of a test on unsaturated highly expansive clay with single face drainage in System *A*.

From the successful test in System *A*, mentioned above, with single face drainage it was established that during equalisation water flowed into the sample. In tests in System *B* with the double drainage arrangement under identical suction and stress conditions to the test in System *A*, a very small rate (0.03 cm^3/hr) of water outflow to the water volume change unit was however noticed. More importantly, water flowed into the sample for the first two days and on the third day outflow from the sample started, which then stabilised to a constant rate. It should be noted that no air was noticed in the drainage line. This suggested there was a very tiny leakage of water. The leakage was masked initially because a larger amount of inflow occurred to the sample and when this inflow decreased to a relatively low level after about two days, the leakage gradually became dominant before stabilising to a constant rate. Since no leakage was noticed in the test with single drainage, the source of leakage was likely to be on the drainage line that connected to the top cap. At this stage, it was suspected that the leakage was due to an imperfect glued seal of the high air entry ceramic filter into the acrylic mounting ring. Different gluing arrangements and gluing materials were used in an attempt to eliminate the leakage. The leakage however continued indicating that something else was the cause. It is worth mentioning that the rate of leakage was now so small that it took about 10 days to check the effect of any change (the saturation of filters took about 5 days and in order to determine the leakage rates, tests were required to be continued for at least 5 days).

In a further test, the high air entry filter assemblies for the top and bottom faces were swapped. The high air entry filter assembly, now attached to the top cap, had been tested beforehand for no leakage by attaching it to the pedestal. In this test, it was found that even the already tested high air entry filter assembly leaked when attached to the top cap. In contrast no leakage was found in the high air entry filter assembly that was now attached to the bottom face drainage line (it had shown leakage when it was attached to the top cap). This eliminated the filter and the associated gluing arrangement as one of the various possible sources of leakage.

The flexible tubes providing the water drainage connections from the top cap to the cell base were finally identified as the cause of leakage. In total it took about three months to identify this final source of leakage. The leakage occurred at the interface between the flexible tubes and the fittings used to connect the tubes to the top cap and the cell base. This was perhaps because of the fact that these fittings were designed to provide a good seal if the pressure inside the tube was higher than the pressure outside, whereas in this application the internal pressure (pore water pressure u_w) was lower than the external pressure (cell pressure σ_3). This differential pressure resulted in compression of the flexible tube, which tended to separate the sealing surfaces of the fitting (whereas a high internal pressure would actually improve the sealing action). By using 3 mm outer diameter thick-walled tubes the leakage problem was eliminated. New fittings suitable for 3 mm outer diameter tubes were used for making the connections. The new fittings were also compression type, but worked satisfactorily with the new tube, which was stiffer in compression than the tube previously used. Additionally, Locktight 542 glue was used to seal the connections. These tubes and fittings were then used in the other two Systems *A* and *C* and then tests with the double drainage arrangement were started.

4.5 Calibration

Calibration of the 5 transducers (3 pressure transducers and 2 volume change measurement transducers) and of the volume changes associated with the cell and the water drainage line were carried out for each System (*A*, *B* and *C*).

4.5.1 Calibration of pressure transducers

All three pressure transducers i.e. the pore air pressure u_a, pore water pressure u_w, and cell pressure σ_3 transducers were calibrated using a digital pressure indicator containing a pressure transducer with high accuracy. All the pressure transducers were calibrated using three full

cycles of increasing and decreasing pressures. No significant hysteresis was observed and linear calibration equations gave standard errors of less than 1 kPa.

4.5.2 Calibration of Imperial College volume change measurement devices

Before calibration of the Imperial College volume change units, these were de-aired using freshly de-aired water by filling and emptying the units several times. For dissolution of any remaining air, the units were kept pressurised at 200 kPa for one day. This procedure for de-airing was followed in calibration as well as in all the tests involving Imperial College change measurement devices. For calibration, a known amount of water was transferred into or out of the unit from a 10 cm^3 graduated burette with a precision of 0.02 cm^3, and the output from the displacement transducer attached to the Imperial college volume change unit was monitored. The layout of the calibration system is schematically illustrated in Figure 4.15. Calibrations were carried out at line pressures of 50, 250, and 500 kPa with full cycles of filling and emptying at each pressure. The calibrations were found to be independent of line pressure for all the units, with a linear relationship between the volume change and the voltage output from the displacement transducer. All the calibrations were performed at least twice, in order to check repeatability. The maximum error in the volume measurement was estimated to be ± 0.06 cm^3 over a measurement range of 20 cm^3.

4.5.3 Calibration of burette type volume change measurement devices

The burette was first carefully cleaned of any dirt or grease and then the attached tubes and the burette were flushed with de-aired water to remove any trapped air from the system. The layout used for calibration was similar to that shown in Figure 4.15. A known amount of water was transferred into or out of the unit from a 10 cm^3 graduated burette with a precision of 0.02 cm^3. The output from the differential pressure transducer attached to the volume change measurement unit was monitored. Special care was taken to transfer the water into or out of the burette at a very slow rate because, in spite of good cleaning of the burette walls, water was observed to stick to the burette walls if the flow of water was not steady and slow.

Calibrations at line pressures of 0, 50, 250, and 500 kPa were carried out. At each pressure a full cycle involving filling with water and then emptying the volume change unit was used for these calibrations. The calibrations for each line pressure were found to be linear, but varied non-linearly with the line pressure. Calibration was thus in two stages:

1. For a particular line pressure the volume of water in the burette V was correlated to voltage output X linearly and calibration factor $Cal\ Fact$ was of the following form:

$$V = \frac{1}{CalFact} X \tag{4.2}$$

2. The calibration factor *Cal Fact* is function of line pressure P and was found to vary as second order polynomial of the following form:

$$CalFact = aP^2 + bP + c \tag{4.3}$$

Where a, b and c are calibration constants.

Sivakumar (1993) found that the volume change, from the burette device, was independent of the line pressure at an output voltage of zero. This is shown schematically in Figure 4.16, which shows that the calibration curves for different line pressures all intersected at zero volts. For example, volume change from point A (at a line pressure of 100 kPa) to point B (at line pressure of 300 kPa) was calculated as follows:

$$VolumeChange = \frac{X_B}{CF_B} - \frac{X_A}{CF_A} \tag{4.4}$$

where CF_B and CF_A are the calibration factors calculated from Equation 4.3. In a test, volume change was directly logged, as Equation 4.4 was built into the control and logging software.

The values of the constants a, b, and c in Equation 4.3 are given in Table 4.2. All calibrations were performed at least twice, to confirm repeatability. The maximum error in volume measurement was estimated to be $\pm$ 0.07 cm^3.

4.5.4 Cell calibration

The double-walled cell required calibrations consisting of two parts.

- Firstly, there was the immediate volume change caused by a change of cell pressure, which was due to compression of the water in the cell and slight expansion of the cell valves and the short lengths of connecting tubing.
- Secondly, there was the continuing apparent volume change, caused by water absorption by the acrylic cell wall (see Wheeler (1988)).

These calibrations, for apparent volume change of the inner cell, were very time-consuming. It took about four weeks to calibrate each cell.

Before calibrating a cell, all the drainage lines in the system were flushed with freshly de-aired water to remove any trapped air and the water drainage line was then closed. A dummy sample, made of stainless steel, was mounted on the pedestal within the inner cell. A rubber membrane was then sleeved on to the dummy sample and two o-rings were used to seal each face of the

sample (top and bottom). The inner cell was then filled with de-aired water and the air vent was plugged. The outer cell was then assembled and filled with water, and the air vent hole was plugged. The sample volume change measurement device was connected to the cell for recording of volume change, but the valve on this line was kept closed and was opened just before starting the calibration test. After connecting the outer cell to the pressure line, the valves on the outer and the inner cell lines were opened simultaneously. To increase the cell pressure to a target value of cell pressure, the logging and control programme was used. The cell pressure was increased/decreased to 100, 300, 500, 300, and 100 kPa. Each increment or decrement of cell pressure was applied relatively quickly (at a rate of about 4.2 kPa/min). After achieving the particular value of cell pressure, the cell was left at that pressure for a period of at least 4 days. This requirement was for each step of cell pressure to get sufficient data so that the rate of water absorption by the acrylic cell could be calculated. A typical plot between cell volume change and time during the calibration exercise is shown in Figure 4.17.

The immediate volume change for each step change of cell pressure was calculated from the corresponding plots and then the cumulative volume change against cell pressure was plotted as shown in Figure 4.18. The variation of immediate volume change with cell pressure was fitted to a second order polynomial. Relevant equations and the values of calibrations are given in Tables 4.2 to 4.4. The immediate volume changes in the calibrations were very similar to what had been observed earlier by Sivakumar (1993), except for the first calibration of System *B*. A later calibration for System *B* agreed with Sivakumar. The reasons for the lack of agreement of the first calibration for System *B* with the calibration reported by Sivakumar (1993) are not fully understood (it may have been that something non-standard was done at this early stage of testing). This calibration was, however, used for only one test.

For the rate of water absorption by the acrylic cell, rates of water absorption corresponding to each step of cell pressure were calculated. The water absorption had an approximately linear variation with time at each level of cell pressure. The rate of water absorption thus calculated was plotted against cell pressure, as shown in Figure 4.19. The variation of rate of water absorption with cell pressure was approximated by a linear relationship and the calibration factors along with the relevant equations are given in Tables 4.2 to 4.4. For System *B*, two calibrations were carried out. The first calibration was followed by one test and System *B* was then used for development of the double drainage arrangement before carrying out the final calibration. In the first calibration the rates of water absorption at cell pressures of 100 and 300 kPa were much higher during the stage when the cell pressure was increasing than during

measurement when the cell pressure was decreasing. This suggested that the water content of the acrylic was still changing significantly with time; a consequence of the fact that the cell had not been used at elevated cell pressures for some considerable time. The earlier experience of Sivakumar (1993) indicated that after a few months use, the calibration showed little further change with time. For the first test, in which the calibration factors from this calibration were used, the calibration factors for rate of water absorption were calculated from the data corresponding to decreasing cell pressure path only rather than the full cycle. These calibration factors, reported in Table 4.2, were very similar to the factors reported by Sivakumar (1993), but clearly the cell needed another calibration quite soon for confirmation of these factors. In the subsequent calibration the rate of water absorption was confirmed, on the basis of data from the full cycle, at a level very similar to that reported by Sivakumar (1993).

For system *A*, again two calibrations were carried out. The first calibration was followed by two tests and then the final calibration was completed, which was used for the remaining tests.

For System *C*, one calibration sufficed, because the acrylic cell had been kept under pressurised water for several months prior to the start of testing with this system. From Table 4.4, it evident that the calibration factors for rate of water absorption were similar to the factors reported for the other two cells in Tables 4.2 and 4.3. This suggests that keeping the acrylic cell walls under pressurised water is much more effective in preventing changes in rate of water absorption than keeping the acrylic immersed in water at atmospheric pressure (which was done for the cell walls in Systems *A* and *B* in the few months prior to the start of testing), especially if the cells are not in use for a long period.

4.5.5 Calibration of water drainage line

The flow of water into the sample was measured during a test with the second volume change unit that was connected to the water drainage lines. If the back pressure on the water drainage line (connecting the sample to the volume change unit) changed, this could cause expansion of the drainage line and the connectors, thereby interfering with measurement of water inflow to the sample. To account for these effects a calibration was carried out. Only the tubes outside the cell were included in this calibration, as the nylon tubes used inside the cell for top face drainage were thick-walled, had high stiffness in compression, and only short lengths of the tube (about 20 cm) were used, whereas the tubes outside were about 1.5 m in length as well as of larger inner diameter. Finally, even the effect of pressure change on the tubes outside cell was very small, as shown in Tables 4.2 to 4.4.

CHAPTER 5

MATERIAL SELECTION AND TESTING PROCEDURE

This chapter starts with a description of work related to material selection and characterisation, followed by a description of the sample preparation method. Finally, the procedure used in carrying out the tests is described, together with the steps involved in calculation of various parameters from the logged data.

5.1 Selection of a Highly Expansive Soil

5.1.1 Considerations in soil selection

The first consideration in the material selection was that the soil should be highly expansive. Another important consideration was that the tests should be of reasonable duration. Not only is the behaviour of unsaturated soils more complex than that of saturated soils, but the testing of unsaturated soils in the laboratory is a very slow process. This is mainly because of the fact that, as the degree of saturation reduces, the water permeability decreases and therefore the dissipation of excess pore water pressures developed during testing becomes very slow. Like saturated soils, the test duration or rate of dissipation of excess pore water pressure depends very much on the type of soil, for example sandy soils drain much faster than clayey soils. In this project the problem of test duration was exacerbated by the very low permeability (even in a saturated state) of highly expansive clays.

The constraint of test duration was particularly severe for this experimental programme because it involved testing in an isotropic version of a triaxial cell rather than in an oedometer apparatus. The typical height of samples used in oedometer tests is 20 mm, with drainage from both top and bottom, giving a maximum drainage path length of 10 mm. In contrast, 50 mm diameter samples used in triaxial tests are typically 100 mm high (height-to-diameter ratio of 2:1, to minimise the strain non-uniformities caused by restraints at the two ends and to allow freedom for development of shear planes). With drainage from one end only, the drainage path length for such a sample is 100 mm. Given that the time for dissipation of excess pore water pressures varies with the square of the maximum drainage path length, triaxial tests can take as much as 100 times longer than oedometer tests.

Unfortunately, as the degree of expansivity of a clay increases, the permeability generally decreases, and therefore the time required for excess pore water pressure dissipation increases.

The requirements of high expansivity and short test duration were therefore in conflict. To identify a suitable soil, providing a reasonable compromise between these two requirements, a comparative study of the swell-time characteristics of various possible soil types was undertaken using oedometer rather than isotropic testing, as the former was faster.

Compacted samples prepared from industrially refined components were preferred over natural samples, so that features of the mechanical behaviour of the soil could be examined without interference from complications such as variability between samples, heterogeneity within a sample, bonding, ageing and variability of chemical or mineralogical composition. The effects of these factors associated with natural soils could, however, be taken up in future research along the lines suggested by Burland (1990) for saturated soils.

5.1.2 Bentonite-kaolin mixes

For comparative study of swell-time characteristics, mixes of bentonites and kaolin were investigated. Three types of bentonite and two types of kaolin were used. The three types of bentonite were a natural calcium bentonite, sodium activated bentonite and a natural sodium bentonite from Wyoming. The two types of kaolin were speswhite kaolin (fine, with D_{50} value of 0.75 μm) and grade-E kaolin (coarse, with D_{50} value of 4 μm). Samples of 20% bentonite with 80% kaolin (by weight) were prepared with different combinations of bentonite type and kaolin type. On the basis of the results from these tests the most suitable combination of bentonite type and kaolin type was chosen. Using this combination, the percentages of bentonite and kaolin were then varied to select the optimum mix proportions.

5.1.3 Oedometer tests and swell-time characteristics

Samples for all the soil mixes were prepared using the same procedure. First the bentonite and kaolin were mixed dry in the required proportions and then water was added to give a water content of 25% by weight. A commercial food mixer was used for thorough mixing of the water and soil. The wet soil was sieved using a 1.18 mm aperture sieve to ensure that the largest packets of soil were considerably smaller than the minimum dimension of the soil sample (50 mm). The sieved material was packed in a polythene bag and left in an airtight chamber for 24 hours for homogenisation. Subsequently, the soil was placed into an oedometer ring, on top of which a purpose-built extension collar was fixed. The soil sample was statically compacted to 400 kPa at a displacement rate of 1.5 mm per minute using a compression frame. Surplus soil from the top of the oedometer ring was carefully trimmed using a spatula, so that the sample height was the same as the ring height.

The sample was weighed and mounted on to the oedometer apparatus, which was fitted with a dial gauge to measure the swelling or compression of the sample to a precision of 0.01 mm. A vertical stress of 10 kPa was applied. Soil samples were left for about 5 minutes to come to equilibrium under the applied vertical stress of 10 kPa. The sample was then inundated with water. The volumetric swelling strain on inundation was plotted against time (with the latter on a logarithmic scale).

The swell-time curves for grade-E kaolin mixed with calcium bentonite, sodium activated bentonite or Wyoming sodium bentonite are shown in Figure 5.1 (with the bentonite forming 20% by weight in each case). Inspection of Figure 5.1 shows that the sample containing calcium bentonite swelled only about 4%. In contrast, the other two samples swelled more than 16%. On the basis of this result the calcium bentonite was ruled out as being insufficiently expansive. The sample containing Wyoming sodium bentonite ultimately swelled more than the sample containing sodium activated bentonite, but for this swelling to occur the former took longer than the latter (see Figure 5.1). From these results, it was unclear whether the sodium activated bentonite or the Wyoming sodium bentonite provided the better choice.

Figure 5.2 shows the swell-time curves of Wyoming sodium bentonite and sodium activated bentonite mixed with either grade-E kaolin or speswhite kaolin (with the bentonite forming 20% by weight in each case). Of the four mixes, the sample of speswhite kaolin and Wyoming sodium bentonite gave the maximum final swelling and the fastest swelling. This mix was therefore selected for further investigation to arrive at an optimum percentage of bentonite in the mix.

Figure 5.3 shows the swell-time results of various percentages of Wyoming sodium bentonite (0%, 10%, 12%, 15% and 20%) mixed with speswhite kaolin. Inspection of Figure 5.3 shows that as the percentage of the bentonite increases, the swelling magnitude increases, but so does the time required to achieve full swelling. As a compromise the mixture of 10% Wyoming sodium bentonite with 90% speswhite kaolin was selected as the main test material, giving about 11% swelling under the conditions of the oedometer test shown in Figure 5.3. McKeen (1992) proposed a classification system for expansive soils. According to this classification, soils that swell less than 1.8% on wetting are considered as "non-expansive", those that swell 1.8 to 5.3% are termed "moderately expansive", swelling of 5.3 to 10% corresponds to "highly expansive" and finally soils that swell more than 10% are considered as "very highly expansive". The mix

of 10% Wyoming sodium bentonite with speswhite kaolin therefore corresponded to a "highly expansive" or "very highly expansive" clay.

5.2 Selection of a Non-Expansive Soil

During the main series of isotropic tests on the unsaturated highly expansive bentonite/kaolin clay, it became clear that a few tests on a non-expansive clay would provide useful information. Data were already available for monotonic loading or wetting behaviour of unsaturated non-expansive clays (see, for example, Sivakumar (1993)), but data were scarce for cycles of wetting and drying. For modelling the behaviour of unsaturated highly expansive clays it was considered important to identify the distinguishing features of these soils that should be incorporated into the modelling framework. To achieve this objective, a limited series of tests on a non-expansive clay was planned, for purposes of comparison.

Speswhite kaolin was selected as a suitable material to represent typical non-expansive clays. The advantages in selecting kaolin, included:

- As reported in Section 5.1, a mix of bentonite and speswhite kaolin was selected as a highly expansive clay. Speswhite kaolin therefore formed the natural choice as a non-expansive clay for comparison, so that any observed differences in behaviour could be attributed solely to the presence of the highly expansive bentonite in the bentonite/kaolin mix.
- Kaolin has a water permeability higher than most other clayey soils, which meant the test duration could be kept within manageable limits.
- Data generated in this project would complement the data reported for speswhite kaolin by various other authors, including Sivakumar (1993) and Zakaria (1994).

5.3 Atterberg Limits for the Selected Soils

Liquid and plastic limits for the speswhite kaolin were 65% and 32% respectively, giving a plasticity index of 33%. These Atterberg limits for speswhite kaolin are consistent with the values reported by previous researchers such as Al-Tabba (1987) and Kim (1996). For the mix of 10% Wyoming sodium bentonite with 90% speswhite kaolin the liquid and plastic limits were 93% and 33% respectively, giving a plasticity index of 60%.

5.4 Compaction Characteristics

Samples of unsaturated soil could be prepared either by compaction or by de-saturating initially saturated samples. Both these methods of sample preparation are important and represent two different situations, which can occur in the field. The compaction method simulates compacted

fills, whereas the de-saturation method simulates unsaturated natural soils above the water table. Ideally experimental tests should be carried out on samples prepared by both the methods. Since this was not feasible within the duration of the project, the compaction method was selected.

Various possible methods of compaction were available, including "static" (non-impact monotonic loading), dynamic (repeated impact) or kneading. Sivakumar (1993) tried different methods of compaction to prepare triaxial samples, and found that static compaction (carried out in 9 layers each containing equal amounts of material and each layer compacted to the same stress level) gave the most satisfactory samples, in terms of uniformity and repeatability. Zakaria (1994) further confirmed this procedure to be satisfactory. This information, along with experience from a few trials for bentonite/kaolin mix, was used in selecting static compaction for sample preparation.

The main test programme was based on a single compaction water content. In recent research, the compaction water content has been found to influence significantly the behaviour of compacted speswhite kaolin (Sivakumar and Wheeler (in press)). This effect is such that soil samples compacted at different water contents effectively behave as different soils (with different values to some of the soil constants within the constitutive model described in Section 2.10). In the comparative study of swell-time characteristics of various soil mixes, described in Section 5.1, the compaction water content was kept at 25%. To decide on an appropriate compaction water content to be used in the main research programme, it was essential to examine the compaction characteristics of the soil. Compaction curves were prepared for 50 mm diameter triaxial samples prepared by static compaction under a pressure of 400 kPa (the compaction pressure applied by Sivakumar (1993), corresponding to a significantly lower degree of compaction than the standard Proctor method). For comparative purposes, similar compaction curves were also prepared for larger samples prepared by the standard Proctor method.

The clays were first oven-dried at 105^0C for 24 hours, because the bentonite was found to absorb up to 15% moisture content in storage at ambient humidity and temperature. The speswhite kaolin absorbed less than 1% moisture from the air at ambient conditions, but it was also oven-dried. After removal from the oven, the dried soil was allowed to cool down within a sealed container and then the dry bentonite and dry kaolin were mixed in the required proportions. The required quantity of water was added to the soil mixture, so that water contents between 18% and 36% could be achieved. The soil was then sieved through a 1.18 mm aperture sieve for all the water contents except the two highest of 32% and 36%. At 32% or 36% water content the

soil became sticky and could not be sieved. The bigger lumps of soil resulting from mixing of the soil with water were, however, broken down to smaller size by hand.

Soil from a given batch was used for preparation of both a standard Proctor sample and a 50 mm diameter triaxial test sample. The Proctor sample was prepared in three layers using the standard equipment and 27 blows of the standard hammer on each layer. Triaxial samples were prepared in 9 layers using static compaction of 400 kPa at a displacement rate of 1.5 mm per minute on each layer. Thereafter the wet weights of the samples were taken and moisture contents were determined after oven drying at 105^0C for 24 hours.

Moisture contents of 18.6%, 20.6%, 25%, 28.5%, 32%, and 36% were obtained and the respective dry densities were determined for both the standard Proctor samples and the 400 kPa static compaction samples. The results are shown in Figure 5.4. It is clear from the plots that the optimum moisture content for standard Proctor compaction was approximately 29%, whereas for 400 kPa static compaction the optimum moisture content was slightly higher. At 25% moisture content, which is about 4% dry of standard Proctor optimum, a dry density of 1.39 Mg/m^3 was obtained for standard Proctor samples, whereas the corresponding dry density was 1.24 Mg/m^3 for the triaxial samples statically compacted to 400 kPa.

A compaction water content of 25% was finally selected because of the following advantages. Firstly, the magnitude of swelling or collapse which occurred on subsequent wetting was likely to be largest for samples compacted dry of optimum, so that the extremes of soil behaviour could be investigated. Secondly, it was easier to produce samples with good repeatability on the dry side of optimum than on the wet side. Thirdly, the data generated in this research would be complementary to, and to some extent could be compared with, earlier work by Sivakumar (1993) on speswhite kaolin compacted at 25% water content.

In the field, unsaturated compacted soils occur both wet and dry of optimum. An ideal situation therefore would have been to test samples compacted on both sides of optimum. It would have been, however, very difficult to investigate fully two different compaction water contents within the duration of this research. It was decided to examine the dry side first, leaving to future researchers investigation of the behaviour of samples compacted wet of optimum.

Samples for most tests were prepared by static compaction under a vertical stress of 400 kPa, but in view of the emerging test results a few samples of the highly expansive bentonite/kaolin mix prepared by compacting to pressures of 800 and 3200 kPa were also tested (see Section 6.7).

5.5 Sample Preparation Technique

5.5.1 Sample Size

In deciding the dimensions of the samples for isotropic testing, the following points were considered:

- The sample dimensions had to be substantially larger than the dimensions of the largest soil packets forming the soil macro-fabric.
- The height of the sample had to be as small as possible, because the time required for a test increased with square of the water drainage path length.

The sample size for isotropic testing was selected as 50 mm in diameter and 50 mm in height. The maximum size of soil packets forming the soil macro-fabric was 1.18 mm, because the soil was sieved through a sieve of 1.18 mm aperture. For samples used in triaxial shear tests the height-to-diameter ratio is typically 2:1, to minimise the non-uniformities caused by restraint at the two ends and to allow freedom for the development of shear planes. In this research programme, a height-to-diameter ratio of 1:1 was used. This ratio was considered adequate as only isotropic tests were carried out and therefore shear planes were not envisaged and strain non-uniformity over the length of the sample was unlikely to be as pronounced as in a triaxial test involving shearing.

5.5.2 Sample preparation procedure

Speswhite kaolin and Wyoming sodium bentonite were oven-dried at 105^{0} C for 24 hours. After removal from the oven, the dried material was allowed to cool in sealed containers and the kaolin and sodium bentonite were then mixed to give 10% (by weight) of sodium bentonite in the mix. De-aired water was added to the dry soil mix (to give a water content of 25%) in a domestic food mixer for 3 to 5 minutes. Large lumps of soil formed during the mixing were broken down to smaller size by a mortar and pestle. The material was then sieved through a 1.18 mm aperture sieve and the material passing through the sieve was transferred to a plastic bag. The soil retained on the sieve was again broken down with mortar and pestle and sieved, and this process was repeated until only a very small amount of soil was retained on the sieve. To avoid loss of moisture, grinding and sieving was done as quickly as possible, and generally took about 45 minutes. The plastic bag containing the sieved material was then emptied into a tray to mix the material thoroughly before transferring the soil again into the plastic bag, which was then

sealed with tape. For equalisation of moisture throughout the soil mix, the plastic bag containing the soil was stored in an airtight chamber for 7 days.

Samples were prepared in a split compaction mould (see Figure 5.5), which consisted of three sections: a top collar, a middle section, and a bottom collar. Each section was split vertically into two halves. The middle section was 100 mm high and the top and the bottom collars were for preparing overlength samples, which were then trimmed to the required height. To prepare samples of 50 mm height, a steel piece of 50 mm diameter and 50 mm height was inserted at the bottom end of the mould before assembling it. Silicon grease was applied to the inner surface of the mould to reduce friction during compaction.

Soil was poured into a tray from the plastic bag and mixed thoroughly. Six equal portions of the soil each of 51 g were prepared and kept in small sealed plastic bags to prevent loss of moisture whilst each portion of soil was compacted. A portion of soil was poured into the mould and compacted to a vertical stress of 400, 800 or 3200 kPa in a compression frame at a displacement rate of 1.5 mm per min. Before adding the next portion of soil, the surface of the compacted soil was scarified, so that there was a good bond between adjacent layers of soil and then the next portion of the soil was also compacted to 400, 800 or 3200 kPa. This procedure was repeated for all the portions of soil. The mould was released and opened to take out the sample. The steel piece, with the sample sitting on top of it, was again placed inside the middle section of the mould and then sample was trimmed to the height of the middle section using a spatula, to give a 50 mm long sample. It was easy to open the middle section of the mould without any damage to samples compacted to 400 or 800 kPa, but for samples compacted to 3200 kPa, it was difficult to open the middle section of the mould. In an attempt to open the mould the sample split apart. Samples compacted to 3200 kPa were therefore extruded from the mould and trimmed to 50 mm length. The samples were left in the ambient environment for about 30 minutes before setting up in the cell, to allow for any rapid swelling due to equalisation of pore air pressure in the body of the sample. Samples of bentonite/kaolin were prepared by static compaction to 400, 800 or 3200 kPa, whereas all samples of pure kaolin were compacted to 400 kPa only.

5.6 Testing Procedure

General features of testing procedure are described in this section, whereas the details of specific tests are reported with the test results in Chapter 6.

5.6.1 Setting up

Whilst the sample was standing for 30 minutes, the water drainage tubes were flushed with de-aired water. The drainage connections are shown schematically in Figure 5.6. For tests with drainage from the bottom of the sample only, the water drainage line incorporated valves V_1, V_2, and V_3 only. This water drainage line was extended by including the portion with valves V_4 and V_5 for tests with water drainage from both bottom and top of the sample.

Before setting up in the cell, the height of the sample was checked for any change during the standing period and then the sample was weighed. Two lengths of fuse wire (0.30 mm diameter and 30 mm long), each arranged as a semi-circle, were positioned on the acrylic ring of the high air entry filter assembly attached to the base of isotropic cell in order to temporarily prevent contact between the sample and the filter (see Section 4.3.6). The sample was carefully positioned centrally on the high air entry filter and a rubber membrane was sleeved on to the sample using a membrane stretcher. Two o-rings were then placed on the bottom end of the membrane for sealing on the pedestal. For tests with pore water drainage from the bottom face only, a low air-entry filter (50 mm diameter disc) was placed on the top of the sample followed by the acrylic top cap. For tests with pore water drainage from both top and bottom, a pair of fuse wires was placed on top of the sample, followed by the acrylic mounting ring shown in Figure 4.13 (incorporating a dry annular low air entry filter for pore air pressure control and a water-saturated central high air entry filter for pore water pressure control). The rubber membrane was then sealed on to the top cap with a second pair of o-rings. Excess rubber membrane at the top and bottom was cut off with scissors to avoid trapping any air within the folds of the membrane, which could have caused inaccuracies in the measurement of sample volume change using the double-walled cell technique.

The inner cell was assembled and the top plate of this cell was screwed into position with the help of 3 tie rods. The air vent hole in the inner cell top plate was left open, the cell was then filled with de-aired water and the vent hole was plugged when the cell was full. The top plate for the inner cell, was machined so that the air vent hole was at the highest point within the cell, to ensure that no air was trapped within the cell. The outer cell was then assembled and filled with water from the bottom with air venting from the hole in the outer cell top plate. The inner cell was connected to the sample volume change measuring device, whilst the outer cell was connected to an air water interface which was on the same air pressure line as the sample volume change measuring device. All the valves were then closed.

5.6.2 Initial equalisation stage

Valves to the inner and outer cells were opened with zero pressure applied and then the cell pressure was manually increased to 50 kPa to make the fuse wire embed into the sample so that contact was achieved between the soil and the high air entry filter. Valve V_6 (see Figure 5.6) on the air drainage line and valves V_1, V_2 and V_4 (see Figure 5.6) on the water drainage lines were opened and air back pressure and the water back pressure were manually increased to 40 kPa and 15 kPa respectively. It was important to apply a positive value of water back pressure as quickly as possible after the sample came into contact with high air entry filter, to prevent the possibility of cavitation caused by negative pressure in the water drainage connections within the cell. Readings of sample volume change and water inflow to the sample were recorded manually during this process.

Having decided on the values of mean net stress $p_c'' = \sigma_3 - u_a$ and matrix suction $s_c = u_a - u_w$ at which initial equalisation was to occur for a given test, appropriate values of cell pressure σ_3, pore air pressure u_a, and pore water pressure u_w were then selected. These target pressure values were inserted into the control software, together with the pressure ramping rate and the logging rate. After changing the stepper motor control from manual to auto, the control software was started. The cell pressure, air back pressure, and water back pressure were ramped at a relatively fast rate of about 4 kPa per minute and the targets were reached within about 2 hours, depending upon the specific target values for individual tests. The equalisation stage was then continued until the flow of water fell to 0.05 cm^3 per day, corresponding to a change of specific water volume of about 0.001 per day. The time required for equalisation varied between tests, but was generally 4 to 6 days.

5.6.3 Wetting and drying stages

Wetting and drying paths at constant mean net stress p'' were incorporated within a substantial number of tests. In these wetting or drying stages, to keep the mean net stress $p'' = \sigma_3 - u_a$ constant, cell pressure σ_3 and pore air pressure u_a were kept constant at the specified target values of these pressures using the control loop of the software. Each pressure was controlled to a precision of ±0.5 kPa. To follow a wetting path (decrease of suction) the pore water pressure u_w was increased at a specified rate to a specified value whilst the pore air pressure u_a was kept constant at its specified value. Likewise for a drying path (increase of suction), the pore water pressure u_w was decreased at a specified rate to a specified value whilst keeping the pore air pressure u_a constant. After the target value of pore water pressure for a wetting or drying path was reached, the pore water pressure within the sample was allowed to equilibrate to the applied

value of the water back pressure applied to the sample boundary. This equilibration was continued until the rate of water flow to or from the sample had reduced to 0.05 cm^3 per day.

Ideally during wetting or drying paths the water back pressure u_w should have been varied at a rate that was sufficiently slow that at any time the pore water pressure throughout the sample differed very little from the water back pressure applied to the sample boundary. If the wetting or drying were carried out at a faster rate, large changes in the volume of water within the sample as well as overall volume of the sample would occur after achieving the target value of the pore water pressure applied at the sample boundary. This feature of the soil behaviour was used to select a suitable rate of wetting/drying. For example, if the water inflow or outflow to the sample occurring after achieving the target value of the pore water pressure was low (within 10% of the total inflow or outflow during the stage), the rate was considered suitable. This was, however, not a straightforward process, given the very slow rates of wetting or drying required and the requirement of two or more wetting and drying cycles in some tests. For the first 7 tests, the pore water pressure was varied at a constant rate, which was as low as 0.8 kPa per hour in one test. At such a rate, a period of 21 days was taken to decrease the suction from an initial value of 400 kPa to a final value of 20 kPa and another 3 days were then needed for subsequent equilibration of excess pore water pressure within the sample.

During the early tests, where suction was varied at a linear rate with time during wetting or drying stages, it was observed that the magnitudes of water inflow and sample volume change occurring during a stabilisation period at the end of a test stage were much larger at the end of a wetting stage (when the suction was low) than at the end of a drying stage (when the suction was high) (see Chapter 6). This was consistent with expectations that water inflow and sample volume changes occurred non-linearly with suction, with a given magnitude of suction increment or decrement having larger influence at low suction than at high suction. This meant that, to obtain satisfactory results, it was necessary to vary suction very slowly at the end of wetting stage or the beginning of a drying stage, but that it might be possible to vary suction more rapidly when the suction magnitude was greater. It was therefore decided, in the later tests, to vary suction at a non-linear rate with time during wetting or drying stages, in an effort to shorten test duration whilst ensuring satisfactory test quality.

One possible form of non-linear suction variation would have been to vary the logarithm of suction at a linear rate with time (an appropriate course of action if it were thought that the sample response varied with the logarithm of suction). This would however have excluded the

possibility of wetting to zero suction. In the development of their elasto-plastic constitutive model Alonso *et al* (1990) avoided this difficulty by assuming that elastic volume changes caused by wetting or drying varied with the logarithm of $s + p_{at}$, where p_{at} was atmospheric pressure (see Equation 2.39). The addition of p_{at} was, however, entirely arbitrary. For the current work, it was therefore decided that it would be less arbitrary and more logical to vary the logarithm of $p'' + s$ at a linear rate with time, based on the argument that as saturated conditions are approached $p'' + s$ tends to the effective stress p' and therefore, at least at the saturated limit, the soil response might be expected to vary with the logarithm of $p'' + s$.

For wetting or drying performed at constant p'', with the logarithm of $p'' + s$ varied at a linear rate with time, then:

$$\ln(p'' + s) = \ln(p'' + s_0) + kt \tag{5.1}$$

where s_0 is the initial suction at $t = 0$ and k is a constant, with k taking a positive value during drying stages (increase of suction) and a negative value during wetting stages (decrease of suction). Rearranging Equation 5.1:

$$p'' + s = (p'' + s_0)\exp(kt) \tag{5.2}$$

Differentiating Equation 5.2, with p'' held constant, gives:

$$\frac{ds}{dt} = k(p'' + s_0)\exp(kt) \tag{5.3}$$

Inspection of Equation 5.3 shows that with $k > 0$, the magnitude of ds/dt gradually increases during a drying path, whereas during a wetting path with $k < 0$, the magnitude of ds/dt gradually decreases. Combining Equations 5.3 and 5.2:

$$\frac{ds}{dt} = k(p'' + s) \tag{5.4}$$

The control software initially had the facility only for constant rate of variation of cell pressure, air back pressure, and water back pressure with time. The software was therefore modified so that each of the pressures could be varied either at a constant or at an exponential rate, as indicated by Equation 5.3. In fact, this feature was used only for variation of water back pressure during wetting or drying stages. The absolute magnitudes of the rate of suction variation were determined by specifying the value of the constant k. A value of $k = 0.00016$ min^{-1} was used for the majority of tests in which exponential variation of suction was employed. In wetting/drying cycles at $p'' = 10$ kPa, this gave $ds/dt = 4$ kPa/hour at $s = 400$ kPa and $ds/dt = 0.1$ kPa/hour at $s = 0$ kPa (see Equation 5.4). This value of k enabled test durations to be kept within manageable

limits whilst achieving better results than that had been achieved with even the slowest constant rate of suction variation with time (see Section 6.3).

5.6.4 Loading and unloading stages

In test stages involving loading (increase of p'') or unloading (decrease of p''), the mean net stress $p'' = \sigma_3 - u_a$ was varied by changing the cell pressure σ_3, whilst the suction $u_a - u_w$ was kept constant by maintaining the pore air pressure u_a and pore water pressure u_w at specified target values.

With the double-walled cell technique of sample volume measurement, Sivakumar (1993) did not vary $\sigma_3 - u_a$ by controlling the cell pressure σ_3, because he was worried that, if he reduced σ_3 during an unloading stage, dissolved air might come out of solution as the cell pressure was reduced, and this air might affect the measurement of sample volume change. To check this aspect, two trial tests were carried out. From these tests, it became clear that dissolved air did not come out of solution during reduction of cell pressure as long as the cell pressure was kept greater than the maximum value of air pressure previously applied to the sample. By operating within this constraint the possible problem of ex-solution of air within the cell was avoided.

5.6.5 Constant volume wetting and drying stages

In two tests, wetting and drying stages were performed whilst keeping the sample volume constant. Wetting and drying involved respectively increasing or decreasing the water back pressure at a variable rate, as described in Section 5.6.3, whilst keeping the air back pressure constant. The cell pressure σ_3 was then varied by the control software as required to keep the sample volume constant. For example, a tendency for an increase in sample volume was counteracted by increasing the cell pressure (leading to an increase of $p'' = \sigma_3 - u_a$). The sample volume was held constant to an accuracy of ± 0.04 cm^3 (corresponding to a variation of specific volume of less than 0.0008). The control and logging software was modified to carry out the constant volume wetting and drying as the earlier version of the software did not have this facility. In the modified version of the software a trigger volume change value of 0.04 cm^3 was inserted, which meant that a signal was sent to the cell pressure stepper motor if the actual volume change exceeded $\pm$ 0.04 cm^3.

5.7 Use of Logged Data

For all the tests, time t, cell pressure σ_3, air back pressure u_a, water back pressure u_w, increase of sample volume ΔV, and drainage of water into the sample ΔV_w were logged at hourly intervals.

except for the first 24 hours within the equalisation stage when data were logged every 15 minutes. The data could be transferred to a floppy disc while a test was running, so that initial analysis could be undertaken with the test still in progress. This was important in view of the long duration of tests. At the start of each new stage (equalisation, wetting, drying, loading or unloading) within a test, the software needed to be re-started, but this was not a problem as it took only a few minutes. Data were updated for every stage, by combining with the data from previous stages of the test. The logged data were in *.prn file format and were compatible with any commercial spreadsheet, such as *excel*.

The mean net stress p'' and suction s at each logging point were calculated as:

$$p'' = \sigma_3 - u_a \tag{5.5}$$

$$s = u_a - u_w \tag{5.6}$$

In addition specific volume v, specific water volume v_w and degree of saturation S_r were calculated as:

$$v = \frac{V_0 + \Delta V}{V_s} \tag{5.7}$$

$$v_w = \frac{V_{w0} + \Delta V_w + V_s}{V_s} \tag{5.8}$$

$$S_r = \frac{v_w - 1}{v - 1} \tag{5.9}$$

where V_0 was the volume of the sample at the start of a stage, V_s was the volume of solids within the sample (calculated after completion of the test when the dry mass was measured), and V_{w0} was the volume of water in the sample at the start of the stage (calculated for the start of the first stage from the difference between the initial wet mass and the dry mass measured at the end of the test).

CHAPTER 6

EXPERIMENTAL RESULTS

This chapter starts with a summary of the test programme. The experimental results are then presented, with a brief initial discussion, in terms of the stress variables mean net stress p'' and suction s, which are most commonly used in constitutive modelling of unsaturated soils (see Section 2.4).

6.1 Test Programme

A summary of the tests carried out is given in Table 6.1. Out of the total of twenty controlled-suction isotropic tests, twelve involved samples of the bentonite/kaolin mix compacted under a pressure of 400 kPa, four were on bentonite/kaolin samples compacted to higher pressures (800 kPa or 3200 kPa) and four were on samples of pure kaolin (compacted to 400 kPa). The samples for all twenty tests were prepared by compacting at 25% water content as described in Section 5.5.

In all the tests samples were first allowed to equalise at a suction s_e (which varied between 0 and 400 kPa for different tests) under a given mean net stress p_e'' (which varied between 10 and 50 kPa). Subsequently the samples were taken through various different stress paths. In terms of the stress paths, the tests fell into a number of different categories, as outlined below.

Three samples of bentonite/kaolin mix compacted under a pressure of 400 kPa were subjected to wetting and drying cycles (see Tests 1, 2, and 5 in Table 6.1). In these tests, suction was varied whilst holding the mean net stress constant, as described in Section 5.6.3.

Four tests (Nos. 6, 7, 9, and 11, see Table 6.1) on bentonite/kaolin mix compacted under a pressure of 400 kPa involved loading and/or unloading, by increasing or decreasing mean net stress p'' at a constant value of suction, as described in Section 5.6.4.

Two tests (Nos. 8 and 10, see Table 6.1), on samples of bentonite/kaolin mix compacted under a pressure of 400 kPa, were designed in combination with the loading and unloading tests (Nos. 7 and 9) to study the influence of wetting and drying on subsequent loading behaviour of the samples. Tests 8 and 10 therefore involved a wetting/drying cycle followed by a loading stage.

In wetting and drying stages for the tests mentioned above, mean net stress p'' was held constant and the volume of the sample was allowed to vary. Two tests (Nos. 15 and 16, see Table 6.1) were carried out by holding the volume of the sample constant and adjusting the mean net stress during wetting and drying paths. The procedure used in carrying out the constant volume wetting and drying stages is described in Section 5.6.5.

As detailed in Table 6.1, four samples of bentonite/kaolin mix compacted to higher compaction pressures (Samples 3 and 4 under a pressure of 800 kPa and Samples 19 and 20 under a pressure of 3200 kPa) were subjected to wetting and drying cycles.

Finally, four samples of pure kaolin compacted under a pressure of 400 kPa were tested (see Tests 12, 14, 17, and 18 in Table 6.1). In two tests (Nos. 12 and 14) wetting/drying cycles were carried out at a given constant value of mean net stress. In the other two tests (Nos. 17 and 18) loading stages were carried out at a constant value of suction.

6.2 Initial Equalisation

The method of equalisation of soil samples, from an initial suction s_i to a given suction s_e and mean net stress p_e'', was common to all tests although the values of s_e and p_e'' varied for different tests. The results for the initial equalisation stage of all the tests are therefore presented together in this section. The initial equalisation stage generally took 5 days to complete.

In ten tests (Nos. 1, 6, 7, 8, 9, 10, 11, 13, 15, and 16) samples of bentonite/kaolin mix compacted to 400 kPa were equalised at a mean net stress p_e'' of 10 kPa to suctions varying between 100 and 400 kPa. Inspection of Figure 6.1 (i) shows that the specific water volume v_w increased (water flowed into the samples) for all the tests, indicating that the initial suction of the samples was higher than 400 kPa (the highest value of suction to which samples were equalised). This was confirmed by measuring the initial suction for one sample prepared by compaction under a pressure of 400 kPa. The suction was found to be higher than 1000 kPa by using an Imperial College tensiometer (Ridley and Burland (1993)). The precise value of suction could not be ascertained, because the tensiometer could not withstand suctions in excess of 1000 kPa, due to air breaking through the high air entry filter of the tensiometer. The increase in specific water volume was least for tests in which samples were equalised to a suction of 400 kPa. The results from Test No 1, appear somewhat inconsistent with the remaining tests equalised at 400 kPa suction. This was the first test to be performed, before certain aspects of procedure were standardised, and the results should therefore be treated with caution. The increase in the specific

water volume during equalisation increased as the level of suction to which the samples were equalised s_e was decreased. This, of course, simply represents the greater inflow of water as the suction is reduced further.

The specific volume v for each sample increased (see Figure 6.1 (ii)). The maximum increase in specific volume (and hence the maximum swelling) occurred for the sample that was equalised at a suction of 100 kPa and the minimum swelling occurred for samples that were equalised at the highest level of suction (400 kPa). Samples in all these tests swelled and no collapse compression occurred, which indicated that the *LC* yield curve was not reached in any of these tests during initial equalisation. The pattern of swelling response in Figure 6.1 (ii) is qualitatively consistent with the elasto-plastic models for unsaturated non-expansive clays of Alonso *et al* (1990) or Wheeler and Sivakumar (1995). The increased swelling on wetting to a suction of 100 kPa rather than a suction of 400 kPa suggests a value for the swelling index κ_s (see Equation 2.39) of approximately 0.09 (as expected, considerably higher than the value of 0.02 reported for pure speswhite kaolin by Wheeler and Sivakumar (1995).

The results for Tests 2, 5, and 16 are given in Figure 6.2. In these tests, samples of the bentonite/kaolin mix compacted under a pressure of 400 kPa were equalised at a suction of 400 kPa, but the values of mean net stress were 50, 20 and 10 kPa for Tests 2, 5, and 16 respectively. Results from these tests are used to explore the influence of the value of mean net stress on the soil response.

The specific water volume increased for all three tests (see Figure 6.2 (i)), indicating that water flowed into the samples i.e. the initial suction was greater than 400 kPa for all three cases. Inspection of Figure 6.2 (i) shows a general trend that as the mean net stress increased the amount of water inflow into the sample decreased. The inflow of water was least for Test 2 (in which the mean net stress was 50 kPa) and greatest for Test 16 (in which the mean net stress was 10 kPa).

The variation of specific volume v with time is shown in Figure 6.2 (ii). Initially, undrained reduction of specific volume v occurred as the mean net stress p'' was increased from 10 kPa to a final value of 10, 20 or 50 kPa: $\Delta v = 0$ in Test 16, $\Delta v = -0.009$ in Test 5, and $\Delta v = -0.019$ in Test 2. This undrained reduction in specific volume v is most apparent for Test 2 in which the mean net stress p'' was increased to 50 kPa (see Figure 6.2 (ii)). After this initial undrained compression, swelling occurred as water entered the sample. The amount of wetting-induced

swelling seems to decrease with increasing mean net stress p''. In the constitutive models for unsaturated non-expansive clays of Alonso *et al* (1990) or Wheeler and Sivakumar (1995) the amount of elastic swelling on wetting over a given suction range is assumed to be independent of the value of mean net stress (see Equation 2.39). The swelling response observed in Figure 6.2 (ii) appears inconsistent with this simplification, although the data are not entirely conclusive on this point, because the initial suction at the start of wetting could be different in the three tests (due to the different suction changes induced during the initial undrained loading to p'' = 10, 20, or 50 kPa). The difference in the final values of v achieved at p'' = 10 kPa and p'' = 50 kPa suggests a value of the elastic swelling index κ (see Equation 2.39) of approximately 0.040 (slightly higher than the value of 0.025 suggested by Wheeler (1996) for pure kaolin compacted under the same conditions).

For Tests 3 and 4, samples of the bentonite/kaolin mix were prepared by compacting the mix under a pressure of 800 kPa. The samples for these tests were equalised at a suction of 400 kPa, but the mean net stress was 50 kPa in Test 3 and 10 kPa in Test 4. It is clear from Figures 6.3 (i) and 6.3 (ii) that as the mean net stress increased the amount of water inflow into the sample and the amount of swelling decreased. This general trend is consistent with the trend for samples compacted under a pressure of 400 kPa (see Figures 6.2 (i) and 6.2 (ii)). The difference in the final values of v in the two tests in Figure 6.3 (ii) would suggest a κ value of approximately 0.009 (substantially less than the value of 0.040 calculated from Figure 6.2 (ii) for samples compacted to a lower pressure).

To examine the influence of compaction pressure on the soil behaviour during equalisation, the results for three Tests 4, 16, and 19 are plotted in Figure 6.4. The samples were prepared by compacting the bentonite/kaolin mix under pressures of 400, 800, and 3200 kPa for Tests 16, 4, and 19 respectively. All the samples were equalised at a suction of 400 kPa and mean net stress of 10 kPa. Inspection of Figure 6.4 (ii) shows that the initial specific volume of the samples was, as expected, a function of compaction pressure with the lowest specific volume for the sample that was compacted to the highest compaction pressure. This is consistent with the elasto-plastic models of unsaturated non-expansive clays of Alonso *et al* (1990) or Wheeler and Sivakumar (1995), with the *LC* yield curve being expanded further (producing additional plastic compression and hence lower value of v) on compaction at a higher pressure. The amount of wetting-induced swelling was fairly similar for all three samples (Figure 6.4 (ii)). The initial value of specific water volume v_w was similar in all three tests (see Figure 6.4 (i)), because all samples were compacted at the same water content of 25%. From Figure 6.4 (i) it is evident that

the final value of specific water volume v_w was lowest for the sample compacted to the highest pressure. This is, at least partly, explained by the different values of v: it would have been highly improbable in Test 19 for v_w to increase as high as it did in Test 16, because this would have implied a degree of saturation 98% (unlikely to occur at a suction of 400 kPa).

In Tests 11 and 20 samples of bentonite/kaolin mix compacted under pressures of 400 and 3200 kPa respectively were allowed to equalise at a suction of 100 kPa and mean net stress of 10 kPa. The results for these two tests are presented in Figure 6.5, which are consistent with the results for Tests 16, 4, and 19 (see Figure 6.4).

Four tests (Nos. 12, 14, 17, and 18) were carried out on samples of pure kaolin and all these samples were compacted under a pressure of 400 kPa. The variations of specific water volume v_w and specific volume v against time for Tests 12, 14, and 18 are plotted in Figures 6.6 (i) and 6.6 (ii) respectively. The results for Test 17 are not included in the figure, because of a problem in equalisation. The equalisation for this sample was not fully complete even in 15 days (whereas the equalisation in other tests was generally achieved within 5 days), indicating that there might have been imperfect contact between the ceramic filters and the sample. All the samples of kaolin were equalised at a mean net stress of 10 kPa, but suction varied from 400 to 200 kPa. Inspection of Figure 6.6 (i) shows that the specific water volume increased for all the tests, indicating that water flowed into the samples. This means that the initial suction after compaction was higher than 400 kPa for the samples of kaolin. The amount of water inflow into the samples, as expected, was higher for the sample equalised at a suction of 200 kPa than for the samples equalised at a suction of 400 kPa. From Figure 6.6 (ii), the results for Tests 12 and 14 (both brought to a suction of 400 kPa) are slightly inconsistent, showing significantly greater swelling in Test 12. Comparing the final value of v from Test 12 with the final value of v achieved in Test 18 (suction = 200 kPa) suggests κ_s value of about 0.035 (not dissimilar to the value of 0.02 reported by Wheeler and Sivakumar (1995) for speswhite kaolin), whereas comparing Test 14 with Test 18 suggests a κ_s of about 0.10 (similar to the value of 0.09 calculated for the highly expansive bentonite/kaolin mix from Figure 6.1).

6.3 Wetting and Drying Stages

In this section results from wetting/drying cycles are presented from multistage tests on samples of bentonite/kaolin mix compacted under a pressure of 400 kPa. There were six such tests (Nos. 1, 2, 5, 8, 16, and 10) that involved wetting/drying cycles at a given value of mean net stress.

The format, used for presentation of results from these tests, is explained with reference to Figure 6.7 (Test 1). Figure 6.7 (i) shows the test path in the $s : p''$ plane, indicating two complete cycles of wetting and drying performed at a mean net stress p'' of 10 kPa. Labels *a*, *b*, *c*, *d* and *e* represent start and finish points of individual test stages, presented in alphabetic order. Figures 6.7 (ii) and 6.7 (iv) show specific volume v plotted against suction s, with the suction either on a linear scale (Figure 6.7 (ii)) or a logarithmic scale (Figure 6.7 (iv)). Similarly, Figure 6.7 (iii) and 6.7 (iv) show degree of saturation S_r plotted against suction s, with s on linear or logarithmic scale.

The degree of saturation S_r is used instead of specific water volume v_w, because it is important and useful to know the relative amounts of water and air in the voids. In the results for initial equalisation (see Section 6.2), the specific water volume v_w (rather than degree of saturation S_r) was used, because v_w directly gives information about the water flow and during equalisation results it was useful to know whether water flowed into or out of the sample. The information about water flow can though be deduced by combining the results for degree of saturation with specific volume v.

In Figure 6.7 the variations of specific volume v and the degree of saturation S_r are plotted against suction s on both a linear scale (see Figures 6.7 (ii) and 6.7 (iii)) and on a logarithmic scale (see Figures 6.7 (iv) and 6.7 (v)). The semi-logarithmic plots (iv) and (v) appear to provide a clearer indication of soil behaviour. For example, on drying paths *bc* and *de* there are clear indications of yield points (represented by distinct changes of slope) and linear post-yield behaviour in Figure 6.7 (iv) whereas this behaviour is not apparent in Figure 6.7 (ii). Moreover, $v : \ln s$ plots are consistent with the commonly used $v : \ln p'$ plots for saturated soils or $v : \ln p''$ plots for unsaturated soils. The remaining results are therefore presented on semi-logarithmic plots. It should however be noted that plotting zero suction on logarithmic scale is not feasible. To avoid this problem, Alonso *et al* (1990), added atmospheric pressure p_{at} to suction s. The addition of p_{at} was arbitrary and hence is not used here.

6.3.1 Test control and rate of testing

During Test 1 the mean net stress was held constant at 10 kPa and it is satisfying to note that the control system performed very well as the mean net stress fluctuated within a narrow band of 1 kPa (see Figure 6.7 (i)). In all the subsequent tests similar quality of control was achieved (see Figures 6.8 (i) to 6.12 (i)).

Tests 1 and 2 (and also Test 3, performed on a bentonite/kaolin sample compacted to 800 kPa) were carried out with water drainage from the bottom face only of the sample. In the remaining tests water drainage from both bottom and top of the sample was used (see Section 4.4). In Test 1, the wetting/drying cycles were carried out by varying suction at a rate of 2.5 kPa/hour and the test took 68 days to complete. After achieving the suction target at the end of wetting stages *ab* and *cd* (Figure 6.7 (iii)), a significant amount of water flowed into the sample during the subsequent stabilisation period, until the rate of change of specific water volume dropped to the target value of 0.001 per day. The amounts of water that flowed out from the sample during the corresponding stabilisation periods after achieving the suction target at the end of two drying paths *bc* and *de* were much smaller. It was, however, clear that the rate of wetting and drying (2.5 kPa/hour) used in this test was unacceptably fast, because the corresponding changes in specific volume v during the stabilisation periods at the end of wetting stages were large (0.03 at end of *ab*, at a suction of 50 kPa, and 0.08 at the end of *cd* at a suction of zero, see Figure 6.7 (ii)), representing incomplete equalisation of suction within the sample during the test.

.

The rate of variation of suction in Test 2 was reduced to 1.6 kPa/hour. The test took 28 days to complete, despite the fact that only one wetting/drying cycle was performed. The rate of wetting and drying was however still not slow enough, as the change in the specific volume v during the stabilisation period at the end of wetting stage *ab*, at a suction of 100 kPa, was 0.025 (see Figure 6.8 (ii)).

In Test 3 the rate of suction variation was reduced further to 0.8 kPa/hour. One and a half cycles of wetting/drying were completed in 67 days. This rate of suction variation was considered acceptable, because the changes in the specific volume v during the stabilisation periods at the end of wetting stages were reasonably low (0.007 at the end of *ab*, at a suction of 100 kPa, and 0.025 at the end of *cd*, at suction of 10 kPa see Figure 6.27 (ii)).

In Test 4, with water drainage from both top and bottom faces of the sample, a rate of suction variation of 2.0 kPa/hour was used. It was, however, clear that this rate was again unacceptably fast because the corresponding changes in specific volume v during the stabilisation periods at the end of wetting stages were large (0.03 at end of *ab*, at a suction of 100 kPa, and 0.07 at the end of *cd*, at a suction of 10 kPa, see Figure 6.28 (ii)).

In Test 5, with double drainage, suction was varied at a rate of 1.6 kPa/hour. This rate of suction variation was considered acceptable, because the change in specific volume v during the

stabilisation periods at the end of wetting stages were reasonably low (0.006 at the end of *ab*, at a suction of 100 kPa, and 0.014 at the end of *cd*, at a suction of 10 kPa, see Figure 6.9 (ii)).

The suction was varied nonlinearly (with $k = \pm 0.00016\,\text{min}^{-1}$, as described in Section 5.6.3), to improve further the quality of results of subsequent tests that involved wetting and drying stages. The objective of improving the quality of results was achieved, with very small changes occurring in specific volume during stabilisation periods at the end of wetting or drying stages. For example, in Test 8 the change of specific volume during the stabilisation period at the end of wetting *ab* was only 0.005, at a suction of 20 kPa, (see Figure 6.10 (ii)).

6.3.2 Tests 1, 2 and 5

Tests 1, 2 and 5 involved wetting/drying cycles at mean net stress values of 10, 50, and 20 kPa respectively. These low values of mean net stress were chosen because it was intended to explore the possible existence and form of the Suction Decrease (*SD*) and Suction Increase (*SI*) yield curves proposed in the constitutive model for unsaturated expansive clays of Alonso *et al* (1994) (see Section 3.6) without approaching the *LC* yield curve.

In Test 1 (stress path shown in Figure 6.7 (i)), after equalisation at a suction of 400 kPa and mean net stress of 10 kPa, two cycles of wetting/drying (*abc*, *cde*) were carried out at a mean net stress of 10 kPa. These cycles consisted of: first wetting path *ab* with suction decreasing from 400 to 50 kPa; first drying path *bc* with suction increasing from 50 to 380 kPa; second wetting path *cd* with suction decreasing from 380 to 0 kPa; and finally drying path *de* with suction increasing from 0 to 370 kPa. In this test, during drying paths *bc* and *de* the intended suction of 400 kPa could not be achieved because of backlash in the stepper motor-controlled regulator on changing direction of loading. This problem was avoided in subsequent tests by ensuring that the regulators were never operated close to the limit of their range.

Inspection of Figure 6.7 (iv) shows that in both the wetting paths *ab* and *cd* only swelling occurred and the sample did not exhibit wetting-induced collapse compression. This suggests that in neither of these wetting paths was the *LC* yield curve reached. Figure 6.7 (iv) shows further that in first wetting *ab* there was a point at which the slope of the curve increased significantly. This could have been a preliminary indication for the existence of a *SD* type yield curve. In second wetting *cd*, there was, however, no corresponding increase in slope. Had there been an increase in slope on wetting path *cd* at a point where the suction dropped below the minimum suction of 50 kPa achieved in the first wetting *ab*, it could have been construed that

the *SD* type yield curve existed and the curve had been dragged from its previous position during the first wetting path. Given the suggestion of a possible yield point in the first wetting stage *ab*, but not in the second wetting stage *cd*, it was not possible to arrive at a definite conclusion on the existence of the *SD* yield curve from the results of Test 1.

In contrast, points of slope change were relatively clear on both the drying paths *bc* and *de* (see Figure 6.7 (iv)), indicating that a *SI* yield curve might have been reached in these paths. Another feature to be noted is that after the first cycle of wetting/drying there was net shrinkage (compare points *a* and *c* in Figure 6.7 (iv)), and the net shrinkage increased substantially after the second cycle of wetting/drying (compare points *c* and *e*). A clear trend of drying-induced irreversible shrinkage thus emerged. If the yield points identified in the two drying paths corresponded to the *SI* yield curve, then the *SI* yield curve must have been dragged down to relatively low values of suction during preceding wetting stages, by some form of coupled behaviour. Alonso *et al* (1994) argued that the downward movement of the *SI* yield curve could occur as a result of coupling to the *SD* yield curve, but the results shown in Figure 6.7 (iv) are not really consistent with this suggestion, because there is no evidence of the *SD* yield curve in wetting path *cd*.

In Figures 6.7 (iii) and 6.7 (v) the variation of degree of saturation S_r is plotted against suction s. The degree of saturation approached 1.0 when the suction was reduced to zero at the end of the second wetting *cd* (see Figure 6.7 ((iii) and (v)) and the sample remained fully saturated during the subsequent drying stage *de*. In fact, the implied values of S_r during drying stage *de* were generally slightly above 1.0 (reaching a maximum of 1.01), indicating a small measurement error. This was possibly due to flow of water into the low air entry filter on the air drainage line, because, for zero suction, the targets for pore air pressure and pore water pressure were the same. The control of suction was within ± 1 kPa, which meant that the water back pressure could have been higher by 1 kPa than the air back pressure and this could have resulted in water entering the low air entry filter. To avoid this error, in subsequent tests the applied suction was generally kept slightly above zero (see below). Inspection of Figures 6.7 (iii) and 6.7 (v) shows that the degree of saturation S_r at a given value of suction s was higher in a drying path than in the preceding wetting path. Over a full wetting and drying cycle (*abc* or *cde*) there was net increase in the degree of saturation S_r, and this increase in the degree of saturation tended to accumulate over the two cycles. This pattern of behaviour is the hydraulic hysteresis discussed in Section 2.6.

Test 2 was planned to explore the wetting and drying behaviour of the soil at a mean net stress of 50 kPa. In Test 2 (stress path shown in Figure 6.8 (i)), after equalisation at a suction of 400 kPa

and a mean net stress of 50 kPa, a cycle of wetting and drying *abc* was carried out (see Table 6.1).

Inspection of Figure 6.8 (ii) shows that during wetting path *ab* swelling occurred initially and then collapse compression started to occur. The change from swelling to collapse compression was gradual, probably because of non-uniform distribution of suction within the sample. The compression of the sample continued during the stabilisation period after achieving the target suction of 100 kPa at the sample boundary (again, an indication of incomplete equalisation of suction throughout the sample). The occurrence of collapse compression during wetting was a clear indication that the loading collapse *LC* yield curve was reached. The original objective in this test was to get further evidence for or against the existence of the *SD* yield curve. This however was not forthcoming, because of unexpectedly reaching the *LC* curve. In drying path *bc* shrinkage occurred without any indication of yielding of the soil and hence there was no evidence for the *SI* yield curve. The slope of the shrinkage path *bc* in Figure 6.8 (ii) is substantially greater than the pre-yield value of slope for drying paths *bc* and *de* in Figure 6.7 (iv), suggesting that the plastic behaviour could have been occurring throughout the drying stage in Test 2 (although the slope was lower than the post-yield slopes from the drying stages in Figure 6.7 (iv)).

Inspection of Figure 6.8 (iii) shows that the degree of saturation S_r increased in the wetting path *ab* and decreased in drying path *bc*, with S_r being higher in the drying path than in the wetting path at any given value of suction s (the occurrence of hydraulic hysteresis).

Test 5 involved wetting/drying cycles performed at a mean net stress of 20 kPa (intermediate between the values of 10 kPa and 50 kPa used in Tests 1 and 2 respectively). The stress path is shown in Figure 6.9 (i) and explained in Table 6.1.

Inspection of Figure 6.9 (ii) shows that no collapse compression occurred in wetting *ab*, suggesting that the *LC* yield curve was not reached. In the second wetting path *cd* a small amount of collapse compression occurred, suggesting that the *LC* yield curve was just reached. The change from swelling to compression was gradual and most of the collapse compression occurred during the subsequent stabilisation period (indicating non-equalisation of suction within the sample).

In Figure 6.9 (ii) there is no evidence of any sudden increase in the slope of the swelling curves during wetting stages *ab* or *cd*. This means there was no evidence for the existence of the *SD* yield curve. On the drying path *bc* (Figure 6.9 (ii)), shrinkage occurred without any marked yield point. The slope of the drying path in Figure 6.9 (ii) was similar to the corresponding drying curve in Figure 6.8 (ii) and intermediate between the pre-yield and post-yield slopes in Figure 6.7 (iv) (note the different vertical scales in the three figures), so it is possible that plastic behaviour was occurring throughout the drying stage in Test 5. A small amount of net shrinkage occurred over the full wetting/drying cycle *abc* (compare points *a* and *c* in Figure 6.9 (ii)), consistent with the suggestion that a limited amount of plastic compression occurred during drying path *bc*.

From Figure 6.9 (iii), there was evidence of a small amount of irreversibility in the curve of degree of saturation against suction (hydraulic hysteresis). The small amount of irreversibility observed in the swelling/shrinkage behaviour presented in Figure 6.9 (ii) could have been linked to this irreversibility in the variation of S_r.

6.3.3 Tests 8, 16 and 10

In each of Tests 8, 16 and 10, a wetting/drying cycle formed part of a multistage test that was aimed at exploring the influence of a wetting/drying cycle on subsequent behaviour during loading or wetting/drying at constant volume. The results for these wetting/drying cycles are presented in this section. The results for the subsequent loading/unloading stages are presented in Section 6.5 and for wetting/drying at constant volume in Section 6.6.

In Test 8 a cycle of wetting/drying was carried out, after equalisation at a suction of 300 kPa and mean net stress of 10 kPa (see Table 6.1), to study the influence of the wetting/drying cycle on the subsequent behaviour during loading. The stress path for the wetting/drying cycle is shown in Figure 6.10 (i). Inspection of Figure 6.10 (ii) shows that no collapse compression occurred in wetting path *ab* and hence the *LC* yield curve was not reached (consistent with the behaviour observed in Figure 6.7 for Sample 1, which was also tested at $p'' = 10$ kPa). The swelling of the sample continued with decreasing suction along a straight line *ab* without any indication for the existence of the *SD* yield curve. Drying-induced irreversible shrinkage occurred with some indication for yielding commencing at a suction of about 30 kPa. The slope of the post-yield drying path was clearly steeper than the slope of the swelling line *ab* and was approaching the value of the post-yield slopes of the drying paths for Sample 1 in Figure 6.7 (iv). This could be an indication for the existence of a *SI* yield curve, but for this to be the case the *SI* yield curve

would have to have been dragged from an initial position at a suction of more than 400 kPa to a position at a suction of about 30 kPa during the wetting path. Such a large coupled movement of the *SI* yield curve seems, however, unlikely, suggesting that the yielding during drying could be due to some other reason. From Figure 6.10 (iii), clear evidence emerged for irreversible behaviour of the soil in terms of degree of saturation S_r (hydraulic hysteresis).

In Test 16, a cycle of wetting and drying (see Table 6.1 and Figure 6.11 (i)) was carried out, after equalisation at a suction of 400 kPa and mean net stress of 10 kPa, to study the influence of wetting and drying on the subsequent response of the clay mix during constant volume wetting/drying. The general pattern of soil behaviour from the wetting/drying cycles of Test 16 (see Figures 6.11 (ii) and 6.11 (iii)) is consistent with the results from Test 8 (see Figure 6.10).

In Test 10 a cycle of wetting and drying was performed at a mean net stress of 10 kPa. This test began with a loading/unloading cycle *abc*, which was then followed by the wetting/drying cycle *cde* shown in Figure 6.12, before a final loading/unloading cycle *efg*. After equalisation at a mean net stress of 10 kPa and a suction of 200 kPa loading *ab* (increase of mean net stress p'' from 10 kPa to 100 kPa) and then unloading *bc* (decrease of mean net stress p'' back to10 kPa) were performed prior to wetting/drying cycle *cde*. The stress path for the wetting/drying cycle is shown in Figure 6.12 (i) and detailed in Table 6.1. The results for this cycle of wetting and drying *cde* are presented in Figure 6.12, and the results for loading/unloading stages are presented in Section 6.5.

Inspection of Figure 6.12 (ii) shows that in the wetting path *cd*, the *LC* yield curve was not reached, as no collapse compression occurred. During the wetting path *cd*, there was no suggestion of a yield point and hence no evidence of the *SD* yield curve emerged. It should be noted that no net shrinkage occurred during wetting/drying cycle *cde* (points *c* and *e* coincide in Figure 6.12 (ii)), whereas over wetting/drying cycles in other tests drying-induced irreversible shrinkage was a general feature. In fact, the volumetric response in Test 10 during wetting/drying cycle *cde* was approximately reversible (elastic) given that the vertical step at the end of wetting path *cd* was caused by incomplete equalisation of suction within the sample and the flatter section at the start of drying part *de* could have been caused by the same phenomenon. This absence of net shrinkage over a wetting/drying cycle (in contrast to other tests) could have been linked to the fact that the *LC* yield curve had been pushed out from its initial position during the loading path *ab* that preceded the wetting/drying cycle. This suggests that the drying-

induced irreversible shrinkage in the 5 tests discussed previously could have been linked in some way to the proximity of the stress path to the *LC* yield curve in these tests.

6.4 Loading and Unloading Stages

In Tests 6, 7, 9, 11, and 13 samples of bentonite/kaolin mix compacted under a pressure of 400 kPa were subjected to isotropic loading/unloading at a given value of suction. In two tests (Nos. 6 and 7) the samples were subjected to a loading/unloading cycle at a constant suction of 300 kPa, in another two tests (Nos. 9 and 13) loading/unloading was performed at a suction of 200 kPa, and in Test No. 11 the loading/unloading was conducted at a suction of 100 kPa. Results for each of these tests are presented on a common format, consisting of three plots, in Figures 6.13 to 6.17. The first plot shows the stress path followed in a test. In the second and third plots, the variations of specific volume v and degree of saturation S_r are plotted against mean net stress p'' (on a logarithmic scale). The rate of loading or unloading for all these tests was 1.5 kPa/hour. Inspection of Figures 6.13 to 6.17 shows that in all tests the suction was successfully held constant during loading or unloading with an accuracy of ±1 kPa.

The stress path for Test 6 is given in Figure 6.13 (i). The intention was to increase the mean net stress from 10 kPa to 100 kPa during loading path *ab* and then reduce the mean net stress from 100 kPa to 10 kPa in unloading path *bc* with the suction held at 300 kPa throughout. Unfortunately towards the end of loading path *ab* the air pressure in the supply line dropped, and as a consequence loading stopped at p'' = 94 kPa and the mean net stress then dropped suddenly to 75 kPa, from which point the unloading stage *bc* was started. Inspection of Figure 6.13 (ii) shows that there was a suggestion of a change in the slope of the compression curve during loading stage *ab*, corresponding to a yield point on the *LC* yield curve. Further evidence for the existence of the *LC* yield curve emerged from the results of other tests (Nos. 7, 9, 11, and 13, presented in Figures 6.14 (ii) to 6.17 (ii) respectively). Test 9 (see Figure 6.15) involved a first loading stage *ab*, from p'' = 10 kPa to p'' = 100 kPa, followed by unloading *bc* to p'' = 10 kPa, loading *cd* to p'' = 250 kPa and then unloading *de* to p'' = 100 kPa (all conducted at s = 200 kPa). During first loading *ab* the yielding was relatively gradual (see Figure 6.15 (ii)). In the subsequent unload/reload loop some small mechanical hysteresis is evident, then a fairly distinct yield point occurred during reloading at p'' = 100 kPa, corresponding to the maximum mean net stress previously applied.

Inspection of Figures 6.15 ((iii) shows that the degree of saturation S_r varied elasto-plastically with p'' and followed a general (although reverse) pattern to that observed in the $v : \ln p''$ plot (compare Figures 6.15 (ii) and (iii)).

The compression curves for Tests 7, 9, 11, and 13 are plotted in Figure 6.18. Test 13 was a repeat test for the first loading stage of Test 9 and it is satisfying to note that the repeatability was good. For each of these tests, there was a clear indication that the soil yielded as the mean net stress was increased. The yield points were rather vague (compared to re-loading as in Test 9), suggesting a difference between the yield behaviour after compaction and the yield behaviour after loading in a triaxial cell, perhaps caused by non-uniform distribution of stresses within the sample in the compaction process resulting in a more gradual process of subsequent yielding. As expected, Figure 6.18 shows that the location of the post-yield normal compression line varied with suction, with the normal compression lines for higher values of suction lying above those for lower values of suction (consistent with the occurrence of collapse compression on wetting of samples loaded to virgin states). The slopes of the normal compression lines for suction of 100, 200 and 300 kPa appear very similar (as reported for pure speswhite kaolin by Sivakumar (1993)).

Values of yield stress were estimated from Figure 6.18 by the method of intersection of two straight lines. The value of yield stress increased with increasing suction. The estimated values of yield stress corresponding to each test (at a given suction) are plotted in the $s : p''$ plane in Figure 6.19. By joining the yield points for tests at different values of suction the initial location of the LC yield curve is sketched for the bentonite/kaolin mix compacted under a pressure of 400 kPa. Also shown in Figure 6.19 is the LC yield curve for pure kaolin compacted under a pressure of 400 kPa, as reported by Sivakumar (1993). The LC yield curve for the bentonite/kaolin mix lies to the left of the LC yield curve for pure kaolin, indicating that the same compaction procedure seems to have expanded the LC yield curve by different amounts in two different soils.

Collapse compression occurred during wetting in Test 2 (see Figure 6.8 (ii)), in which a wetting/drying cycle was performed at $p'' = 50$ kPa. Inspection of Figure 6.19 suggests that at $p'' = 50$ kPa, the LC yield curve would be reached at a suction of about 140 kPa, which is broadly consistent with the results from Test 2, although the change from swelling to collapse compression was gradual, which makes the precise comparison hard.

6.5 Influence of Wetting and Drying on Loading Behaviour

Tests 8 and 10 were designed in combination with Tests 7 and 9 to study the influence of wetting/drying on subsequent behaviour of the bentonite/kaolin mix during isotropic loading. Test 8 differed from Test 7 only in that an additional wetting/drying cycle *abc* was carried out in the former whereas no wetting/drying cycle was involved in the latter. The stress path for Test 8 is shown in Figure 6.20 (i). After equalisation at a suction of 300 kPa and mean net stress of 10 kPa, wetting/drying cycle *abc* was performed before loading stage *cd* in which the mean net stress p'' was increased from 10 kPa to 175 kPa. The results for the wetting/drying cycle *abc* have already been presented in Section 6.3.3 (see Figure 6.10). The compression curve for loading stage *cd* is given in Figure 6.20 (ii), which shows that the soil yielded with increasing mean net stress. The value of yield stress of 70 kPa was obtained by intersection of two straight lines. This yield point corresponds to a point on the *LC* yield curve.

To understand the influence of wetting/drying cycle *abc* on the subsequent loading behaviour in Test 8 the results for the loading stages of Tests 7 and 8 are presented together in Figure 6.21. Assuming that the repeatability between the two tests was within acceptable limits, the difference in the response of the two samples during the loading stage can be attributed to the preceding wetting/drying cycle *abc* that was performed in Test 8. The initial value of specific volume in Test 7 was 2.27. In Test 8 the initial value of specific volume was 2.26 and then the specific volume v decreased to 2.09 in the wetting/drying cycle *abc*. Figure 6.21 (i) shows that the yielding was gradual in both tests and given the level of uncertainty created by this, it was difficult to say whether the value of the yield stress had been affected by the additional wetting/drying cycle in Test 8. Any influence on the yield stress was, however, relatively small. The results do however suggest that the post-yield compression curves were significantly different for Tests 7 and 8. This is inconsistent with the model of Alonso *et al* (1994), which would predict that the substantial irreversible (plastic) compression that occurred during the preceding wetting/drying cycle in Test 8 would result in a significant increase in the yield stress observed during subsequent constant suction loading, but the post-yield compression curves would then be predicted to be the same for Test 7 and 8. Figure 6.21 (ii) shows that the degree of saturation was substantially higher during the loading stage of Test 8 than in the corresponding stage of test 7 (due to the net increase of S_r in the preceding wetting stage), and the difference in compression behaviour observed in Figure 6.21 (ii) may therefore be linked to this difference in S_r.

In Tests 9 and 10 the problem of accurately identifying a yield point during a gradual yielding process was reduced by fixing the yield points more precisely by performing a loading/unloading cycle at the start of each of the tests. The stress path for Test 10 is shown in Figure 6.22 (i). After equalisation at a suction s of 200 kPa and mean net stress p'' of 10 kPa, loading ab was performed by increasing mean net stress from 10 kPa to 100 kPa followed by unloading bc back to a mean net stress of 10 kPa. After this loading/unloading abc, wetting cd from a suction of 200 kPa to a suction of 20 kPa and then drying de from suction of 20 kPa to a suction of 200 kPa were completed before the final loading ef in which the mean net stress was increased from 10 kPa to 250 kPa. Finally the sample was unloaded fg to a mean net stress of 10 kPa. Test 9 differed from Test 10 only in that the wetting/drying cycle cde was omitted from the former.

The results for the wetting/drying cycle cde of Test 10 have already been presented in Section 6.3.3 (see Figure 6.12). The results for loading and unloading stages are given in Figure 6.22 (ii), which shows that the soil gradually yielded in the first loading ab with increasing mean net stress. In subsequent unloading bc the sample swelled along a typical swelling line bc. During wetting/drying cycle cde there was no net shrinkage (point c and point e coincide in Figure 6.22 (ii)). In the second loading ef the soil yielded with increasing value of mean net stress. The compression curve for Test 10 (see Figure 6.22 (ii) indicates that the effect of wetting and drying was to shift the yield point to lower value of about 80 kPa (whereas the yield stress prior to wetting/drying cde was 100 kPa, fixed by the loading ab). The variation of degree of saturation S_r against mean net stress p'' is given in Figure 6.22 (iii), which shows that the degree of saturation increased with increasing value of mean net stress. The points c and e are different in Figure 6.22 (iii) because the degree of saturation of the sample increased during the wetting/drying cycle cde although there was no net volume change.

To understand the influence of wetting/drying cycle cde, in more detail, on the subsequent loading behaviour, the results for loading stages of Tests 9 and 10 are presented together in Figure 6.23. Inspection of Figure 6.21 (i) shows that the yield stress on re-loading was slightly reduced in Test 10 and the post-yield compression curves for the two tests were initially slightly different, with a steeper slope in Test 9 than in Test 10. The post-yield compression curves finally began to merge together after loading to a mean net stress of about 200 kPa.

Clearly the soil behaviour in Tests 9 and 10 was different to that observed in Tests 7 and 8. This could be linked to the fact that there was significant net shrinkage during wetting/drying

in Test 8, but not in Test 10. The soil behaviour in Test 10 is still not consistent with the model of Alonso *et al* (1994), which would predict the same yield stresses in Tests 9 and 10. The values of S_r during re-loading are very different in Tests 9 and 10, and this may explain the observed difference in yielding behaviour.

6.6 Constant Volume Wetting and Drying

Tests 15 and 16, involving wetting and drying under constant volume conditions, were performed with the purpose of:

1. Exploring the soil response during wetting/drying at constant volume.
2. Studying the influence of a previous cycle of wetting/drying at constant p'' on the response of soil during subsequent constant volume wetting/drying.

In Test 15, equalisation at a suction of 400 kPa and mean net stress of 10 kPa was followed by loading *ab* from mean net stress of 10 to 40 kPa. Wetting *bc* from a suction of 400 to 20 kPa and drying *cd* from 20 to 55 kPa were then carried out while keeping the volume of the sample constant by allowing the mean net stress to vary. In Test 16 after equalisation at a suction of 400 kPa and mean net stress of 10 kPa, a cycle of wetting/drying (see path *abc* in Figure 6.11), involving variation of suction from 400 to 20 and then back to 400 kPa, was completed, before loading the sample along path *cd* from mean net stress of 10 to 40 kPa. The additional wetting/drying cycle *abc* was carried out in the normal way, with p'' held constant and the sample volume free to vary. With the sample at a suction of 400 kPa and a mean net stress of 40 kPa, wetting *de* from a suction of 400 to 20 kPa and then drying *ef* from 20 to 105 kPa were carried out by holding the volume of the sample constant and allowing the mean net stress to vary. In terms of stress paths the only difference between Tests 15 and 16 was, therefore, that an additional wetting/drying cycle (see *abc* in Figure 6.11) at constant p'' was completed in Test 16. The results of the final constant volume wetting and drying stages for Tests 15 and 16 are presented in this section.

The results for Test 15 are given in Figure 6.24. Inspection of Figure 6.24 (i) shows that the volume of the sample was held constant within a very narrow band ($\Delta v = \pm 0.0008$). From Figure 6.24 (ii), it emerges that, during wetting *bc*, the mean net stress initially remained almost unchanged (p'' at about 40 kPa) as the suction was decreased from 400 kPa to about 240 kPa and then p'' marginally increased to about 43 kPa before finally beginning to decrease (reaching a value of 20 kPa at the end of wetting at $s = 20$ kPa). The decrease in the mean net stress started at a suction of about 220 kPa. This decrease in mean net stress with decreasing suction suggests

that wetting-induced collapse compression had commenced, which was compensated by swelling resulting from a decrease in the mean net stress. This implies that, had the mean net stress been held constant during this wetting, the sample would have begun to collapse at a suction of about 220 kPa, indicating that the *LC* yield curve had been reached. The trend of decreasing mean net stress continued during the stabilisation period after achieving the target suction of 20 kPa at the end of the wetting path. In subsequent drying the mean net stress continued to decrease, indicating the sample had a tendency to shrink due to drying, which was counterbalanced by the swelling resulting from the decrease in mean net stress. It is useful to compare the trend from this test with the results of Test 2 (see Figure 6.8) in which wetting was carried out at a constant mean net stress of 50 kPa (fairly similar to the initial mean net stress in Test 15 of 40 kPa). The sample in Test 2 initially swelled by a small amount and then started to collapse, and this collapse compression continued during the stabilisation period. Shrinkage occurred during subsequent drying. This means that these two tests produced a consistent pattern, and it is useful to know that the collapse compression feature of the soil behaviour is verifiable from two different types of tests.

From the results of Test 16 in Figure 6.25 (ii), it emerges that during wetting *de* the sample mean net stress initially increased from 40 kPa at a suction of 400 kPa to 70 kPa at a suction of 100 kPa, suggesting that the sample would have swelled if the mean net stress had been held constant. This indicates that the *LC* yield curve had not yet been reached. From a suction of about 100 kPa the mean stress began to decrease (suggesting that the *LC* yield curve had been reached) finally reaching a value of 40 kPa at the end of wetting when the suction was 20 kPa. The collapsing tendency of the sample continued during the rest period, after achieving the target suction of 20 kPa. The continued reduction of p'' during the drying stage *ef* was evidence of the normal tendency to shrink on drying.

To compare the response of the samples in Tests 15 and 16, results for the constant volume wetting and drying stages of the two tests are plotted together in Figure 6.26. The main differences were that Test 16 showed a much more substantial increase in p'' during the early stages of wetting than Test 15 and the onset of the reduction in p'' is substantially delayed in Test 16. This is equivalent to saying that Test 16 showed much greater tendency for swelling in the early stages of wetting and the onset of collapse compression was significantly delayed. This would be consistent with *LC* yield curve having been pushed out significantly in Test 16 as a consequence of the irreversible shrinkage occurring during the preceding wetting/drying cycle.

6.7 Influence of Compaction Pressure

Four Tests (Nos. 3, 4, 19 and 20) were carried out on bentonite/kaolin samples compacted under pressures higher than 400 kPa. The samples for Tests 3 and 4 were prepared under a compaction pressure of 800 kPa, whereas the compaction pressure was 3200 kPa for Tests 19 and 20. The intention of higher compaction pressures was to push the *LC* yield curve out so that the existence of the *SD* and *SI* yield curves could be investigated without reaching the *LC* yield curve and to explore whether net swelling occurred during wetting/drying cycles, as reported by authors such as Chu and Mou (1973), if the wetting/drying cycles occurred well inside the *LC* yield curve.

The stress path for Test 3 (sample compacted to 800 kPa) is shown in Figure 6.27 (i) and explained in Table 6.1. Inspection of Figure 6.27 (ii) shows that no collapse compression occurred in wetting paths *ab* and *cd*, indicating that the *LC* yield curve was not reached. Furthermore, no yielding occurred in either of the wetting paths to indicate existence of the *SD* yield curve. Interestingly, the volumetric response in wetting/drying cycle *abc* was almost reversible with no net shrinkage or swelling (compare points *a* and *c* in Figure 6.27 (ii)). This means there was no evidence for the existence of the *SI* yield curve. From Figure 6.27 (iii), hydraulic hysteresis was evident, with the degree of saturation showing a net increase over the wetting/drying cycle *abc*.

The stress path for Test 4 (on a sample compacted to 800 kPa) is shown in Figure 6.28 (i) and detailed in Table 6.1. Interpretation of the results from Test 4 is hampered by the fact that the test was conducted rather fast, resulting in substantial non-equalisation of suction within the sample, as indicated by the large changes of v and S_r occurring during the stabilisation period at the end of wetting stages (as discussed in Section 6.3.2).

Inspection of Figure 6.28 (ii) shows that in both the wetting paths *ab* and *cd* only swelling occurred and the sample did not show collapse compression. This suggests that the *LC* yield curve was not reached in these wetting paths. Another feature to be noted is that after the first cycle of wetting and drying (*abc*) there was a small amount of net shrinkage (compare points *a* and *c* in Figure 6.28 (ii)). There was no indication of yielding in either of the wetting paths *ab* or *cd*. This means there was no evidence to support the existence of a *SD* yield curve. Likewise in drying *bc* there is no clear evidence for the existence of a *SI* yield curve.

Hydraulic hysteresis was evident from Figure 6.28 (iii). The final degree of saturation approached unity at the end of wetting *cd*, suggesting that the sample became almost fully saturated although the suction was at 10 kPa.

The stress path for Test 19 is shown in Figure 6.29 (i) for a bentonite/kaolin sample compacted to a pressure of 3200 kPa. After equalisation at a suction of 400 kPa and mean net stress of 10 kPa, the intention was to have wetting path *ab* from a suction of 400 to a suction of 100 kPa and then a drying path back to a suction of 400 kPa. During drying, however, air broke through one of the high air entry filters and therefore the drying path *bc* was terminated at a suction of 175 kPa.

In the wetting path *ab* (see Figure 6.29(ii)) only swelling occurred and this suggests that in this wetting path the *LC'* yield curve was not reached. Moreover there was no yielding in the path *ab*, to suggest the existence of a *SD* yield curve. Although drying could not be completed there was a suggestion of net swelling over a wetting/drying cycle, in contrast to the net shrinkage over a wetting/drying cycle observed for the majority of the bentonite/kaolin samples compacted to a pressure of 400 kPa (see, for example, Section 6.3). From Figure 6.29 (iii) a general pattern of hydraulic hysteresis was again evident, with a net increase of S_r over a wetting/drying cycle.

With some indication for net swelling over a wetting/drying cycle from Test 19, it was considered useful to explore this aspect further in another test on a second sample of bentonite/kaolin compacted to 3200 kPa. The stress path for Test 20 is shown in Figure 6.30 (i) and explained in Table 6.1. Inspection of Figure 6.30 (ii) shows that in the wetting path *ab* only swelling occurred, which means that in this path the *LC'* yield curve was not reached. With no indication for yielding in the wetting path *ab*, there was no evidence to suggest the existence of a *SD* yield curve. Net swelling occurred over the wetting/drying cycle *abc*. This means that for a wetting/drying cycle well inside the *LC'* yield curve net swelling occurred. It is noted that for samples of the bentonite/kaolin mix compacted under a pressure of 400 kPa, net shrinkage occurred over a wetting and drying cycle (see Section 6.3). This suggests that both the contrasting types of soil behaviour reported by Alonso *et al* (1995) and Chu and Mou (1973) can therefore occur on the same soil material.

Inspection of Figure 6.30 (iii) shows that at the end of wetting *ab* the degree of saturation approached unity, indicating that sample became fully saturated and in the subsequent drying the sample remained saturated.

6.8 Tests on Kaolin

Tests on non-expansive clay were needed to find out which features, if any, of the behaviour of highly expansive clays were different from the behaviour of non-expansive clays, and possible ways of taking into account these additional features within a constitutive model. With a mixture of bentonite and kaolin being tested as a highly expansive clay, pure kaolin was considered appropriate as a typical non-expansive clay.

A relatively short duration test (No. 12) was carried to ascertain the appropriate rate of wetting and drying for kaolin. After equalisation at a suction of 400 kPa and mean net stress of 10 kPa the sample was wetted from a suction of 400 to a suction of 100 kPa and then dried again to a suction of 400 kPa. The stress path for the test is shown in Figure 6.31 (i). An exponential rate of wetting was selected, as described in Section 5.5.3, with $k = -0.00049\,\text{min}^{-1}$ (three times faster than the value of k selected for testing bentonite/kaolin samples) for wetting path *ab*. During drying path *bc* a value of $k = +0.00024\ \text{min}^{-1}$ was selected (i.e. half that selected for wetting), because the step change in specific volume v during the stabilisation period at the end of the wetting path was considered too large at 0.02 (see Figure 6.31 (ii)) indicating that the wetting was carried out at an unacceptably fast rate. Although the rate of drying *bc* was decreased in comparison to the rate for wetting *ab*, the step increase in specific volume during the stabilisation period at the end of drying was still considered rather large, at 0.008 (see Figure 6.31 (ii)). In view of this, it was decided for subsequent tests to adopt the same variable rate of wetting and drying for kaolin that was used for the samples of bentonite/kaolin mix ($k = \pm 0.00016\,\text{min}^{-1}$).

The stress path for Test 14 is shown in Figure 6.32 (i) and explained in Table 6.1. No stabilisation period was possible after final wetting *ef* because of a power shut down in the lab. The results for Test 14 are presented in Figure 6.32. Prior to looking into these results it should be noted that the location of the *LC* yield curve identified by Sivakumar (1993) for pure speswhite kaolin was shown in Figure 6.19. Given this position of the *LC* yield curve, it was expected that the wetting and drying paths for Test 14 (mean net stress of 10 kPa) would be entirely within the *LC* yield curve. Inspection of Figure 6.32 (ii) shows that no collapse compression occurred in any of the wetting paths *ab*, *cd*, or *ef*, which confirmed that the *LC* yield curve was not reached in any of the stress paths. Furthermore, there was no point at which the slope of the swelling curve suddenly increased in any of the wetting paths (*ab*, *cd* and *de*). In fact wetting paths *cd* and *de* were parallel straight lines. There was therefore no evidence to

suggest the existence of a *SD* yield curve. Since the wetting and drying paths did not reach the *LC* yield curve, the models of Alonso *et al* (1990) and Wheeler and Sivakumar (1995) for non-expansive clays would suggest elastic behaviour. Inspection of Figure 6.32 (ii), however, shows that the volumetric behaviour of kaolin was irreversible in cycles of wetting/drying. In the first wetting/drying cycle *abc*, there was net shrinkage, as point *c* lies below point *a*. In the second wetting/drying cycle *cde* (over a slightly greater suction range), the net shrinkage of the sample was three times larger than the shrinkage in the first wetting/drying cycle. Inspection of drying paths *bc* and *de* shows no dramatic points of slope change and it is unclear whether plastic straining was occurring throughout the drying paths in order to produce the net shrinkage over each wetting/drying cycle.

Figure 6.32 (iii) shows small increase of S_r over each wetting/drying cycle. This is the hydraulic hysteresis reported in Section 6.3 for tests on samples of the bentonite/kaolin mix and previously discussed in Section 2.6. The irreversibility of variation of specific volume discussed above might be linked to this hydraulic hysteresis.

Tests 17 and 18 were aimed at studying the influence of wetting and drying on loading behaviour of kaolin. In Test 17, after equalisation of the sample at a suction of 200 kPa and mean net stress of 10 kPa, isotropic loading to p''= 300 kPa was carried out while holding the suction constant at 200 kPa. In Test 18, after equalisation of the sample at suction of 200 kPa and mean net stress of 10 kPa, a wetting/drying cycle was performed, with the suction decreased from 200 kPa to 20 kPa and then increased again to 200 kPa, prior to loading the sample while holding the suction constant at 200 kPa.

The results for the loading path carried out in Test 17 are presented in Figure 6.33. From Figure 6.33 (ii), it is clear that the *LC* yield curve was reached in this loading path *ab*. The variation of S_r with increase of p'' (see Figure 6.33 (iii)) seems to follow an elasto-plastic pattern, similar to the variation of v.

As pointed out above, Test 18 was similar to Test 17, but involved an additional wetting/drying cycle before the loading stage. The results for the wetting/drying stage are presented in Figure 6.34. With no collapse compression occurring in wetting path *ab* (see Figure 6.34 (ii)), it was clear that the *LC* yield curve was not reached. Furthermore, no evidence emerged for yielding during wetting, suggesting no indication of a *SD* yield curve. Over the wetting/drying cycle *abc* there was small amount of net swelling (compare point *a*

and c in Figure 6.34 (ii)). From Figure 6.34 (iii) there was again evidence for irreversibility in the variation of degree of saturation S_r, with a small net increase over the wetting/drying cycle.

Results from the isotropic loading stage cd that followed the wetting/drying cycle abc in Test 18 are given in Figure 6.35. From Figure 6.35 (ii), it is clear that the kaolin sample started to yield with increasing mean net stress p'' and the LC yield curve was reached in the loading path cd.

To understand the effect of a wetting/drying cycle on the subsequent behaviour of kaolin during loading, compression curves for Tests 17 and 18 are plotted together in Figure 6.36. Following the small amount of net swelling in the preceding wetting/drying cycle in Test 18, the yield stress during loading for Test 18 was slightly lower than the corresponding value in Test 17 (about 85 kPa instead of about 100 kPa). The post-yield curves were virtually identical for the two tests. This pattern of behaviour, observed for non-expansive kaolin, is actually qualitatively consistent with predictions of the model of Alonso *et al* (1994) for highly expansive clays, slightly in contrast to the behaviour of bentonite/kaolin samples shown in Figures 6.14 and 6.20.

6.9 Conclusions

From the results presented in this chapter some important conclusions emerged that are worth noting briefly at this stage:

- The existence of the LC yield curve was confirmed for both bentonite/kaolin and pure kaolin clays. The occurrence of both collapse compression in wetting paths and yielding of the soil in loading paths was verified. The results from constant volume wetting/drying tests provided further evidence for the existence of the LC yield curve.
- For both types of clay there was no evidence to support the existence of the SD type of yield curve (wetting-induced swelling occurred without any sharp increase in the rate of swelling with decreasing suction) proposed in the models for unsaturated highly expansive clays of Gens and Alonso (1992) and Alonso *et al* (1994).
- For samples of bentonite/kaolin mix compacted under the lowest pressure of 400 kPa, wetting/drying cycles inside the LC yield curve produced net shrinkage during each cycle. This net volume reduction over a wetting/drying cycle is similar to the pattern reported for highly expansive Boom clay by Alonso *et al* (1995).
    1. Sometimes the net shrinkage over a wetting/drying cycle was accompanied by evidence of yielding during the drying stage, in other cases there was no evidence of a yield point

(suggesting, perhaps, that irreversible (plastic) shrinkage strains were occurring throughout the entire drying stage).

2. Although the occurrence of irreversible shrinkage during drying stages could be construed as evidence of an *SI* yield type curve (as proposed in the model of Alonso *et al* (1994)) the location of the onset of plastic behaviour (either right at the start of a drying stage or early in a drying stage) was inconsistent with the model of Alonso *et al* (1994), because in the model the *SI* yield curve can only be dragged down some distance behind the *SD* yield curve during wetting.

- On bentonite/kaolin samples compacted to 3200 kPa, during wetting/drying cycles there was a net volume increase over each wetting/drying cycle. This is similar to the pattern of behaviour reported for a highly expansive soil by Chu and Mou (1973).
- This means that both net shrinkage over a wetting/drying cycle and net swelling over a cycle can occur with same soil. This type of behaviour could, in theory, be represented by the model of Alonso *et al* (1994), but highly complex coupling relationships would be required between the *SI*, *SD*, and *LC'* yield curves (see Section 3.6.2) and distinct yield points would be predicted during each wetting and drying path (in contrast to the observed behaviour).
- Irreversibility in volumetric behaviour occurs over subsequent cycles (not just the first cycle). Yield points were never observed during both drying and wetting stages of the same cycle, as would be required in the model of Alonso *et al* (1994) if irreversible behaviour were to continue during subsequent cycles.
- The degree of saturation S_r varied significantly between wetting and drying stages and S_r generally showed a net increase over each wetting/drying cycle. There is therefore the possibility that net shrinkage or swelling over a cycle may be linked to the irreversible variation of S_r (hydraulic hysteresis). The hydraulic hysteresis is not included in the existing elasto-plastic models for highly expansive or non-expansive soils (see Section 2.10.3).
- Net shrinkage or swelling over a wetting/drying cycle remaining inside the *LC'* yield curve was also observed for samples of kaolin (a non-expansive or moderately expansive clay) so that the irreversible behaviour was not restricted to highly expansive clays.
- The existing elasto-plastic models for non-expansive clays, such as Alonso *et al* (1990) or Wheeler and Sivakumar (1995) account for the wetting-induced collapse compression and yielding during loading very well. Various other features of observed behaviour, such as irreversibility in wetting/drying paths within the *LC'* yield curve cannot be represented by these models. Although the elasto-plastic models for unsaturated highly expansive clays

suggested by Gens and Alonso (1992) and Alonso *et al* (1994) do predict irreversible behaviour during wetting/drying cycles inside the *LC* yield curve, the detailed form of behaviour predicted is not consistent with experimental observations.

- Given that the observed irreversibility of shrinkage or swelling may be linked to the irreversible variation of S_r (hydraulic hysteresis), it would be worth considering new constitutive modelling approaches employing alternative stress variables, as described in Section 2.5.

CHAPTER 7

DISCUSSION AND CONSTITUTIVE MODELLING

The experimental results were presented in Chapter 6 without detailed interpretation and discussion. Moreover the results were presented in terms of mean net stress p'' and suction s, which are most commonly used in constitutive modelling of unsaturated soils. It was, however, evident in Section 6.9 that some important features of unsaturated soil behaviour cannot be explained within the framework of existing constitutive models that are developed in terms of mean net stress p'' and suction s. In this chapter, selection of appropriate stress variables is re-examined, before presenting a new conceptual model. The patterns of soil behaviour are explained in the new conceptual framework and experimental results are briefly re-examined to assess the performance of the new model .

7.1 Features of Unsaturated Soil Behaviour

The patterns of unsaturated soil behaviour that emerged from the experimental results were summarised in Section 6.9. The behaviours of highly expansive (bentonite/kaolin mix) and non-expansive (pure kaolin) clays were found to be similar in many respects, suggesting that a suitable unified modelling framework could be feasible for both non-expansive and highly expansive unsaturated soils. The occurrence of irreversible volume changes during wetting/drying cycles inside the LC yield curve, even for pure kaolin, indicated that there are important features of unsaturated soil behaviour that cannot be represented by the current form of the existing elasto-plastic models for non-expansive soils of Alonso *et al* (1990) and Wheeler and Sivakumar (1995). In addition, the precise forms of irreversibility appear inconsistent with the elasto-plastic models for highly expansive soils proposed by Gens and Alonso (1992) and Alonso *et al* (1994). Furthermore, there was a suggestion that some of the observed irreversibility of volumetric behaviour during wetting/drying cycles might be linked to the occurrence of hydraulic hysteresis in the variation of degree of saturation S_r. This hydraulic hysteresis is not included in the existing elasto-plastic models for non-expansive soils or highly expansive soils. This means that the modelling approach for unsaturated soils needs a fundamental re-examination.

7.2 Selection of Suitable Stress State Variables

In Section 2.4, it was pointed out that the single effective stress approach does not work for unsaturated soils, and an additional stress variable is required to account for the influence of

suction within meniscus water on the soil behaviour. In Section 2.5, the link between possible stress variables and conjugate strain parameters was outlined. From the point of view of work input considerations, several alternative combinations of stress variables are possible (see Section 2.5). One such set of stress variables, for isotropic loading, is the mean net stress p'' and suction s. Although the mean net stress p'' and suction s have been most commonly used in elasto-plastic models for unsaturated soils, certain features of soil behaviour are difficult to represent by such constitutive models: for example, the observed forms of irreversibility in volumetric behaviour during wetting/drying paths.

A particular omission of the existing elasto-plastic models, defined in terms of p'' and s, is to take any account of the influence of hydraulic hysteresis on the stress-strain behaviour. As described in Section 2.6, two samples of the same soil, at the same suction but one on a drying curve and the other on a wetting curve, would have different values of S_r and hence would be expected to exhibit different mechanical properties, because of the different proportions of bulk water and meniscus water in the samples. The influence of degree of saturation S_r on mechanical behaviour should therefore be included in any rigorous model, and this is not possible with an elasto-plastic constitutive model defined solely in terms of p'' and s. This shortcoming of existing models is likely to be most important during stress paths involving reversals or cycles of suction, and may not be apparent in tests involving only monotonic variation of suction (such as the tests of Sivakumar (1993)). The occurrence of cyclic wetting and drying of unsaturated soils is, however, very common in the field. This means that accounting for the behaviour of these soils in wetting/drying cycles is crucially important if constitutive models are to be of practical use.

The importance of hydraulic hysteresis is most strongly apparent during transition between saturated and unsaturated conditions, and this is therefore an aspect of behaviour that is modelled particularly badly by existing models. In constitutive models developed in terms of mean net stress p'' and suction s, it is normally assumed that suction of zero uniquely corresponds to a degree of saturation of unity, whereas in practice during drying from a fully saturated state a finite value of suction s_{ae} (the air entry value) must be applied at the soil boundary before S_r drops below 1. Proper modelling of this feature would require sudden discontinuities of yield curve shape in a model defined in terms of p'' and s. The shape of the LC yield curve is considered in Figure 7.1, for a soil drying from saturated state and then subsequently wetted, to illustrate the difficulty of correctly modelling transition between saturated and unsaturated conditions. Figure 7.1 (i) shows the required shape of yield curve

during the process of drying from a fully saturated condition, with point A representing the isotropic yield stress for the initial saturated condition. It should be noted that until the applied suction reaches the air entry value s_{ae}, the sample will remain saturated and the behaviour of the soil would be controlled by the mean effective stress p', which can be expressed in terms of mean net stress p'' and suction s as:

$$p' = p - u_w = (p - u_a) + (u_a - u_w) = p'' + s \tag{7.1}$$

The yield curve up to the air entry point B (see Figure 7.1 (i)) is therefore a straight line inclined at 45^0 to the p'' axis, corresponding to a constant value of $p'' + s$. The yield value of p'' therefore decreases with increasing suction while the soil remains saturated. In contrast, as soon as the soil becomes unsaturated, experimental evidence shows that the yield value of p'' increases with increasing suction (see BC' in Figure 7.1 (i)), consistent with the stabilising effect of meniscus water at inter-particle contacts in unsaturated soil. With progressive desaturation of the voids, an increasing number of particle contacts would be influenced by meniscus water, which in turn would lead to further increase in the yield stress.

Clearly a yield curve of the shape shown in Figure 7.1 (i) would be rather complicated to model. Worse still, as soon as desaturation occurs the yield curve shape would suddenly change from that shown in Figure 7.1 (i) to that shown in Figure 7.1 (ii), because the soil would now remain unsaturated on wetting right down to zero suction. This requirement of a sudden change of yield curve shape would be extremely difficult to model.

To remove the above outlined deficiencies of the constitutive models developed in terms of mean net stress p'' and suction s, there is need to re-examine the use of appropriate combinations of stress variables. Alternative sets of stress variables were discussed in Section 2.5 and one of the various possible combinations, for isotropic stress states, is given by the following expressions:

$$p^* = p - S_r u_w - (1 - S_r) u_a \tag{7.2}$$

$$s^* = ns \tag{7.3}$$

Houlsby (1997) showed that the strain increment parameters conjugate to the stress variables p^* and s^* (defined by Equations 7.2 and 7.3), are the volumetric strain increment $d\varepsilon_v$ and the decrement of degree of saturation $-dS_r$ respectively. The strain increment parameter $-dS_r$ conjugate to the stress variable s^* is readily integrable; an advantage over models defined in

terms of p'' and s, where the strain parameter $d\varepsilon_v$ (see Equation 2.15) conjugate to s is not integrable.

In Section 2.2, it was pointed out that the effects of pore water pressure in bulk water and meniscus water on the soil behaviour are qualitatively different. In developing constitutive models, it is therefore important to recognise this distinction. The stress variable p^*, defined in Equation 7.2, is likely to represent the influence of applied total stress, pore air pressure, and pore water pressure within bulk water, assuming that the weighted pore pressure can be based simply on the relative proportions of voids occupied by air and bulk water (and assuming that the volume of meniscus water is negligible). The variable p^* reduces to effective stress for saturated soil ($S_r = 1$) and dry soil ($S_r = 0$). It should be noted that in the set of stress variables p'' and s, the mean net stress $p'' = \left(p - u_a\right)$ does not necessarily reduce to effective stress $p' = \left(p - u_w\right)$ when the soil becomes saturated (given that a soil can be fully saturated even when a non-zero value of suction is applied to the soil boundary).

Although the stress variable p^* is expected to include the influence of pore water pressure within bulk water, it cannot represent the influence of pore water pressure within meniscus water. Initial expectations would therefore be that the influence of suction within meniscus water must be represented by the second stress parameter s^* (see Equation 7.3)

The forms of LC' yield curves during drying from a saturated state and then subsequent wetting, in terms of the stress variables p^* and s^*, are shown schematically in Figures 7.2 (i) and 7.2 (ii). During drying from a saturated state the LC' yield curve is a vertical straight line up to the air entry value s^*_{ae} (see Figure 7.2 (i)), because for a saturated soil ($S_r = 1$), p^* reduces to conventional effective stress and hence the yield value of p^* does not change with increasing suction, while the soil remains saturated. After the air entry value of the soil has been exceeded, some voids desaturate and the particle contacts begin to be influenced by meniscus water. This means that, as s^* is increased with increasing suction, beyond s^*_{ae}, the yield value of p^* would be expected to increase with increasing s^*, as shown schematically in Figure 7.2 (i). The LC' yield curve during subsequent wetting is shown schematically in Figure 7.2 (ii). Once again there has to be a sudden change of yield curve shape (compare Figures 7.2 (i) and 7.2 (ii)), because the soil now remains unsaturated right down to zero suction. Therefore, it is not immediately apparent that the new choice of stress parameters has resulted in any significant improvement in

the modelling of transition between saturated and unsaturated conditions. This aspect is explored further in the next section.

7.3 Conceptual Model in Terms of New Stress Variables

A qualitative framework, for isotropic conditions, in terms of stress variables p^* and s^* is outlined in this section, whereas predictions from the model are explored in Section 7.4.

In Section 2.9, the influence of suction in meniscus water on inter-particle forces was analysed. The analysis showed that, for idealised spherical particles of radius R, the additional normal component of inter-particle force ΔN_s, arising from the presence of meniscus water at inter-particle contacts, varies with s (or s^*) in the manner shown by the solid curve ABC' in Figure 7.3. If a given inter-particle contact becomes influenced by meniscus water rather than bulk water (as adjacent voids dry out) at zero suction (and hence at zero s^*), the value of ΔN_s immediately takes a value of $4\pi TR/3$ (see Section 2.9.1), represented by point B in Figure 7.3. On subsequent increase of suction (or s^*) the value of ΔN_s tends to a limiting value of $2\pi TR$ (C' in Figure 7.3), which is only 50% greater than the corresponding value at zero suction. Furthermore, in practice, voids will actually empty of bulk water at finite values of suction, so that a lens of meniscus water will form at a given inter-particle contact at a finite value of suction rather than at zero suction. This means that the variation of ΔN_s with suction at a given inter-particle contact will actually vary in the manner shown by the solid line $ADEC'$ in Figure 7.3. As a first approximation, therefore, the variation of ΔN_s can be represented by the idealised dashed line $ADFC'$ in Figure 7.3, where the value of ΔN_s is zero until the lens of meniscus water forms and then assumed to be constant with increasing suction (or s^*) from then on. This approximation, that the value of ΔN_s is unaffected by suction once the meniscus water forms, is likely to be even more applicable to platy particles than to spherical particles (as shown by the analysis in Section 2.9.2).

The argument presented above suggests that the influence of meniscus water (arising from the occurrence of additional inter-particle normal forces) is likely to be controlled predominantly by the proportion of particle contacts affected by meniscus water, and not by the actual values of suction within these menisci. This suggests that the role of meniscus water on mechanical behaviour is likely to be dominantly a function of degree of saturation S_r, rather than s^*. The LC' yield curve would therefore be expected to be a straight vertical line in the $s^*:p^*$ plane (over the full range of s^*, not just saturated conditions), but degree of saturation S_r will act as a hardening parameter. An increase of S_r suggests a decrease in the stabilising effect of menisci, and hence an

inward movement of the yield curve (see Figure 7.4), with a decrease of S_r producing a corresponding outward movement of the yield curve. These movements of the yield curve produced by changes of S_r occur even if the stress state is well inside the yield curve, and do not correspond directly to any occurrence of plastic strains.

The form of the *LC* yield curve in the $S_r : p^*$ plane is shown schematically in Figure 7.5. The soil behaviour in any test path inside the *LC* yield curve would be reversible (elastic), whereas a test path reaching the *LC* yield curve would result in the onset of plastic strains. The shape of the *LC* yield curve shown in Figure 7.5 represents an increase in the yield value of p^* with decreasing degree of saturation, indicating the stabilising effect of meniscus water on yielding of the soil. The dotted *LC* yield curves in Figure 7.5 represent the expansion of the original yield curve due to plastic compression of soil occurring once the yield curve is reached. The transition between saturated and unsaturated conditions, at $S_r = 1$, is handled completely smoothly with a yield curve presented in the $S_r : p^*$ plane, with none of the problems that occur with yield curves described in either the $s : p''$ plane (see Figure 7.1) or the $s^* : p^*$ plane (see Figure 7.2).

The yield curves presented in Figure 7.5 are not shown extending down to a degree of saturation of zero (dry conditions). In analysing the influence of meniscus water on the additional normal component of inter-particle force ΔNs (see Figure 7.3) it was assumed that as s^* tends to infinity, and S_r tends to zero, the lens of meniscus water tends to an infinitesimally small size, but does not disappear completely. In consequence, it was calculated that ΔNs tended asymptotically to a finite limiting value as s^* tended to infinity (see Figure 7.3). In practice, however, there would come a point at which the inter-particle contact would dry out completely, and ΔNs would suddenly drop to zero for that contact. The *LC* yield curve shown in Figure 7.5 should, at very low values of S_r, therefore show a rapid drop of p^* with decreasing S_r, with the yield value of p^* dropping to the saturated value once more at $S_r = 0$ (given that p^* represents the mean effective stress p' for $S_r = 1$ and $S_r = 0$). This expected drop in the yield value of p^* at very low values of S_r, and the corresponding transition to fully dry conditions, could be of importance in unsaturated sands, but is unlikely to be of practical importance in unsaturated clays, because the values of suction at which this would occur would be extremely high in clays.

If the influence of meniscus water (arising from the additional inter-particle normal forces) is controlled by the value of S_r rather than by the value of the stress parameter s^*, then, logically, the component of elastic strains attributable to meniscus water effects is likely to be a function of

changes of S_r, rather than changes of s^*. Elastic strains, under isotropic stress conditions, are therefore likely to be the result of changes of p^* (representing the influence of applied total stress, pore air pressure and pore water pressure within bulk water) and changes of S_r (the meniscus water effect), with compressive elastic volumetric strains caused by an increase of p^* or a decrease of S_r.

Degree of saturation S_r has clearly become an important parameter in the proposed stress-strain framework. The final component of the proposed framework would be to link S_r to s^* by means of a hysteretic soil-water characteristic relationship, of the type illustrated in Figure 7.6. Authors from Soil Science, such as Mualem (1974, 1977), have proposed hysteretic soil-water characteristic relations, but expressed in terms of S_r and suction s. These authors tend, however, to assume an incompressible soil skeleton (n = constant), so in their case values of s could be converted to corresponding values of s^* by a simple scaling. In the proposed new framework it would appear logical to use s^*, rather than s, as the stress parameter for the soil-water characteristic curve, because s^* is conjugate to $-dS_r$ in a work input equation expressed in terms of p^* and s^*.

The proposal, for a deformable soil, of a hysteretic relationship between S_r and s^*, rather than between S_r and s, is supported by experimental data from Sivakumar (1993). Sivakumar performed a variety of different types of constant suction shearing (fully drained, constant p'' or constant v), as illustrated in Figure 7.7. For the fully drained and constant p'' shearing, the porosity n varied during shearing and, as a consequence, s^* varied even though suction s was maintained constant. In these tests, it was observed that the degree of saturation S_r varied significantly during shearing (see Figure 7.7). In contrast, for tests involving shearing at constant v (and hence n) s^* was held constant, and it was observed in these tests that the degree of saturation remained approximately constant (see Figure 7.7).

Summarising the overall form of proposed constitutive framework for isotropic conditions, the stress variables are p^* and s^*, and the corresponding strain variables are volumetric strain ε_v and S_r, but the basic elasto-plastic stress-strain model relates volumetric strains to changes of p^* and S_r (rather than s^*), with S_r then related to changes of s^* through a coupled hysteretic model for the soil-water characteristic curve.

Assuming that the behaviour of a saturated soil can be adequately represented by the Modified Cam Clay model, the yield surface for an unsaturated soil can be extended to triaxial stress

conditions in $q : p^* : S_r$ space, as shown schematically in Figure 7.8. Inspection of Figure 7.8 clearly indicates that the size of the elliptical yield curves grows with decreasing degree of saturation S_r.

7.4 Qualitative Performance of the New Modelling Framework

In this section the performance of the new modelling framework is assessed by examining qualitative features of behaviour that would be predicted by the new framework, and comparing these with observations from the experimental tests. The subsequent section then sets out the various equations that would be required in order to develop the proposed framework to a full mathematical model.

7.4.1 Elastic cycles of wetting and drying

The LC yield curve in $S_r : p^*$ plane represents a boundary inside which the soil response (in terms of volumetric strains) is expected to be reversible (elastic), whereas any test path which reaches the LC yield curve would give rise to irreversible (plastic) volumetric strains. For example, consider path ABC in Figure 7.9 (i), in which a sample is wetted at a constant value of p^*, by increasing the degree of saturation S_r, from A to B and then dried (a decrease of S_r) back to point C. In Figure 7.9, points A and C represent the same values of p^* and S_r. The expected volumetric response of the soil is sketched in Figure 7.9 (ii). During wetting AB the sample swells, due to the elastic increase in volume caused by the decrease of S_r (representing only the meniscus water effect), and in the subsequent drying BC shrinkage occurs. Over the full cycle of wetting and drying there is no net change in the volume of the sample, indicating that the soil response remains fully reversible (elastic). Likewise in a loading/unloading path (variation of p^*) inside the LC yield curve, a closed test path in the $S_r : p^*$ plane would be expected to produce no net change in sample volume.

The next step is to consider a more conventional wetting/drying cycle conducted at a constant value of mean net stress p'', with suction s varied over a specified range. Such wetting/drying cycles, in which p'' was held constant, were performed in several experimental tests (see Table 6.1). Figure 7.10 (i) shows the stress path ABC for such a wetting/drying cycle plotted in the $s : p''$ plane. The corresponding soil-water characteristic curve in the $S_r : s^*$ plane is shown in Figure 7.10 (ii). During wetting AB the suction s, and hence s^*, decreases and the degree of saturation S_r shows a corresponding increase. During subsequent drying BC the degree of saturation S_r falls again, but because of the hysteretic nature of the soil-water characteristic curve the value of S_r at any point during drying is greater than at the same value of s^* during the

preceding wetting (see Figure 7.10 (ii)). The final suction s at point C' is identical to the initial value at point A, but the final value of s^* is likely to be slightly different to the initial value, because a net change of sample volume over the cycle (see below) corresponds to a change of porosity n.

Figure 7.10 (iii) shows the test path plotted in the $S_r : p^*$ plane. During wetting AB the degree of saturation S_r increases and inspection of Equation 7.2 shows that the stress variable p^* decreases, because both S_r and u_w increase, which means that the term $S_r u_w$ increases more than the decrease of $(1 - S_r)u_a$, giving a net decrease of p^*. During drying BC', S_r decreases and p^* increases. At point C', at the end of drying, S_r is higher than the initial value at point A (because of the effects of hydraulic hysteresis, see Figure 7.10 (ii)). Rearrangement of Equation 7.2 shows:

$$p^* = p'' + S_r s \qquad (7.4)$$

Hence the net increase of S_r between A and C' also implies a net increase of p^* (given that p'' and s each have identical values at A and C'), as shown in Figure 7.10 (iii). It is clear from Figure 7.10 (iii) that in the $S_r : p^*$ plane the path followed during drying is different to that followed during wetting, and there are net changes of both S_r and p^* over the cycle.

Figure 7.10 (iv) shows the predicted variation of specific volume v during the wetting/drying cycle, plotted against suction s. For stress paths remaining inside the LC' yield curve (which is now plotted in the $S_r : p^*$ plane, as shown in Figure 7.10 (iii)), elastic swelling occurs during wetting AB (due to the reduction of p^* and the increase of S_r) and elastic compression (shrinkage) during drying BC'. In the $v : s$ plot the wetting and drying paths, however, do not coincide, even though the behaviour is essentially elastic, because the test paths followed in $S_r : p^*$ plane are different during wetting and drying, and it is the variables S_r and p^* which are now assumed to control the development of volumetric strain. At the end of the cycle at C' the value of p^* is greater than the initial value at A, and this would suggest an elastic decrease of specific volume v over the cycle. In contrast, however, the degree of saturation S_r shows a net increase over the cycle, and this would suggest a net elastic increase of v (the component of elastic volume change arising from the meniscus water effect). Overall, therefore, there could be either a net increase or a net decrease of v over the cycle (as indicated by the two possible drying paths BC' in Figure 7.10 (iv)), depending upon which of the two components of the elastic change of v is the larger. Porosity n could therefore show either a net increase or a net decrease over the cycle, and hence the stress parameter $s^* = ns$ could show either a net increase or net

decrease for a wetting/drying cycle performed over a fixed range of suction s (see Figure 7.10 (ii)).

The soil behaviour during multiple wetting/drying cycles, performed at a constant value of mean net stress p'', and with the test path in the $S_r : p^*$ plane remaining within the LC' yield curve for all cycles, is illustrated in Figure 7.11. The pattern of soil behaviour in wetting/drying cycles after the first cycle is broadly similar to the behaviour in first cycle. The irreversible volumetric behaviour can continue over a number of wetting/drying cycles (not just the first wetting/drying cycle) (Figure 7.11 (iv)), because in each cycle the drying path in the $S_r : p^*$ plane is different to the preceding wetting path (see Figure 7.11 (iii)), as a consequence of the hysteretic nature of the $S_r : s^*$ relationship (Figure 7.11 (ii)). If all the wetting/drying cycles are performed over the same range of suction, the amount of irreversible volume change occurring over a cycle would be expected to decrease over each subsequent cycle. Ultimately the test path should tend to a closed hysteretic loop in the $S_r : s^*$ plane and hence in the $S_r : p^*$ and $v : s$ planes.

In the proposed new elasto-plastic framework the mechanism described above (and sketched in Figures 7.10 and 7.11) is the only means by which net increases of v could occur over a wetting/drying cycle. This would explain the net swelling over a wetting/drying cycle reported by Chu and Mou (1973) (see Figure 3.10). It would also explain the results observed in Tests 19 and 20 of the current experimental programme. For example, Figure 7.12 shows results from Test 19 in terms of the new stress and strain variables.

Prior to discussing the results of Test 19, shown in Figure 7.12, it is useful to note the format in which experimental results are presented in this chapter. Six plots are used (see, for example, Figure 7.12). The first four plots (i, ii, iii, iv) are laid out in such a way that the two axes of a plot are common to other plots. This layout is useful in gaining an overall picture by being able to project from one plot to another. Plot (i) shows the test path in the $S_r : p^*$ plane. A logarithmic scale is used for p^* in this plot, and therefore the qualitative appearance of the test path and the LC' yield curve may be different to that sketched in Figures 7.10 and 7.11 (which assume a linear scale). Plot (ii) gives the soil-water characteristic curve in the $S_r : s^*$ plane. The variation of specific volume v is plotted against p^* and s^* in plots (iii) and (iv) respectively. Finally the stress path in the $s^* : p^*$ plane and the strain path in $S_r : v$ plane are given in plots (v) and (vi) respectively.

In Test 19, a sample of bentonite/kaolin compacted under a pressure of 3200 kPa was subjected to a wetting/drying cycle at $p'' = 10$ kPa (this was not a complete cycle of wetting and drying, because the suction was decreased from 400 kPa to 50 kPa during wetting *ab*, but then increased back to only 175 kPa during drying *bc*). The test paths in the $S_r : p^*$ plane (see Figure 7.12 (i)) presumably, remained inside the *LC'* yield curve, which had been pushed out by a substantial amount during the compaction under a high pressure of 3200 kPa. As expected, in terms of the new modelling framework, in the $S_r : p^*$ plane the test paths in wetting and drying are different (see Figure 7.12 (i)). This is a consequence of hydraulic hysteresis in the $S_r : s^*$ relationship, as illustrated in Figure 7.12 (ii). From Figures 7.12 (iii) and 7.12 (iv), clear evidence for net swelling over the wetting/drying cycle emerged, which is consistent with the prediction from the new modelling framework. The wetting and drying stress paths in the $s^* : p^*$ plane (see Figure 7.12 (v)) are almost indistinguishable from each other. This is due to the fact that an increase in p^* in the drying path (relative to a point at the same suction in the wetting path), due to the higher value of S_r in the drying path, is accompanied by an increase in s^* due to the increased porosity n during drying. Hence the point simply moves further up the stress path in the $s^* : p^*$ plane. The fact that in the $s^* : p^*$ plot (Figure 7.12 (iv)) the wetting and drying stages follow similar paths whereas in the $S_r : p^*$ plot (Figure 7.12 (i)) they follow different paths, reinforces the suggestion that the volumetric behaviour (which clearly follows different paths during wetting and drying, see Figure 7.12 (iii) and 7.12 (iv)) is fundamentally linked to S_r and p^* rather than s^* and p^*. A similar pattern of behaviour emerges from Test 20 (see Figure 7.13).

The mechanism described above (and sketched in Figure 7.10) could also explain the occurrence of net decreases of v over a wetting/drying cycle. Net decreases of v could, however, also be the result of yielding on the *LC'* yield curve occurring either during the wetting path (see Section 7.4.2) or during the drying path (see Section 7.4.3).

7.4.2 Yielding during wetting

Wetting-induced collapse compression is a fundamental feature of unsaturated soil behaviour. It would therefore be useful to examine the capabilities of the new modelling framework to represent collapse compression behaviour. If a test path reaches the *LC'* yield curve during wetting, plastic strains begin to occur. For example, consider path *AB* in Figure 7.14, in which a wetting stage is performed at a constant value of mean net stress p''. The wetting path is plotted in Figure 7.14 (i) in the $s : p''$ plane. The corresponding soil-water characteristic curve in the $S_r : s^*$ plane is sketched in Figure 7.14 (ii). During wetting *AB*, suction s, and hence s^*, reduces

and the degree of saturation S_r increases correspondingly. The wetting path is shown in the $S_r : p^*$ plane in Figure 7.14 (iii) and the volumetric response is shown in Figure 7.14 (iv). The initial position of the LC yield curve is shown by LC_i (see Figure 7.14 (iii)). During wetting from point A to Y the sample undergoes elastic swelling as shown in Figure 7.14 (iv). At point Y the LC yield curve is reached, and with further wetting from point Y to point B collapse compression occurs as shown in Figure 7.14 (iv) and the LC yield curve is expanded to a new position LC_B in the $S_r : p^*$ plane (Figure 7.14 (iii)).

Figure 7.15 shows the results from Test 2, in which a sample of bentonite/kaolin compacted under a pressure of 400 kPa was subjected to a wetting/drying cycle at a mean net stress of 50 kPa (see Table 6.1). Wetting and drying paths (ab and bc) are shown in the $S_r : p^*$ plane in Figure 7.15 (i). Hydraulic hysteresis is clearly evident in the $S_r : s^*$ plot in Figure 7.15 (ii). During wetting ab the sample initially swells before exhibiting collapse compression from a value of s^* of about 150 kPa (see Figure 7.15 (iv)). The possible initial location of the LC yield curve (LC_i) is sketched in the $S_r : p^*$ plane in Figure 7.15 (i), together with the possible subsequent location of the curve at the end of wetting (LC_b).

The representation of wetting-induced collapse compression by the new modelling framework does not represent an advance over previous constitutive models, because this feature is well accounted for by the existing elasto-plastic constitutive models for non-expansive soils, such as the models of Alonso *et al* (1990) or Wheeler and Sivakumar (1995). The capability of any new framework to model collapse compression is however an important test.

7.4.3 Yielding during drying

The possibility of yielding during drying is examined in this section. A test involving a wetting/drying cycle performed at a constant value of mean net stress p'' is considered. Wetting and drying paths AB and BC are shown in the $s : p''$ plane in Figure 7.16 (i). The corresponding hysteretic relationship between degree of saturation S_r and the stress variable s^* is shown schematically in Figure 7.16 (ii). Test paths in the $S_r : p^*$ plane are given in Figure 7.16 (iii), which also shows the movement of the LC yield curve. The volumetric response of the soil is sketched in Figure 7.16 (iv). During wetting AB, the LC yield curve is not reached (see Figure 7.16 (iii)) and therefore only elastic swelling occurs (see Figure 7.16 (iv)). During subsequent drying from point B to Y elastic shrinkage occurs, because this portion of the drying path lies inside the LC yield curve. With further drying beyond point Y, plastic compression occurs as the

LC yield curve is pushed out from its initial position LC_i to a new position shown by LC_e in Figure 7.16 (iii).

From Figure 7.16, it is evident that the new modelling framework can represent the occurrence of yielding during the drying stage of a wetting/drying cycle without accompanying yielding occurring during the preceding wetting stage, whereas according to the model of Alonso *et al* (1994) yielding on the *SI* curve during drying should be preceded by yielding on the *SD* curve during the previous wetting stage. Furthermore the new modelling framework can predict yielding during drying over a number of wetting/drying cycles and not just the first cycle. In multiple wetting/drying cycles each subsequent drying stage can produce additional plastic compression (corresponding to further expansion of the LC yield curve), because of progressive increases in S_r over several cycles, arising from the hysteretic nature of the soil-water characteristic curve in the S_r:s^* plane (see Figure 7.17). The amount of additional drying-induced plastic compression should decrease with each subsequent cycle, with the compression curve gradually converging to a closed hysteretic loop (see Figure 7.17 (iv)), corresponding to a closed hysteretic loop on the soil-water characteristic curve (see Figure 7.17 (ii)).

The mechanism outlined above and sketched in Figures 7.16 and 7.17 can explain the occurrence of net shrinkage over a wetting/drying cycle with yield points evident during drying stages. This fits with the oedometer results on a highly expansive clay presented by Alonso *et al* (1995) (see Figure 3.11). It would also explain the results observed in many of the tests within the current experimental programme. For example, results for Test 1 are shown in Figure 7.18. In this test a sample of bentonite/kaolin compacted under a pressure of 400 kPa was subjected to two complete wetting/drying cycles at p'' = 10 kPa (see Table 6.1). Inspection of the test path in the S_r:p^* plane (Figure 7.18 (i)) shows that it is quite conceivable that the LC yield curve was reached during each of the drying stages *bc* and *de*, consistent with the strong suggestion from the volumetric response (Figure 7.18 (iv)) of yield points during both drying stages. The possible initial and subsequent locations of LC yield curve are sketched in Figure 7.18 (i). Similar behaviour is shown for Test 8 in Figure 7.19.

If net shrinkage occurs over a wetting/drying cycle but there is no clear evidence of a yield point during the drying stage, this could indicate two different possibilities: either plastic behaviour is occurring throughout the entire drying stage (so that the yield point corresponds to the very start of the stage) or the net shrinkage may be solely as a result of elastic effects, as described in Section 7.4.1. Test results where net shrinkage over a cycle occurs but where yield points during

drying are either absent or inconclusive include Test 14 on pure kaolin (see Figure 7.20). Inspection of the magnitude of compression occurring during drying stages of such tests may indicate whether the behaviour during drying is likely to involve plastic straining throughout or is likely to be exclusively elastic behaviour.

According to the new modelling framework, yielding on drying could easily occur during a drying stage immediately following a wetting stage in which wetting-induced plastic collapse compression occurred. Therefore the drying stage *bc* in Test 2 (see Figure 7.15) could correspond to either plastic shrinkage or elastic shrinkage. The sketched positions of *LC* yield curve, in Figure 7. 15 (i), suggest that plastic behaviour is likely.

7.5 Equations Required for a New Model

In the previous section some of the qualitative patterns of behaviour emerging from the proposed new framework were described and compared with experimental results. This section describes the forms of equation that would be required in order to develop the framework to a full mathematical model. No attempt has been made to develop explicit constitutive equations or to present quantitative predictions of soil behaviour that could be compared with experimental data. This has been left for a later stage in the development of this work.

An elasto-plastic constitutive model fitting the proposed new framework would consist of two coupled components:

- an elasto-plastic stress-strain model, similar to that proposed by Alonso *et al* (1990) or Wheeler and Sivakumar (1995), but with mean net stress p'' replaced by p^* and the role of suction s replaced by degree of saturation S_r,
- a hysteretic model for the soil-water characteristic curve, linking S_r to the stress parameter s^* (including the full history of the variation of s^*, not just the current value).

Assuming isotropic elastic behaviour, the increment of elastic volumetric strain $d\varepsilon_p^e$ would be related to the increments of p^* and S_r. A possible form of equation would be:

$$d\varepsilon_p^e = \frac{\kappa dp^*}{vp^*} - a dS_r \qquad (7.5)$$

where κ is the conventional saturated elastic swelling index and a would involve a new soil constant and a function of the stress state variables. The elastic shear strain increment $d\varepsilon_q^e$ would be given by:

$$d\varepsilon_q^e = \frac{dq}{3G} \tag{7.6}$$

where G is the elastic shear modulus.

For isotropic stress states the LC yield curve would be defined by an expression relating the yield value of p^* to the corresponding isotropic yield stress under fully saturated conditions p^*_{0sat} and the degree of saturation S_r:

$$f\left(p^*, S_r, p^*_{0sat}\right) = 0 \tag{7.7}$$

Assuming that the model tends to Modified Cam Clay at the saturated limit, the hardening law would relate changes of p^*_{0sat} to the plastic volumetric strain increment $d\varepsilon_p^p$ by:

$$\frac{dp^*_{0sat}}{p^*_{0sat}} = \frac{v}{\lambda_{sat} - \kappa} d\varepsilon_p^p \tag{7.8}$$

where λ_{sat} is the virgin compression index for $S_r = 1$ (termed $\lambda(0)$ in the existing models).

Equations 7.8 and 7.5 would predict an isotropic normal compression line for saturated conditions ($S_r = 1$) with a slope λ_{sat} in the $v : \ln p^*$ plane:

$$v = N_{sat} - \lambda_{sat} \ln p^* \tag{7.9}$$

where N_{sat} is an additional soil constant defining the intercept of the saturated normal compression line. There would also be unique normal compression lines in $v : \ln p^*$ plane for other values of degree of saturation S_r. The form of these could be predicted by combining Equations 7.5 and 7.9, using a procedure analogous to that employed by Wheeler and Sivakumar (1995) (described in Section 2.10.2).

The LC yield curve expression of Equation 7.7 could be extended to anisotropic stress states by inclusion of deviator stress q, to define a yield surface in $p^* : q : S_r$ space (as sketched in Figure 7.8):

$$f\left(p^*, q, S_r, p^*_{0sat}\right) = 0 \tag{7.10}$$

A flow rule, defining the ratio of plastic strain increments $d\varepsilon_q^p / d\varepsilon_p^p$ in terms of the current soil state, would complete the definition of the elasto-plastic stress-strain component of the overall constitutive model. This would also result in the prediction of a unique critical state line for each value of S_r in the $q : p^*$ plane and the $v : p^*$ plane.

The second component of the overall model would consist of a hysteretic soil-water characteristic relationship, linking S_r to s^*, as illustrated by Figure 7.6. Various authors from Soil

Science, such as Mualem (1974, 1977) have suggested possible mathematical forms for such a relationship (albeit these proposals were expressed in terms of s rather s^*).

The form of hysteretic relationship can be reduced to defining a unique "primary drying curve", for drying from a fully saturated state, (see curve AB in Figure 7.6) and a unique "primary wetting curve", for wetting from the driest possible state, (see curve CD in Figure 7.6). Any other drying curve, starting at a lower value of S_r (such as Y in Figure 7.6), can then be predicted as a suitably scaled version of the virgin drying curve. Similarly, wetting curves, such as YZ in Figure 7.6, take the form of suitably scaled versions of the virgin wetting curve.

The two components of the overall model would be cross-coupled. If the variation of s^* were known, the hysteretic soil-water characteristic relation could be used to calculate the variation of S_r, which would then feed into the elasto-plastic stress-strain component of the model. In general, however, the variation of suction s, rather than s^*, would be specified. The volumetric strains from the elasto-plastic model would therefore be required in order to calculate the variation of porosity n and hence the variation of s^*, for input into the hysteretic soil-water characteristic equation. Clearly, because of this cross-coupling, the equations arising from both components of the model would need to be solved simultaneously, rather than consecutively.

7.7 Future Testing Requirements

Given the form of the proposed constitutive modelling framework, revised forms of laboratory testing would be useful in the future. In particular, it would be useful to conduct tests in which the variables p^* and S_r were each controlled either to remain constant or to vary in a specified fashion. For example, in order to validate more conclusively a fundamental principle of the proposed framework, that the LC yield curve is uniquely defined in the $S_r : p^*$ plane, rather than in terms of some alternative combinations of stress variables or stress and strain variables, it would be useful to conduct pairs of tests of the type illustrated in Figure 7.21. Figure 7.21 shows one sample loaded by increasing p^* while holding S_r constant along test path AB, to identify a yield point on the LC yield curve. A second sample, with identical history, could then be subjected to a constant p^* wetting/drying cycle ACD, with the degree of saturation at D equal to the initial value at A, before constant S_r loading along DE. If the two samples yielded at similar values of p^*, this would be a strong indication of a unique yield curve in the $S_r : p^*$ plane. Figure 7.21 (ii) shows the wetting/drying cycle for the second sample in the $S_r : s^*$ plot, indicating that the two samples would be at very different values of s^* during final loading. Similarly, the two

samples would have very different values of s during loading, as shown by the stress paths sketched in the $s : p''$ plane in Figure 7.21 (iii).

Once the proposed modelling framework had been validated and developed to a full mathematical model, tests in which the variables p^* and S_r were each varied in turn, whilst holding the other variable constant, would also be ideal for measuring the values of the various soil constants within the model. Tests of this type could be performed with the type of computer-controlled equipment described in Chapter 4, with suitable changes to the control software. Variation of p^* at constant S_r could be achieved by increasing or decreasing cell pressure σ_3 (in order to vary p^*) whilst continuously calculating S_r (by combining measurement of sample volume change and measurement of water outflow from the sample) and adjusting u_w (and hence s) so as to maintain S_r constant. Similarly, variation of S_r at constant p^* would most easily be achieved by varying u_w (and hence s) to produce a change of S_r, whilst continuously calculating S_r and adjusting σ_3 so as to maintain p^* constant.

7.7 Comparison with Other Models

Most of the developments in constitutive modelling of unsaturated soils over the last 30 years have used net stress $\sigma - u_a$ and suction $s = u_a - u_w$ as stress state variables. Several authors have, however, put forward proposals involving alternative stress state variables, as summarised by Wheeler and Karube (1996), and a few of these suggested use of a stress variable of the form:

$$\sigma^* = \sigma - S_r u_w - (1 - S_r) u_a \qquad (7.11)$$

Corresponding to one of the stress variables in the current proposal.

Bishop (1959) was, of course, the first to suggest use of a stress variable similar to that given by Equation 7.11, because his proposal for the effective stress in an unsaturated soil (see Equation 2.3) converts to the stress variable of Equation 7.11 if it is assumed that $\chi = S_r$. Bishop, however, proposed that the soil behaviour could be described solely in terms of his single effective stress, whereas the current proposal includes an additional stress variable s^* which influences the soil behaviour via a hysteretic relationship linking s^* and S_r (which then feeds into the stress-strain model).

Bolzon *et al* (1996) developed a constitutive model (which happened to be in the form of a generalised plasticity model) in terms of σ^* and suction s. The work of Houlsby (1997) suggests that this would form an acceptable set of stress variables (in terms of a work input equation) and

the strain increment variable conjugate to s would be $-ndS_r$. This strain increment variable has the disadvantage of not being integrable.

Jommi and di Prisco (1994) proposed an elasto-plastic constitutive model in terms of σ^* and degree of saturation S_r: the same variables as involved in the current proposals. They then assumed, however, a unique soil-water characteristic equation relating S_r to suction s, rather than any form of hysteretic soil-water characteristic relationship. The model of Jommi and di Prisco (1994) therefore reverts to one expressed in terms of σ^* and s.

The unique features of the current proposal are that a model has been developed in terms of σ^* and s^*(which provides particularly simple conjugate strain increment variables), and that the influence of s^* is expressed via a hysteretic relationship between S_r and s^*, with degree of saturation S_r then feeding into the elasto-plastic component of the constitutive model. This latter feature enables the influence of hydraulic hysteresis on the stress-strain behaviour to be incorporated (including the otherwise difficult transition between saturated and unsaturated conditions).

CHAPTER 8

CONCLUSIONS AND RECOMMENDATIONS

Previous researchers had suggested that the behaviour of unsaturated highly expansive clays was fundamentally different to that of unsaturated non-expansive clays, and that the constitutive models developed for unsaturated non-expansive clays were inappropriate for highly expansive clays. Given the high cost of damage to buildings, structures and roads caused by unexpected ground movements associated with unsaturated highly expansive clays and the increasing use of compacted expansive clays for engineered barriers for environmental protection and other purposes, it was considered important to investigate further the behaviour of these soils.

This final chapter covers the main conclusions of the research described in this thesis, together with recommendations for future work on the behaviour of unsaturated soils.

8.1 Conclusions

The programme of research described in this thesis has provided considerable insight into the behaviour of unsaturated soils. In the following sections, conclusions from various aspects of this research are summarised.

8.1.1 Conceptual aspects of unsaturated soil behaviour

- A detailed analysis of the influence of suction within meniscus water on the inter-particle forces was carried out (see Section 2.9) which showed that:
    1. For millimetre-sized spherical particles (sand grains or packets of clay containing many platelets) the contribution of suction in meniscus water to inter-particle contact stresses is negligible (less than 1 kPa).
    2. For micron-sized clay platelets the contribution of suction in meniscus water to inter-particle stresses is largely dependent on platelet size (and independent of suction value), with contributions in excess of 100 kPa possible for clay-sized platelets.
    3. Given that meniscus water around individual clay platelet contacts can occur only at suctions above about 100 kPa, and that meniscus water around contacts between millimetre-sized spherical particles can never contribute substantially to inter-particle stresses, within the range of suction from zero to 100 kPa the most significant effect of suction within meniscus water on inter-particle stresses arises from water around

contacts between silt-sized bodies (either individual silt particles or silt-sized aggregations of clay platelets).

- The effects of unsaturated conditions on swelling and shrinkage of clays are explained with the aid of simple conceptual features (see Section 3.3.5). These aids along with the new fabric model (see Section 3.4) provide useful insight into the soil behaviour.
- A conceptual model for the fabric of compacted highly expansive clays is proposed in Section 3.4 and three levels of fabric are clearly identified. The feasibility of occurrence of unsaturated conditions within all three levels of fabric is explored, which helps in checking the appropriateness of assumptions employed in constitutive models such as that proposed by Gens and Alonso (1992).

8.1.2 Experimental techniques

- A new technique of water drainage from the top and bottom of a triaxial sample, with air drainage from one end only, was developed for controlled-suction testing of unsaturated soils using the axis translation technique (see Section 4.4).
- It was found that ex-solution of air within cell water during reductions of cell pressure could be avoided if the cell pressure was never reduced below the maximum value of pore air pressure previously applied. As a consequence, it was possible to vary cell pressure σ_3, pore air pressure u_a and pore water pressure u_w (rather than just u_a and u_w, as was used by Sivakumar (1993)), during stress path testing of unsaturated soils, without causing problems for sample volume change measurement based on monitoring the flow of cell water.
- A new procedure for non-linear variation of suction with time was developed and used for carrying out wetting/drying cycles (see Section 5.6.3). The non-linear variation of suction proved useful in improving the quality of results (see Section 6.3.1).

8.1.3 Main experimental results

A programme of experimental tests was performed on samples of a compacted bentonite/kaolin mix (with a few additional tests on kaolin samples). All testing was limited to isotropic stress conditions (q = 0), with controlled variation of mean net stress $p'' = p - u_a$ and suction $s = u_a - u_w$. From the experimental results some important conclusions emerged that are summarised here:

- Loading and wetting tests indicated the existence of a Loading Collapse LC yield curve, a fundamental feature of existing elasto-plastic models for non-expansive clays.
- For samples of bentonite/kaolin mix compacted under the lowest pressure of 400 kPa, wetting and drying cycles apparently inside the LC yield curve produced net shrinkage

over each cycle, with an irreversible component of shrinkage during each drying stage. This is similar to the pattern reported by Alonso *et al* (1995).

- In contrast, for samples of bentonite/kaolin mix compacted under the highest pressure of 3200 kPa, wetting/drying cycles remaining inside the *LC* yield curve produced net swelling, with an irreversible component of swelling during each wetting stage. This is similar to the pattern of behaviour reported by Chu and Mou (1973). The contrasting types of behaviour reported by Alonso *et al* (1995) and Chu and Mou (1973) therefore both occurred for the same soil
- The occurrence of net shrinkage or net swelling for wetting/drying cycles apparently remaining inside the *LC* yield curve, cannot be represented by the existing elasto-plastic constitutive models for non-expansive unsaturated soils proposed by Alonso *et al* (1990) and Wheeler and Sivakumar (1995), but can, in principle, be represented by the elasto-plastic models for highly expansive unsaturated soils proposed by Gens and Alonso (1992) and Alonso *et al* (1994).
- Irreversible shrinkage or swelling occurred during subsequent wetting/drying cycles, not just during the first cycle. This aspect of behaviour can be represented by the model of Alonso *et al* (1994), with suitable coupling of the *SD* and *SI* yield curves.
- Net shrinkage during a wetting/drying cycle was sometimes accompanied by a distinct change of stiffness (a yield point) during the appropriate drying path, but at other times was not. The latter was not consistent with the model of Alonso *et al* (1994). Yield points were never observed during both drying and wetting stages of a cycle, as would be required in the model of Alonso *et al* (1994) if irreversible behaviour were to continue during subsequent cycles.
- The value of yield stress observed during isotropic loading at constant suction was affected by the occurrence of a previous wetting/drying cycle (as predicted by the model of Alonso *et al* (1994)), but the location of the post-yield compression curve in the $v : p''$ plane was also affected (inconsistent with the model).
- Net shrinkage or swelling during a wetting/drying cycle was always accompanied by a substantial net change of degree of saturation S_r during the cycle (termed hydraulic hysteresis, see for example, Wheeler and Karube (1996)).
- Although the magnitudes of both reversible and irreversible components of swelling and shrinkage were smaller, the qualitative patterns of behaviour observed for pure kaolin (a non-expansive clay) were identical to those for the highly expansive bentonite/kaolin mix.

8.1.4 New model for unsaturated soils

The behaviour of unsaturated non-expansive and highly expansive soils was found not to be fundamentally different (see Sections 6.9 and 7.1), which suggested that unified modelling for both types of soils is desirable. A new constitutive modelling framework is therefore proposed (see Sections 7.3 to 7.5). Some of the important features of the proposed model are:

- The stress variables $p^* = p - S_r u_w - (1 - S_r)u_a$, q and $s^* = n(u_a - u_w)$, used in the model, are conjugate with the strain increment parameters $d\varepsilon_p$, $d\varepsilon_q$ and $-dS_r$ respectively. It should be noted that in the existing elasto-plastic models, stress variables were seldom linked with conjugate strain increment parameters. With this linkage of stress variables to strain parameters, new constitutive models would be capable of providing complete and consistent stress-strain relationships.
- For isotropic stress states, the influence of externally applied total stresses, pore air pressure and pore water pressure within bulk water is expressed through the stress variable p^*. The influence of meniscus water is expressed through the degree of saturation S_r, which is linked to the final stress variable s^* by a hysteretic soil-water characteristic relationship.
- For triaxial stress states the form of proposed constitutive model would consist of an elasto-plastic stress-strain model, with a yield surface in $p^* : q : S_r$ space, coupled to a hysteretic soil-water characteristic relationship linking S_r to s^*.
- Hydraulic hysteresis is an integral part of the new constitutive framework, which therefore provides improved modelling capabilities for stress paths involving reversals and cycles of suction, including the difficult transition between saturated and unsaturated conditions.
- The model is in very simple form, but seems to capture the major features of unsaturated soil behaviour (see Section 7.4). More importantly, the model is promising in solving several outstanding problems associated with constitutive modelling of unsaturated soils (including the occurrence of net shrinkage or swelling during wetting/drying cycles and proper modelling of the transition between saturated and unsaturated conditions). The framework will need to be developed to a full mathematical model (see Section 7.5) and will need to be fully validated by experimental data (see Section 7.6), including extension to triaxial stress states.

8.2 Recommendations for Future Work

The research reported in this thesis has resulted in a better understanding of the behaviour of unsaturated soils. Many questions are, however, still unanswered and there are several lines of research which could usefully be pursued in the future. These future research opportunities include development of constitutive models, improvement to laboratory testing techniques, and other areas (such as numerical implementation of the constitutive models).

8.2.1 Development and validation of new constitutive model

- The new modelling framework proposed in Sections 7.3 and 7.4 should be developed to a full mathematical model, along the lines set out in Section 7.5. Quantitative predictions of stress-strain curves from the model should then be compared with the existing experimental data presented in Chapter 6, and the model refined, if necessary.
- Additional experimental tests, including shear testing, should be conducted to complete the model validation. This additional experimental programme could include tests in which the variables p^* and S_r were varied in a controlled fashion, as described in Section 7.6.
- In subsequent phases the constitutive model could be refined to include second order effects, such as the influence of anisotropic stress histories, non-linear small strain behaviour and the occurrence of plastic strains inside the state boundary surface (by use of nested kinematic yield surfaces or bounding surface plasticity).

8.2.2 Improvements to laboratory testing techniques

- Experience gained in the current research confirmed earlier experience (Sivakumar (1993)) that monitoring the flow of water into a triaxial cell provided measurements of sample volume change of acceptable quality, but that calibration and use of the double-walled acrylic cells was very cumbersome and time-consuming. It is therefore recommended that, in future, the double-walled acrylic cells are replaced with single-walled metal cells (sacrificing visual observation of the sample, but avoiding problems of creep, hysteresis and water absorption by the cell walls). Metal-walled cells are now being used for unsaturated soil testing at both Oxford University and Glasgow University.
- The technique of providing drainage of pore water from both top and bottom of a sample (with drainage of pore air from one end), developed in the current work for an isotropic cell, should be extended to a full triaxial cell.
- The axis translation technique removes the possibility of cavitation within pore water, and therefore may not correctly represent behaviour in the field during initial desaturation from a saturated state. It would therefore be desirable for any test programme aimed at studying soil behaviour during transition between saturated and unsaturated conditions to be based on a technique in which true negative values of pore water pressure are applied (such as the osmotic technique, see Section 4.1.2). This would require the osmotic method of suction control to be developed to a point where suction could be varied in a continuous fashion, rather than simply as the application of step changes of suction. Furthermore, migration of

chemicals across the semi-permeable membrane used in the osmotic technique needs to be properly investigated (see Section 4.1.2).

8.2.3 Other areas

Other areas in which future research or development would be beneficial include:

- Numerical implementation of the new constitutive model (once it is fully developed) and subsequent application to boundary value problems.
- Dissemination of improved understanding of unsaturated soils to industry, for use in design and analysis at qualitative and quantitative levels.
- Simplification of laboratory testing methods for transfer to the commercial environment.
- Improved interpretation of in-situ test results from unsaturated soils.
- Better methods for measurement of suction in-situ and for predicting the variation of suction with time in the field.
- Application to problems of contaminant transport through the unsaturated (vadose) zone.

In spite of the need for further research, this project has advanced the constitutive modelling process significantly in three respects. Firstly, a unified modelling framework for both unsaturated non-expansive and highly expansive soils is proposed. Secondly, new forms of stress variables with conjugate strain increment parameters are used for the first time in a modelling framework. Finally, the influence of hydraulic hysteresis on stress-strain behaviour is included in the framework.

REFERENCES

Aitchison, G.D. (1961). Relationships of moisture stress and effective stress functions in unsaturated soils. Conf. pore pressure and suction in soils: British National Society of the International Society for Soil Mechanics and Foundation Engineering. London: Butterworths. 47-52.

Alonso, E.E., Gens, A. and Gehling, W.Y.Y. (1994). Elasto-plastic model for unsaturated expansive soils. Proc. 3rd Eur. Conf. Num. Methods Geotech. Eng., Manchester. 11-18.

Alonso, E.E., Gens, A. and Hight, D.W. (1987). Special problem soils. General report. Proc. 9th Eur. Conf. Soil Mech., Dublin, Vol.3, 1087-1146.

Alonso, E.E., Gens, A. and Josa, A. (1990). A constitutive model for partially saturated soils. Géotechnique, Vol.40(3), 405-430.

Alonso, E.E., Lloret, A., Delahaye, C.H., Vaunat, J., Gens, A. and Volckaert, G. (1998). Coupled analysis of a backfill hydration test. Int. J. for Num. and Anal. Methods in Geomech., Vol.22, 1-27.

Alonso, E.E., Lloret, A., Gens, A. and Yang, D.Q. (1995). Experimental behaviour of highly expansive double-structure clay. Proc. 1st Int. Conf. Unsaturated Soils, Paris, Vol.1, 11-16

Al Mukhtar, M., Robinet, J.C. and Liu, C.W. (1993). Hydro-mechanical behaviour of partially saturated low porosity clays. Engineering Fills (Eds. B.G Clarke, C.J.F.P.Jones and A.I.B Moffat). London: Thomas Telford. 87-98.

Al-Tabbaa, A. (1987). Permeability and stress-strain response of speswhite kaolin. PhD thesis, University of Cambridge.

Al-Tabbaa, A. and Wood, D.M. (1989). An experimentally based bubble model for clay. Numerical Models in Geomechanics, NUMOG III (Eds. S. Pietruszczak and G.N. Pande). London: Elsevier. 91-99.

Anandarajah, A., Kuganenthira, N. and Zhao, D. (1996). Variation of fabric anisotropy of kaolinite in triaxial loading. J. of Geotech. Eng., Div., ASCE, Vol.122(8), 633-640.

Araruna, J.T, Harwood, A.H. and Clarke, B.G. (1995). A practical, economical and precise volume change measurement device. Géotechnique, Vol.45(3), 541-544.

Atabek, R.B., Felix, B., Robinet, J.-C. and Lahlou, R. (1991). Rehelogical behaviour of saturated expansive clay materials. Workshop on stress partitioning in engineered clay barriers. Duke University, Durham, N.C.

Atkinson, J.H. and Stallebrass, S.E. (1991). A model for recent history and non-linearity in the stress-strain behaviour of overconsolidated soil. Proc. 7th Int. Conf. Computer Methods & Advances in Geomechanics, Cairns, Vol.1, 553-560.

Aylmore, L.A.G. and Quirk, J.P. (1959). Swelling of clay-water system. Nature, Vol.183(4677), 1752-1753.

Aylmore, L.A.G. and Quirk, J.P. (1960). Domain or turbostratic structure of clays. Nature, Vol.187(4742), 1046-1048.

Barden, L. and Sides, G.R. (1970). Engineering behaviour and structure of compacted clay. J. Soil Mech. and Found. Div., ASCE, Vol.96(SM4), 1171-1200.

Bardet, J.P. (1990). Hypoplastic model for sands. J. of Engineering Mechanics, ASCE, Vol.116(9), 1973-1994.

Bishop, A.W. (1959). The principle of effective stress. Tek. Ukeblad, Vol.39, 859-863.

Bishop, A.W. (1961). The measurement of pore pressure in the triaxial test. Conf. Pore Pressure and Suction in Soils. British National Society of the International Society for Soil Mechanics and Foundation Engineering. London: Butterworths. 26-30.

Bishop, A.W. and Blight, G.E. (1963). Some aspects of effective stress in saturated and partly saturated soils. Géotechnique, Vol 13(3), 177-197.

Bishop, A.W. and Donald, I.B., (1961). The experimental study of partially saturated soils in the triaxial apparatus. Proc. 5th Int. Conf. Soil Mech. Found. Eng., Paris. Vol.1, 13-21.

Bishop, A.W., Kumapley, N.K. and El-Ruwayih, A. (1975). The influence of pore water tension on the strength of clay. Proc. Roy. Soc. 278A, 511-554.

Bocking, K.A. and Fredlund, D.G. (1980). Limitations of the axis translation technique. Proc. 4th. Int. Conf. Expansive Soils, Denver, 117-135.

Bolt, G.H. (1956). Physico-chemical analysis of the compressibility of pure clays. Géotechnique, Vol.6(2), 86-93.

Bolzon, G., Schrefler, B.A. and Zienkiewicz, O.C. (1996). Elastoplastic soil constitutive laws generalized to partially saturated states. Géotechnique, Vol.46(2), 279-289.

Brackley, I.J.A (1973). Swell pressure and free swell in compacted clay. Proc. 3rd Int. Conf. Expansive Soils, Haifa, 169-176.

Brackley, I.J.A (1975). Swell under load. Proc. 6th Reg. Conf. for Africa on Soil Mech. & Found. Eng., Durban, 65-70.

British National Society of the International Society for Soil Mechanics and Foundation Engineering (1961): Conf. Pore Pressure and Suction in Soils. London: Butterworths.

Burland, J.B. (1964). Effective stress in partly saturated soils. Géotechnique, Vol.14, 64-68.

Burland, J.B. (1990). 30th Rankine Lecture: On the compressibility and shear strength of natural clays. Géotechnique, Vol.40(3), 327-378.

Callaghan, I.C. and Ottewill, R.H. (1973). Interparticle forces in montmorillonite gels. Faraday Discussion of the Chemical Society, Vol.57, 110-118.

Casimir, H.B.G. and Polder, D. (1948). The influence of retardation on the London-van der Waals forces. Physical Review, Vol.73(4), 360-372.

Chapman, D.L. (1913). A contribution to the theory of electrocapillarity. Philosophical Magazine, Vol.25(6), 475-481.

Chen, F.H. (1973). The basic physical property of expansive soils. 3rd Int. Conf. Expansive Soils, Haifa, Vol.1, 17-25.

Childes, E.C. (1969). An introduction to the physical basis of soil water phenomena. Wiley Interscience.

Chu, T.Y. and Mou, C.H. (1973). Volume change characteristics of expansive soils determined by controlled suction test. Proc. 3rd Int. Conf. Expansive Soils, Haifa, Vol.1, 177-185.

Clayton, C.R.I. and Khatrush, S.A. (1986). A new device for measuring local axial strain on triaxial specimens. Géotechnique, Vol.36(4), 593-597.

Collins, K. and McGown, A. (1974). The form and function of microfabric features in a variety of natural soils. Géotechnique, Vol.24(2), 223-254.

Costa Filho, L.M. (1980). A laboratory investigation of the small strain behaviour of London clay. PhD thesis, University of London.

Croney, D. (1952). The movement and distribution of water in soils. Géotechnique, Vol.3(1), 1-16.

Cui, Y.J. and Delage, P. (1996). Yielding and plastic behaviour of an unsaturated compacted silt. Géotechnique, Vol.46(2), 291-311.

Dafalias, Y.F. and Popov, E. (1975). A model for nonlinear hardening materials for complex loading. Acta Mechanica, Vol.21(3), 173-192

Delage, P., Howat, M.D. and Cui, Y.J (in press). Relationship between suction and swelling properties in a heavily compacted unsaturated clay. Accepted for publication in the Review of Engineering Geology.

Delage, P. and Lefebvre, G. (1984). Study of the structure of sensitive Champlain clay and of its evolution during consolidation. Canadian Geotech. J., Vol.21, 21-35.

Delage, P., Suraj De Silva, G.P.R. and De Laure, E. (1987). Un nouvel appareil triaxial pour les sols non satures. Proc. 9th Euro. Conf. on Soil Mech., Dublin, Vol.1, 26-28.

Diamond, S. (1970). Pore size distribution in clays. Clays and Clay Minerals, Vol.18, 7-23.

DiMaio, C. (1996). Exposure of bentonite to salt solution: osmotic and mechanical effects. Géotechnique, Vol.46(4), 695-707.

Dineen, K. (1997). The influence of soil suction on compressibility and swelling. PhD thesis, Imperial College, University of London.

Dineen, K. and Burland, J.B. (1995). A new approach to osmotically controlled oedometer testing. Proc.1st Int. Conf. Unsaturated Soils, Paris, Vol.2, 459-465.

Domenico, P.A. and Schwartz, F.W. (1998). Physical and Chemical Hydrogeology, John Wiley & Sons, New York.

Escario, V. and Juca, J.E.T. (1989). Strength and deformation of partly saturated soils. Proc. 12th Int. Conf. Soil Mech. Found. Eng., Redo de Janeiro, Vol.1, 43-46.

Escario, V. and Saez, J. (1973). Measurement of the properties of swelling and collapsing soils under controlled suction. Proc. 3rd Int. Conf. Expansive Soils, Haifa, 195-200.

Escario, V. and Saez, J. (1986). The shear strength of partly saturated soils. Géotechnique, Vol.36(3), 453-456.

Fisher, R.A. (1926). On the capillary forces in an ideal soil: correction of formulae given by W.B. Haines. J. Agr. Sci., Vol.16, 492-505.

Fredlund, D.G. (1975). A diffused air volume indicator for unsaturated soils. Canadian Geotech. J., Vol.12, 533-539.

Fredlund, D.G. (1979). Appropriate concepts and technology for unsaturated soils. Canadian Geotech. J., Vol.16, 121-139.

Fredlund, D.G. and Morgenstern, N.R. (1977). Stress state variables for unsaturated soils. J. Geotech. Eng., Div., ASCE, Vol.103(GT5), 447-466.

Fredlund, D.G., Morgenstern, N.R. and Widger, R.A. (1978). The shear strength of unsaturated soils. Canadian Geotech. J., Vol.15(3), 313-321.

Fredlund, D.G. and Rahardjo, H. (1993). Soil Mechanics for unsaturated soils. John Wiley & Sons: New York.

Fredlund, D.G. and Xing, A. (1994). Equations for the soil-water characteristic curve. Canadian Geotech. J., Vol.31, 521-532.

Fredlund, D.G., Xing, A., Fredlund, M.D. and Barbour, S.L. (1995). The relationship of the unsaturated soil shear strength to the soil-water characteristic curve. Canadian Geotech. J., Vol.32, 440-448.

Gan, J.K.M., Fredlund, D.G. and Rahardjo, H. (1988). Determination of shear strength parameters for unsaturated soil using direct shear test. Canadian Geotech. J., Vol.25, 500-510.

Gan, J.K.M. and Fredlund, D.G. (1996). Shear strength characteristics of two saprolitic soils. Canadian Geotech. J., Vol.33, 595-609.

Gatmiri, B., Tavakoli, S., Moussavi, J. and Delage, P. (1995). Numerical approach of elastoplastic consolidation of unsaturated soils. Proc. 1st Int. Conf. Unsaturated Soils, Paris, Vol.2, 1057-1064.

Gens, A. (1996). Keynote lecture: Constitutive modelling: Application to compacted soils. Proc. 1st Int. Conf. Unsaturated Soils, Paris, Vol.3, 1179-1200.

Gens, A. and Alonso, E.E. (1992). A framework for the behaviour of unsaturated expansive clays. Canadian Geotech. J., Vol.29, 1013-1032.

Gens, A., Vaunat, J. and Ledesma, A. (1995). Analysis of hydration of an engineered barrier in radioactive waste repository scheme using an elastoplastic model. Proc. 1st Int. Conf. Unsaturated Soils, Paris, Vol.2, 1065-1073.

Gleason, M.H. Daniel, D.E., and Eykholt, G.R. (1997). Calcium and sodium bentonite for hydraulic containment applications. J. of Geotech. and Geoenv. Eng., Div., ASCE, Vol.123(5), 438-445.

Goto, S., Tatsuoka, F. Shibuya, S., Kim, Y.S and Sato, T. (1991). A simple gauge for local small strain measurements in the laboratory. Soils and Foundations, Vol.31(1), 169-180.

Gourly, C.S., Newill, D. and Schreiner, H.D. (1993). Expansive soils: TRL's research stratgey, Proc. 1st Int. Symp. Engineering Characteristics of Arid Soils, London.

Gouy, G. (1910). Sur la constitution de la charge electrique a la surface d'un electrolyte. Annales de Physique (Paris), Serie 4, 9, 457-468.

Graber, E.R. and Mingelgrin, U. (1994). Clay swelling and regular solution theory. Environmental Science & Technology, Vol.28(13), 2360-2365.

Graham, J., Oswell, J.M. and Gray, M.N. (1992). The effective stress concept in saturated sand-clay buffer. Canadian Geotech. J., Vol.29, 1033-1043.

Grim, R.E. (1968). Clay Mineralogy, McGraw-Hill, New York.

Gulhati, S.K. and Satija, B.S. (1981). Shear strength of partially saturated soils. Proc. 10th Int. Conf. Soil Mech. Found. Eng., Stockholm, Vol.1, 609-612.

Haines, W.B. (1925). Studies in the physical properties of soils: II A note on the cohesion developed by capillary forces in an ideal soil. J. Agr. Sci., Vol.15, 529-535.

Hilf, J.N. (1956). An investigation of pore water pressure in compacted cohesive soils. Technical Memorandom 654. U.S. Department of Interior Bureau of Reclamation, Denver.

Hird, C.C. and Yung, C.Y. (1989). The use of proximity transducers for local strain measurements in triaxial tests. Geotech. Testing J, ASTM, Vol.12(4), 292-296.

Ho, D.Y.F., Fredlund, D.G. and Rahardjo, H. (1992) Volume change indices during loading and unloading of an unsaturated soil. Canadian Geotech. J., Vol.29, 195-207.

Houlsby, G.T. (1997). The work input to an unsaturated granular material. Géotechnique, Vol.47(1), 193-196.

Houlsby, G.T. and Sharma, R.S. (1997). A conceptual model for the yielding and consolidation of clays. Report No 2130/97, Dept. of Eng. Science, University of Oxford.

Hueckel, T.A. (1992). Water-mineral interaction in hygromechanics of clays exposed to environmental loads: a mixture theory approach. Canadian Geotech. J., Vol.29, 1071-1086.

Iwan, D.W. (1967). On class of models for the yielding behaviour of continuous and composite systems. J. of Applied Mechanics, Sept., 612-617.

Jardine, R.J., Symes, M.J. and Burland, J.B. (1984). Measurement of soil stiffness in the triaxial apparatus. Géotechnique, Vol.34(3) 323-340.

Jayadeva, M.S. and Sridharan, A. (1982). A study on potential distance relationship of clays. Indian Geotech. J., Vol.12, 83-97.

Jennings, J.E.B. (1961). A revised effective stress law for use in prediction of behaviour of unsaturated soils. Conf. Pore Pressure and Suction in Soils: British National Society of the International Society for Soil Mechanics and Foundation Engineering. London: Butterworths.26-30.

Jennings, J.E.B. and Burland, J.B. (1962). Limitations of the use of effective stresses in partly saturated soil. Géotechnique, Vol.12(2), 125-144.

Jommi, C. and di Prisco, C. (1994). Un semplice approcio teorico per la modellazione del comportamento meccanico di terreni granulari parcialmente saturi. Conf. Il ruolo dei fluidi nei problemi di ingegneria geotecnica, Mondovi, 167-188.

Josa, A., Balmaceda, A., Gens, A. and Alonso, E.E. (1992). An elasto-plastic model for partially saturated soils exhibiting a maximum collapse. Proc. 3rd Int. Conf. Computational Plasticity, Barcelona, Vol.1, 815-826.

Justo, J. L, Delgado, A. and Ruiz, J (1984). The influence of stress path in the collapse-swelling of soils at the laboratory. Proc. 5th Int. Conf. Expansive Soils, Adelaide, 67-71.

Kassiff, G. and Ben Shalom, A. (1971). Experimental relationship between swell pressure and suction. Géotechnique, Vol.21(3), 245-255.

Kassif, G., Baker, R. and Ovadia, Y. (1973). Swell-pressure relationships at constant suction changes. Proc. 3rd Int. Conf. Expansive Soils, Haifa, 201-208.

Kim, S.H. (1996). Model testing and analysis of interactions between tunnels in clay. DPhil thesis, University of Oxford.

Kohgo, Y., Nakano, M. and Miyazaki, T. (1993 *a*). Theoretical aspects of constitutive modelling for unsaturated soils. Soils and Foundations, Vol 33(4), 49-63

Kohgo, Y., Nakano, M. and Miyazaki, T. (1993 *b*). Verification of generalised elasto-plastic model for unsaturated soils. Soils and Foundations, Vol 33(4), 64-73

Komine, H. and Ogata, N. (1994). Experimental study on swelling characteristics of compacted bentonite. Canadian Geotech. J., Vol.31, 478-490.

Komine, H. and Ogata, N. (1996). Prediction for swelling characteristics of compacted bentonite. Canadian Geotech. J., Vol.33, 11-22.

Komornik, A., Livneh, M. and Smucha, S. (1980). Shear strength and swelling of clays under suction. Proc. 4th Int. Conf. Expansive Soils, Denver, 206-226.

Krieg, K.D. (1975). A practical two surface plasticity theory. J. Applied Mechanics., Sept., 641-546.

Lagerwerff, J.V. Ogata, G. and Eagle, H.E. (1961). Control of osmotic pressure of culture solutions with polyethylene glycol. Science, Vol.133, 1486-1487.

Lambe, T.W. (1958). The structure of compacted clay. J. of Soil Mech. and Found. Div., ASCE, Vol.84(SM2), 1654.

Lapierre, C., Leroueil, S. and Locat, J. (1990). Mercury intrusion and permeability of Louiseville clay. Canadian Geotech. J., Vol.27, 761-773.

Levy, R., Tanji, K.K. and Whittig, L.D. (1983). Effect of precipitation of alkaline earth carbonates and magnesium hydroxide of Na-Ca-Mg exchange in Wyoming bentonite. Soil Sci. Soc. Am. J.,Vol.47, 906-912.

Lloret, A. and Alonso, E.E. (1985). State surfaces for partially saturated soils. Proc. 11th Int. Conf. Soil Mech. Found. Eng., San Francisco, Vol.2, 557-562.

London, F. (1937). The general theory of molecular forces. Trans. of the Faraday Soc., Vol.33, 8-26.

Maâtouk, A., Leroueil, S. and La Rochelle, P. (1995). Yelding and critical state of a collapsible unsaturated silty soil. Géotechnique, Vol.45(3), 465-477.

Madsen, F.T., and Müller-Venmoos, M. (1985). Swelling pressure calculated from mineralogical properties of Jurassic opalinum shale, Switzerland. Clays and clay minerals, Vol.33, 501-509.

Marinho, F.A.M, Chandler, R.J. and Crilly, M.S. (1995). Stiffness measurement of an unsaturated high plasticity clay using bender elements. Proc. 1st Int. Conf. Unsaturated Soils, Paris, Vol.2, 535-539.

Marinho, F.A.M and Chandler, R.J. (1995). Cavitation and the direct measurement of soil suction. Proc. 1st Int. Conf. Unsaturated Soils, Paris, Vol.2, 623-630.

Maswose, J. (1985). Stress path for a compacted soil during collapse due to wetting. PhD thesis, Imperial College, University of London.

Matyas, E.L. and Radhakrishna, H.S. (1968). Volume change characteristics of partially saturated soils. Géotechnique, Vol.18(4), 432-448.

McKeen, R.G. (1992). A model for predicting expansive soil behaviour. Proc. 7th. Int. Conf on Expansive Soils, Dallas, 1-6.

Mitchell, J.K. (1993). Fundamentals of soil behaviour. John Wiley & Sons, Inc., New York.

Modaressi, A. and Abou-Bekr, N. (1994). Constitutive model for unsaturated soils: validation on a silty material. 3rd Eur. Conf. Numerical Methods in Geotech. Eng., Manchester, 91-96.

Morgenstern, N.R. and Balasubramonian, B.I. (1980). Effects of pore fluid on the swelling of clay-shale. Proc. 4th Int. Conf. Expansive Soils, Denver, 190-205.

Mroz, Z. (1967). On the description of anisotropic workhardening. J. Mech. Phys. Solids, Vol.15, 163-175.

Mualem, Y. (1974). A conceptual model of hysteresis. Water Resources Research, Vol.10(3), 514-520.

Mualem, Y. (1977). Extension of the similarity hypothesis used for modelling the soil water characteristics. Water Resources Resrearch, Vol.13(4), 773-780.

Nageswaran, S. (1983). Effect of gas bubbles on sea bed behaviour. DPhil thesis, University of Oxford.

Nesnas, K. (1995). A finite element implementation of a critical state model for unsaturated soil to simulate drained conditions. PhD thesis, University of Sheffield.

Olsen, R.E. and Mesri, G. (1970). Mechanisms controlling the compressibility of clay. J. Soil Mech. and Found., Div., ASCE, Vol.96(SM6), 1863-1878.

Pousada, E. (1984). Deformabilidad de arcillas expansive bajo succión controlada. Tesis Doctoral, Univ. Polit. Madrid.

Pradhan, T.B.S., Tatsuoka, F. and Molenkamp, F. (1986). Accuracy of automated volume change measurement by means of differential pressure transducer. Soils and Foundations, Vol.26(4), 150-158.

Prevost, J.H. (1978). Anisotropic undrained stress-strain behaviour of clays. J. Geotech. Eng., Div., ASCE, Vol.104(8), 1075-1090.

Price, M. (1985). Introduction to groundwater. Chapman & Hall, London.

Pusch, R. (1982). Mineral-water interactions and their influence on the physical behaviour of highly compacted Na bentonite. Canadian Geotech. J., Vol.19, 381-387.

Ramesh, A. D. (1996). Modelling the thermo/hydraulic/mechanical behaviour of unsaturated soil using an elasto-plastic constitutive relationship. PhD thesis, College of Cardiff, University of Wales.

Richard, B.G. (1978). Application of an experimentally based non-linear constitutive model of soils in laboratory and field tests. Aust. Geomech. J., Vol.G8, 20-30.

Richards, B.G., Peter, P. and Martin, R. (1984). The determination of volume change properties in expansive soil. Proc. 5th Int. Conf. Expansive Soils, Adelaide, 179-186.

Ridley, A.M. and Burland, J.B. (1993). A new instrument for the measurement of soil moisture suction. Géotechnique, Vol.43(2), 321-324.

Romero, E., Facio, J.A., Lloret, A., Gens, A. and Alonso, E.E. (1997). A new suction and temperature controlled triaxial apparatus. 14th Int. Conf. Soil Mech. Found. Eng., Hamburg, Vol.1, 185-188.

Rytwo, G., Nir, S. and Margulies L. (1995). Interactions of monovalent organic cations with montmorillonite, adsorption and model calculations. Soil Sci. Soc. Am. J.,Vol.59, 554-564.

Rytwo, G., Banin, A. and Nir, S. (1996). Exchange reactions in the Ca-Mg-Na-montmorillonite system. Clays and Clay Minerals, Vol.44(2), 276-285.

Schofield, R.K. (1935). The pF of water in soil. Trans. 3rd Int. Cong. Soil science, Vol.2, 37-48.

Seed, H.B. and Chan, C.K. (1959). Structure and strength characteristics of compacted clays. J. Soil Mech. Found. Div., ASCE, Vol.85(SM5), 87-127.

Sham, W.K. (1989). The undrained shear strength of soil containing large gas bubbles. PhD thesis, Queen's University of Belfast.

Shang, J.Q., Lo, K.Y. and Quigley, R.M. (1994). Quantitative determination of potential distribution in Stern-Gouy double-layer model. Canadian Geotech. J., Vol.31, 624-636.

Sharma, R.S. (1984). Effect of stress path on strength deformation characteristics of some intact rocks. M.Tech thesis, Indian Institute of Technology (IIT), New Delhi.

Sivakumar, V. (1993). A critical state framework for unsaturated soil. PhD thesis, University of Sheffield.

Sivakumar, V. and Wheeler, S.J. (in press). Influence of compaction procedure on the elasto-plastic behaviour of an unsaturated clay. Accepted for publication in Géotechnique.

Smart, P. and Tovey, N.K. (1981). Electron microscopy of soils and sediments: examples. Oxford: Clarendon Press.

Sparks, A.D.W. (1963). Theoretical considerations of stress equations for partly saturated soils. Proc. 3rd African Conf. Soil Mech. Found. Eng., Salisbury, Rohdesia, Vol.1, 215-218.

Sposito, G., Jouany, C., Holtzclaw, K.M. and LeVesque, C.S. (1983). Calcium-magnesium exchange on Wyoming bentonite in the presence of adsorbed sodium. Soil Sci. Soc. Am. J.,Vol.47, 1081-1085.

Sridharan, A. and Jayadeva, M.S. (1982). Double layer theory and compressibility of clays. Géotechnique, Vol.32(2), 133-144.

Stern, O. (1924). Zur Theorie der elektrolytischen Doppelschriht. Zeitschrift fur Elektrochemie, Vol.30, 508-516.

Stepkowska, E.T. (1990). Aspects of the clay/electrolyte/water system with special reference to the geotechnical properties of clays. Eng. Geology, Vol.28, 249-267.

Terzaghi, K. (1936). The shearing resistance of saturated soils and the angle between the planes of shear. Proc. 1st Int. Conf. Soil Mech., Vol.1, 54-56.

Thiessen, P.A. (1942). Wechswlseitige Adsorption von Kolloiden, Z. Elektrochem., 48, 675-681.

Vanapalli, S.K., Fredlund, D.G., Pufahl, D.E. and Clifton, A.W. (1996). Model for prediction of shear strength with respect to soil suction. Canadian Geotech. J., Vol.33, 379-392.

van Olphen, H. (1977). An introduction to clay colloid chemistry. John Wiley & Sons, New York.

Wan, A.W.L., Gray, M.N. and Graham, J. (1995). On the relations of suction, moisture content, and soil structure in compacted clays. Proc. 1st Int. Conf. Unsaturated Soils, Paris, Vol.1, 215-222.

Wheeler, S.J. (1986). The stress-strain behaviour of soils containing gas bubbles. DPhil thesis, University of Oxford.

Wheeler, S.J. (1988). The undrained shear strength of soils containing large gas bubbles. Géotechnique, Vol.38(1), 399-413.

Wheeler, S.J. (1991). An alternative framework for unsaturated soil behaviour. Géotechnique, Vol.41(2), 257-261.

Wheeler, S.J. (1996). Inclusion of specific water volume within an elasto-plastic model for unsaturated soil. Canadian Geotech. J., Vol.33, 42-57.

Wheeler, S.J. (1997). A rotational hardening elasto-plastic model for clays. 14th Int. Conf. Soil Mech. Found. Eng., Hamburg, Vol.1, 431-434.

Wheeler, S.J. and Karube, D. (1996). State of the art report: Constitutive modelling. Proc. 1st Int. Conf. Unsaturated Soils, Paris, Vol.3, 1323-1356.

Wheeler, S.J. and Sivakumar, V. (1995). An elasto-plastic critical state framework for unsaturated soil. Géotechnique, Vol.45(1), 35-53.

Whittle, A.J. and Kavvadas, M.J. (1994). Formulation of MIT-E3 constitutive model for overconsolidated clays. J. of Geotech. Eng., Div., ASCE, Vol.120(1), 173-198.

Williams, J. and Shaykewich, C.F. (1969). An evaluation of polyethylene glycol (PEG) 6000 and PEG 20.000 in the osmotic control of soil water matric potential. Canadian J. Soil Science, Vol.49, 397-401.

Yong, R.N. and Mohamed, A.M.O. (1992). A study of particle interaction energies in wetting of unsaturated expansive clays. Canadian Geotech. J., Vol.29, 1060-1070.

Yudhbir (1982). Collapsing behaviour of residual soils. Proc. 7th SE Asian Geotech. Conf., Hong-Kong, Vol.1, 915-930.

Zakaria, I. (1994). Yielding of unsaturated soil. PhD thesis, University of Sheffield.

Zakaria, I., Wheeler, S.J. and Anderson, W.F. (1995). Yielding of unsaturated compacted kaolin. Proc. 1st Int. Conf. Unsaturated Soils, Paris, Vol.2, 811-817.

Zur, B. (1966). Osmotic control of the matric soil-water potential: I soil-water system. Soil Science, Vol.102(6), 394-398.

Saturated solution of	Percentage relative humidity at 20^0 C	Suction (MPa)
Potassium sulphate K_2SO_4	98	2.7
Potassium chloride KCl	85	23
Sodium chloride NaCl	76	33
Calcium Nitrate $Ca(NO_3)_2.4H_2O$	56	79
Calcium Chloride $CaCl_2.6H_2O$	32	158
Lithium Chloride LiCl	11	286
Phosphorous Pentoxide P_2O_5	$<1X10^{-4}$	>1000

Table 4.1: Saturated salt solutions for relative humidity control
(after Al Mukhtar *et al* (1993))

Type of calibration	Form of the equation	July 1996	February , 1997
Air pressure transducer	$ax + b$	a = 7.03622 kPa/mV b = -2.65275 kPa	a = 7.03712 kPa mV b = -2.63275 kPa
Water pressure transducer	$ax + b$	a = 6.99519 kPa/mV b = -4.94327 kPa	a = 7.03712 kPa mV b = -4.84714 kPa
Cell pressure transducer	$ax + b$	a = 6.95382 kPa/mV b = -2.52512 kPa	a = 6.96002 kPa mV b = -2.49195 kPa
Sample volume change measurement unit	$\frac{x}{ap^2 + bp + c}$	a = 13732.12 mV/cm^3/MPa^2 b = -1.412 mV/cm^3/MPa c = -0.00932 mV/cm^3	a = 13729.92 mV/cm^3/MPa^2 b = -1.319 mV/cm^3 MPa c = -0.00712 mV cm^3
Water volume change unit	$\frac{x}{ap^2 + bp + c}$	a = 12965.72 mV/cm^3/MPa^2 b = -4.401 mV/cm^3/MPa c = -0.06339 mV/cm^3	a = 12963.42 mV/cm^3/MPa^2 b = -4.391 mV/cm^3 MPa c = -0.06169 mV cm^3
Cell volume change (Immediate)	$ap^2 + bp + c$	a = 74.36 cm^3/MPa^2 b = -0.803 cm^3/MPa c = 0	a = 75.24 cm^3/MPa^2 b = 1.065 cm^3 MPa c = 0
Water absorption	$ap + b$	a = 0.01 cm^3/MPa/hour b = 0.0004 cm^3/hour	a = 0.004 cm^3 MPa hour b = -0.0005 cm^3 hour
Water drainage line	$ap^2 + bp + c$	a = -1.63 cm^3/MPa^2 b = 1.480 cm^3/MPa c = 0	a = -1.53 cm^3/MPa^2 b = 1.470 cm^3/MPa c = 0

x = output voltage
p = pressure

Table 4.2: Calibration factors for System *A*

Type of calibration	Form of the equation	November 1995	July , 1996
Air pressure transducer	$ax + b$	a = - 0.06604 kPa/mV b = 23.34059 kPa	a = -0.06587 kPa mV b = 22.47878 kPa
Water pressure transducer	$ax + b$	a = -0.06318 kPa/mV b = -7.22908 kPa	a = -0.06308 kPa mV b = -8.74902 kPa
Cell pressure transducer	$ax + b$	a = -0.06489 kPa/mV b = -18.8197 kPa	a = -0.64860 kPa mV b = -19.7341 kPa
Sample volume change measurement unit	ax	a = 0.004895 cm^3/mV	a = 0.004880 cm^3 mV
Water volume change unit	ax	a = 0.00542 cm^3/mV	a = 0.00538 cm^3 mV
Cell volume change (Immediate)	$ap^2 + bp + c$	a = 168.1632cm^3/MPa^2 b = -2.251 cm^3/MPa c = 0	a = 86.88 cm^3/MPa^2 b = 0.895 cm^3/MPa c = 0
Water absorption	$ap + b$	a = 0.0037 cm^3/MPa/hour b = -0.00016 cm^3/hour	a = 0.0030 cm^3/MPa hour b = -0.0006 cm^3 hour
Water drainage line	$ap^2 + bp + c$	a = 19.0 cm^3/MPa^2 b = -0.25cm^3/MPa c = 0	a = 18.0 cm^3/MPa^2 b = -0.20 cm^3/MPa c = 0

x = output voltage
p = pressure

Table 4.3: Calibration factors for System *B*

Type of calibration	Form of the equation	December, 1996
Air pressure transducer	$ax + b$	a = -7.2553 kPa/mV b = 6.6923 kPa
Water pressure transducer	$ax + b$	a = -7.1244 kPa/mV b = -5.1465 kPa
Cell pressure transducer	$ax + b$	a = -7.1940 kPa/mV b = -1.0288 kPa
Sample volume change measurement unit	ax	a = 1.63247 cm^3/mV
Water volume change unit	ax	a = 0.66963 cm^3/mV
Cell volume change (Immediate)	$ap^2 + bp + c$	a = 209.56 cm^3/MPa^2 b = -2.151 cm^3/MPa c = 0
Water absorption	$ap + b$	a = 0.004 cm^3/MPa/hour b = 0.0008 cm^3/hour
Water drainage line	$ap^2 + bp + c$	a = 2.5 cm^3/MPa^2 b = 0 c = 0

x = output voltage
p = pressure

Table 4.4: Calibration factors for System C

Test No	System	Material	Static compaction pressure (kPa)	Drainage	Rate of mean net stress variation during loading/unloading (kPa/hour)	Rate of suction variation (kPa hour) or value of k (min^{-1}) for non-linear variation	Mean net stress p″ (kPa)	Suction (kPa)	Test duration (days)
1	B	*BK*	400	Single	-	2.4	10	400→50→380→0→370	68
2	A	*BK*	400	Single	-	1.6	50	400→100→400	28
3	A	*BK*	800	Single	-	0.8	50	400→100→400→10	67
4	B	*BK*	800	Double	-	2.0	10	400→100→400→10	37
5	A	*BK*	400	Double	-	1.6	20	400→100→400→10	56
6	B	*BK*	400	Double	1.5	1.6	At s = 300 kPa; p'' = 10→94→10	400→300	18
7	B	*BK*	400	Double	1.5	-	At s = 300 kPa; p'' = 10→175→10	300	17
8	B	*BK*	400	Double	1.5	k = ± 0.00016	At s = 300 (b) kPa; p'' = 10→175	300 (a)→20→300 (b)	42
9	C	*BK*	400	Double	1.5	-	At s = 200 kPa; p″ = 10→100→10→250→100	200	23
10	C	*BK*	400	Double	1.5	k = ± 0.00016	At s = 200 (a) kPa; p'' = 10→100→10 At s = 200 (b) p'' = 10→250→10	At p'' = 10 kPa s = 200 (a)→20→200 (b)	66
11	B	*BK*	400	Double	1.5	-	At s = 100 kPa; p'' = 10→200→20	100	19

Table 6.1 : Summary of tests

Test No	System	Material	Static compaction pressure (kPa)	Drainage	Rate of mean net stress variation during loading unloading (kPa hour)	Rate of suction variation (kPa hour) or value of k (min^{-1}) for non-linear variation	Mean net stress p″ (kPa)	Suction (kPa)	Test duration (days)
12	A	*K*	400	Double	-	For wetting path k - 0.00048 For drying path k + 0.00024	10	400→100→400	13
13	C	*BK*	400	Double	1.5	-	At s = 200 kPa; p'' = 10→100	200	10
14	A	*K*	400	Double	-	k = ± 0.00016	10	400→50→400→20→400→5	76
15	B	*BK*	400	Double	1.5	k = ± 0.00016	At s = 400 kPa p'' = 10→40 and then varied to keep the sample volume constant	400→20→55	33
16	B	*BK*	400	Double	1.5	k = ± 0.00016	At s = 400 kPa p'' = 10→40 and then varied to keep the sample volume constant	At p″ = 10 kPa; s = 400→20→400; then at p″ = 40 kPa; s = 400→20→105	71
17	C	*K*	400	Double	1.5	-	At s = 200 kPa; p″ = 10→300	200	34
18	C	*K*	400	Double	1.5	k = ±0.00016	At s = 200 (b) kPa; p″ = 10→300	At p″ = 10 kPa; s = 200 (a)→20→200 (b)	39
19	A	*BK*	3200	Double	-	k = ±0.00016	10	400→50→175	36
20	C	*BK*	3200	Double	-	k = ±0.00016	10	100→1→100	48

Note : *BK* is bentonite/kaolin mix *K* is kaolin

Table 6.1 : Summary of tests

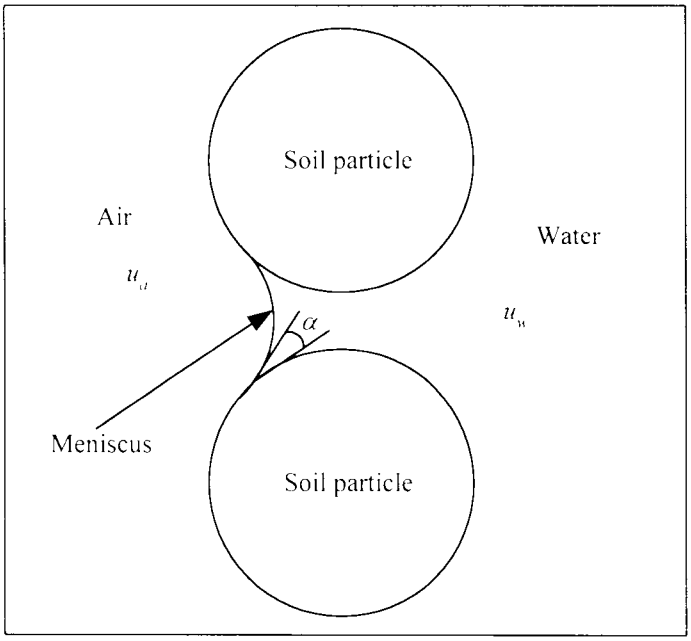

Figure 2.1 : Air-water interface within a soil void

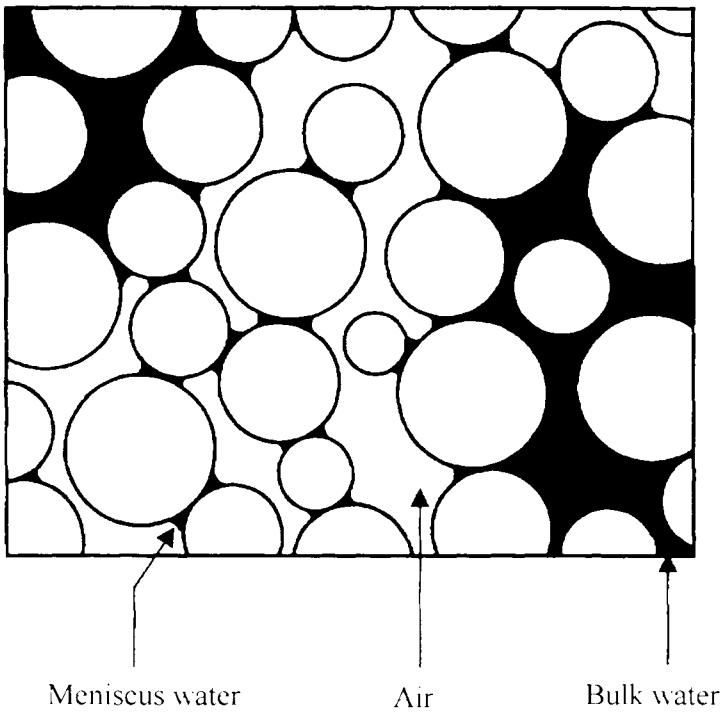

Figure 2.2 : Schematic representation of bulk water and meniscus water (after Wheeler and Karube (1996))

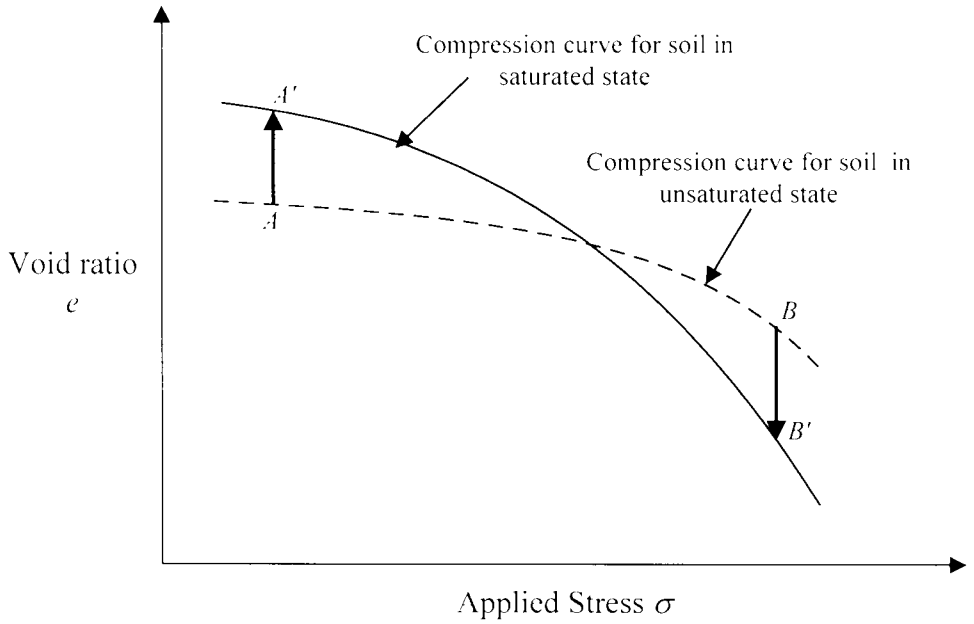

Figure 2.3 : Typical volumetric behaviour of unsaturated soils

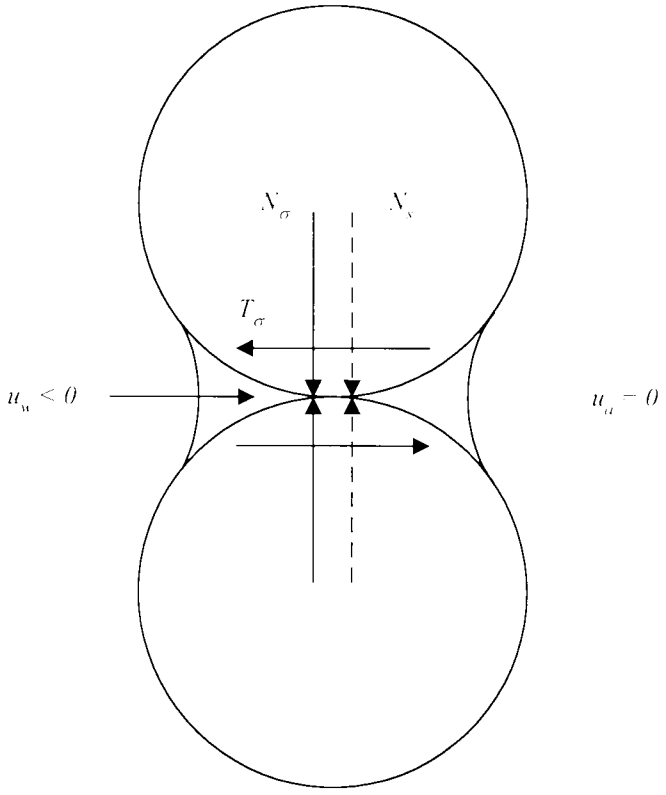

N_σ = normal component of intergranular force due to external stress
N_s = intergranular force due to suction
T_σ = tangential component of intergranular force due to external stress

Figure 2.4 : Influence of external stress and suction on inter-particle forces (after Wheeler and Karube (1996))

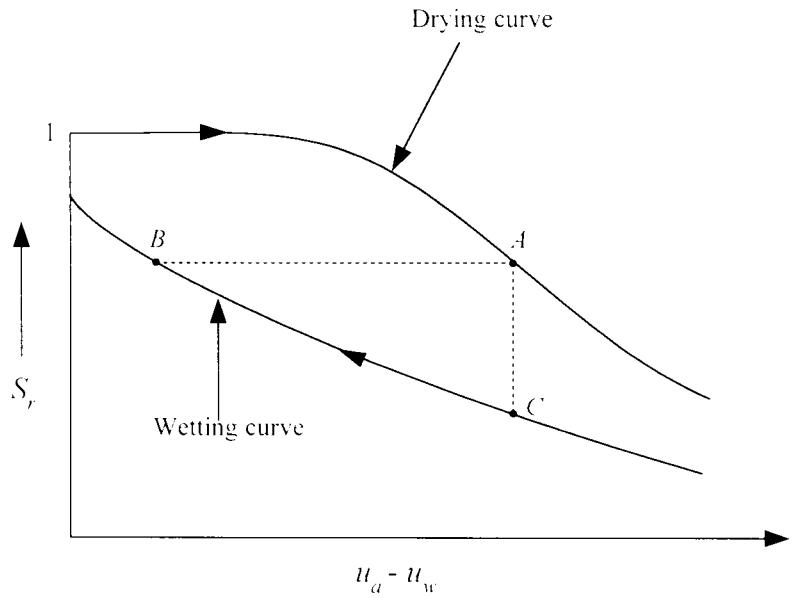

Figure 2.5 : Hysteresis of soil-water characteristic curve

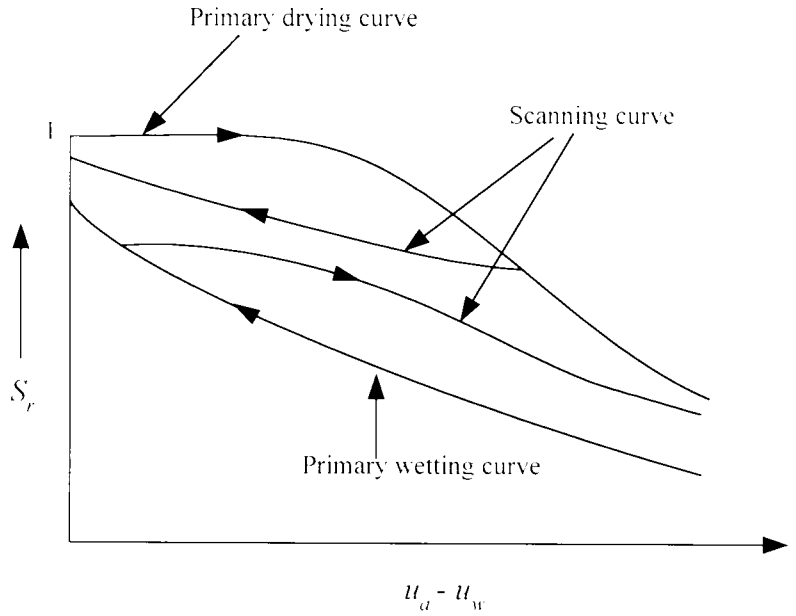

Figure 2.6 : Scanning curves along with primary wetting and drying curves

(i)

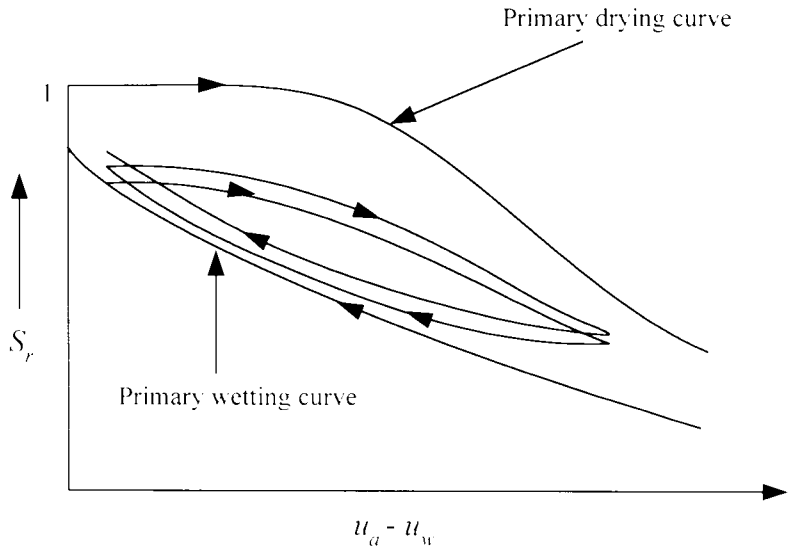

(ii)

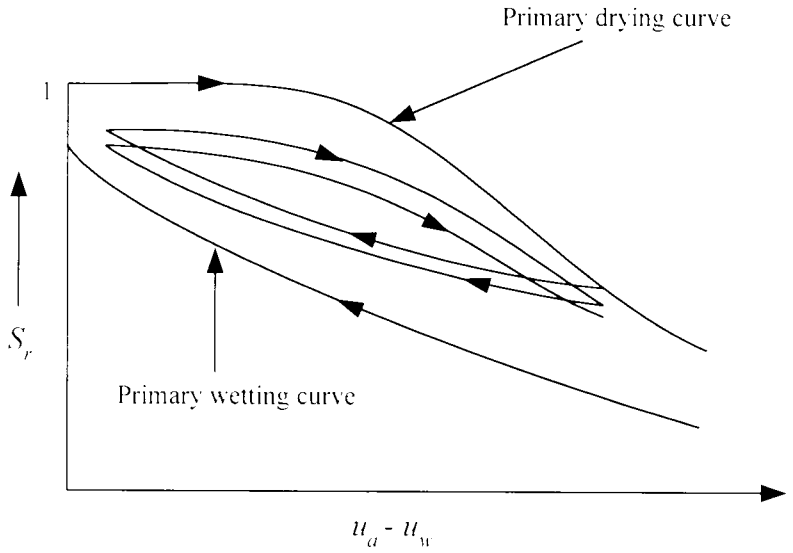

Figure 2.7 : (i) Cycles of wetting and drying starting from a primary wetting curve
(ii) Cycles of wetting and drying starting from a primary drying curve

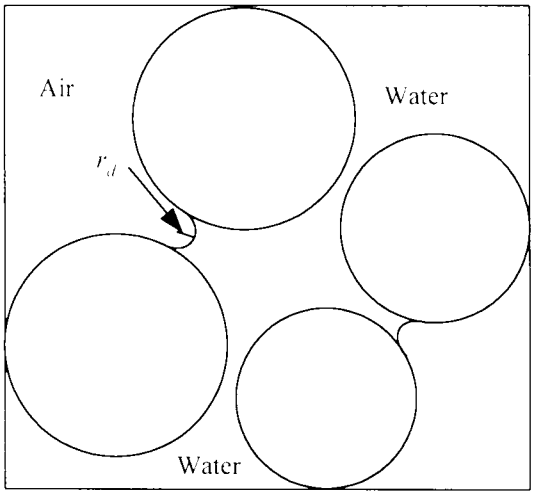

(i) Void about to empty of water during drying (see point A in Figure 2.5)

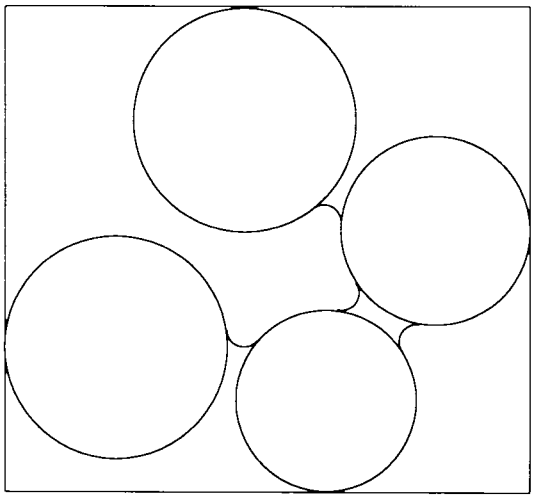

(ii) Void empty of water

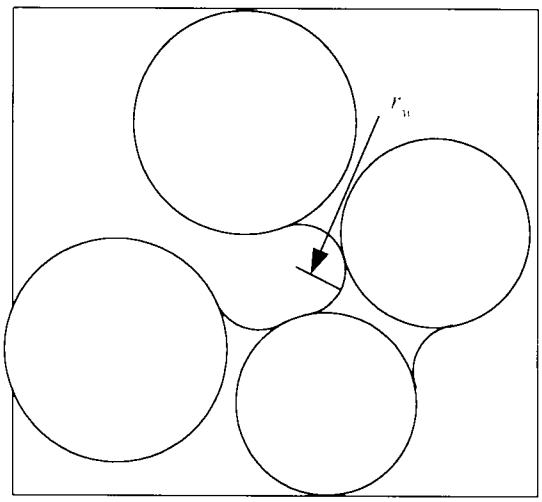

(iii) Void about to flood with water during wetting (see point B in Figure 2.5)

Figure 2.8 : Emptying and flooding of a void during drying and wetting

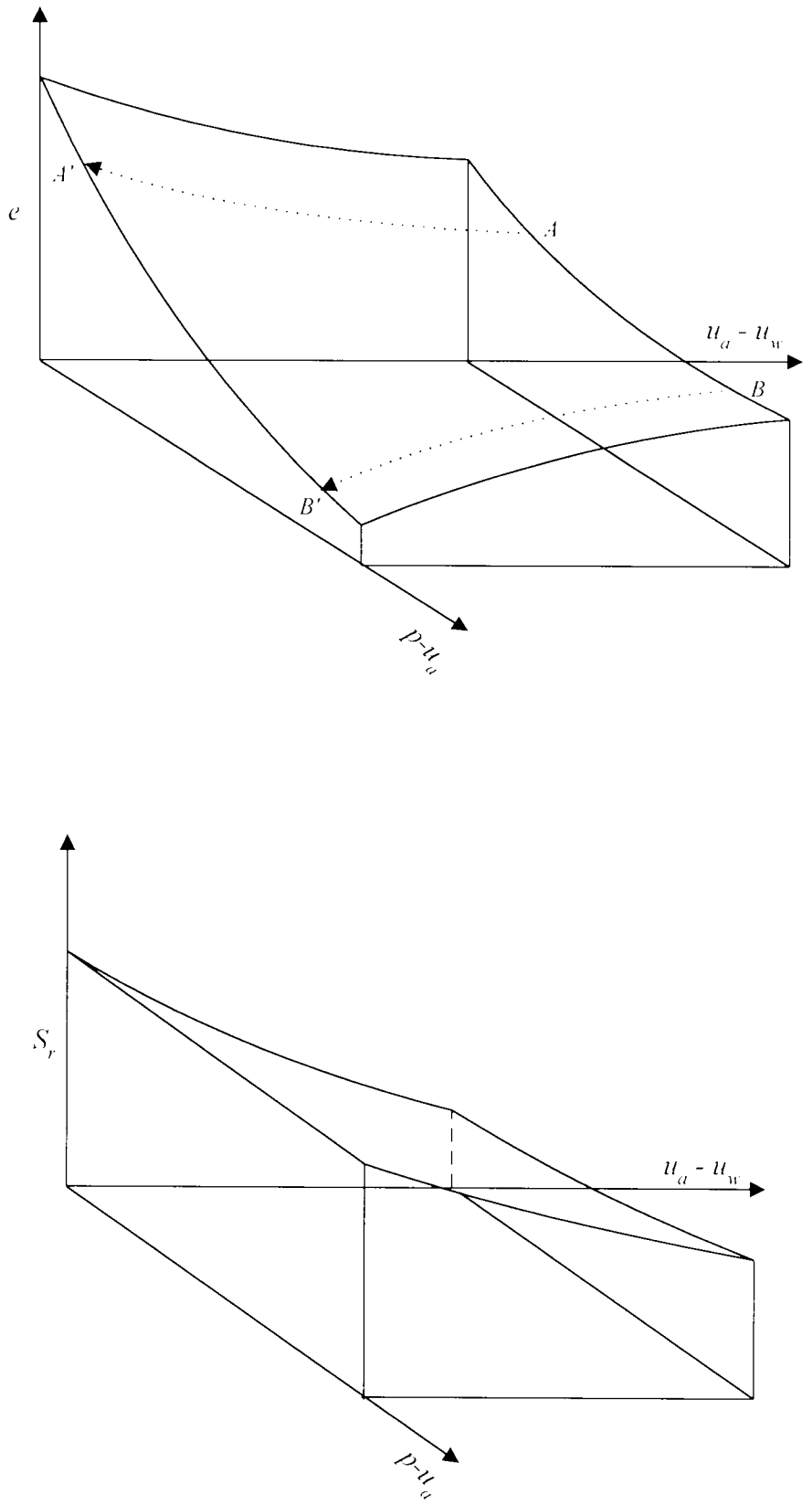

Figure 2.9 : State surfaces for void ratio and degree of saturation (after Matyas and Radhakrishna (1968))

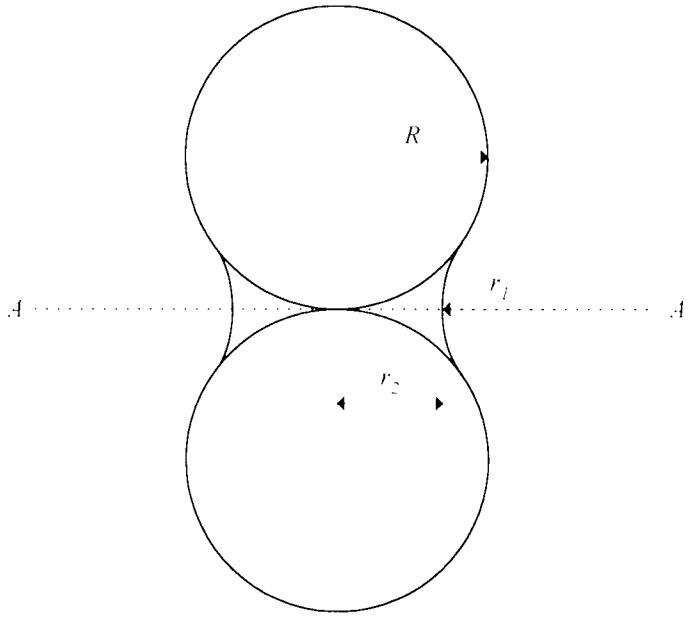

Figure 2.10 : Contact of spherical particles

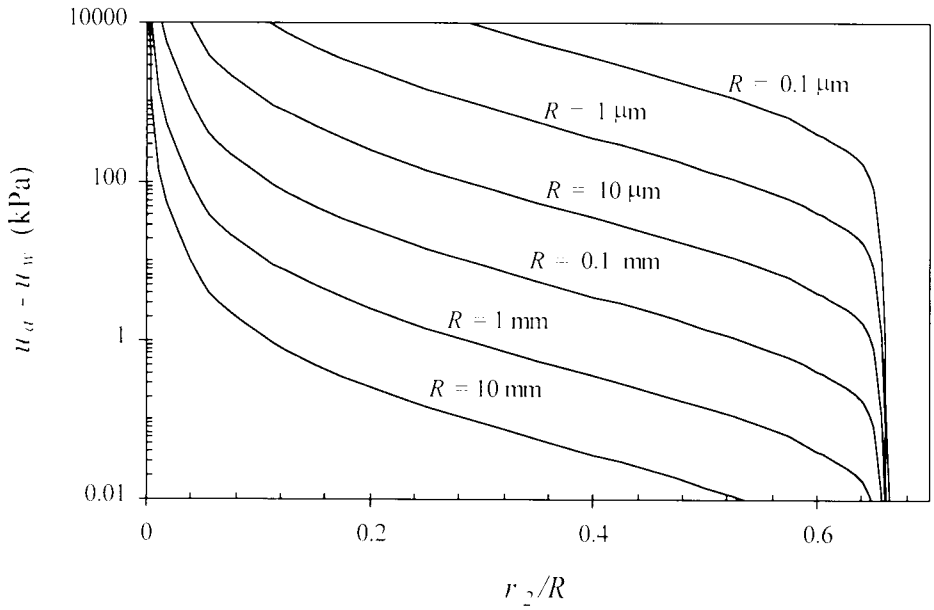

Figure 2.11 : Variation of u_a - u_w with r_2/R for shperical particles

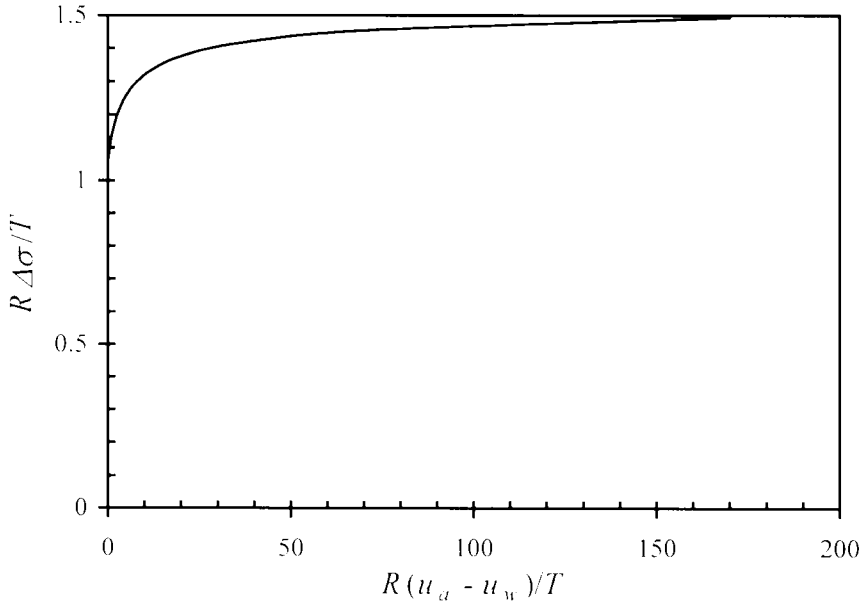

Figure 2.12 : Non-dimensional variation of $\Delta\sigma$ against $u_a - u_w$ for spherical particles

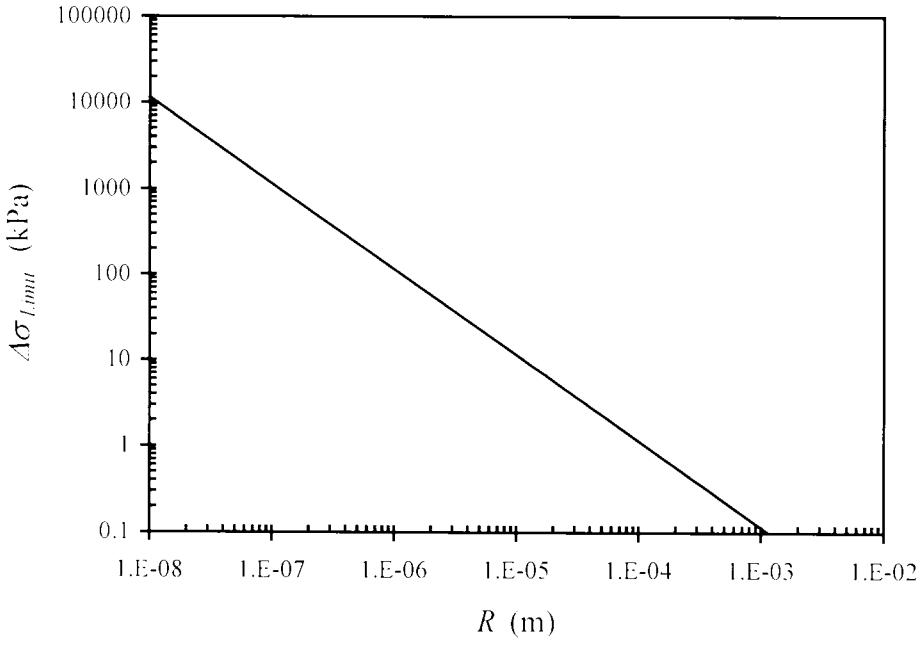

Figure 2.13 : Variation of $\Delta\sigma_{Limit}$ for spherical particles

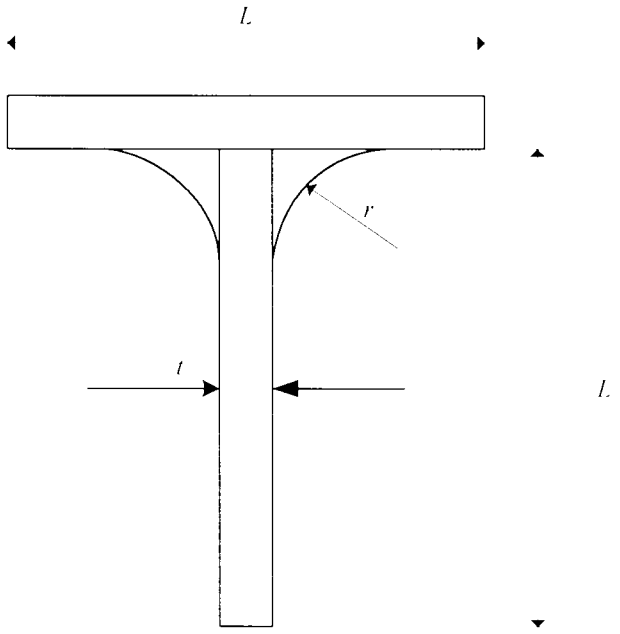

Figure 2.14 : Contact of platy particles

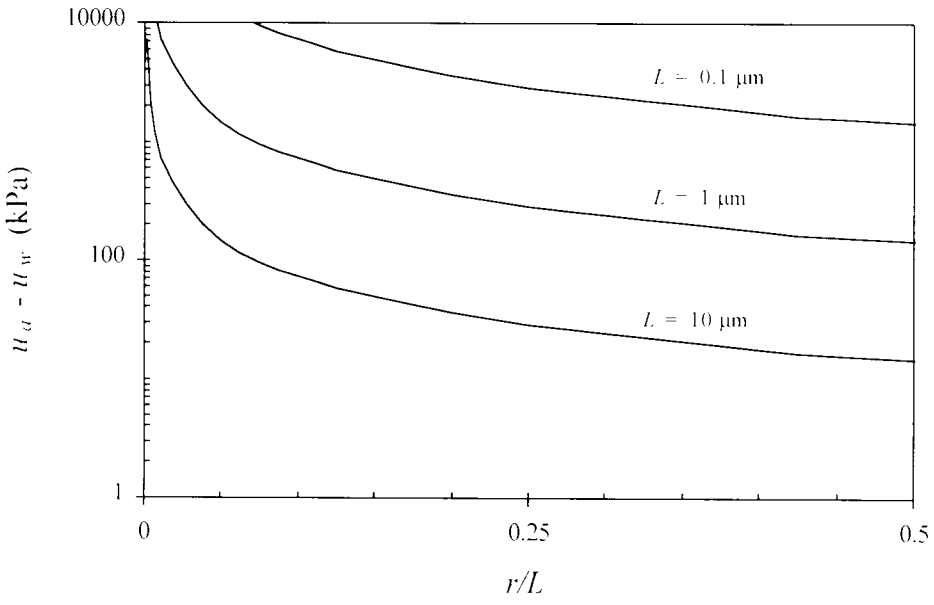

Figure 2.15 : Variation of u_a - u_w with r/L for platy particles

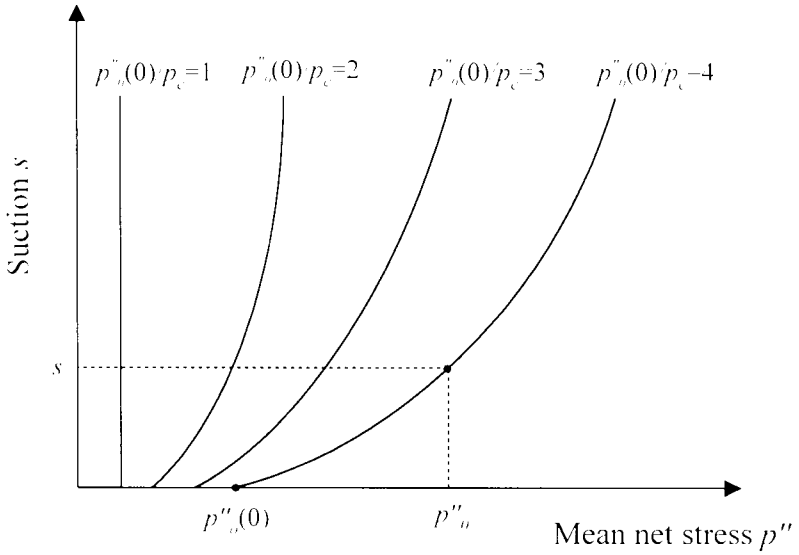

Figure 2.16 :Expansion of the *LC* yield curve
(after Alonso *et al* (1990))

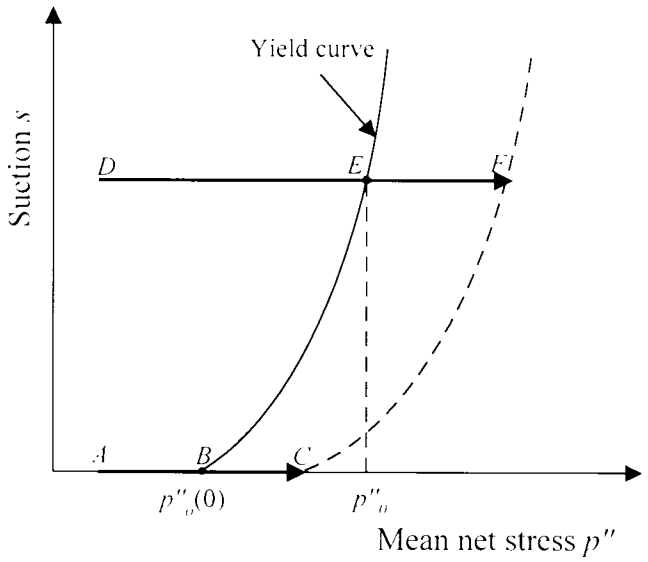

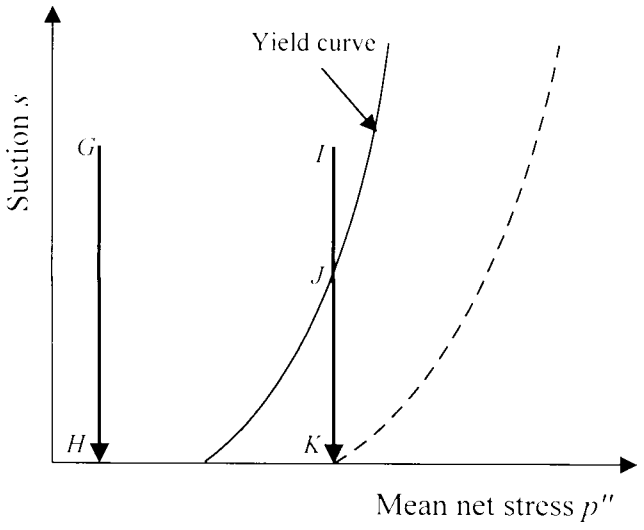

Figure 2.17 : Loading collapse *LC* yield curve
(after Alonso *et al* (1987))

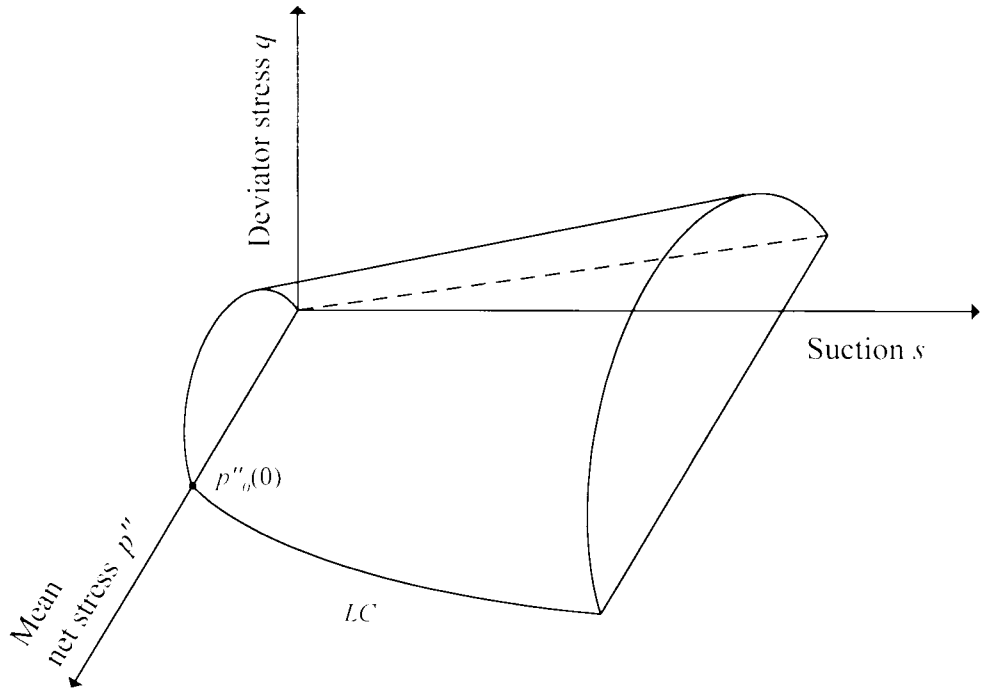

Figure 2.18 : Yield surface in $q : p'' : s$ space
(after Alonso *et al* (1990))

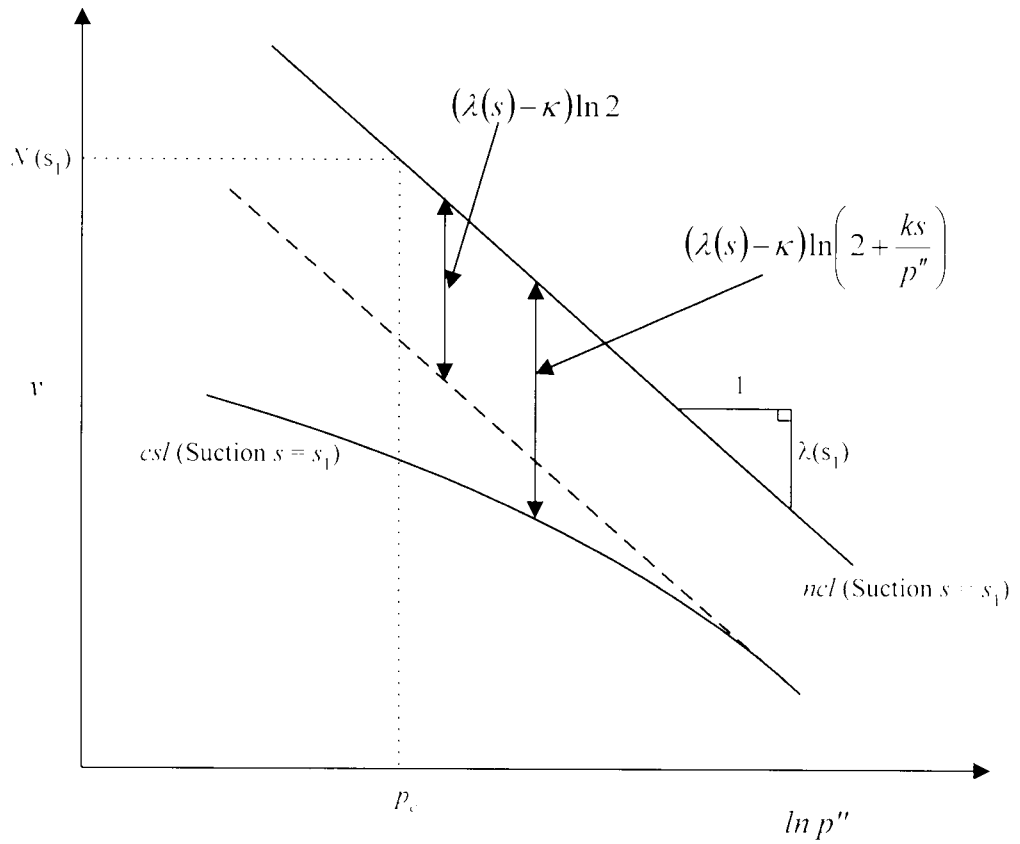

Figure 2.19 : Shape of critical state line (*csl*) in
$v : ln\ p''$ plot predicted by Alonso *et al* (1990)

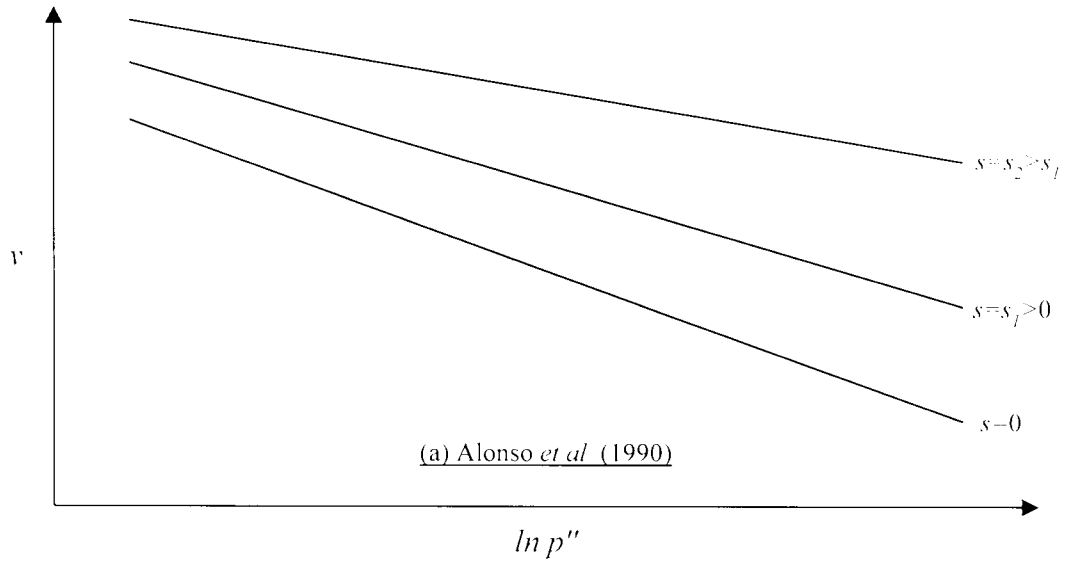

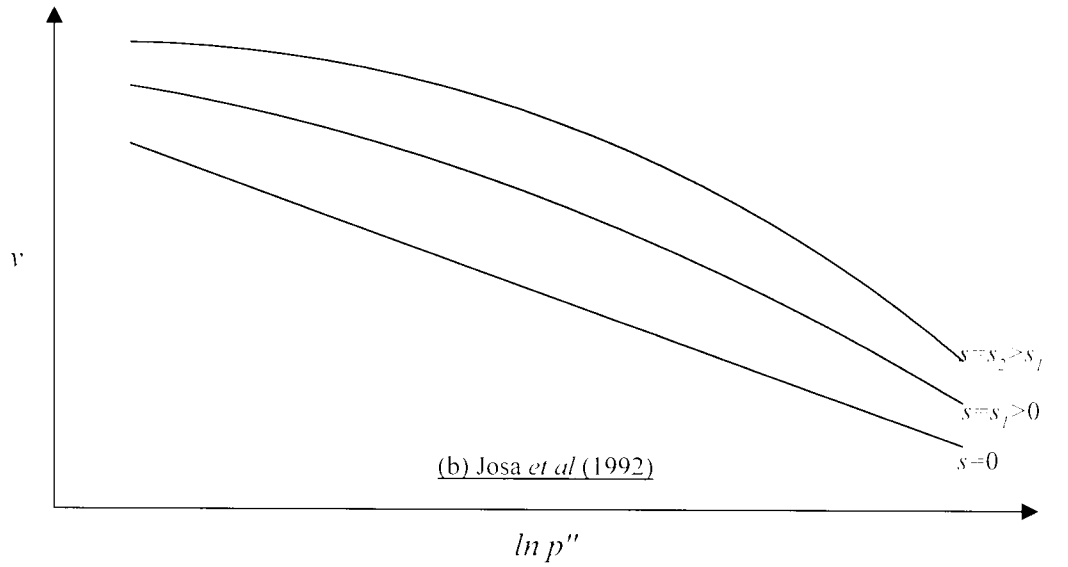

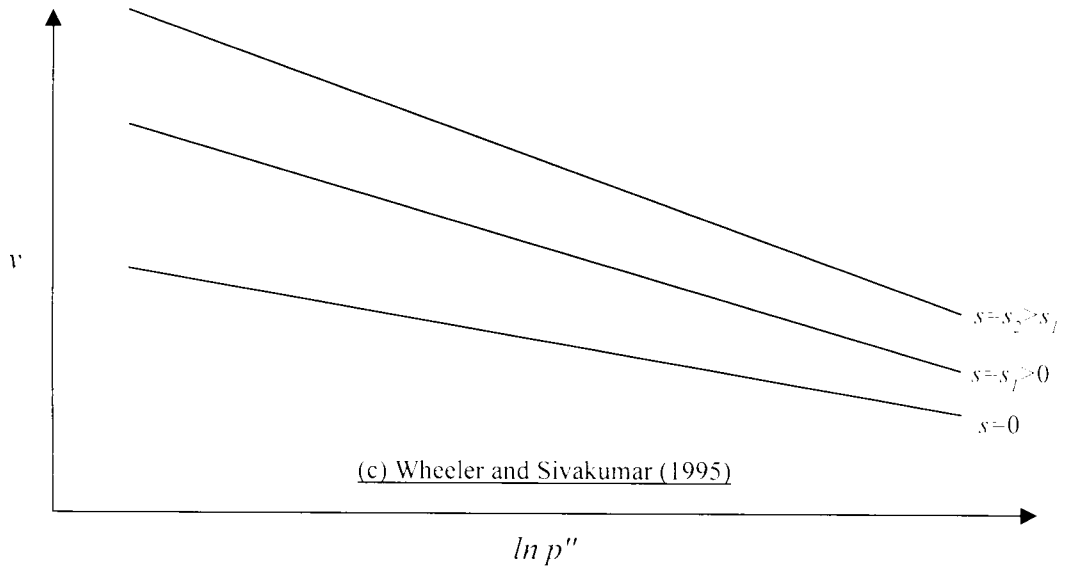

Figure 2.20 : Forms of normal compression lines

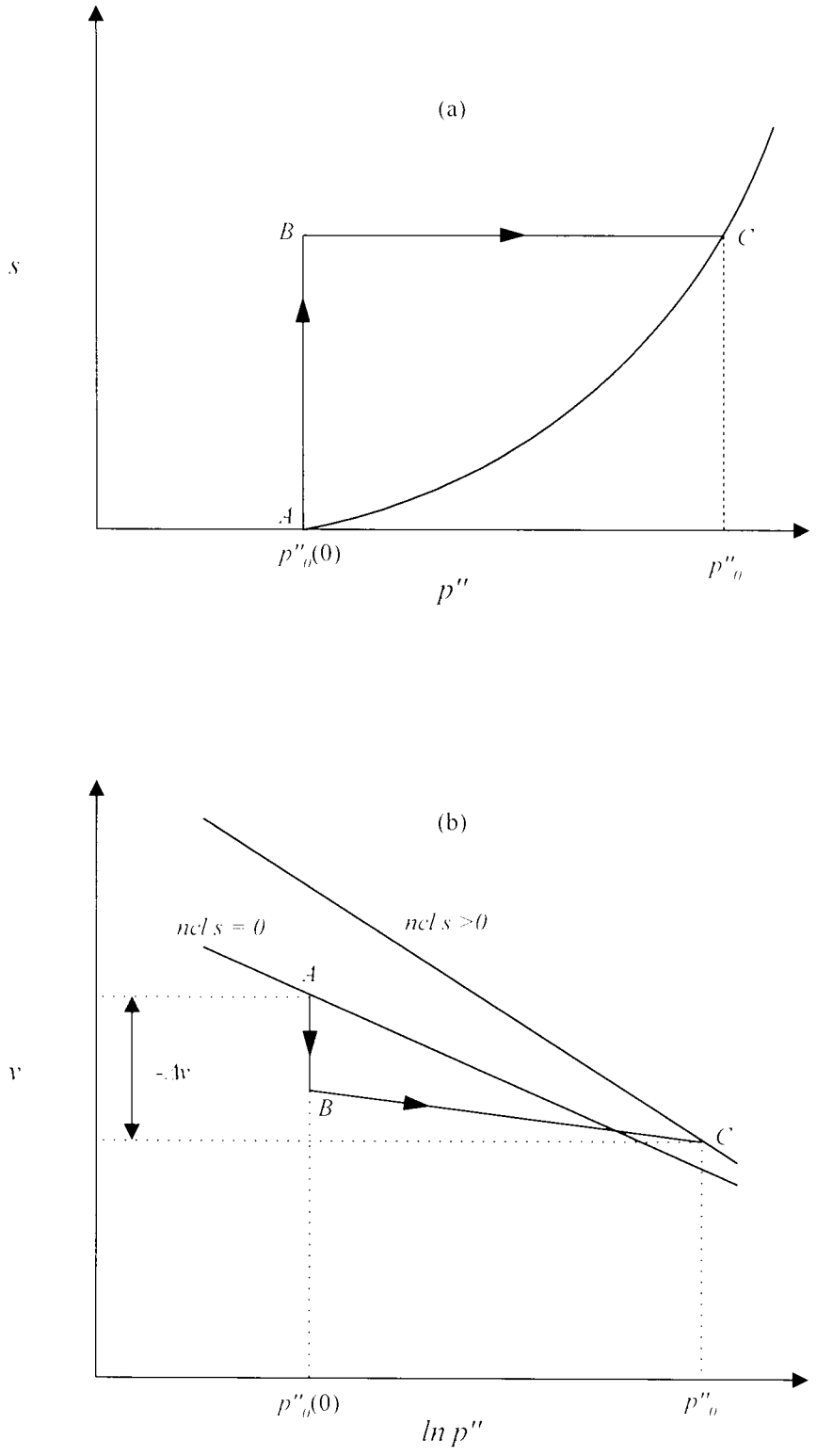

Figure 2.21 : Derivation of *LC* yield curve equation
(Wheeler and Sivakumar (1995))

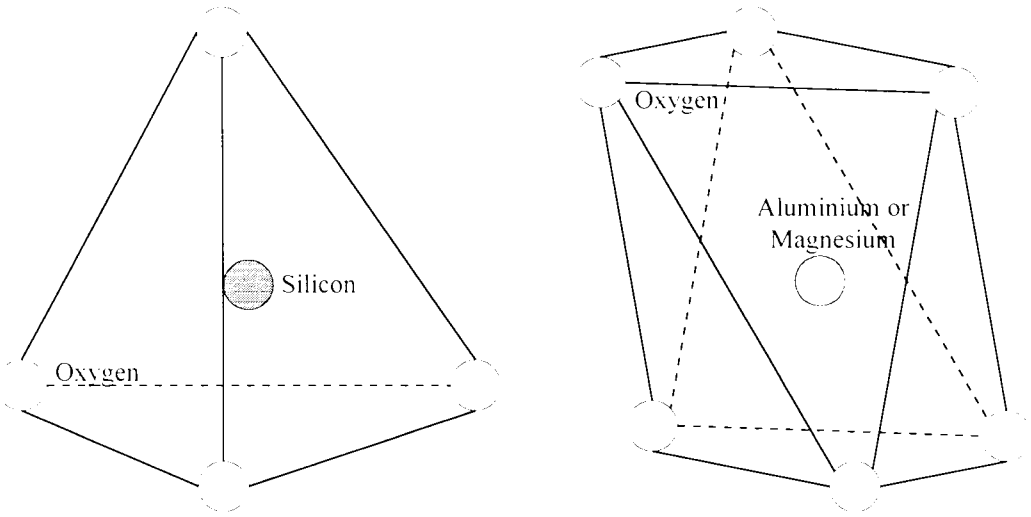

Figure 3.1 : Molecular arrangement in clays

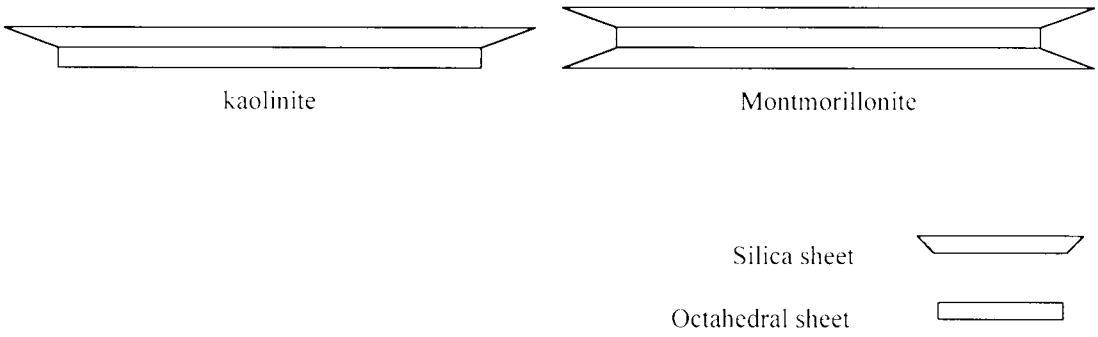

Figure 3.2 : Unit layers

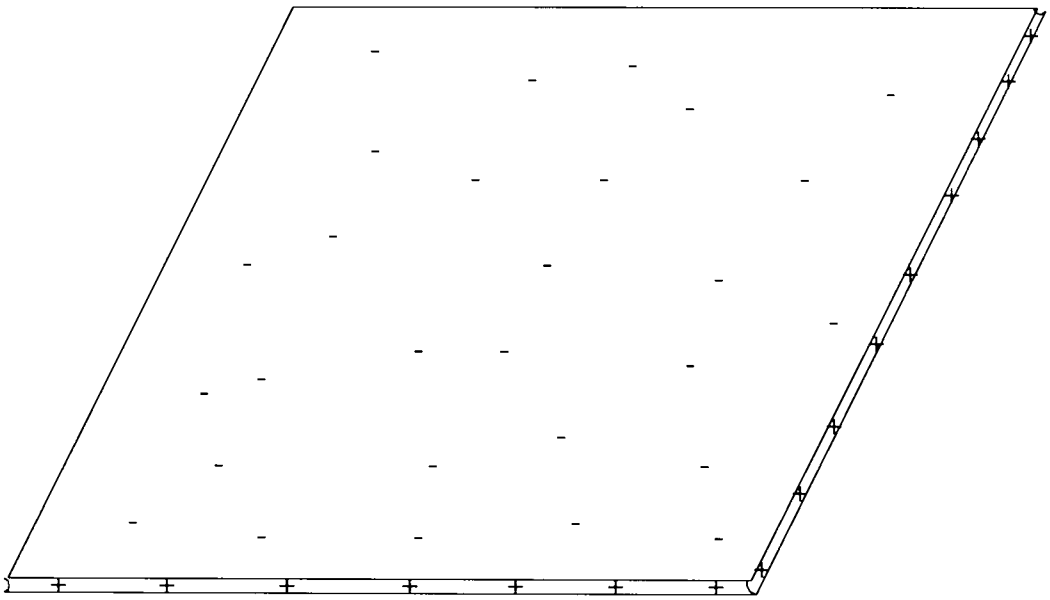

Figure 3.3 : Idealised unit layer with electrical charge

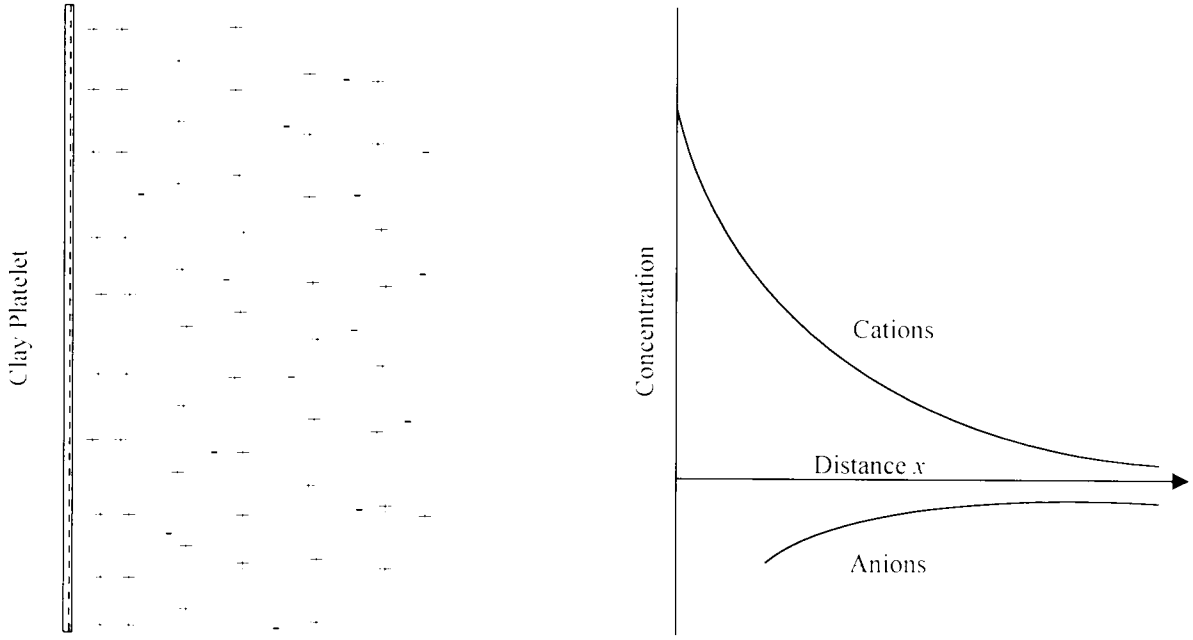

Figure 3.4 : Diffuse double layer and ion distribution
(after Mitchell (1993))

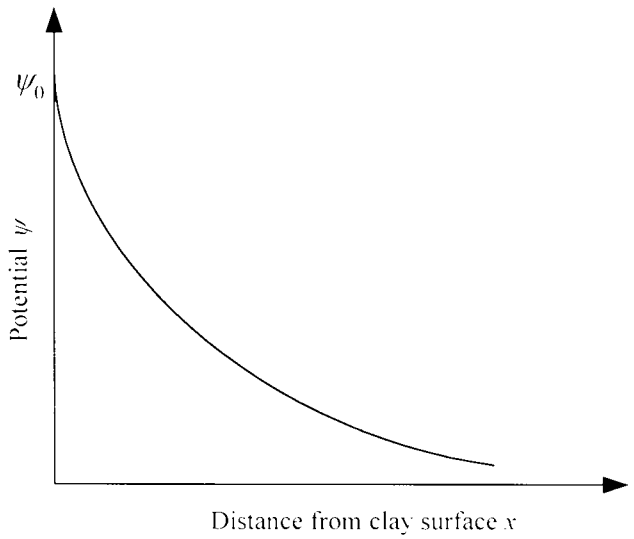

Figure 3.5 : Variation of electrical potential with distance from a clay surface (after Mitchell (1993))

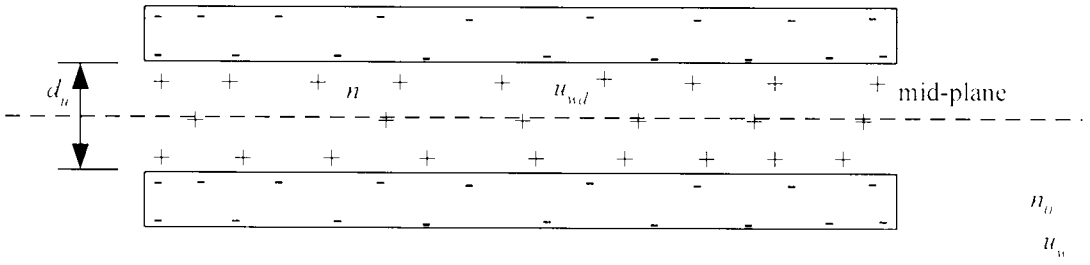

Figure 3.6 (a) : Interaction between *DDLs* of two unit layers in a saturated environment

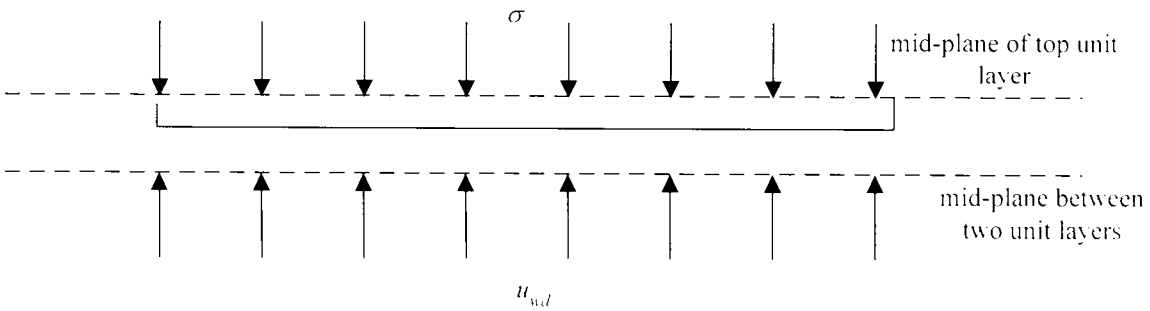

Figure 3.6 (b) : Free body diagram for force equilibrium

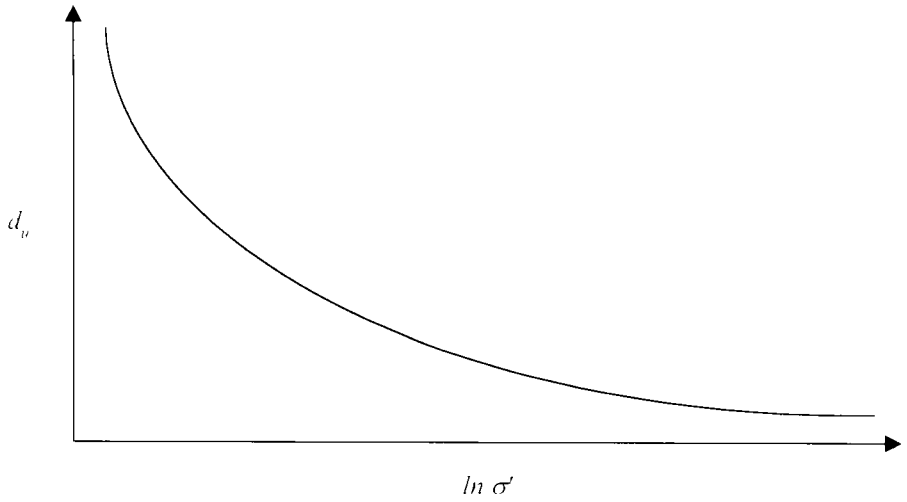

Figure 3.7 : Typical variation of unit layer separation d_u with effective stress for saturated conditions (after Bolt (1956))

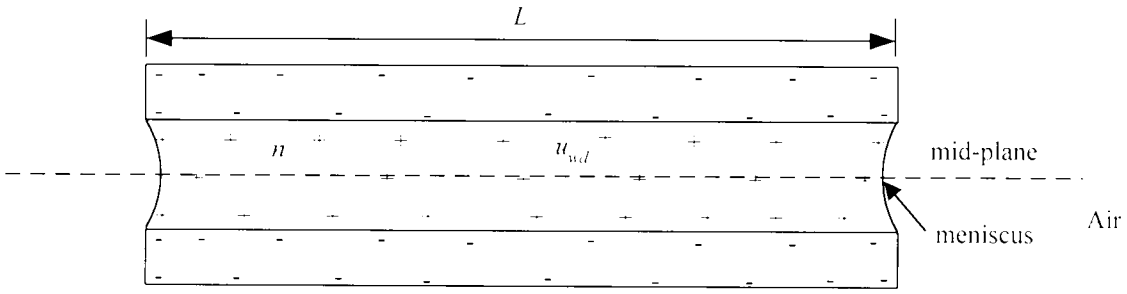

Figure 3.8 : Interaction between *DDLs* of two unit layers in an unsaturated environment

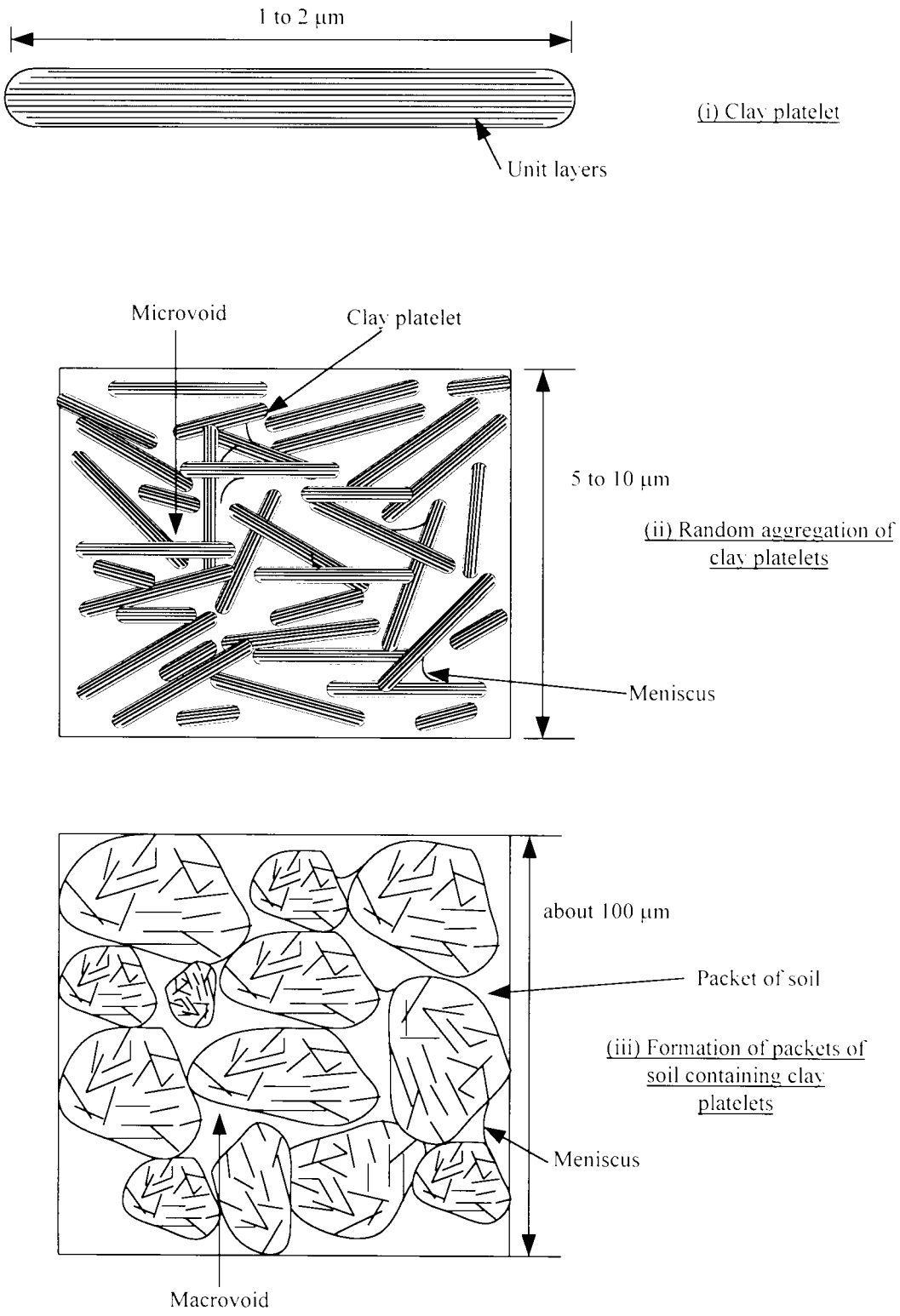

Figure 3.9 : Conceptual model for fabric of compacted clays

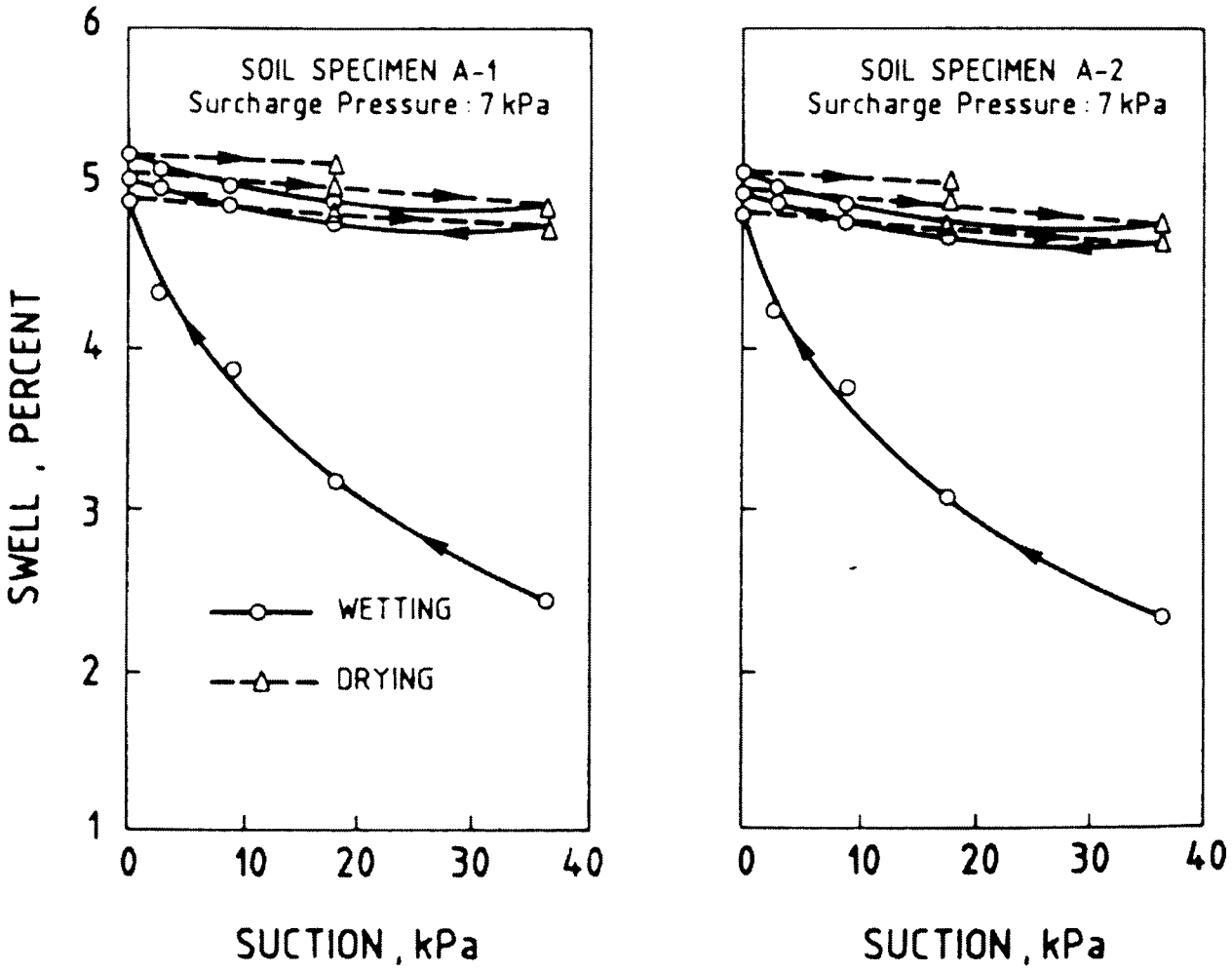

Figure 3.10 : Results for wetting/drying cycles on a highly expansive clay (after Chu and Mou (1973))

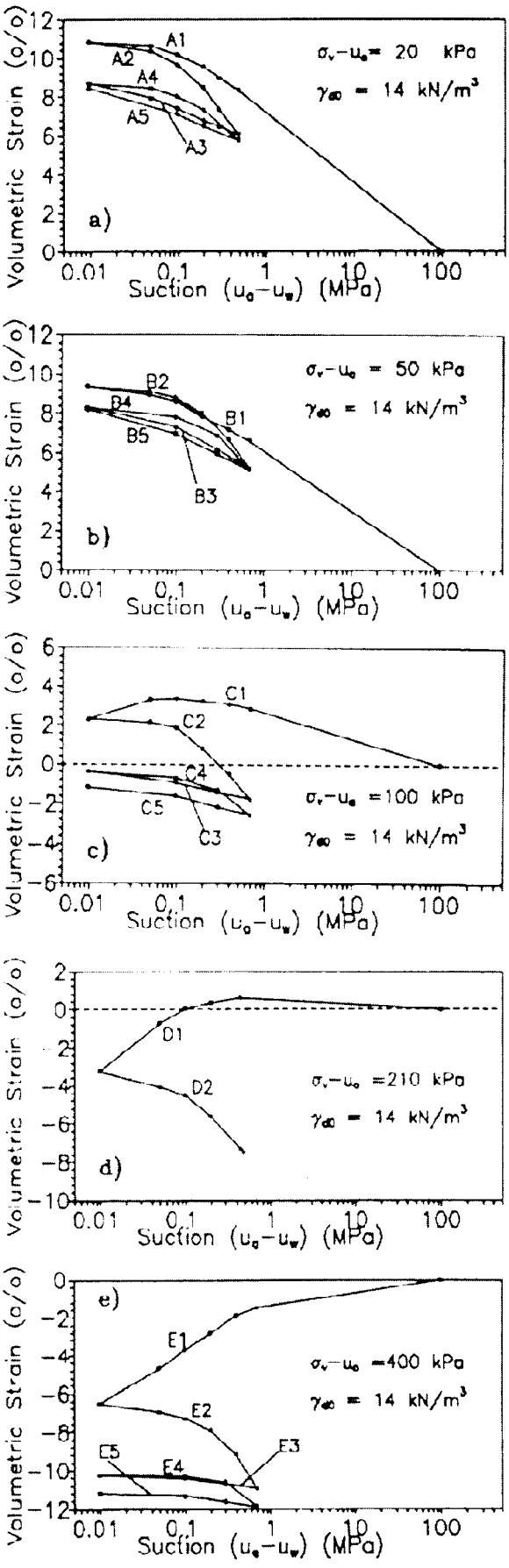

Figure 3.11 : Wetting/drying cycles performed on Boom clay (Alonso et al (1995))

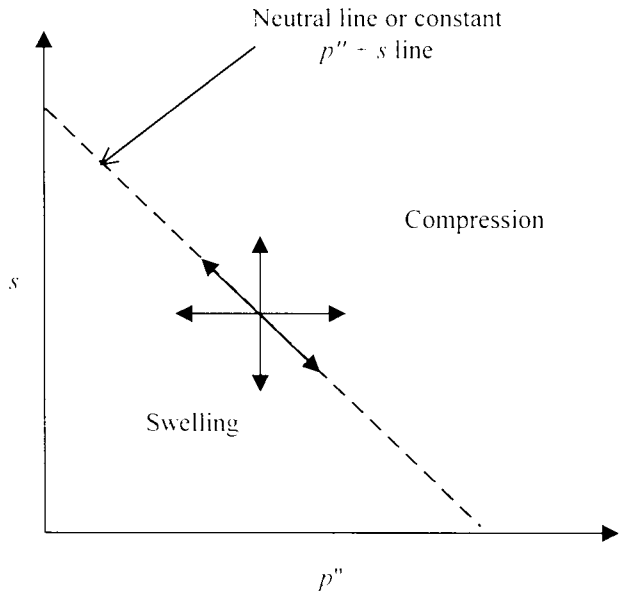

Figure 3.12 : Behaviour of microfabric - concept of neutral line (Gens and Alonso (1992))

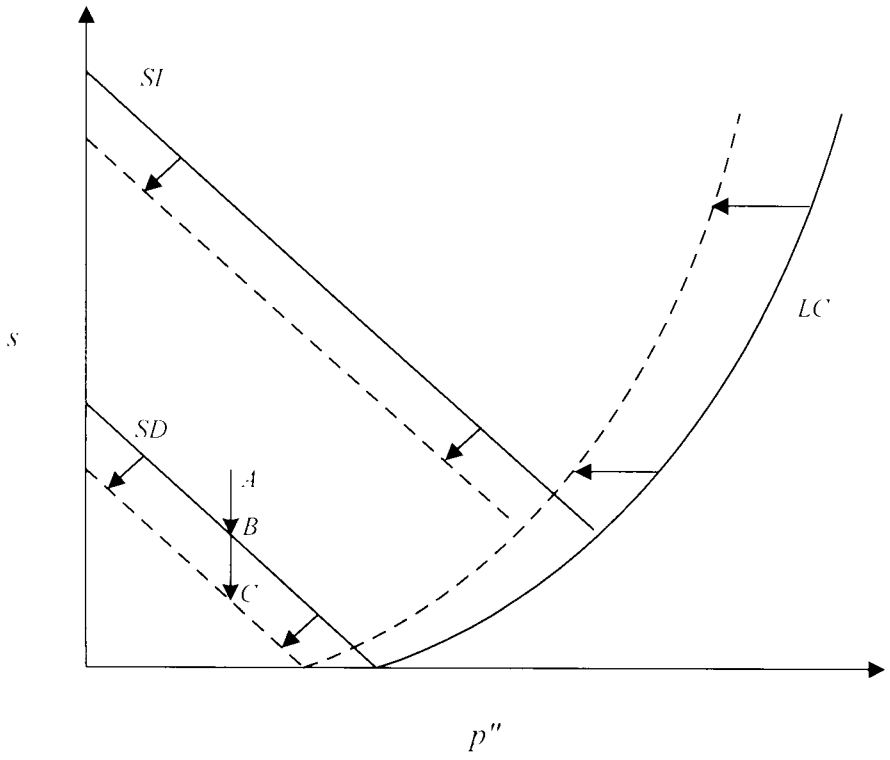

Figure 3.13 : Coupling mechanism between two levels of soil fabric (Alonso *et al* (1994))

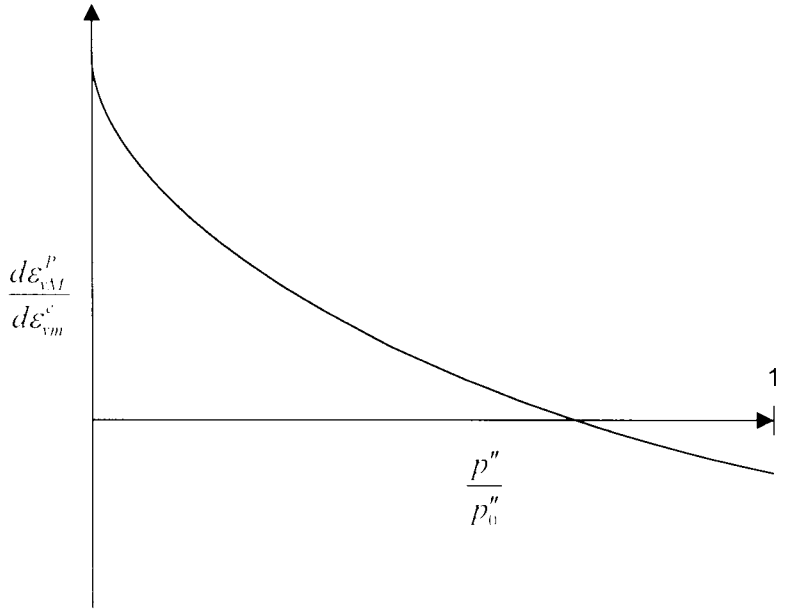

Figure 3.14 : Coupling of strains of micro and macrofabrics for unsatuarted highly expansive clays (Alonso *et al* (1994))

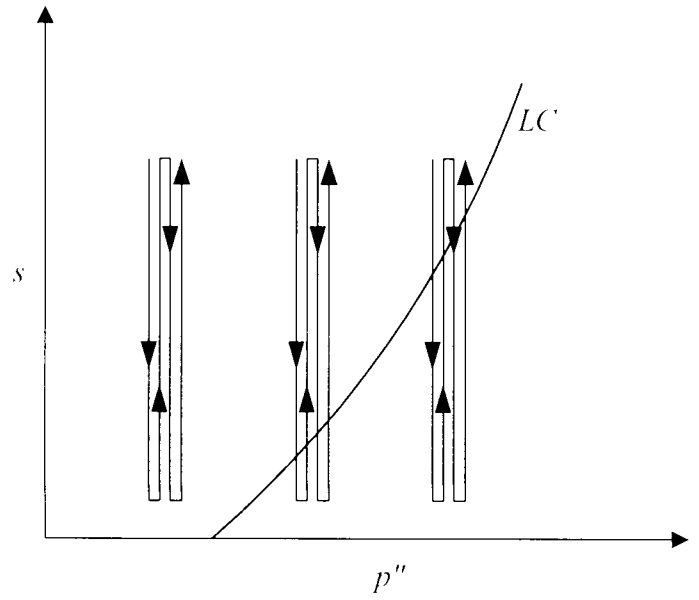

Figure 3.15 : Stress paths for wetting and drying tests

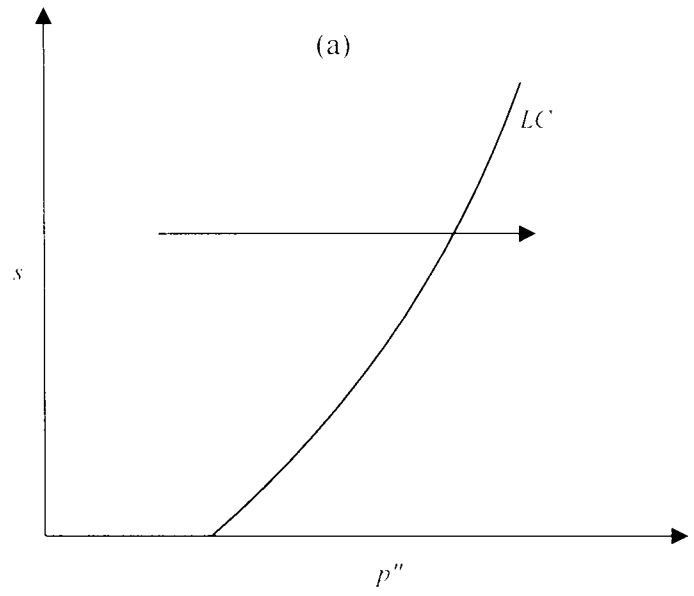

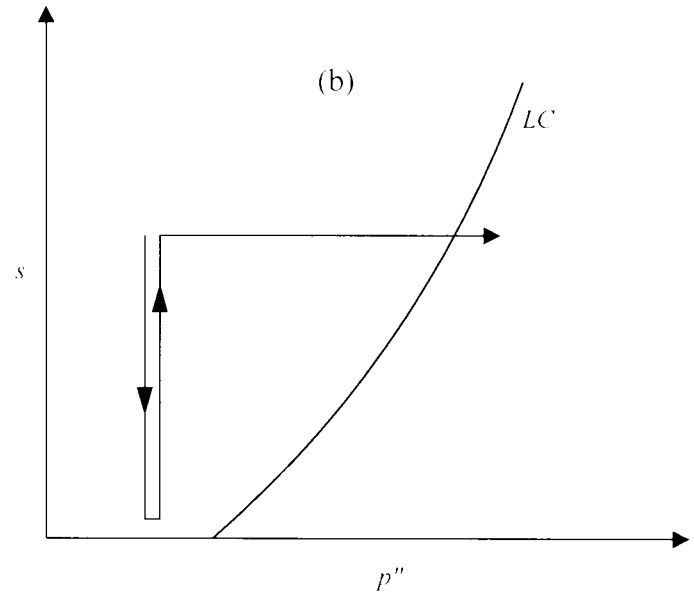

Figure 3.16 : Typical stress paths for tests to explore coupling between the micro and macro levels of soil fabric

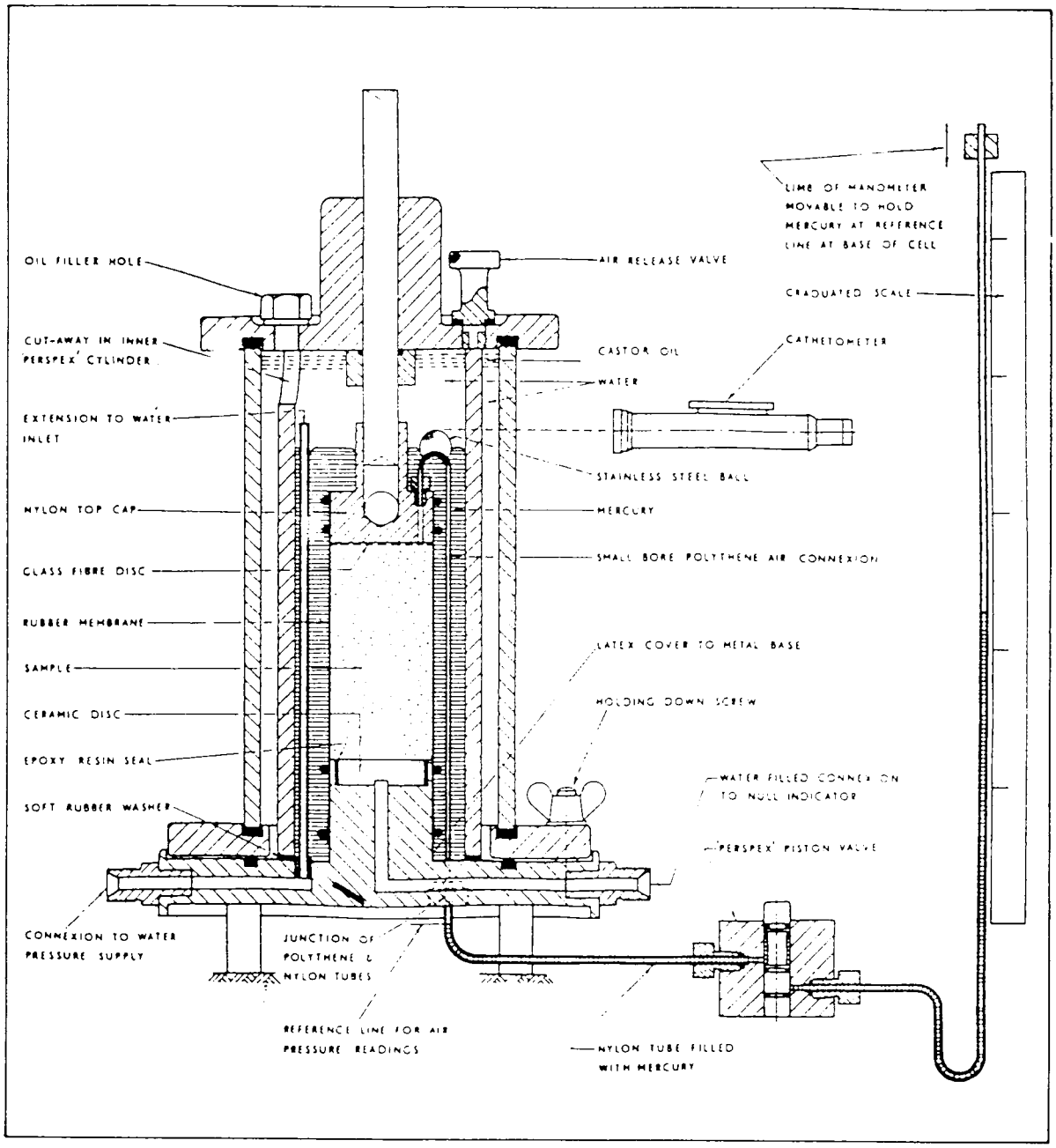

Figure 4.1 : Triaxial apparatus for testing of unsaturated soils
(after Bishop and Donald (1961))

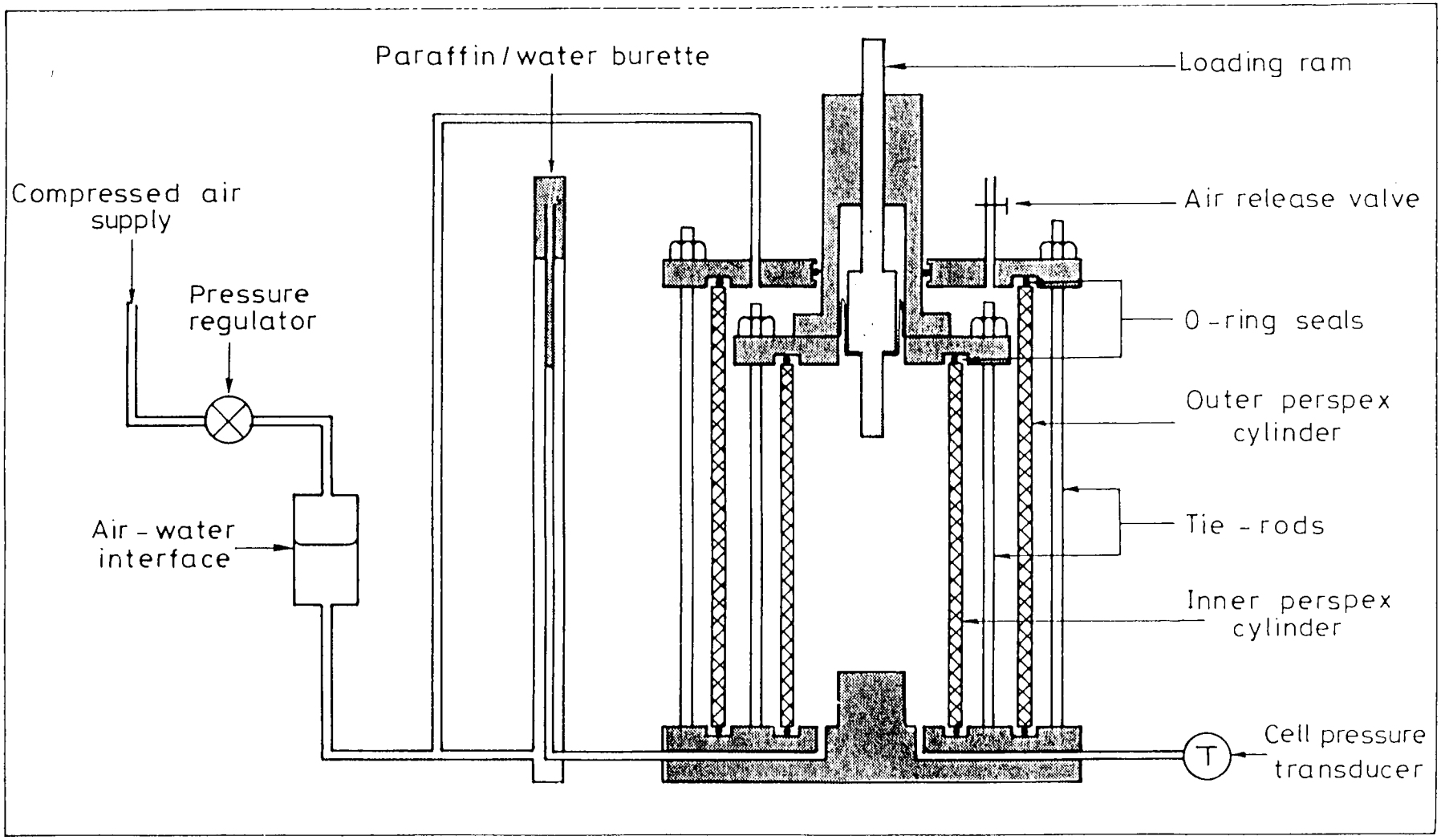

Figure 4.2 : Modified triaxial apparatus for testing of unsaturated soils
(after Wheeler (1986))

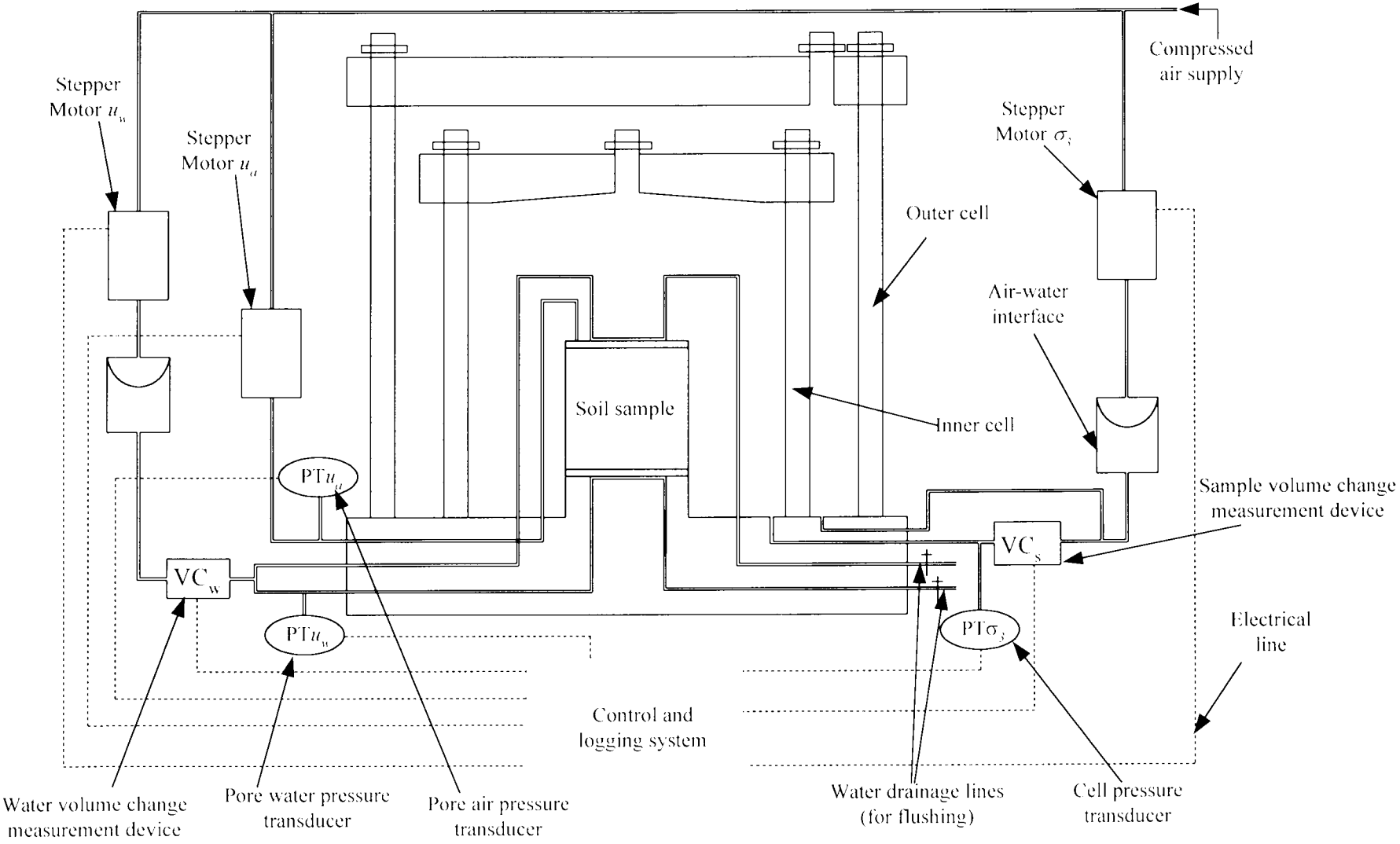

Figure 4.3 : General layout of experimental apparatus

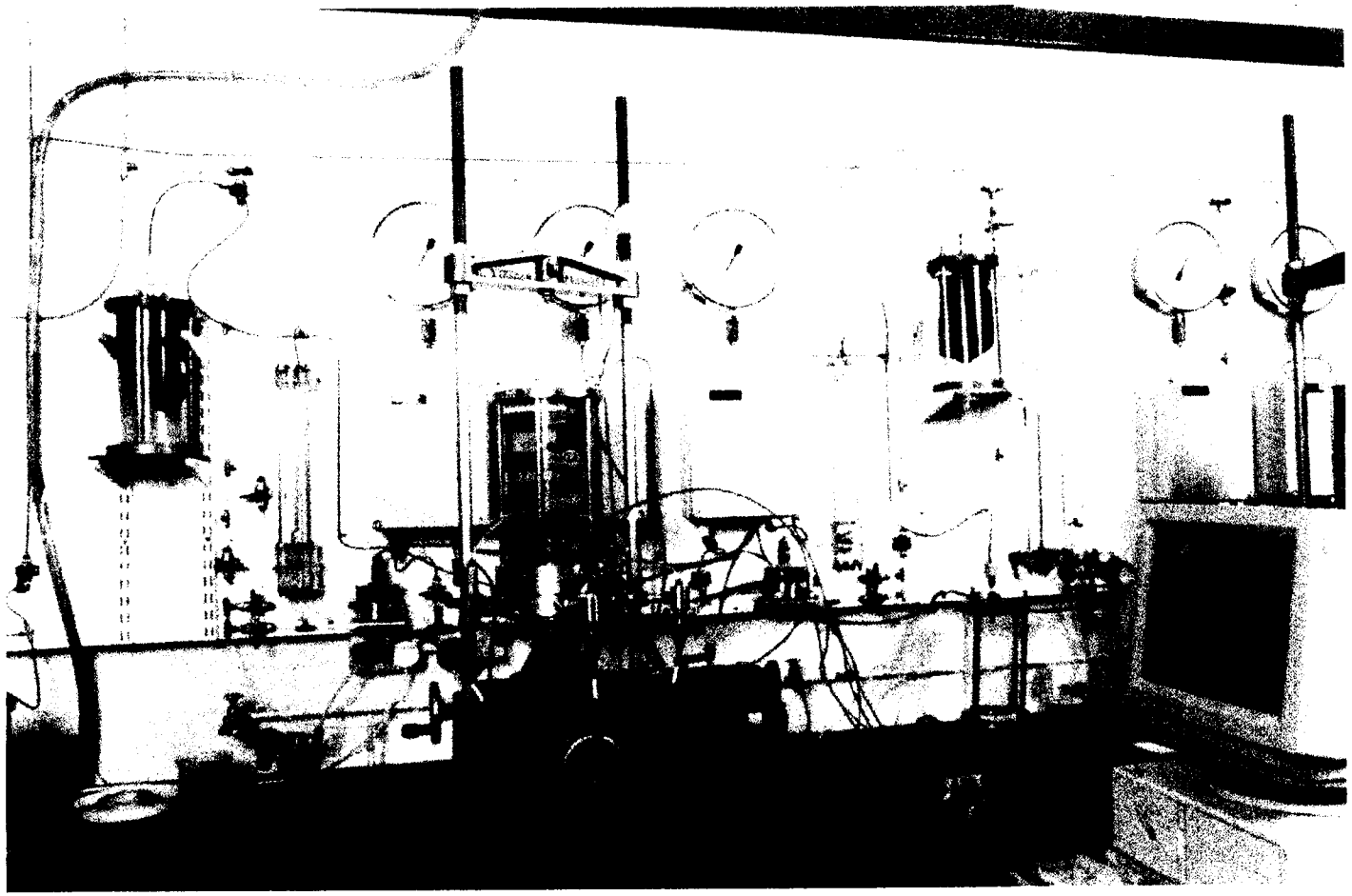

Figure 4.4 : General view of System *A*

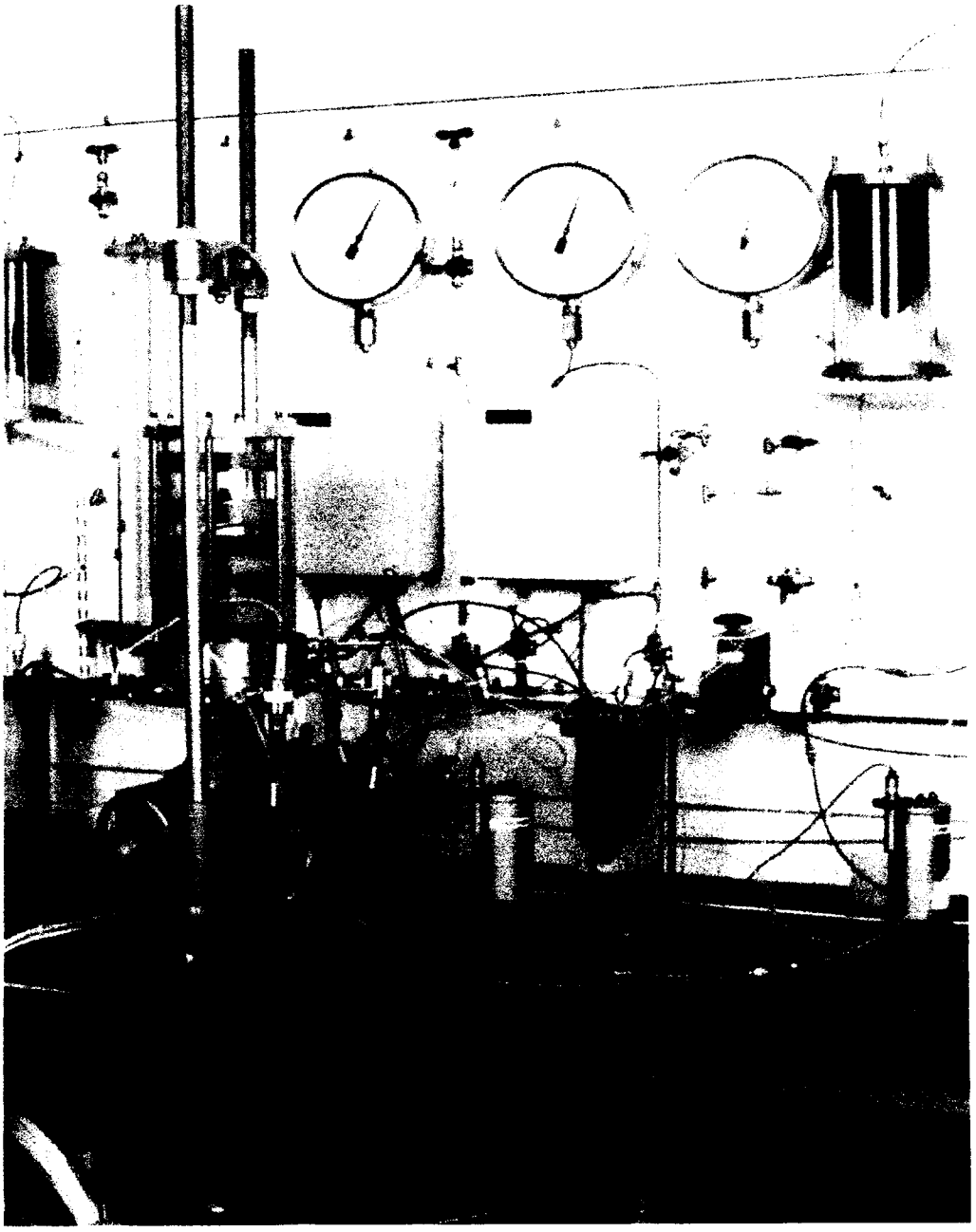

Figure 4.5 : General view of System *B*

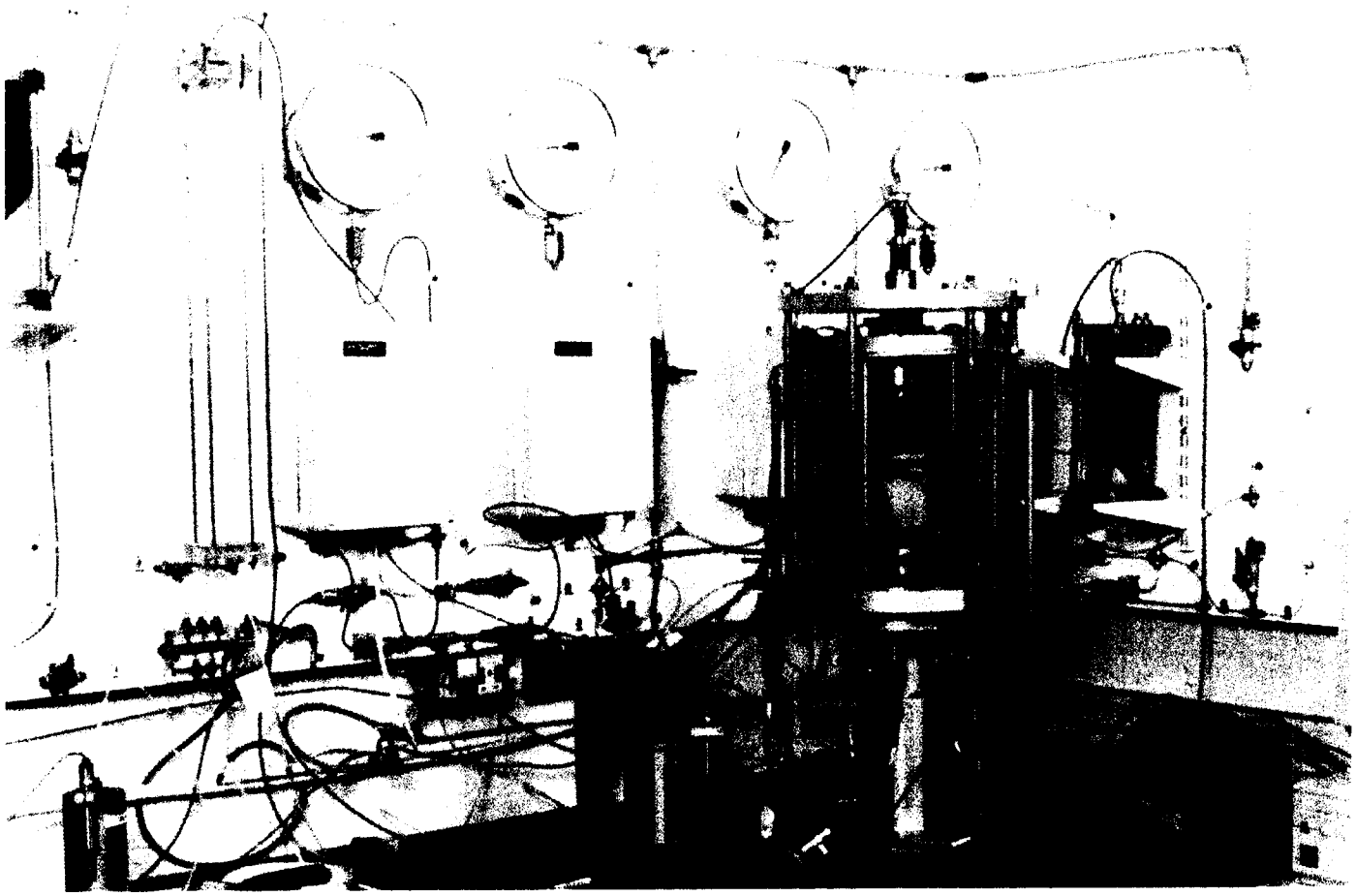

Figure 4.6 : General view of System C

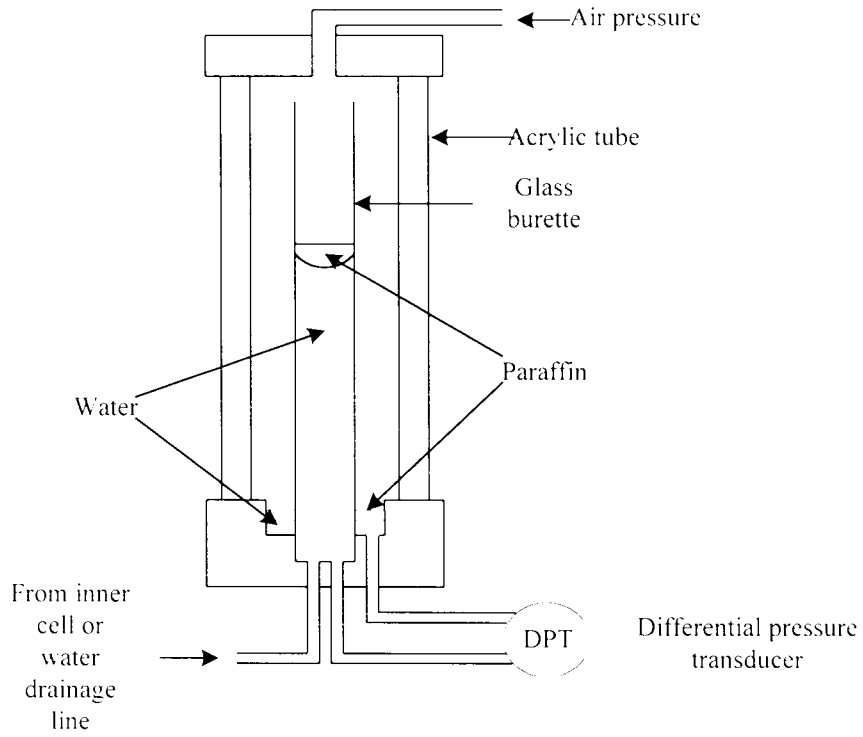

Figure 4.7 : Burette type volume change measurement device

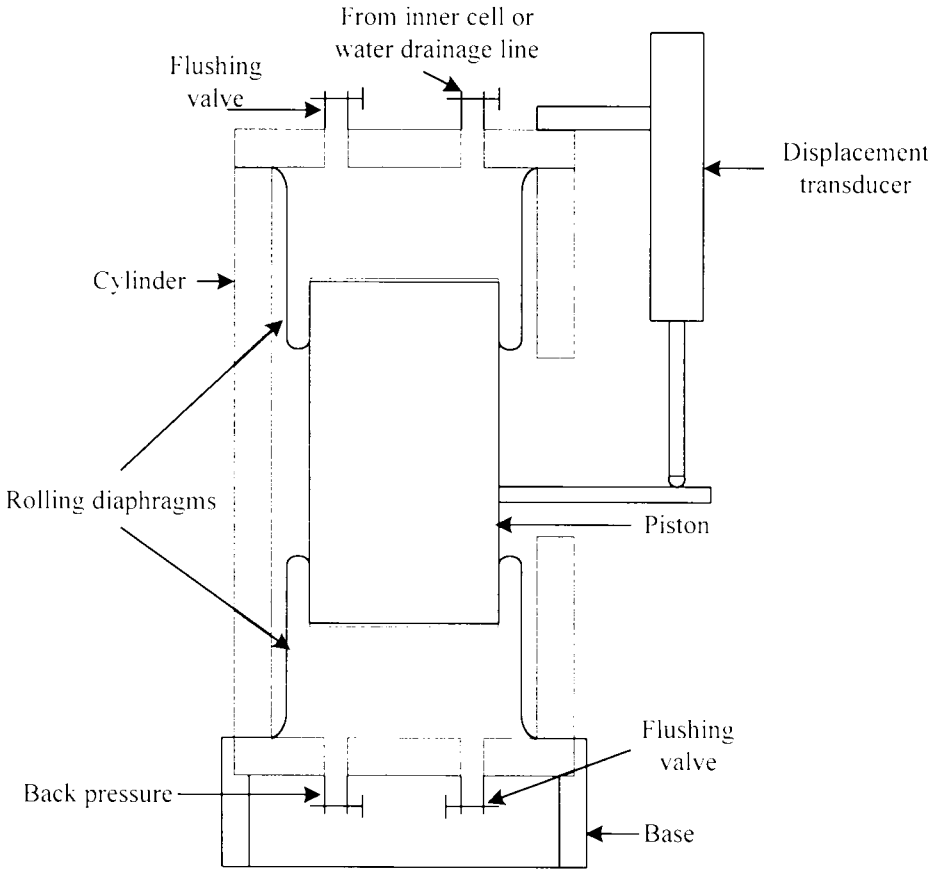

Figure 4.8 : Imperial College volume change measurement device

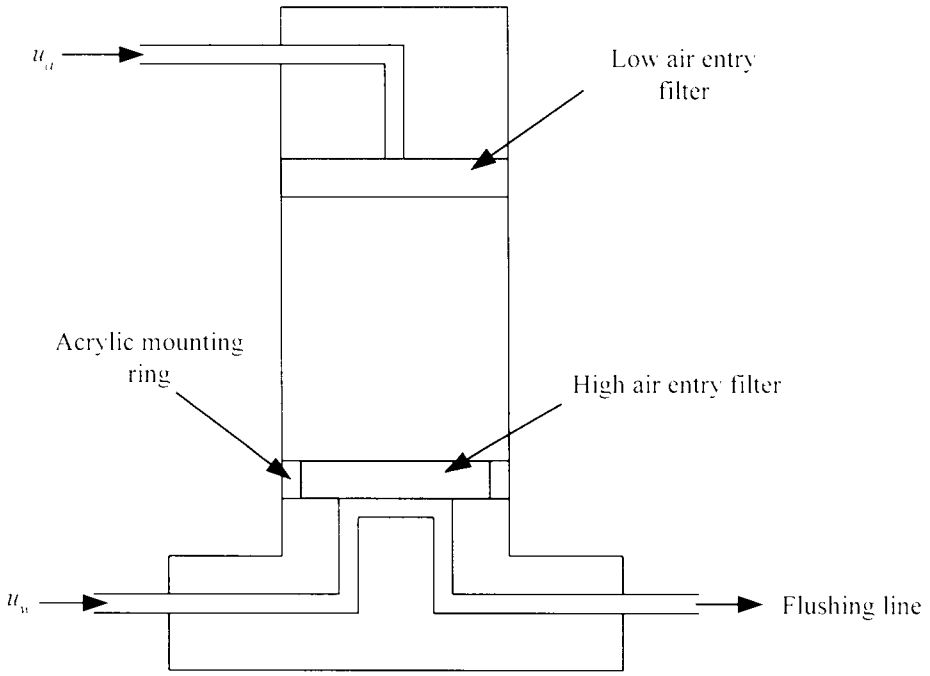

Figure 4.9 : Layout for water drainage from bottom only

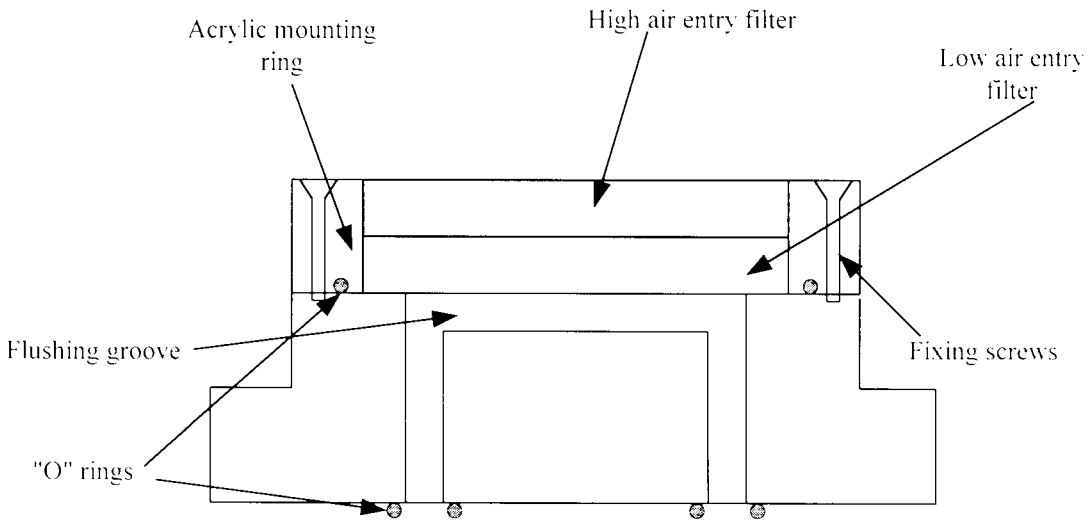

Figure 4.10 : High air entry filter assembly for pedestal

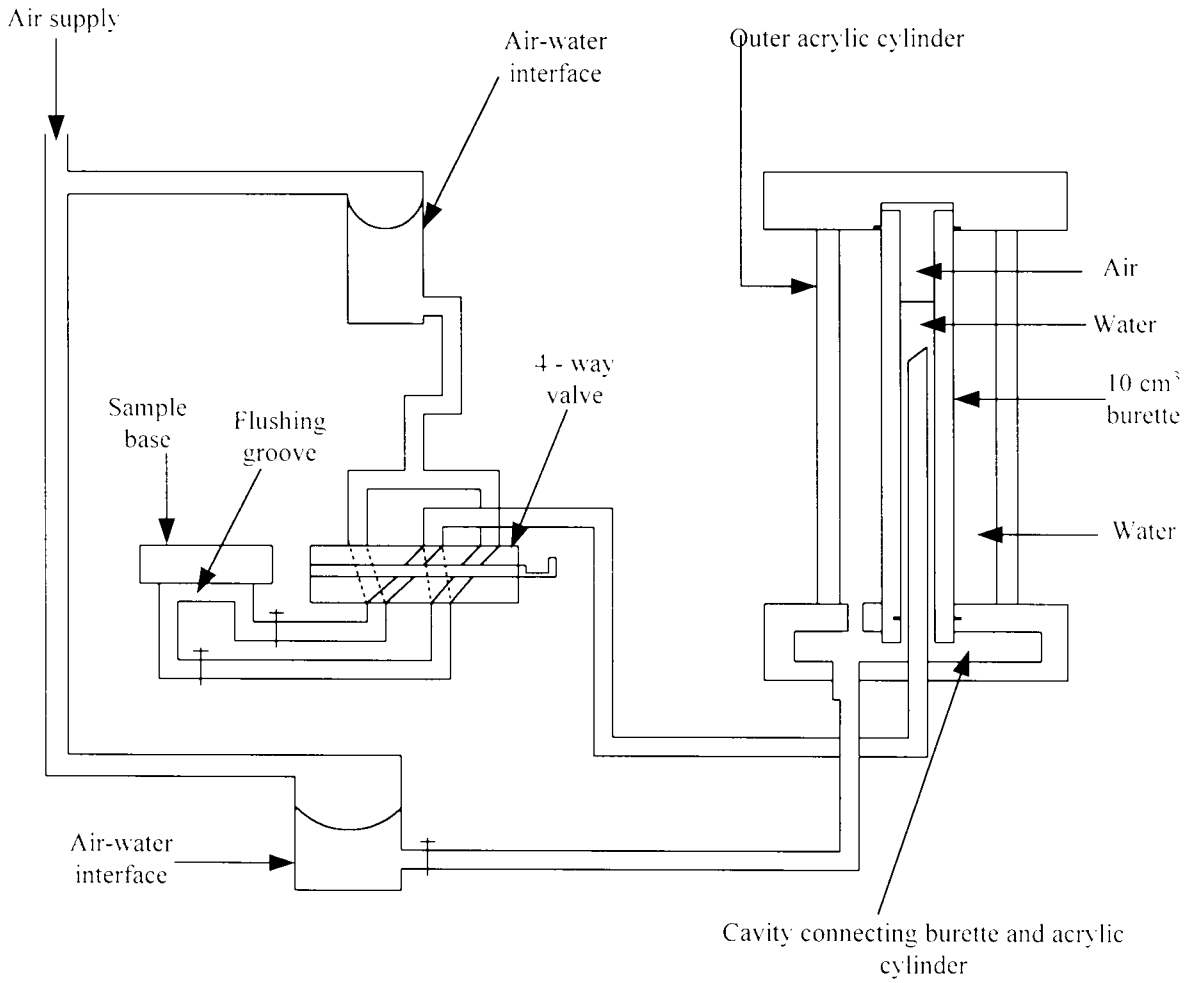

Figure 4.11 : System for flushing of diffused air

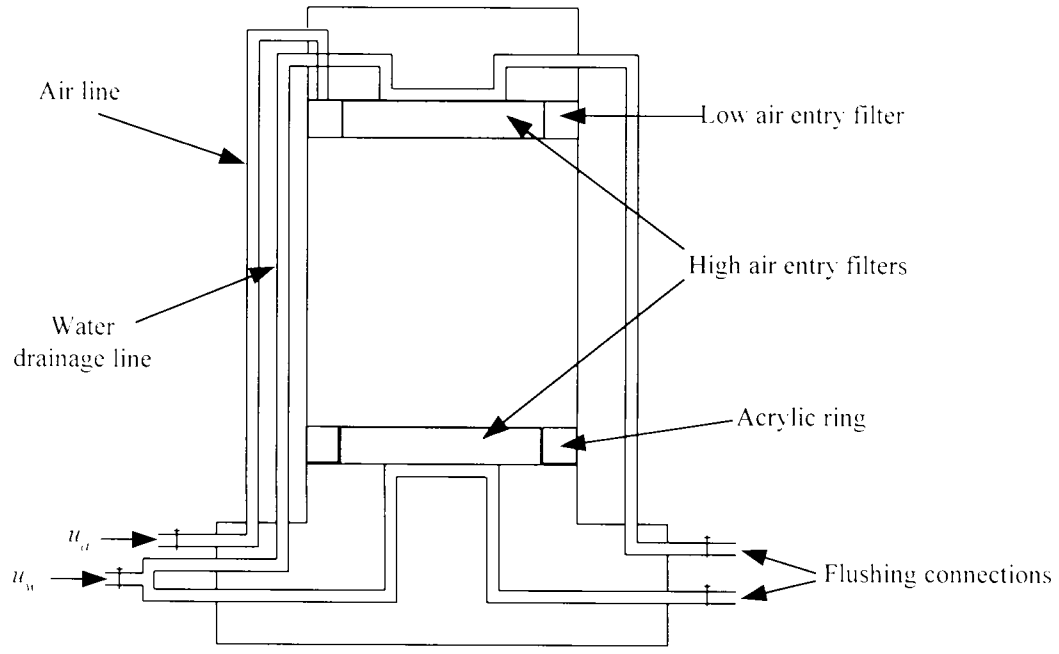

Figure 4.12 : Arrangement for water drainage from both top and bottom of soil sample

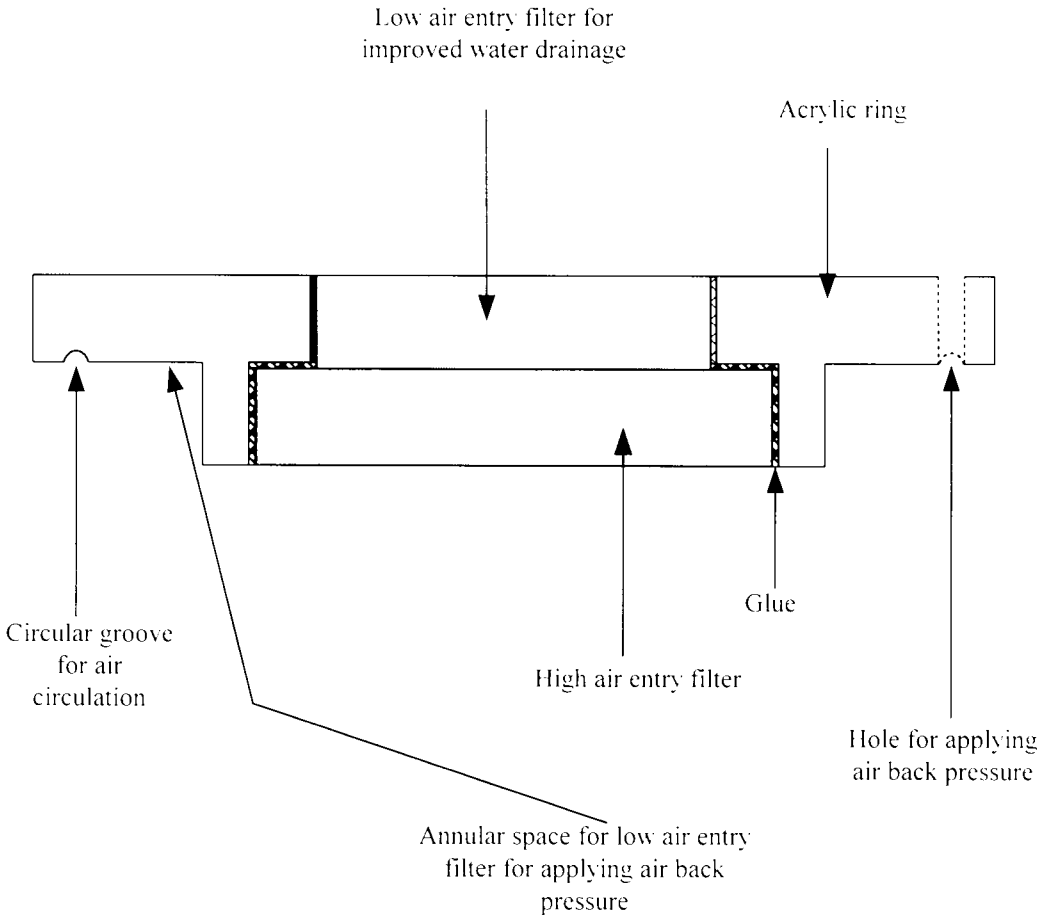

Figure 4.13 : Acrylic mounting ring
containing high and low air entry filters
for drainage from top face of sample

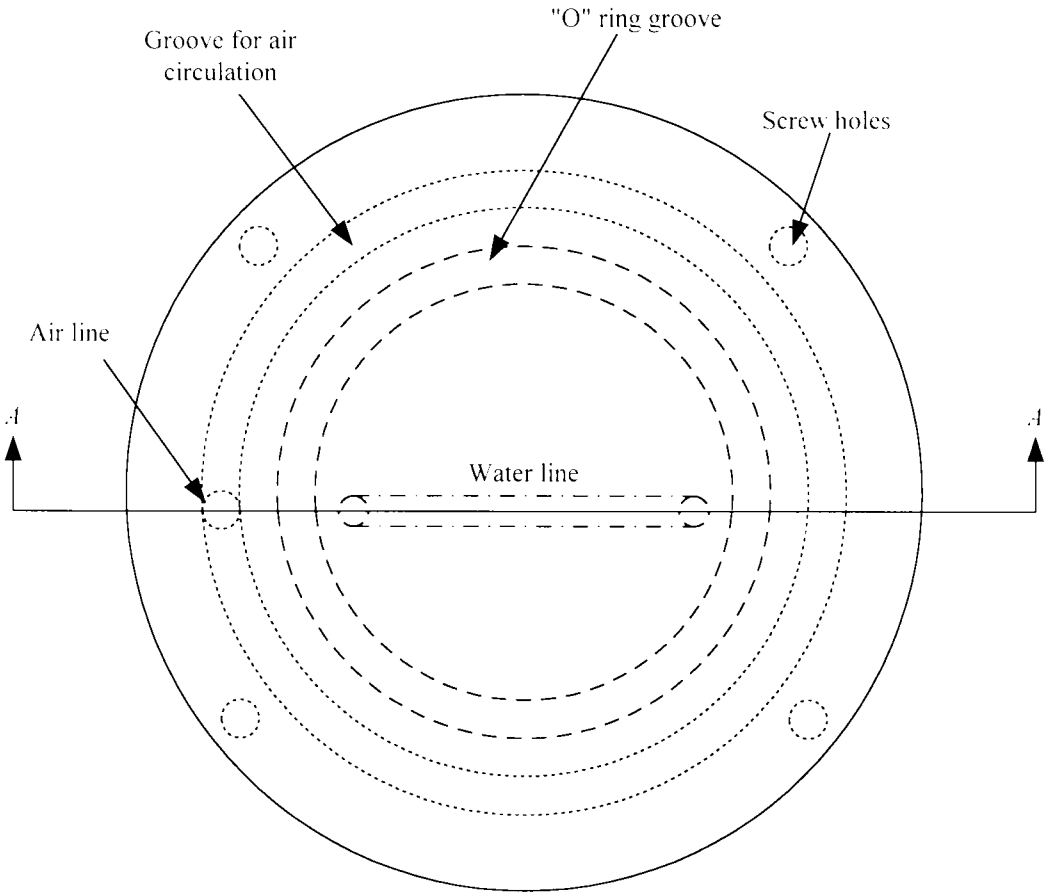

(a) Plan view of bottom face of top cap

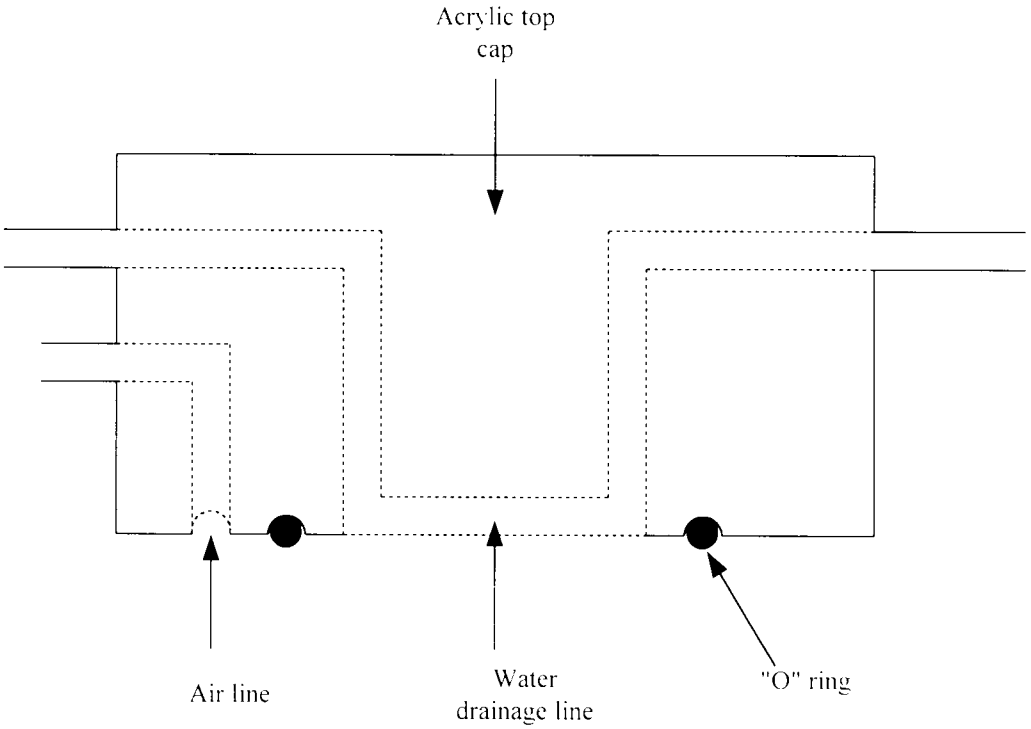

(b) Sectional view of top cap at *AA*

Figure 4.14 : Top cap showing "o" ring sealing arrangement between air and water drainage lines

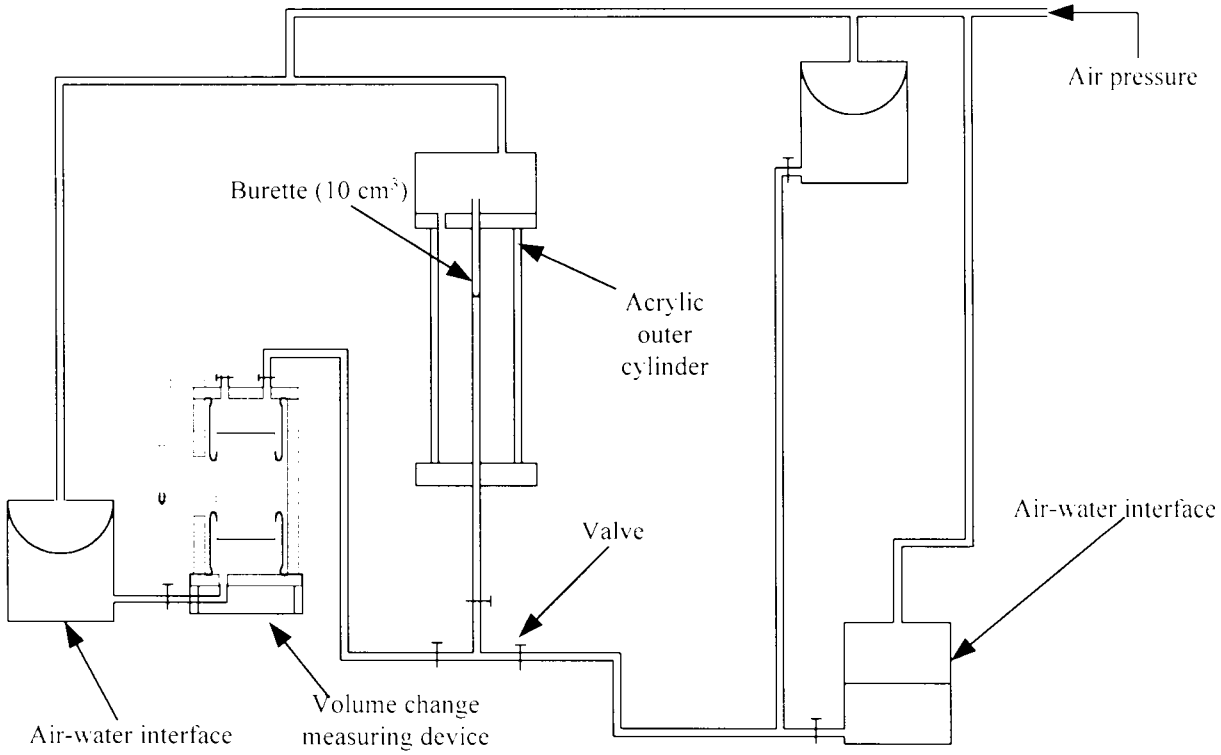

Figure 4.15 : Layout for calibration of volume change measuring devices

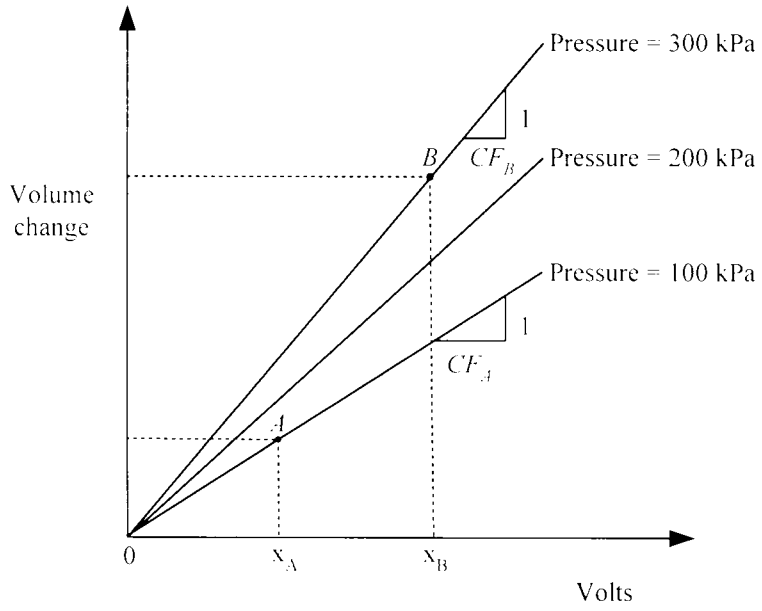

Figure 4.16 : Illustration of volume change calculation from burette type device

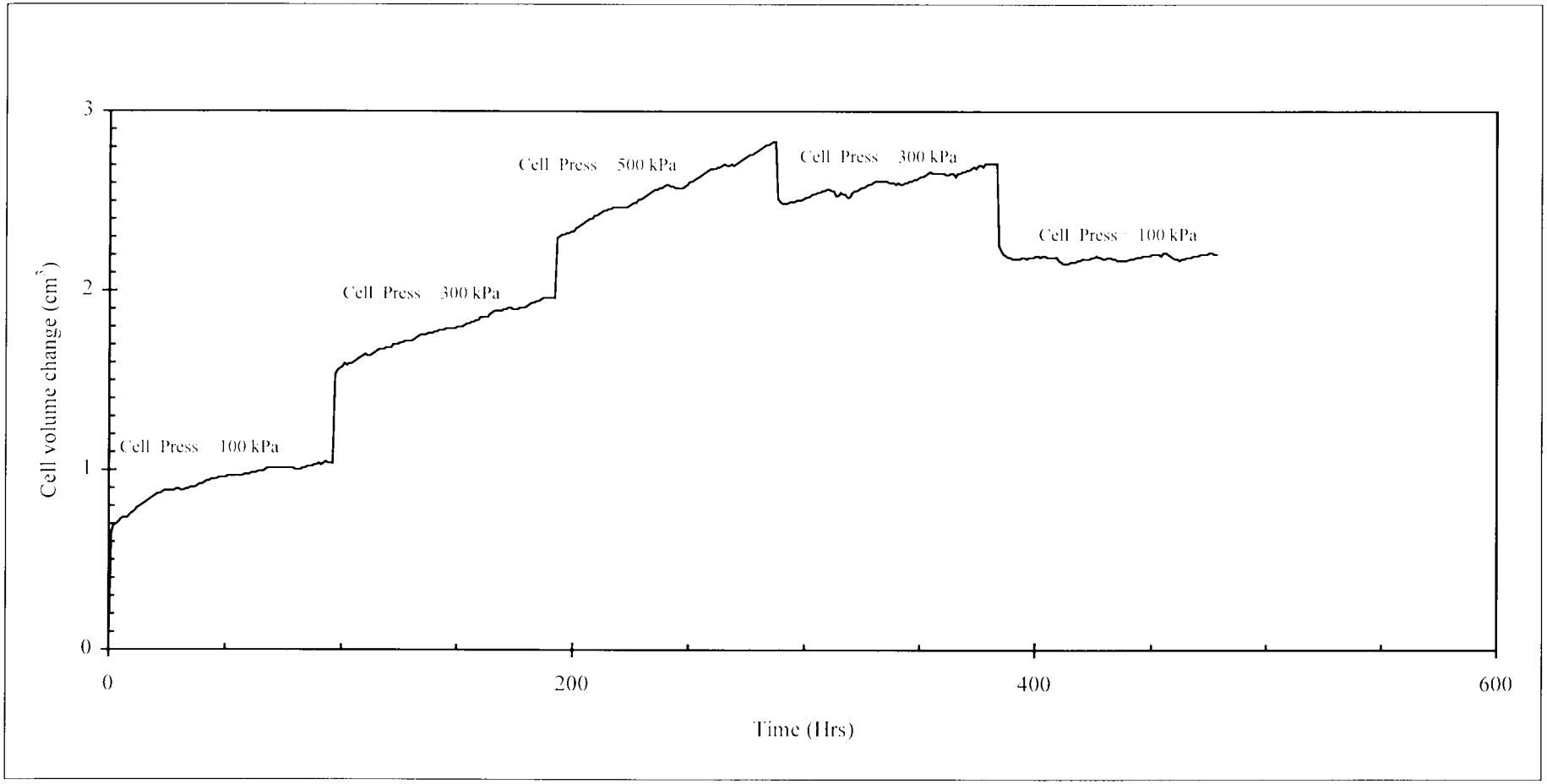

Figure 4.17 : Apparent cell volume change with time

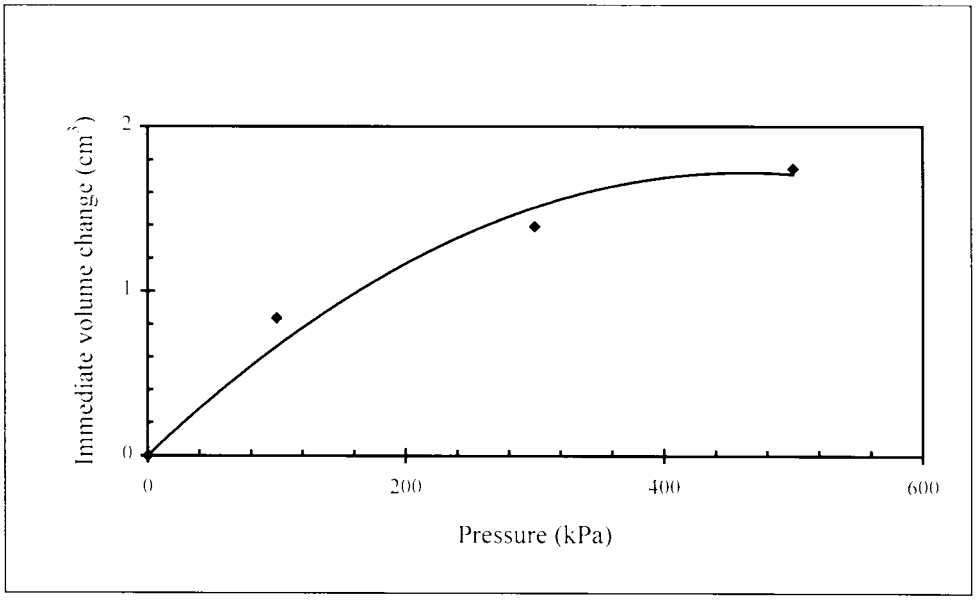

Figure 4.18 : Immediate volume change

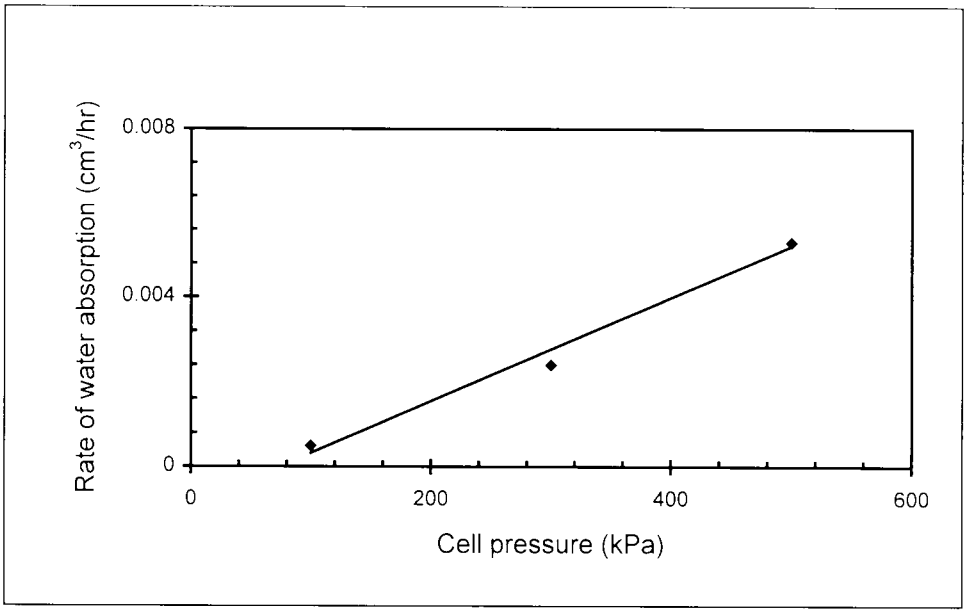

Figure 4.19 : Rate of water absorption

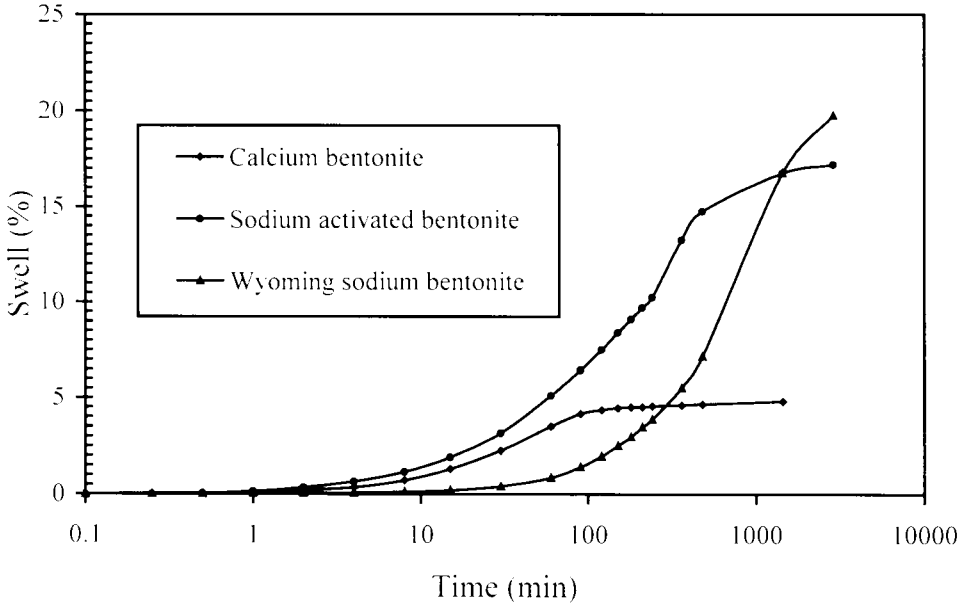

Figure 5.1 : Swell-time curves for grade E kaolin and various types of bentonite (20% by weight in each case)

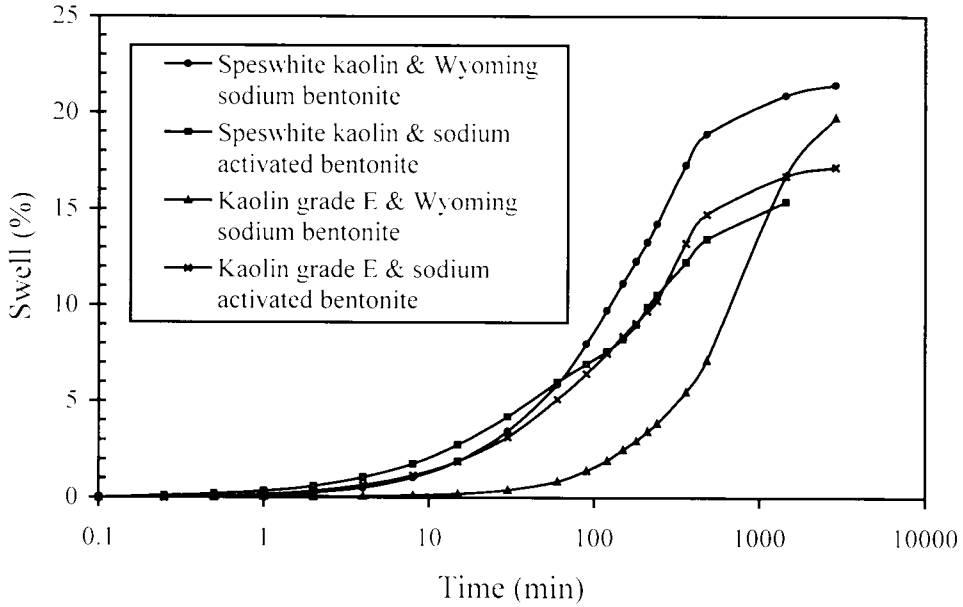

Figure 5.2 : Swell-time curves for kaolin (grade E or speswhite) and bentonite (sodium activated bentonite or Wyoming sodium bentonite, 20% by weight in each case)

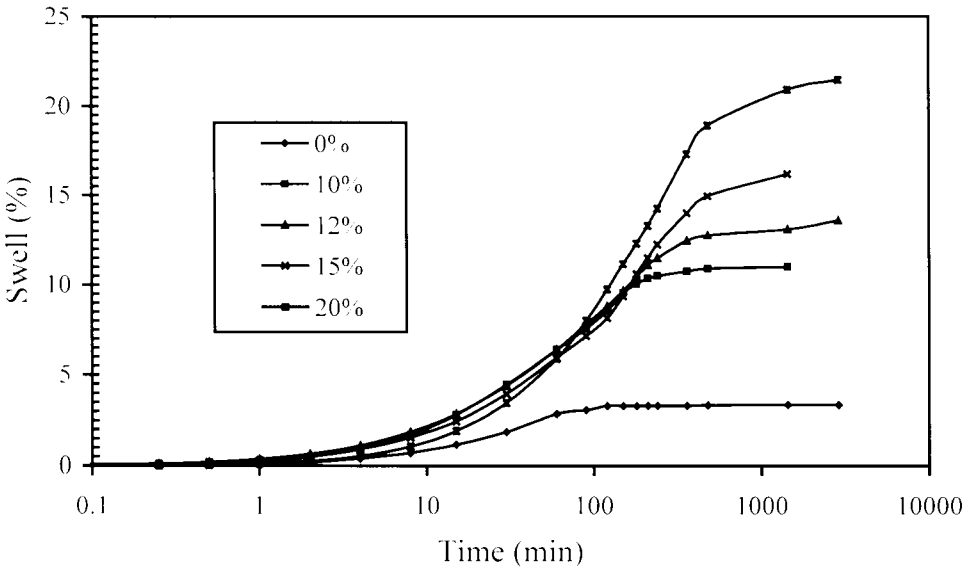

Figure 5.3 : Swell-time curves for speswhite kaolin and Wyoming sodium bentonite

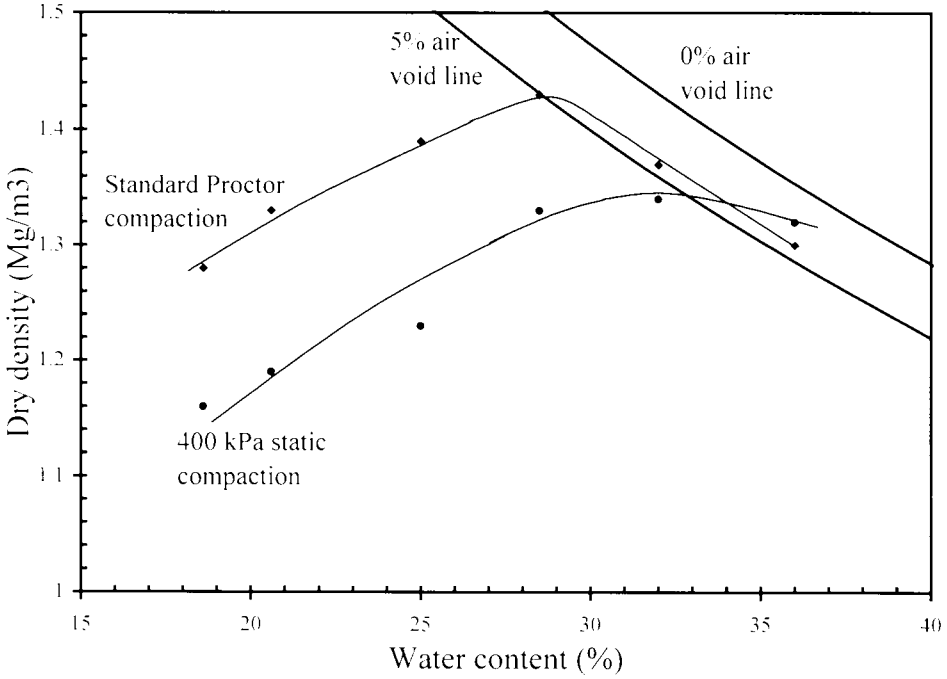

Figure 5.4 : Compaction curves for selected kaolin/bentonite mix

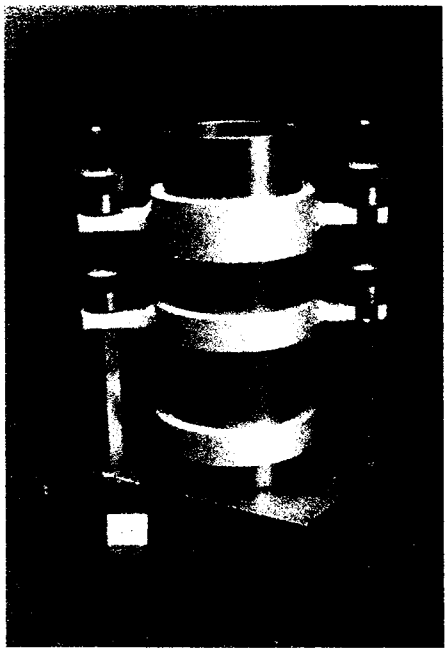

Figure 5.5 : Compaction mould

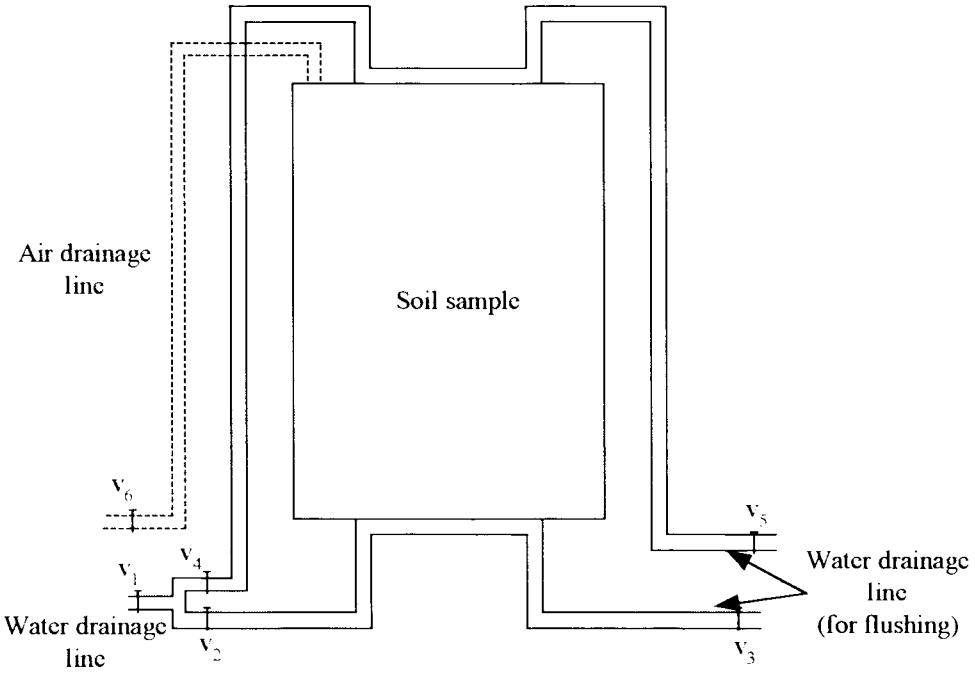

Figure 5.6 : Schematic representation of air and water drainage arrangements

(i)

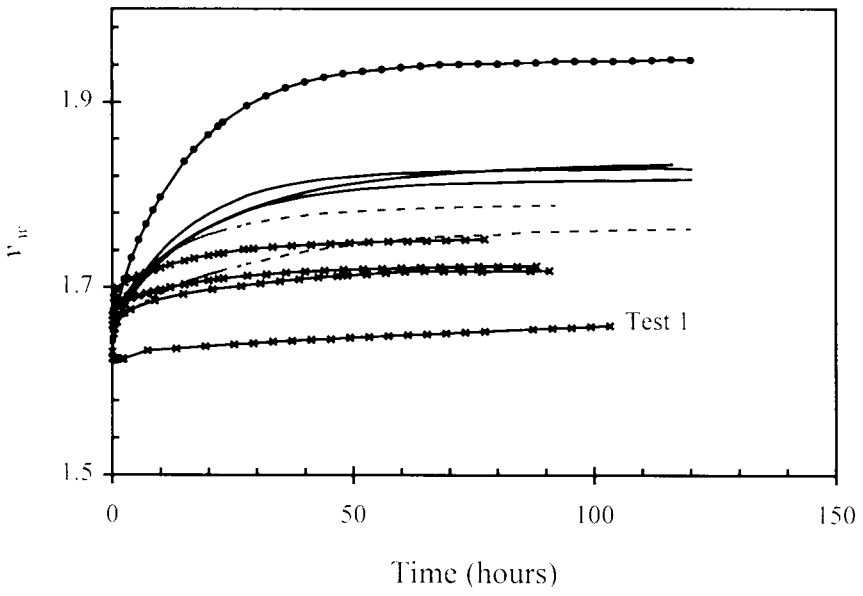

(ii)

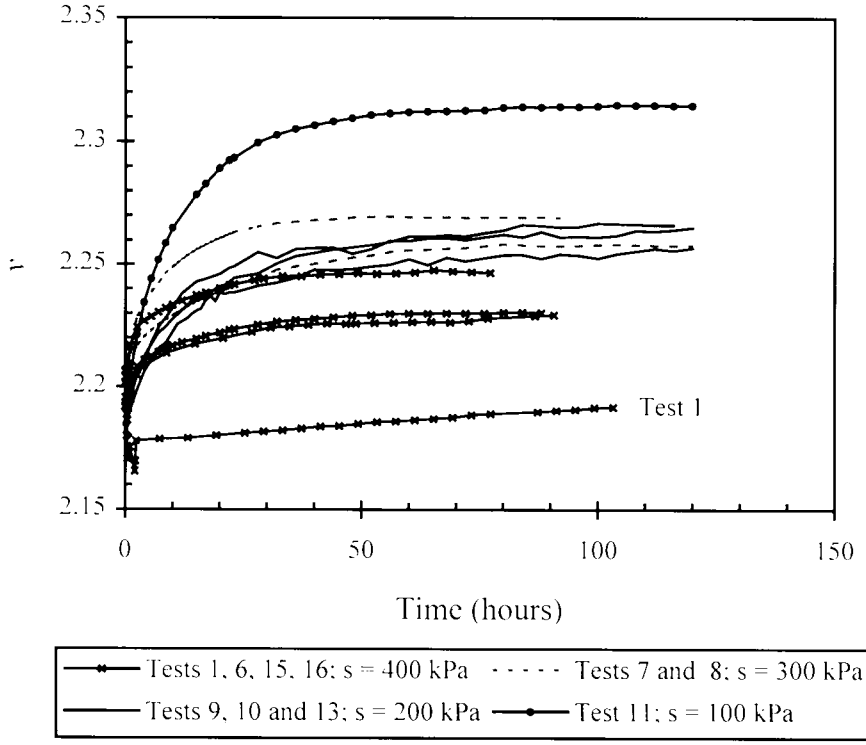

Figure 6.1 : Initial equalisation under mean net stress of 10 kPa of bentonite/kaolin samples compacted to 400 kPa

(i)

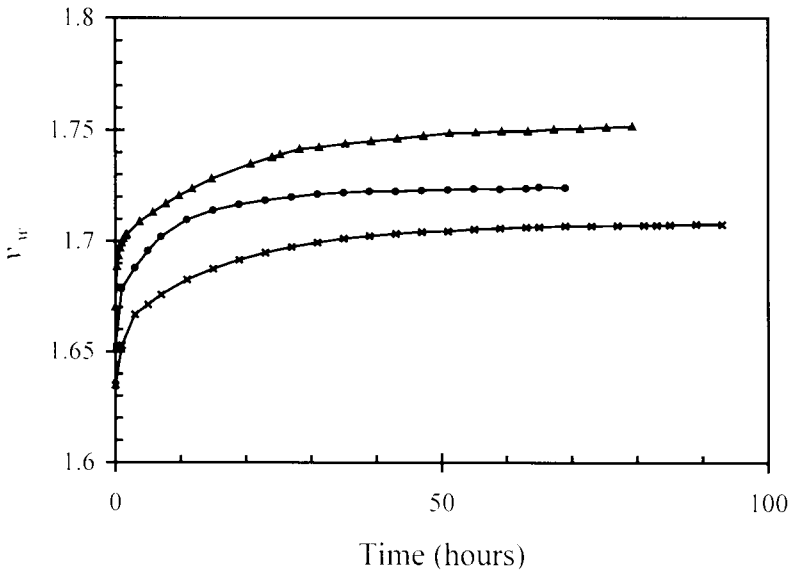

(ii)

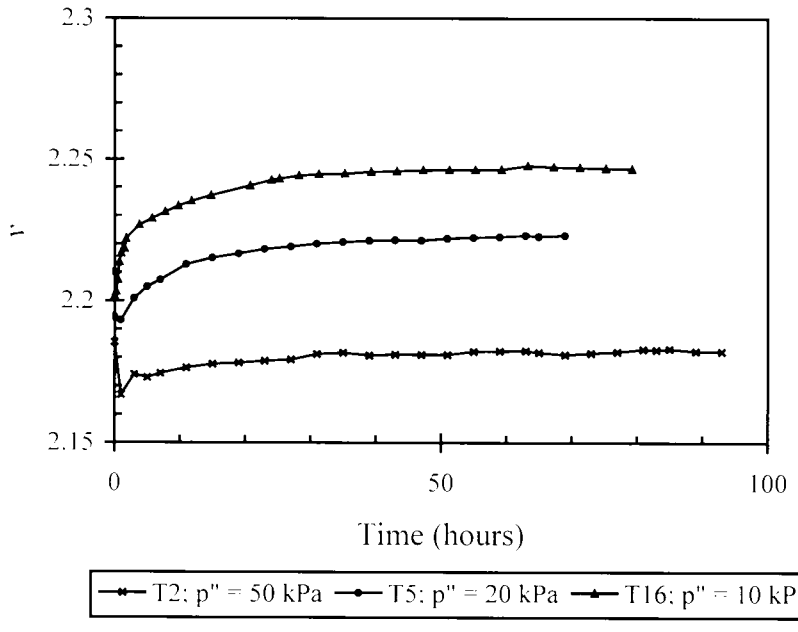

Figure 6.2 : Influence of mean net stress during equalisation (to a suction of 400 kPa) of bentonite/kaolin samples compacted to 400 kPa

(i)

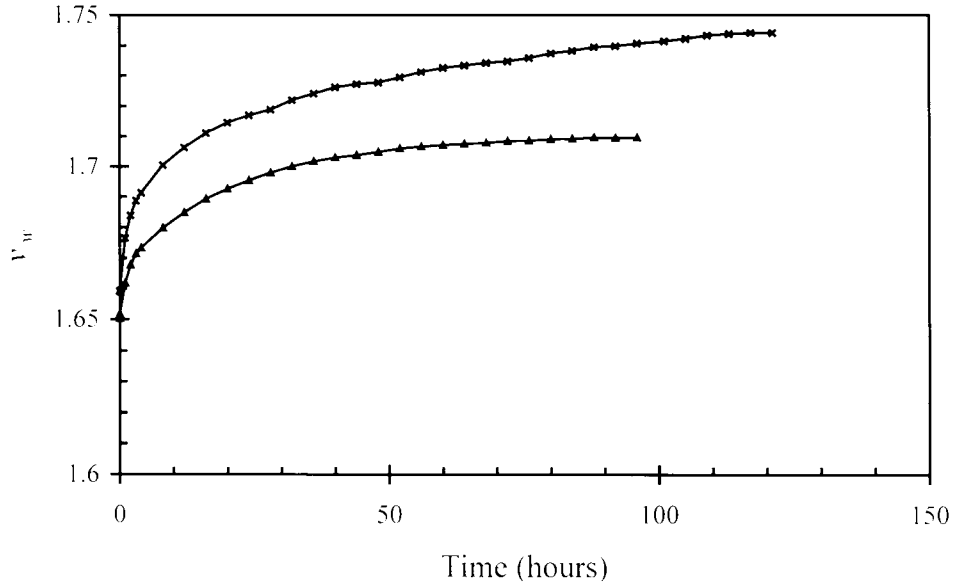

(ii)

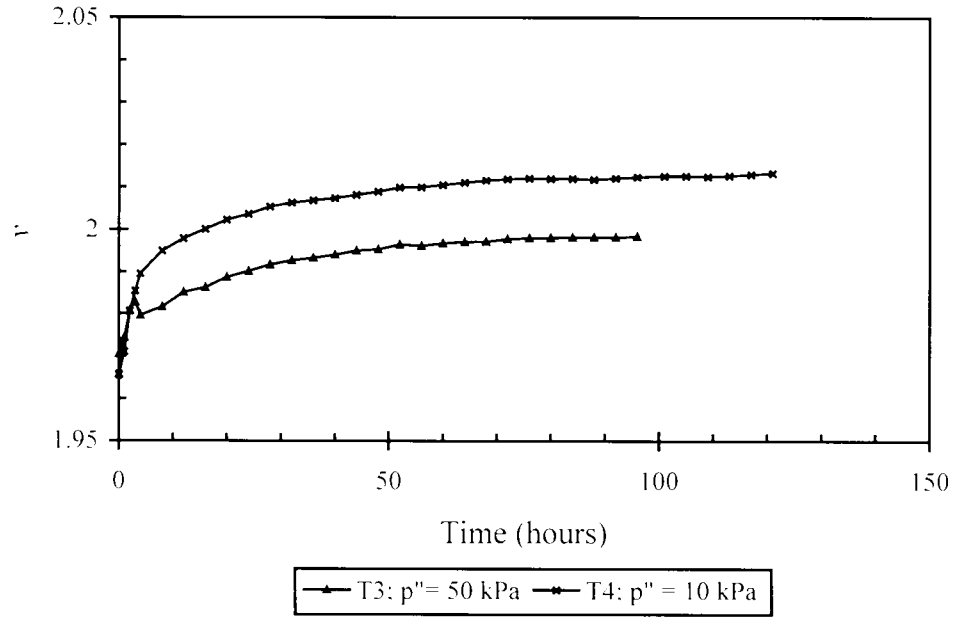

Figure 6.3 : Influence of mean net stress during equalisation (to a suction of 400 kPa) of bentonite/kaolin samples compacted to 800 kPa

(i)

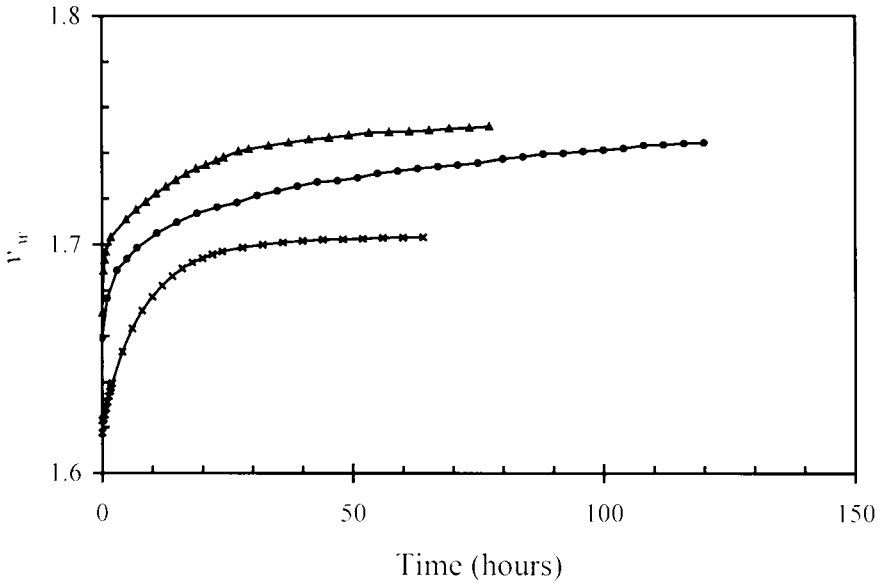

(ii)

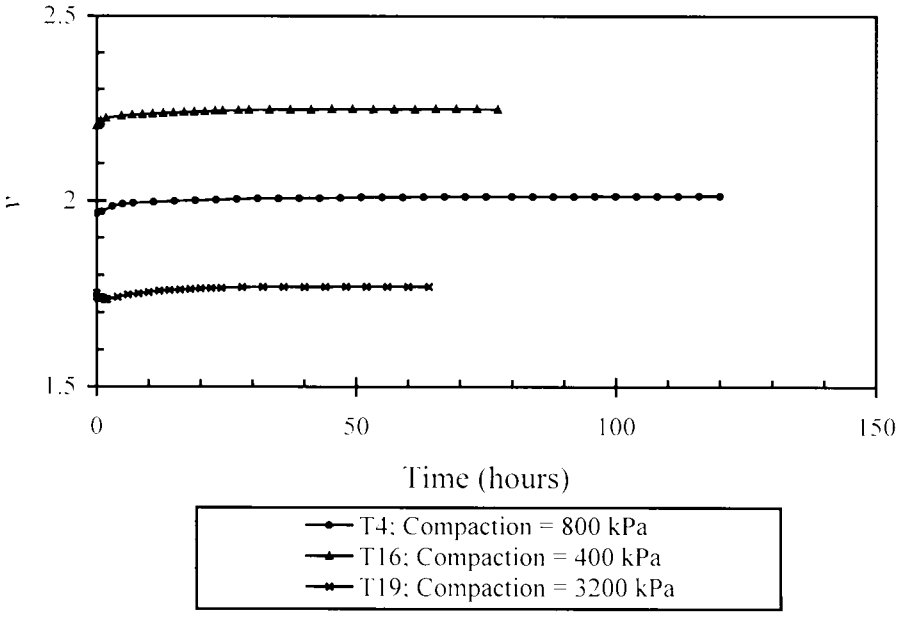

Figure 6.4 : Influence of compaction pressure on subsequent equalisation of bentonite/kaolin samples to a suction of 400 kPa and mean net stress of 10 kPa

(i)

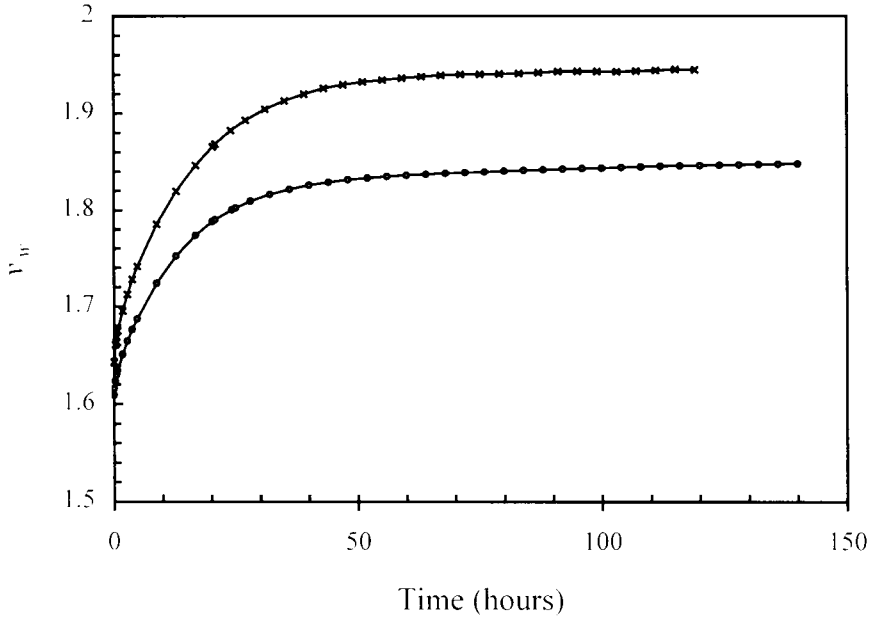

(ii)

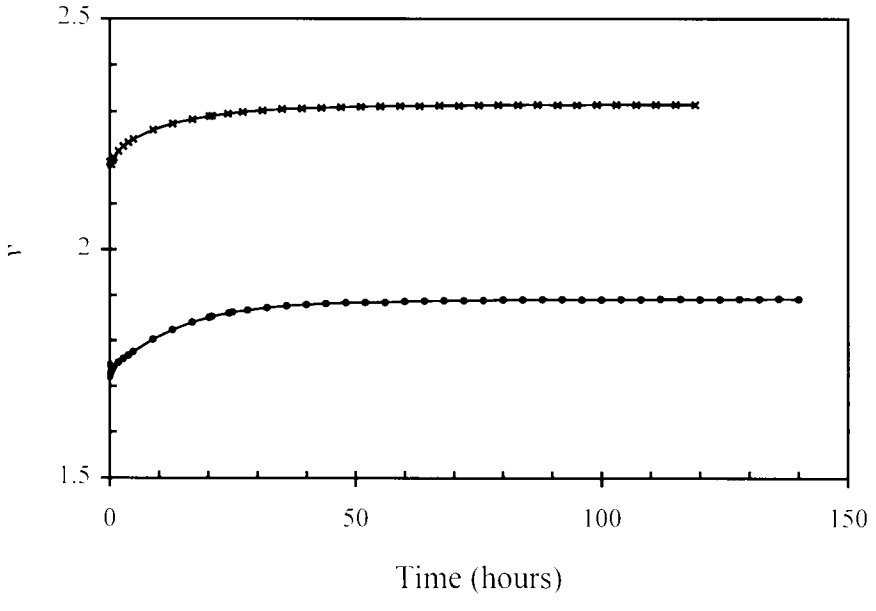

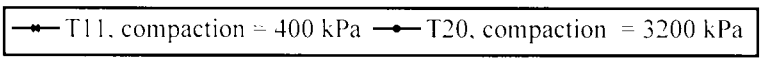

Figure 6.5 : Influence of compaction pressure on subsequent initial equalisation of bentonite/kaolin samples to a suction of 100 kPa and mean net stress of 10 kPa

(i)

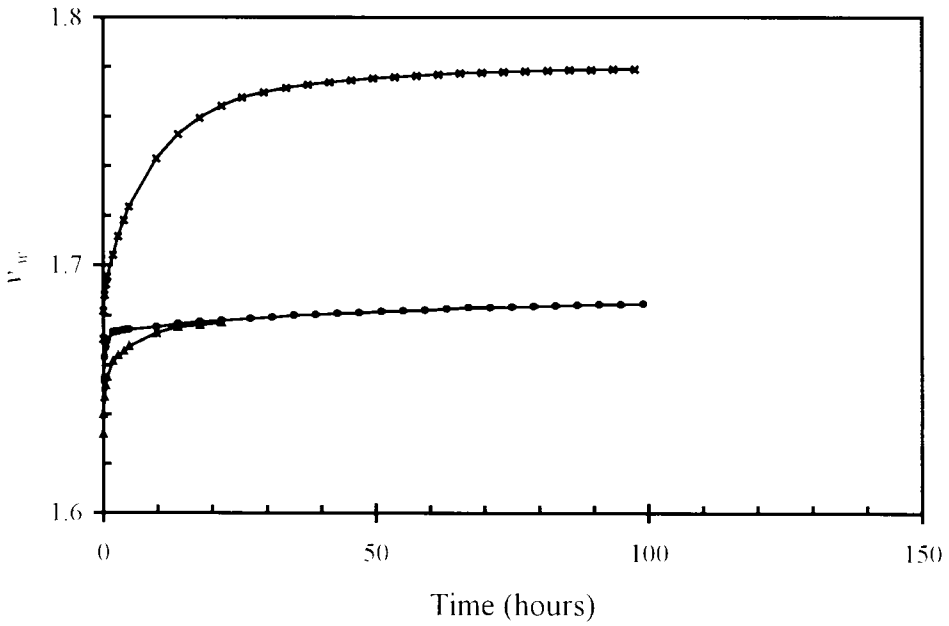

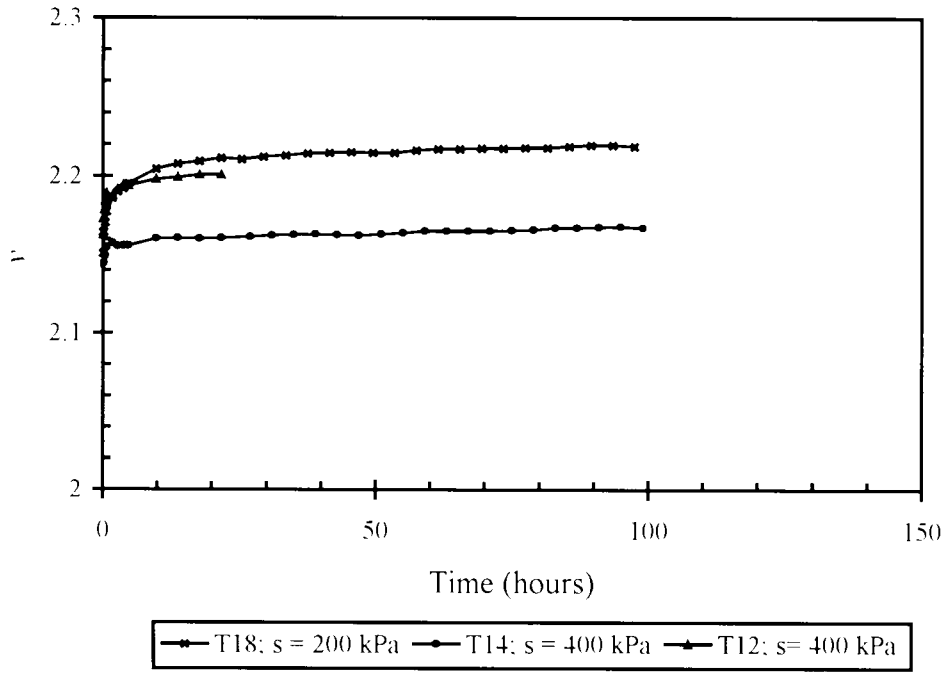

Figure 6.6 : Initial equalisation under mean net stress of 10 kPa of kaolin samples compacted to 400 kPa

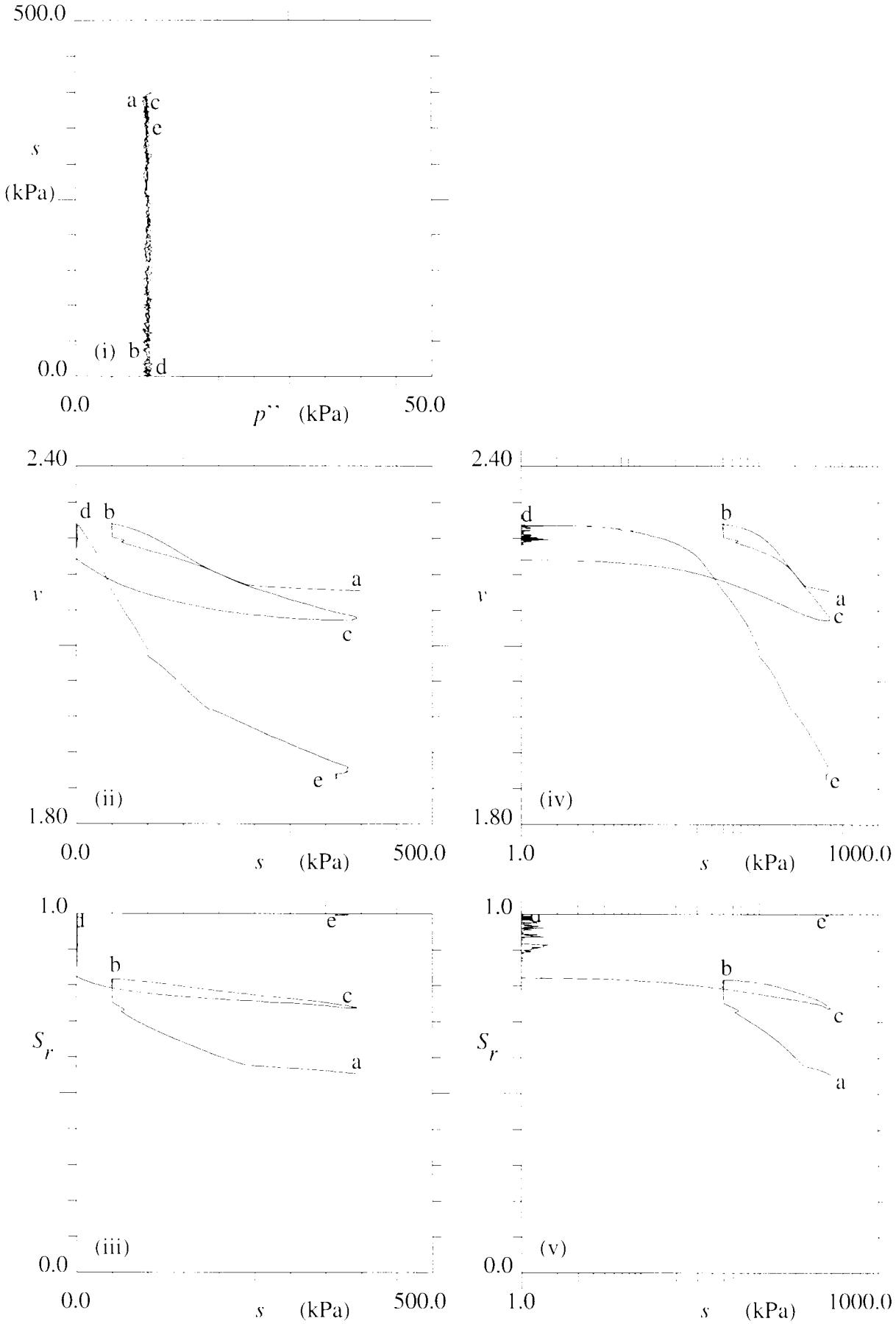

Figure 6.7 : Test 1 (Wetting/drying at p" = 10 kPa; bent/kao sample; comp = 400 kPa)

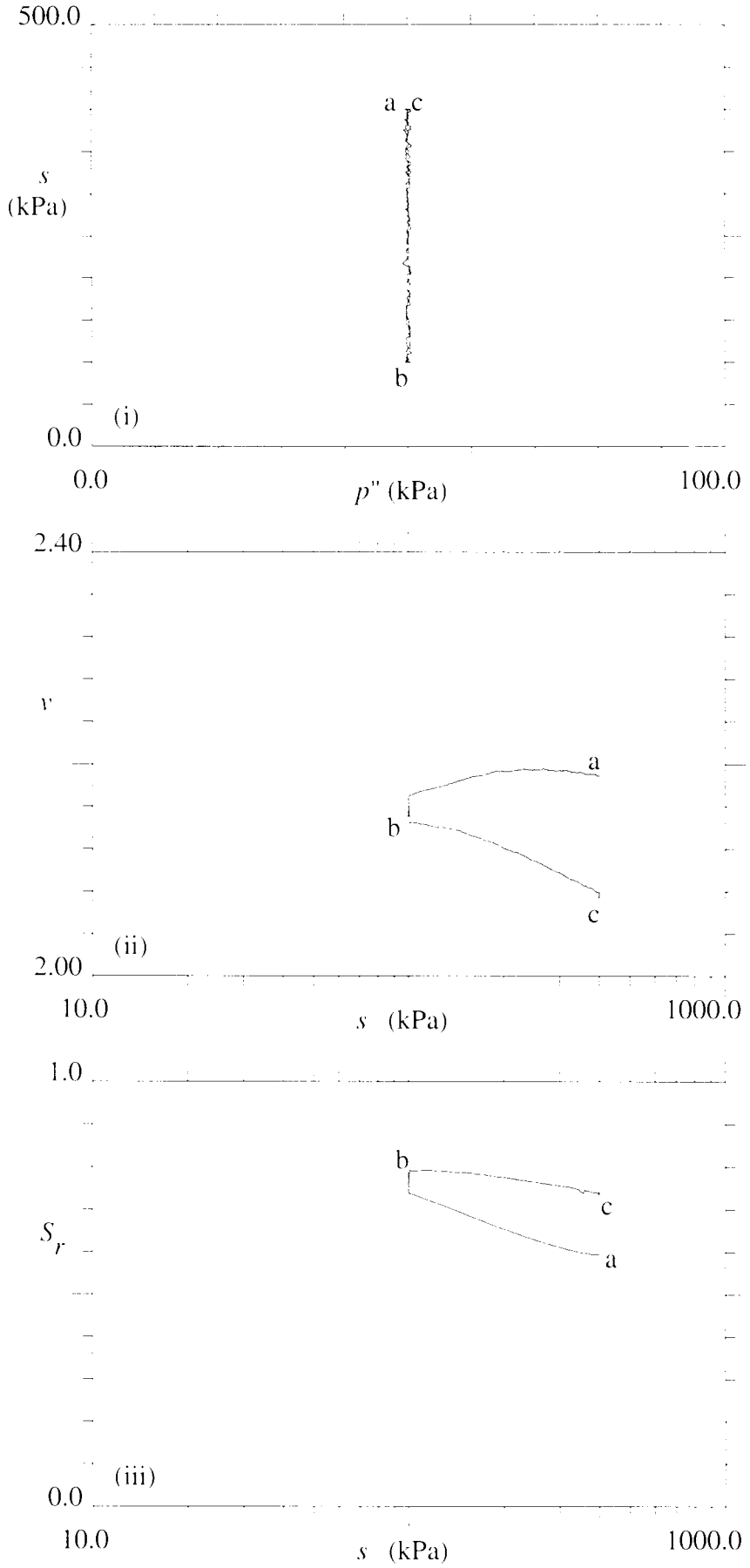

Figure 6.8 : Test 2 (Wetting/drying at p" = 50 kPa; bent/kao; comp = 400 kPa)

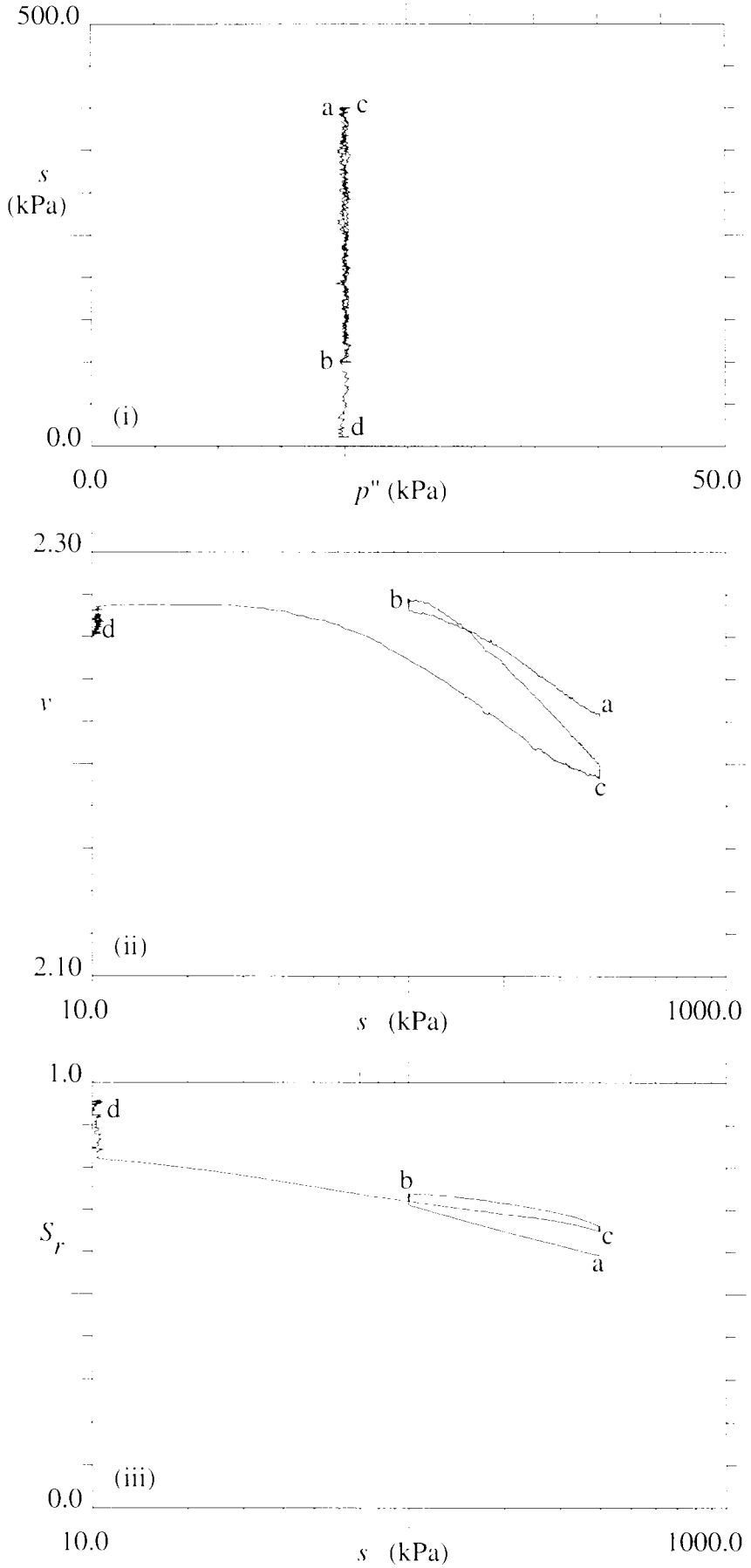

Figure 6.9 : Test 5 (Wetting/drying at p" = 20 kPa; bent/kao; comp = 400 kPa)

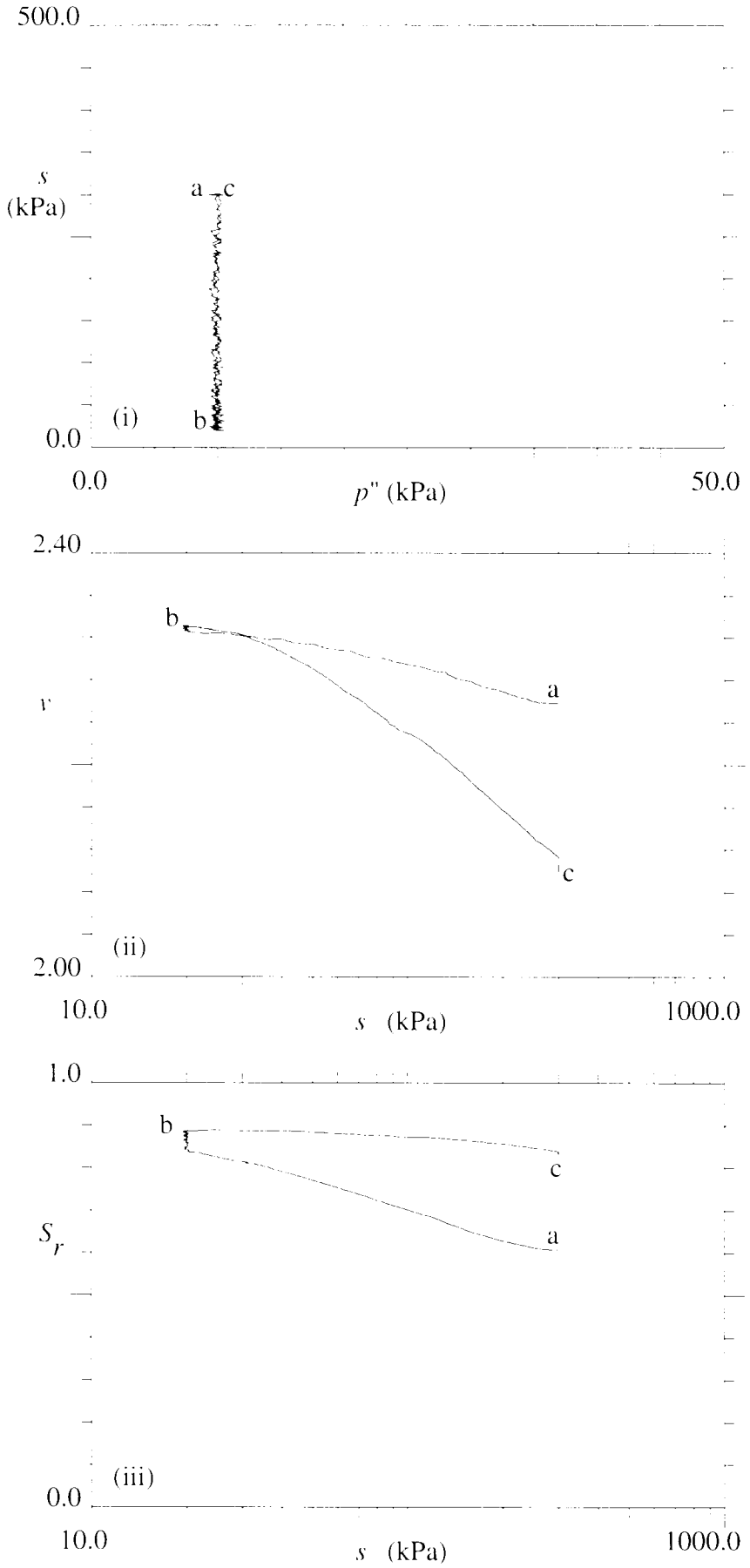

Figure 6.10 : Test 8 (Wetting/drying at p" = 10 kPa; bent/kao; comp = 400 kPa)

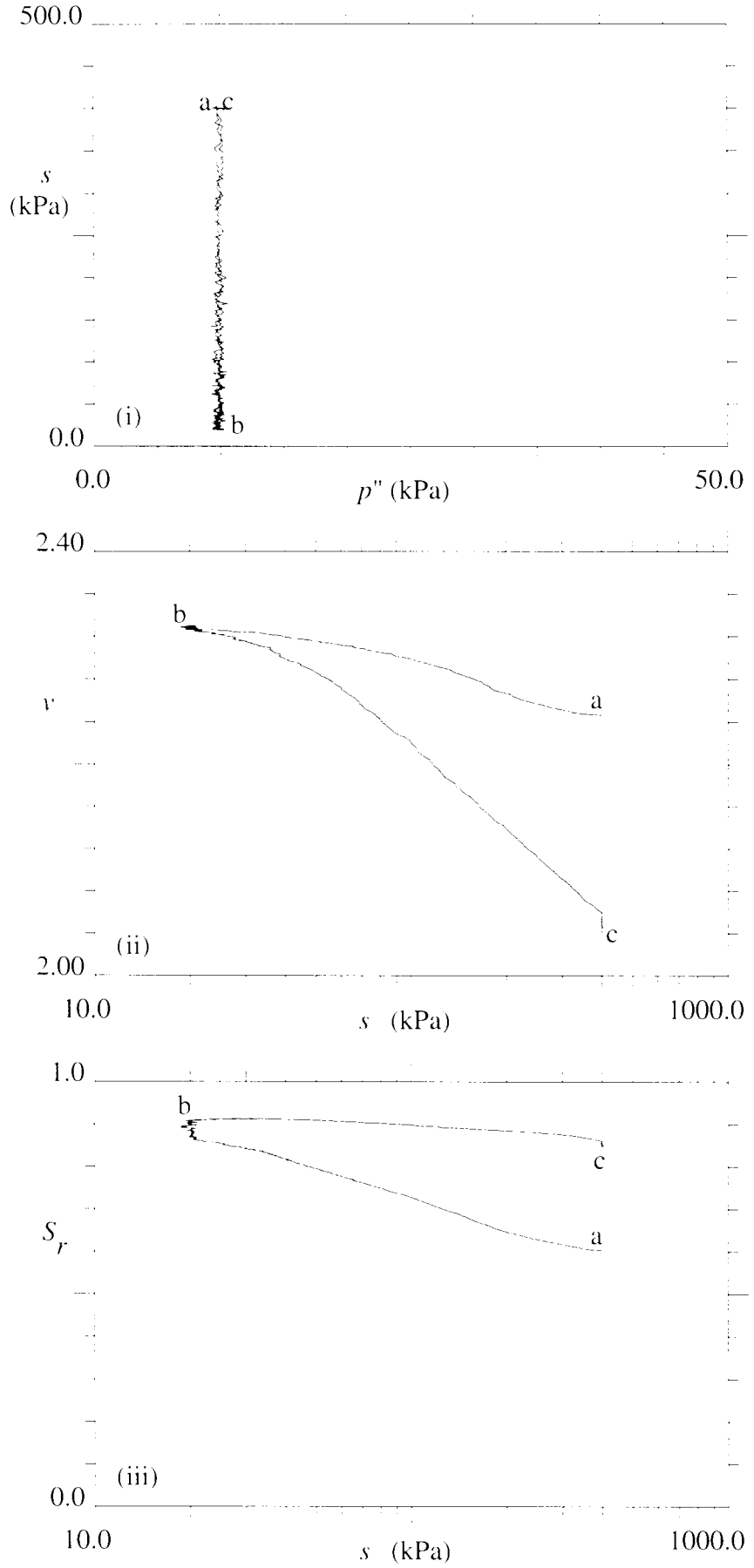

Figure 6.11 : Test 16 (Wetting/drying at p" = 10 kPa; bent/kao; comp = 400 kPa)

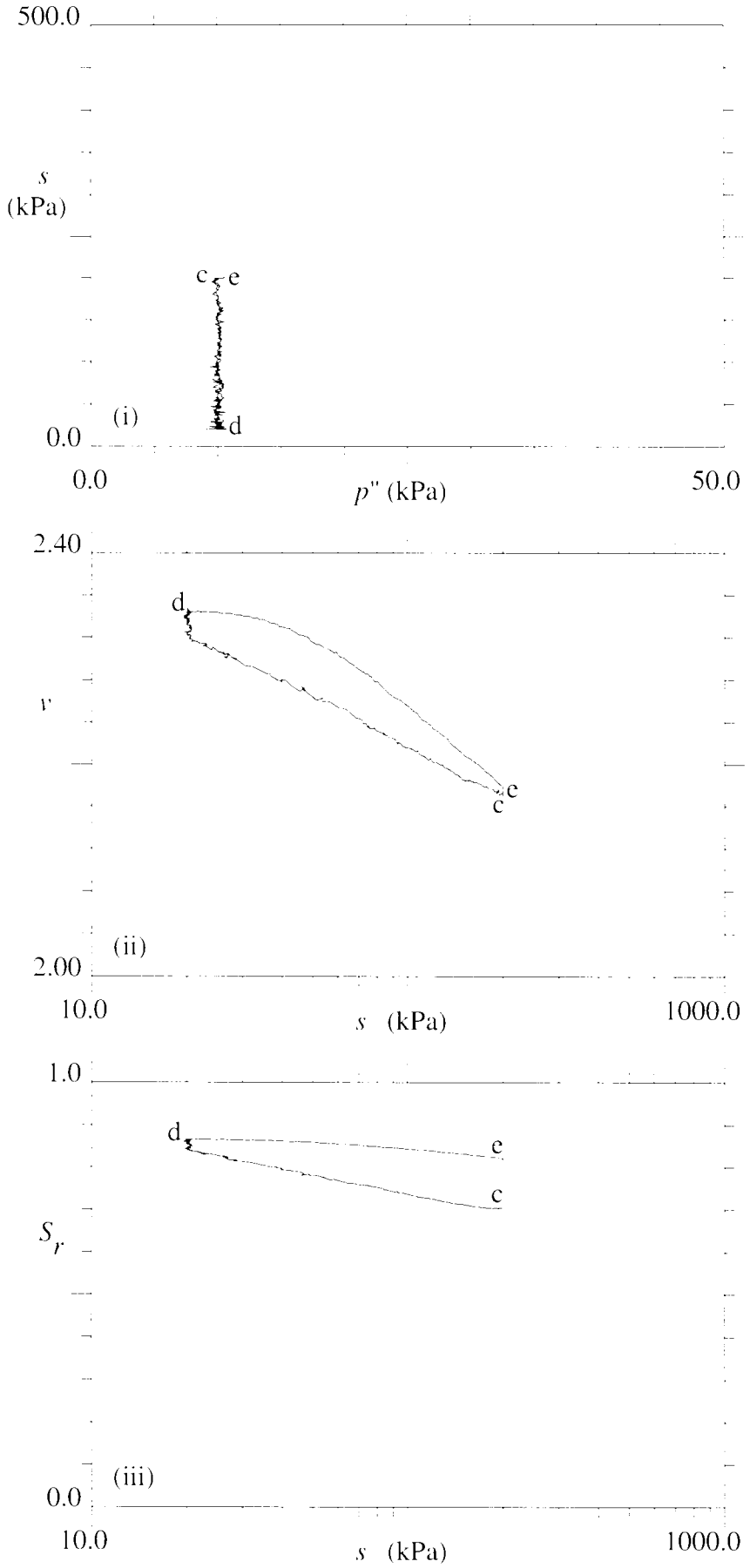

Figure 6.12 : Test 10 (Wetting/drying at p" = 10 kPa; bent/kao; comp = 400 kPa)

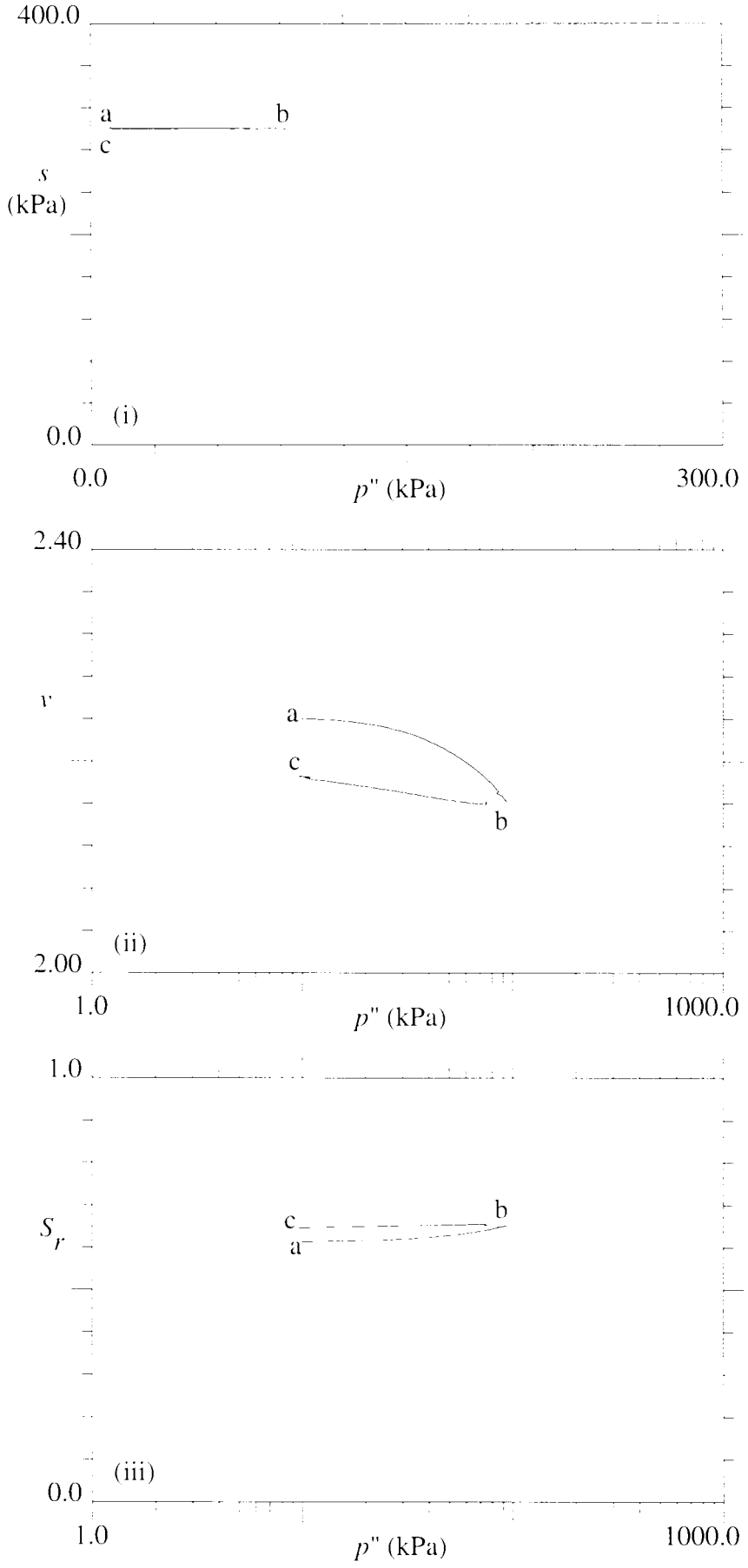

Figure 6.13 : Test 6 (Loading/unloading at s = 300 kPa; bent/kao sample)

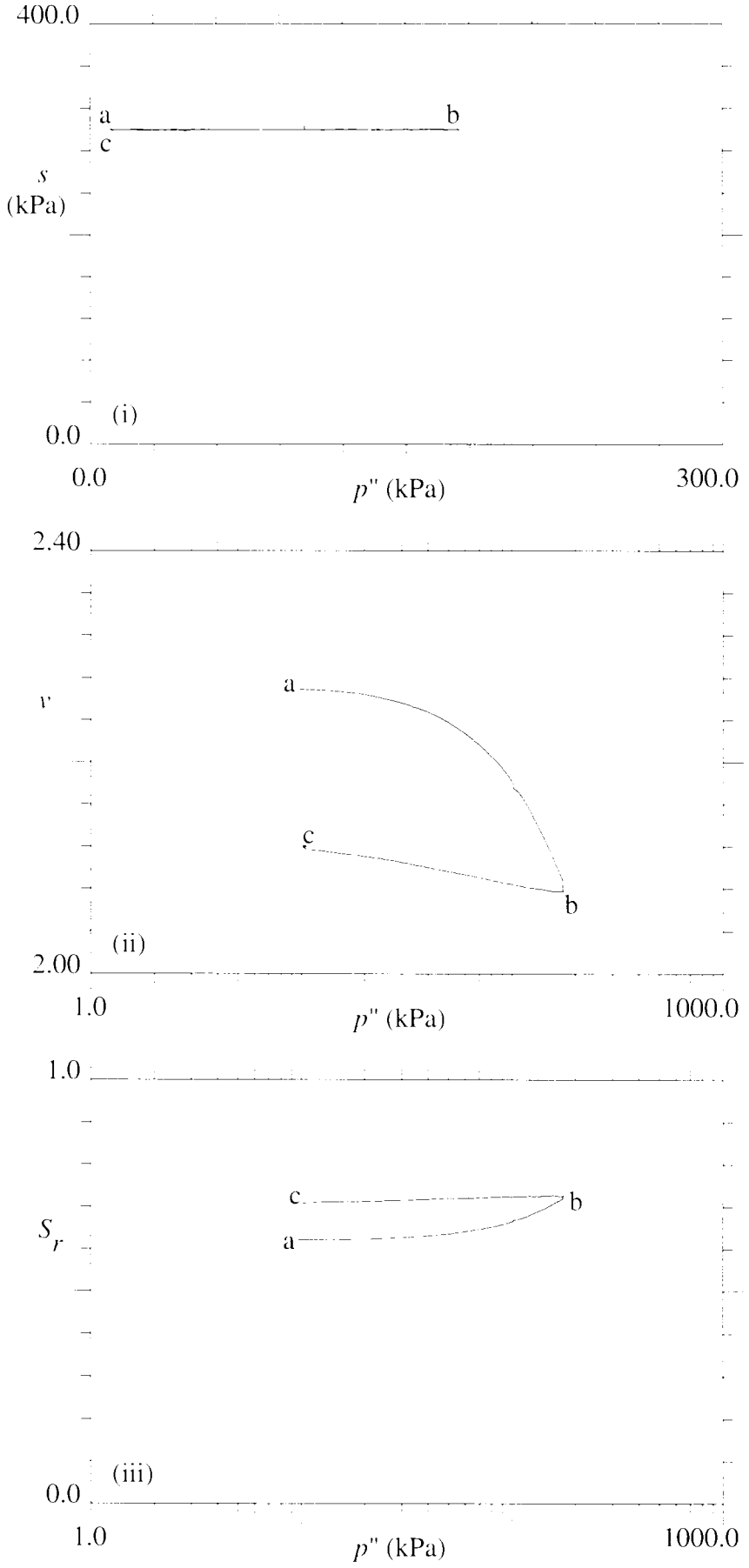

Figure 6.14 : Test 7 (Loading/unloading at s = 300 kPa; bent/kao sample)

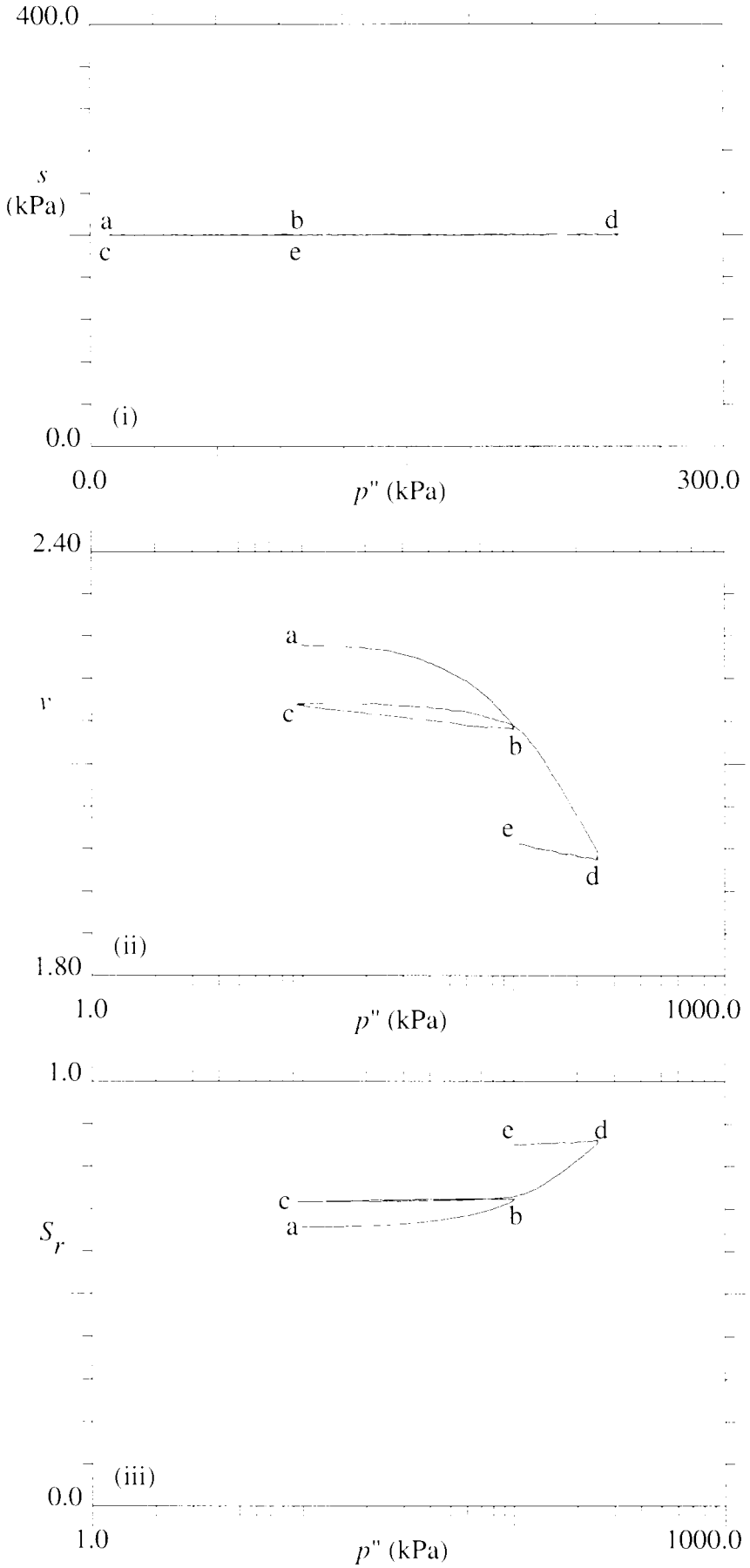

Figure 6.15 : Test 9 (Loading/unloading at s = 200 kPa; bent/kao sample)

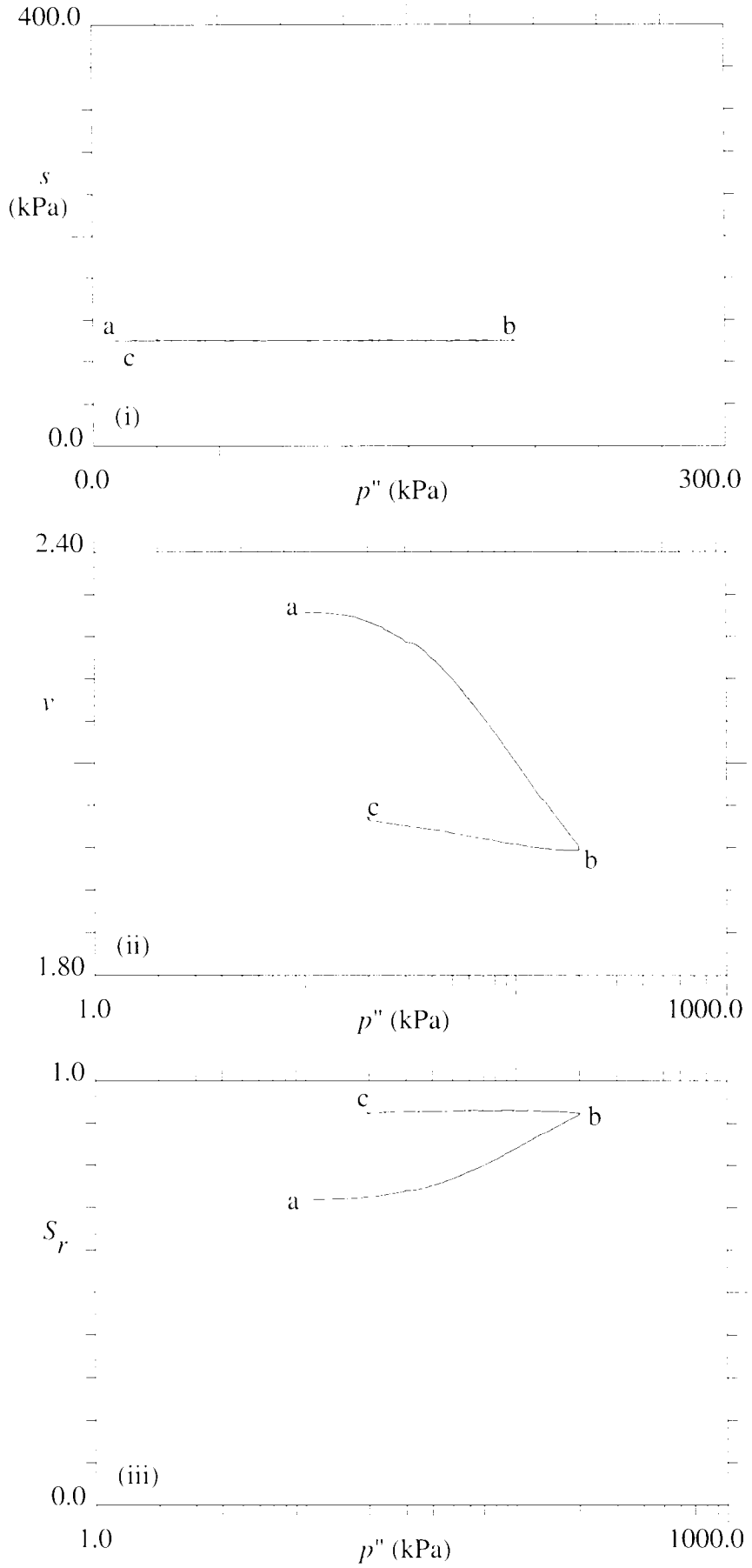

Figure 6.16 : Test 11 (Loading/unloading at s = 100 kPa; bent/kao sample)

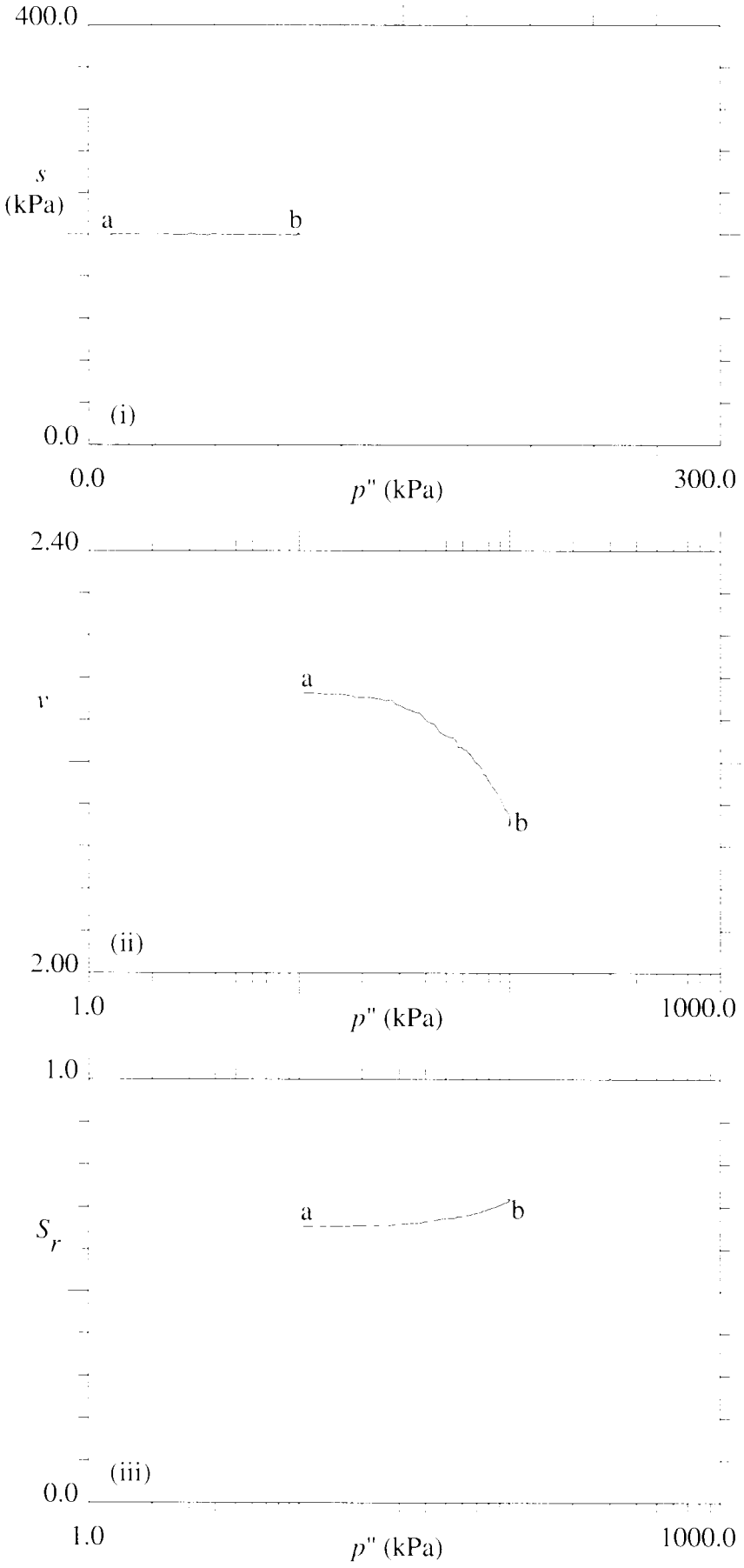

Figure 6.17 : Test 13 (Loading at s = 200 kPa; bent/kao sample)

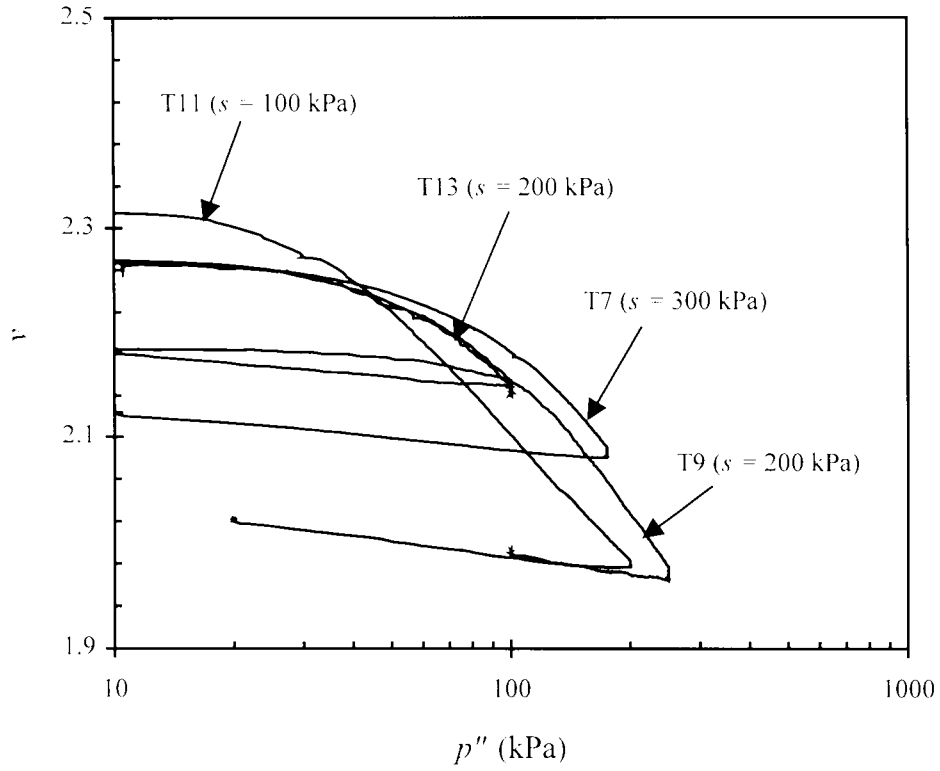

Figure 6.18 : Loading/unloading behaviour of bentonite/kaolin samples prepared by compaction under a pressure of 400 kPa

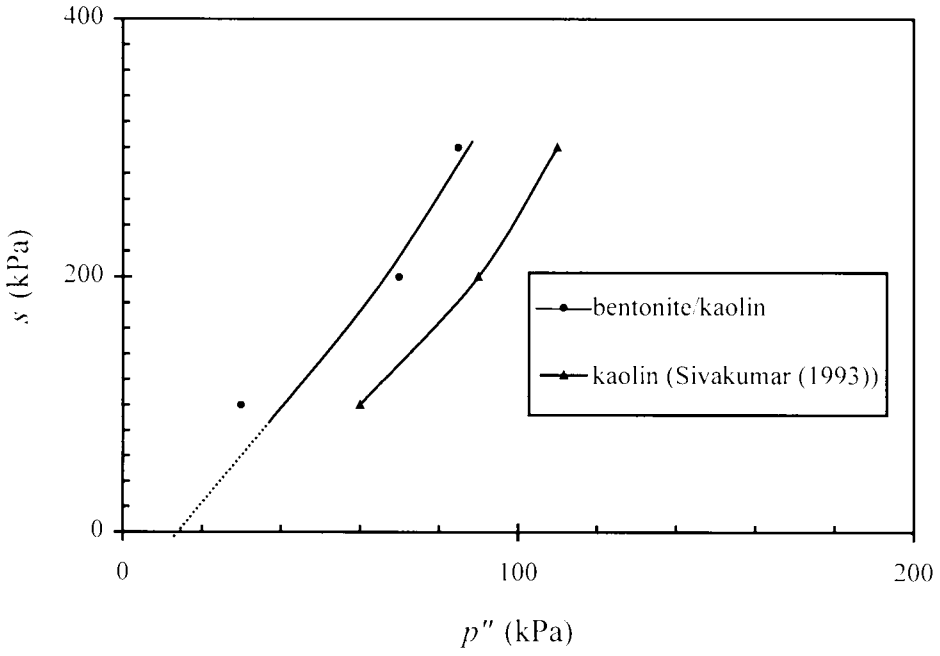

Figure 6.19 : Loading Collapse *LC* yield curves for the bentonite/kaolin mix and pure kaolin compacted under a pressure of 400 kPa

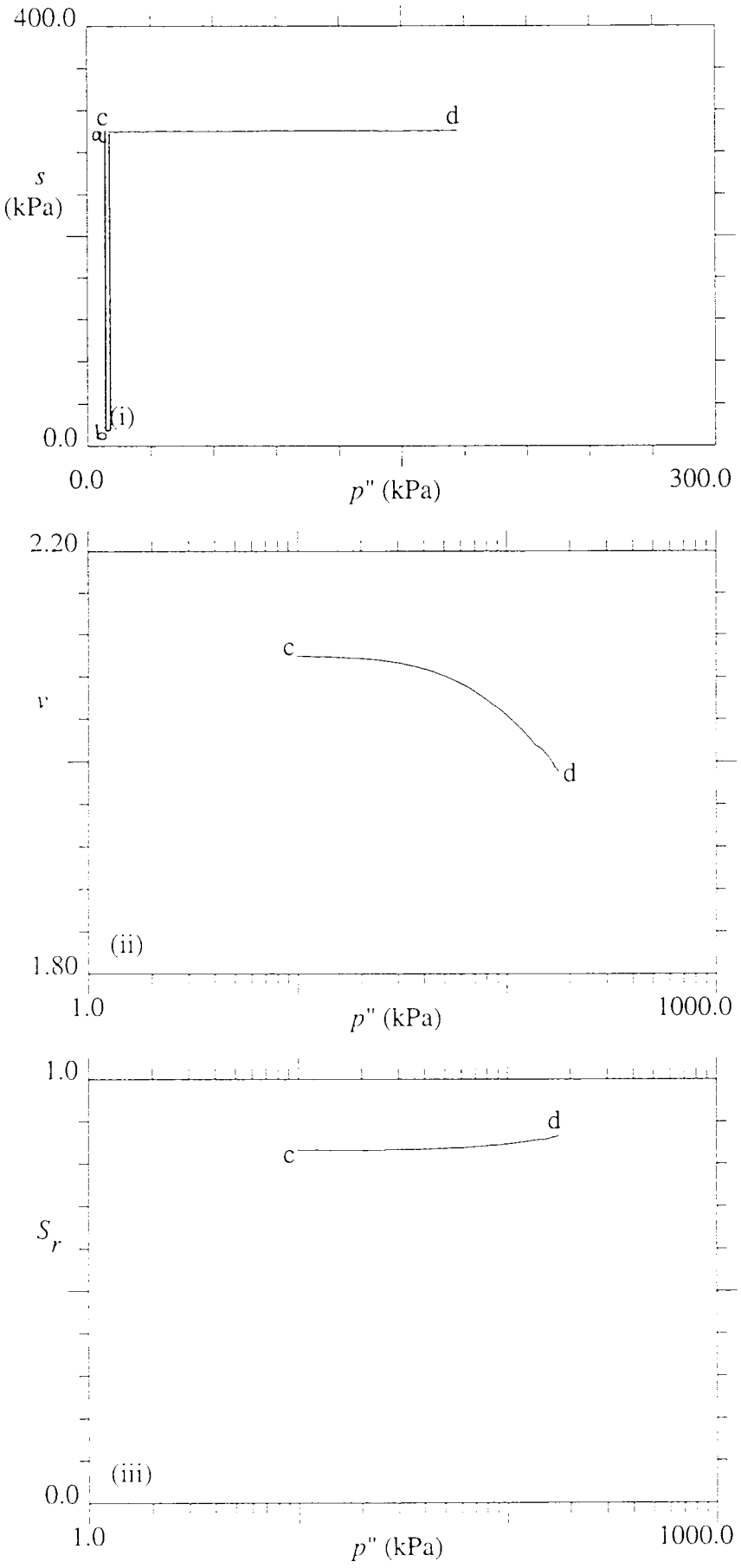

Figure 6.20 : Test 8 (Loading at s = 300 kPa; bent/kao sample)

(i)

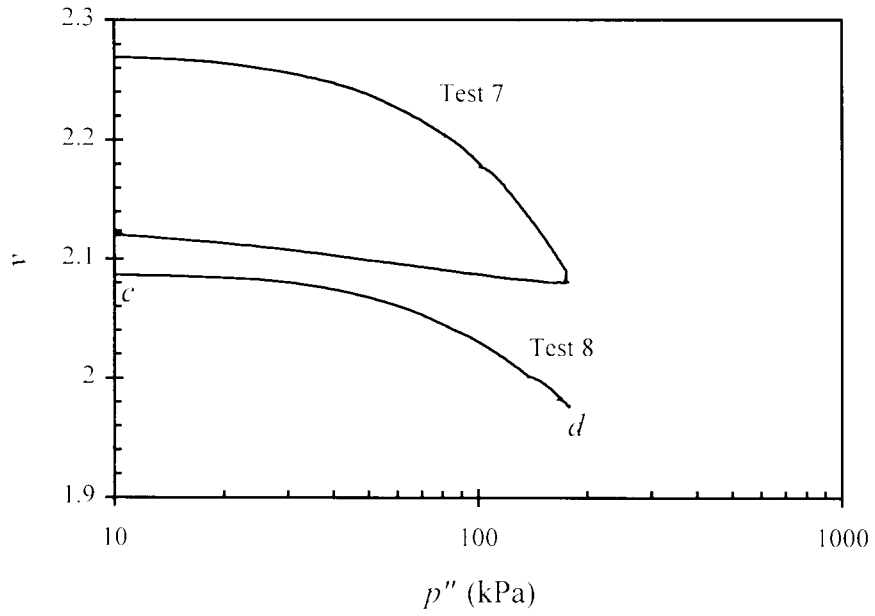

(ii)

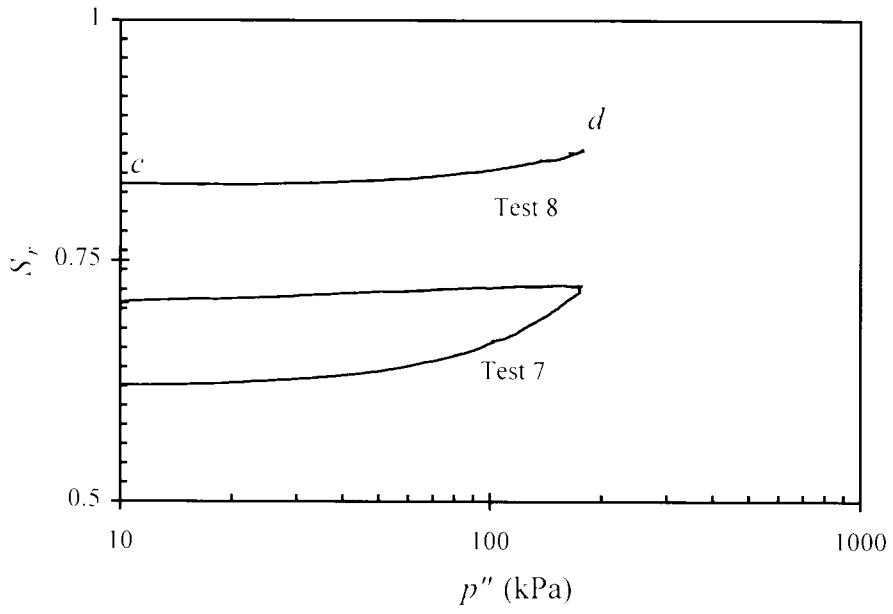

Figure 6.21 : Influence of wetting/drying cycle on subsequent loading behaviour of bentonite/kaolin sample prepared by compaction under a pressure of 400 kPa
(in Test 8 a wetting/drying cycle preceded the loading stage)

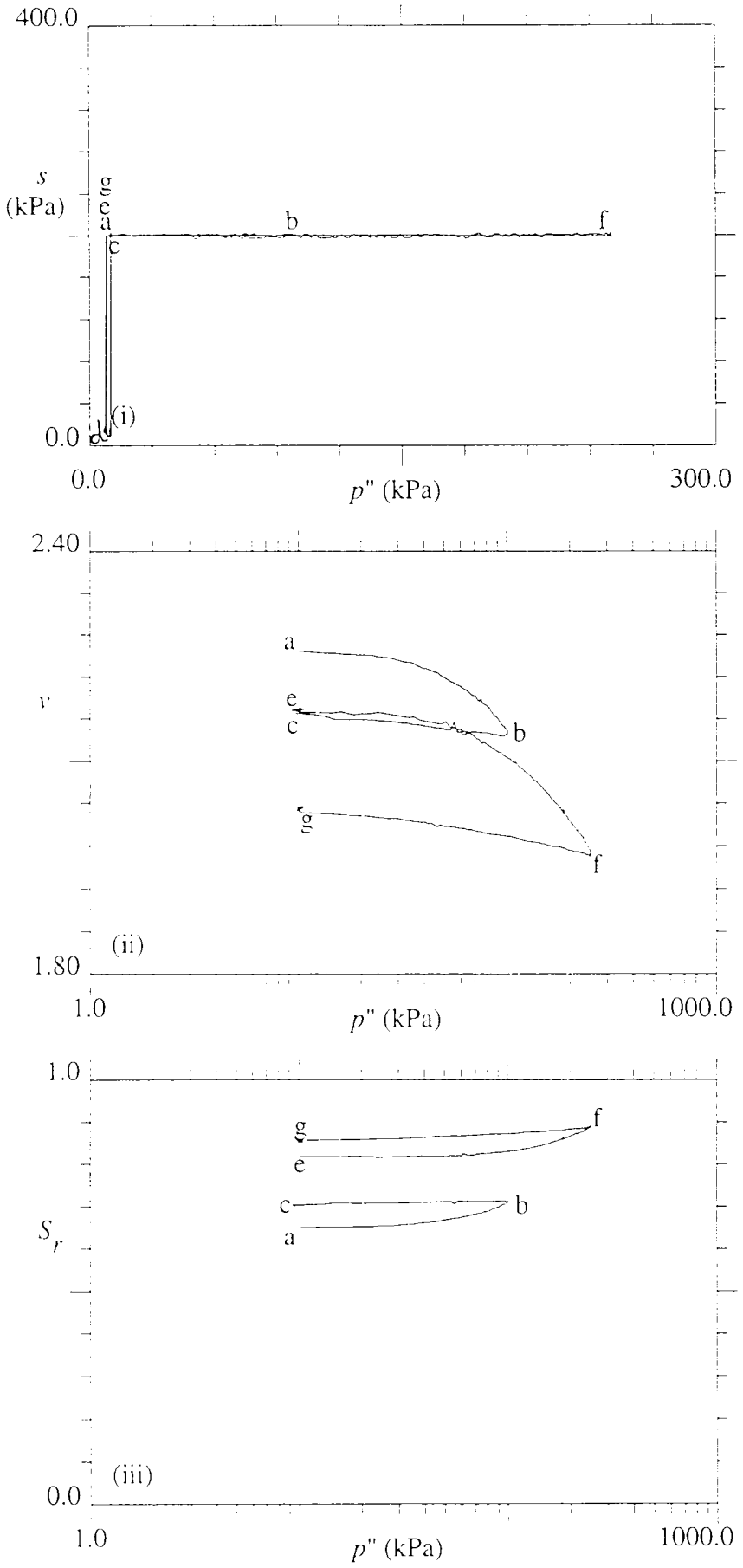

Figure 6.22 : Test 10 (Loading/unloading at s = 200 kPa; bent/kao sample)

(i)

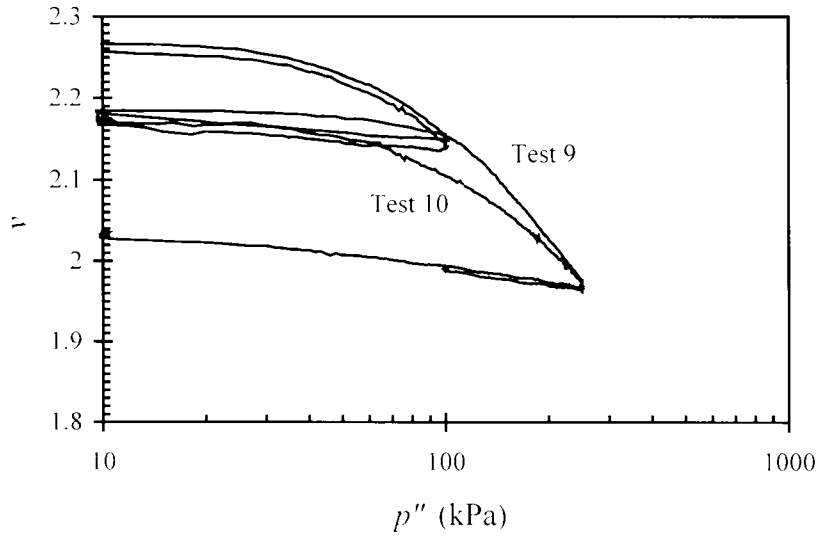

(ii)

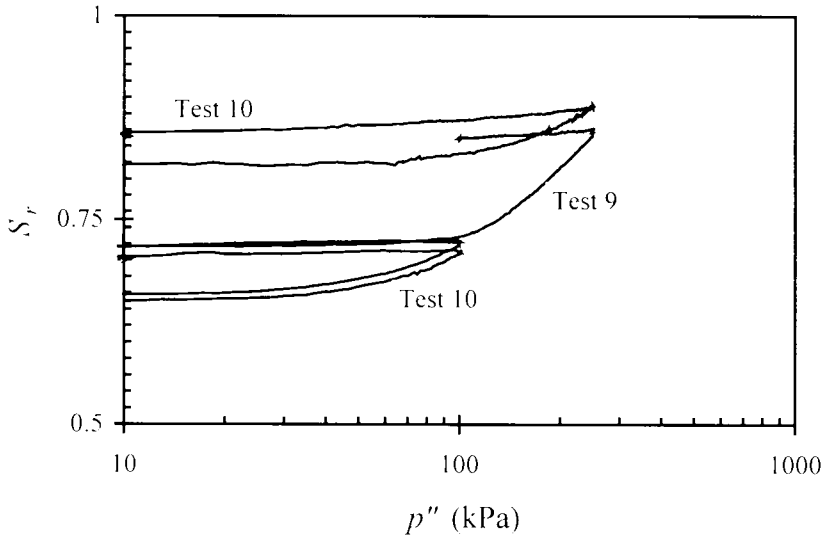

Figure 6.23 : Loading/unloading behaviour of bentonite/kaolin samples prepared by compaction under a pressure of 400 kPa

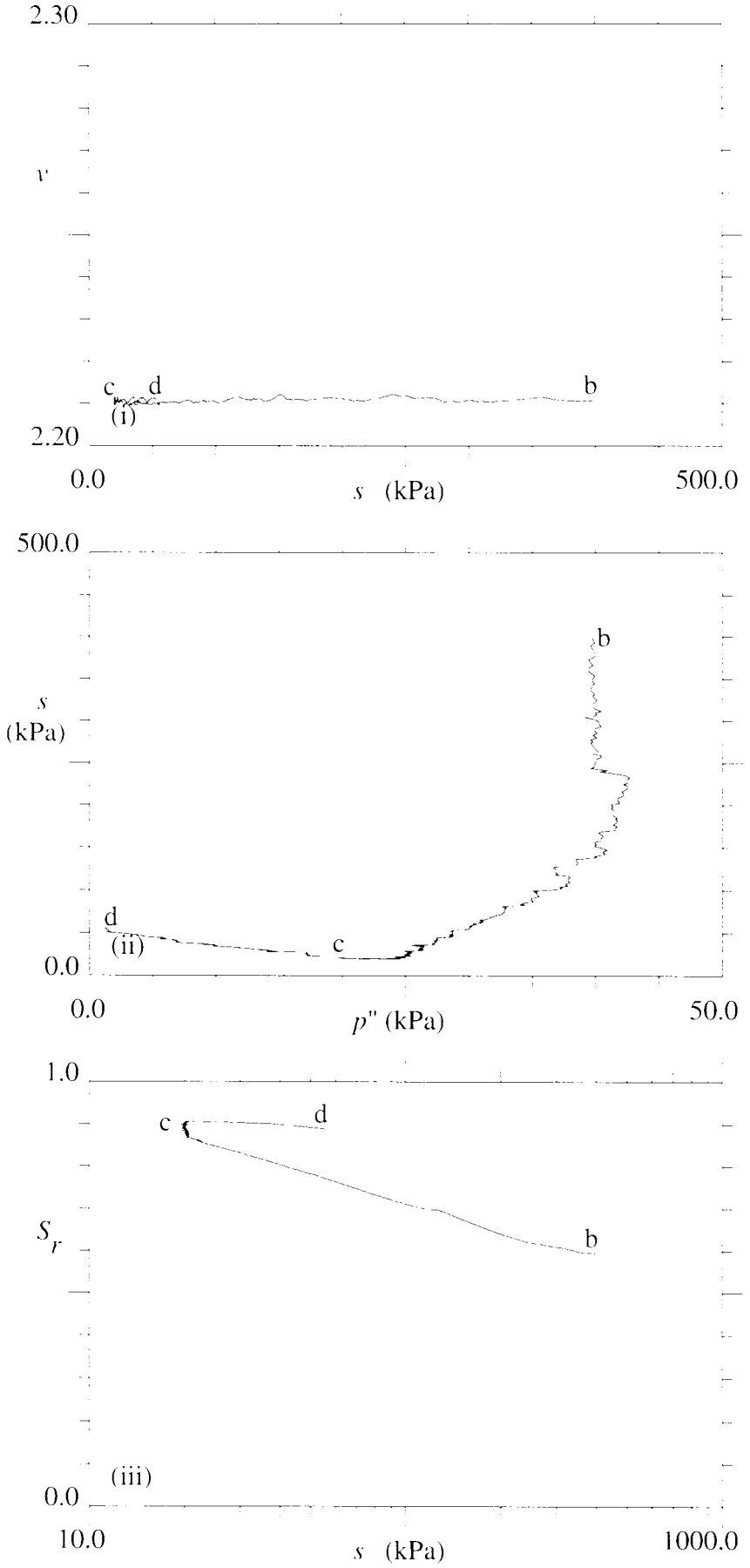

Figure 6.24 : Test 15 (Constant volume wetting and drying)

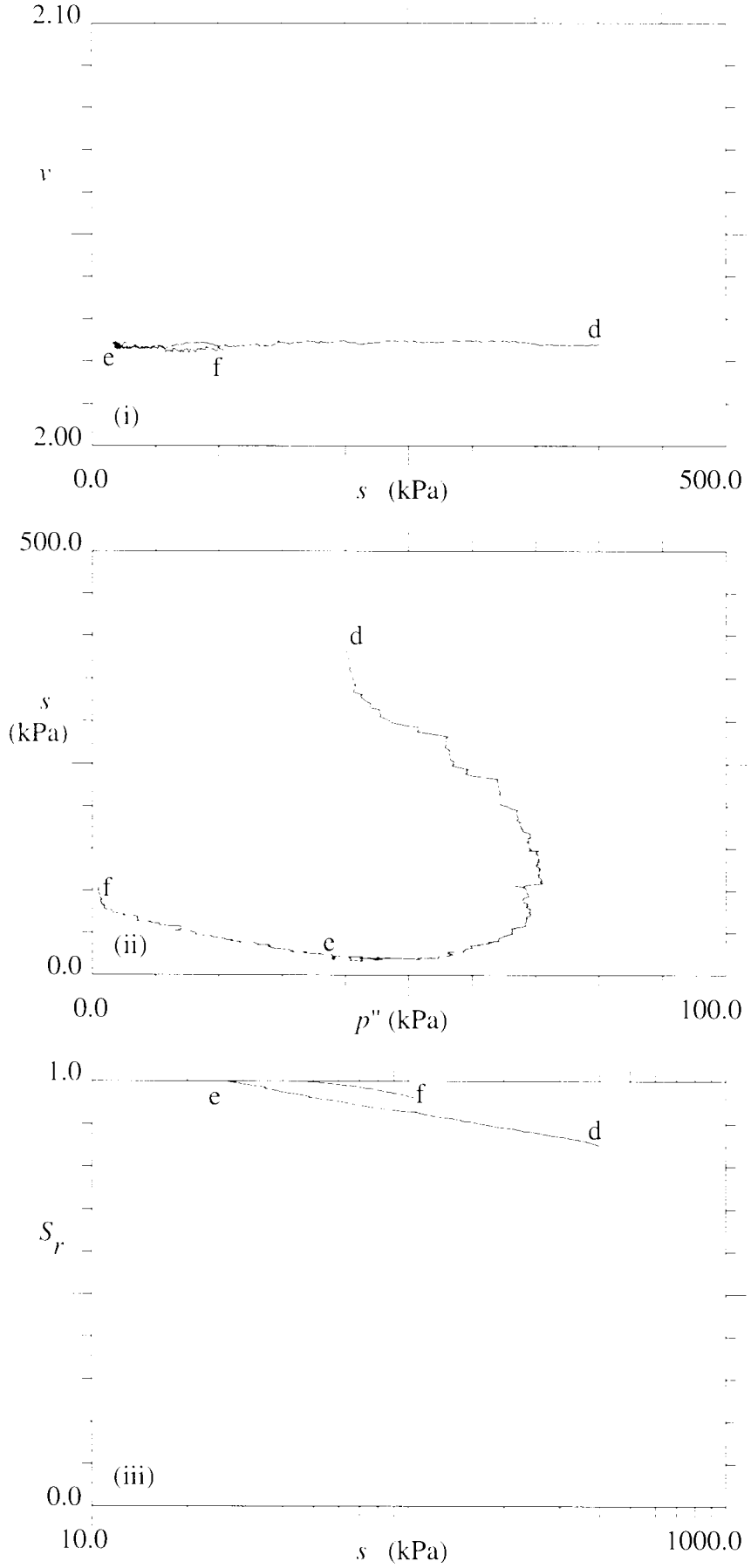

Figure 6.25 : Test 16 (Constant volume wetting/drying after a normal wetting/drying cycle)

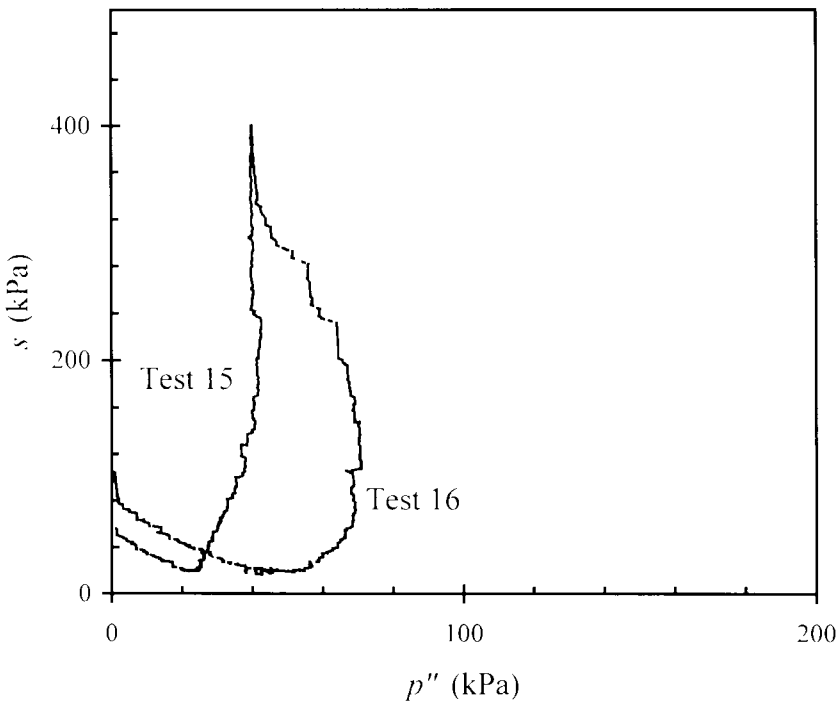

Figure 6.26 : Results of wetting/drying with constant volume of the samples of bentonite/kaolin mix (prepared by compaction under a pressure of 400 kPa)

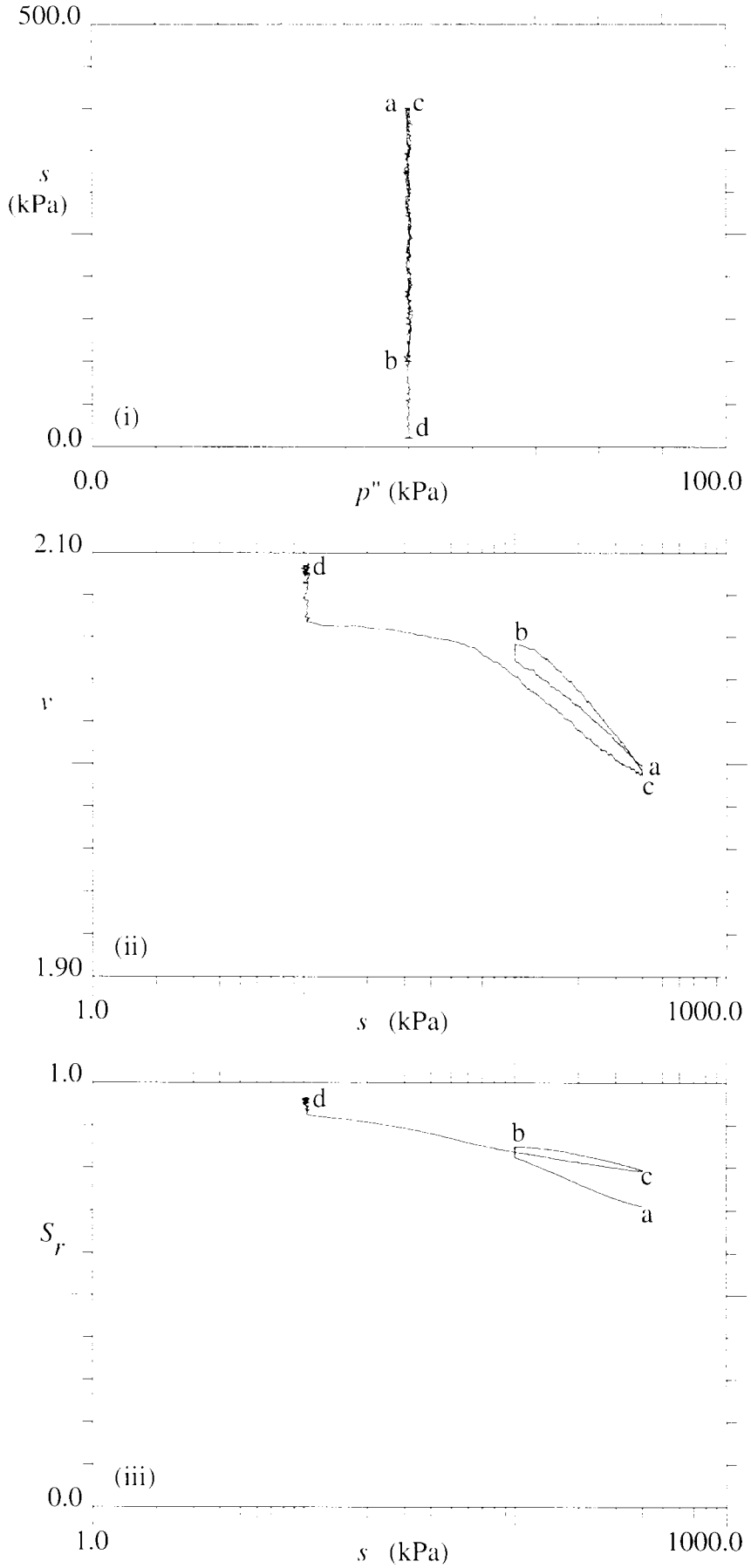

Figure 6.27 : Test 3 (Wetting/drying at p" = 50 kPa; bent/kao; comp = 800 kPa)

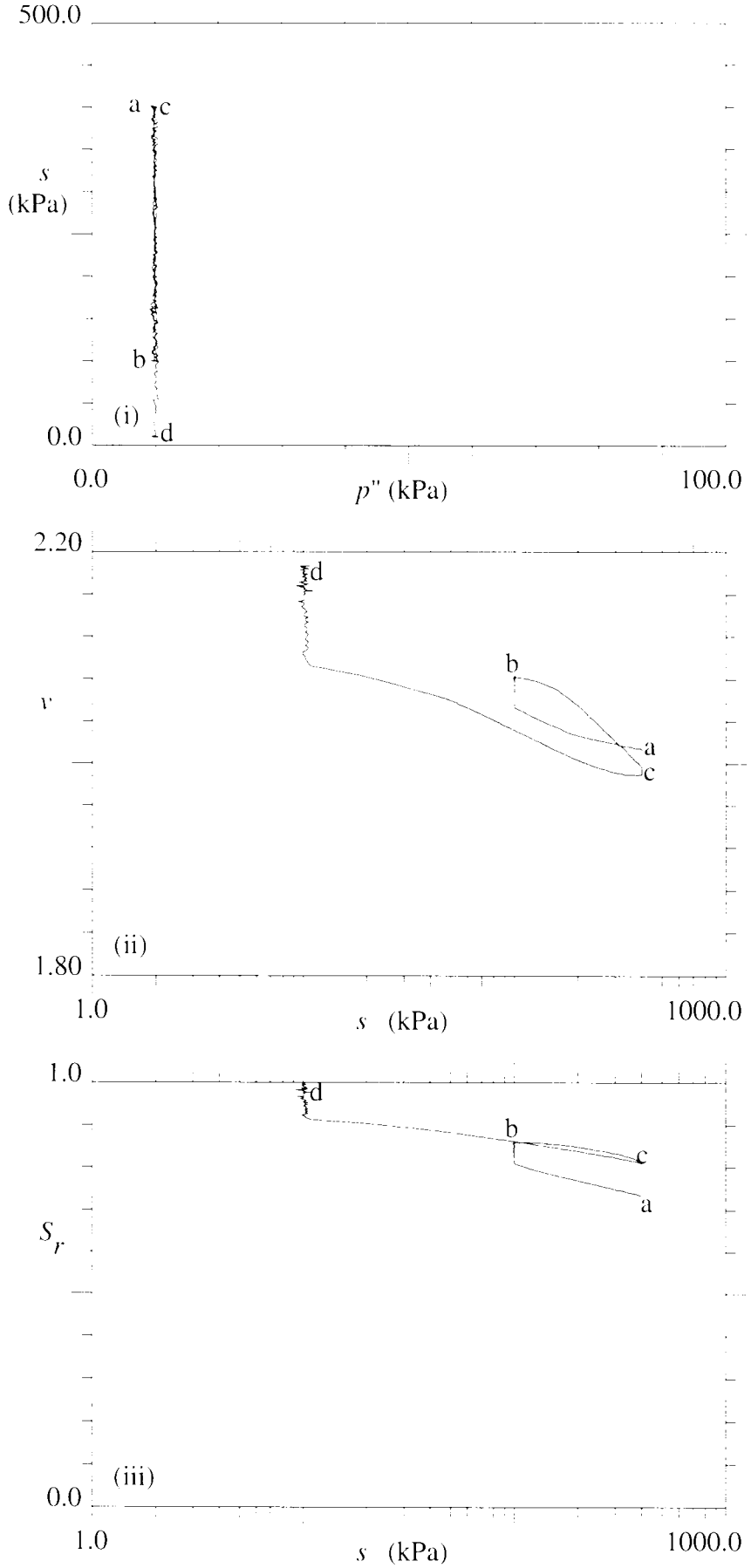

Figure 6.28 : Test 4 (Wetting/drying at p" = 10 kPa; bent/kao; comp = 800 kPa)

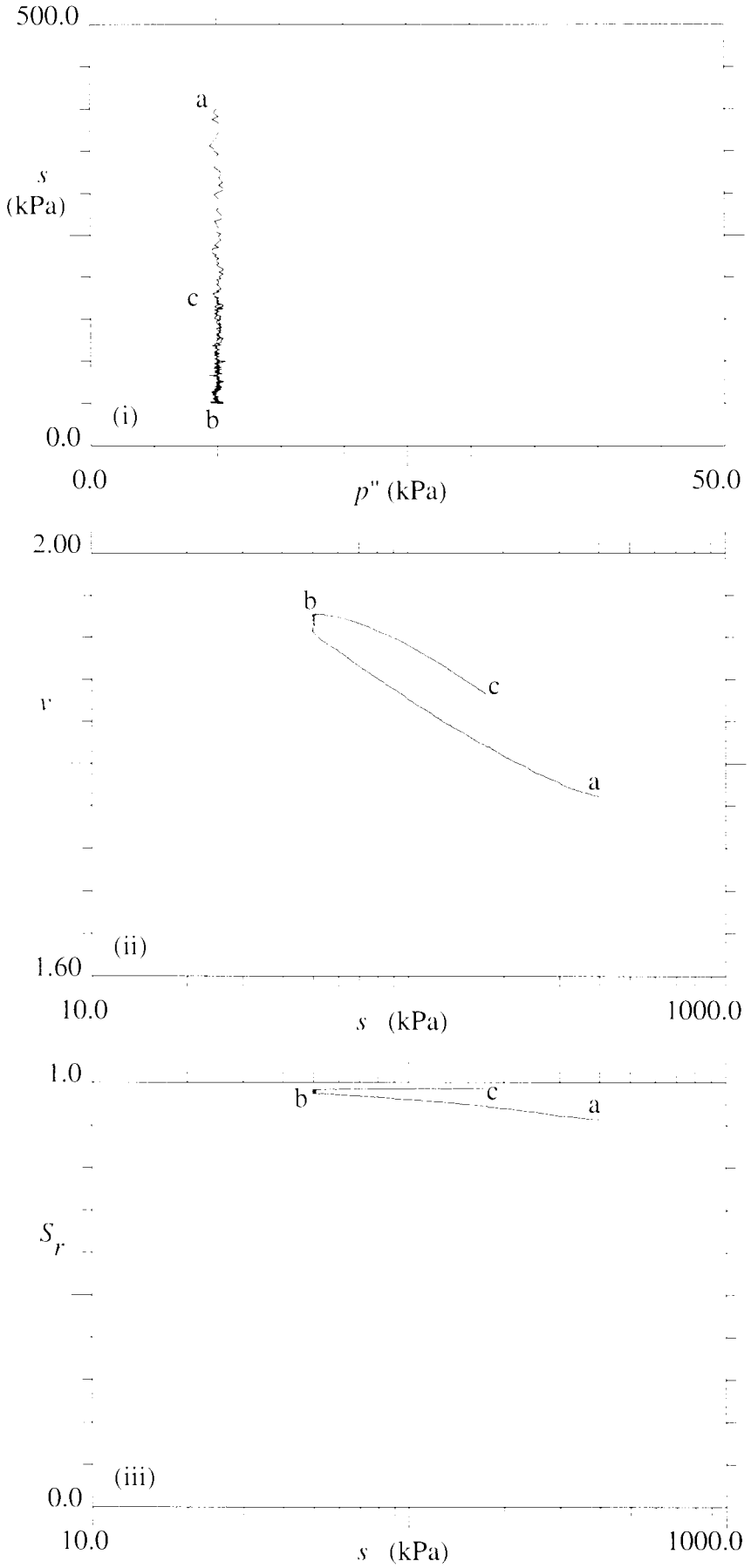

Figure 6.29 : Test 19 (Wetting/drying at p" = 10 kPa; bent/kao; comp = 3200 kPa)

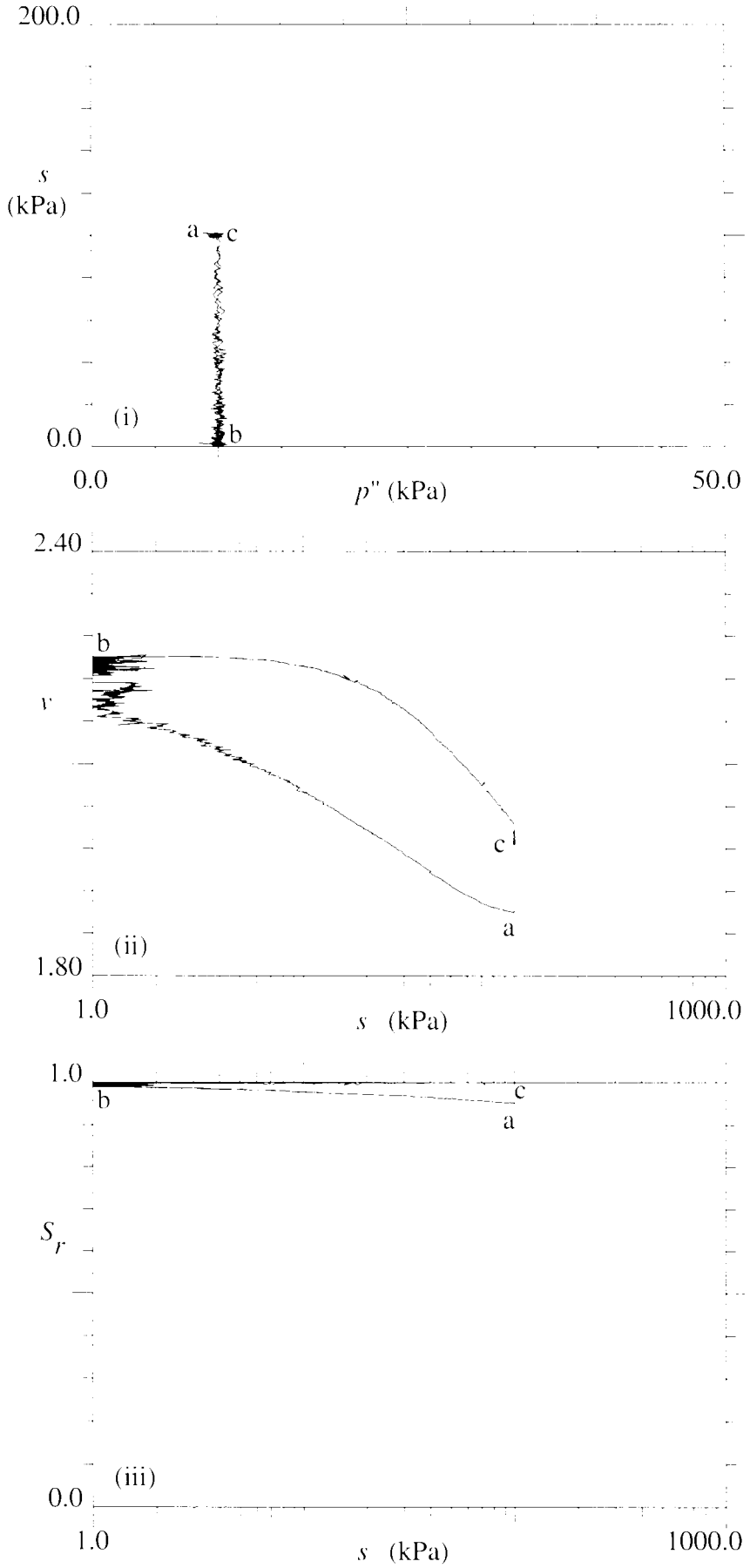

Figure 6.30 : Test 20 (Wetting/drying cycle at p" = 10 kPa; bent/kao; comp = 3200 kPa)

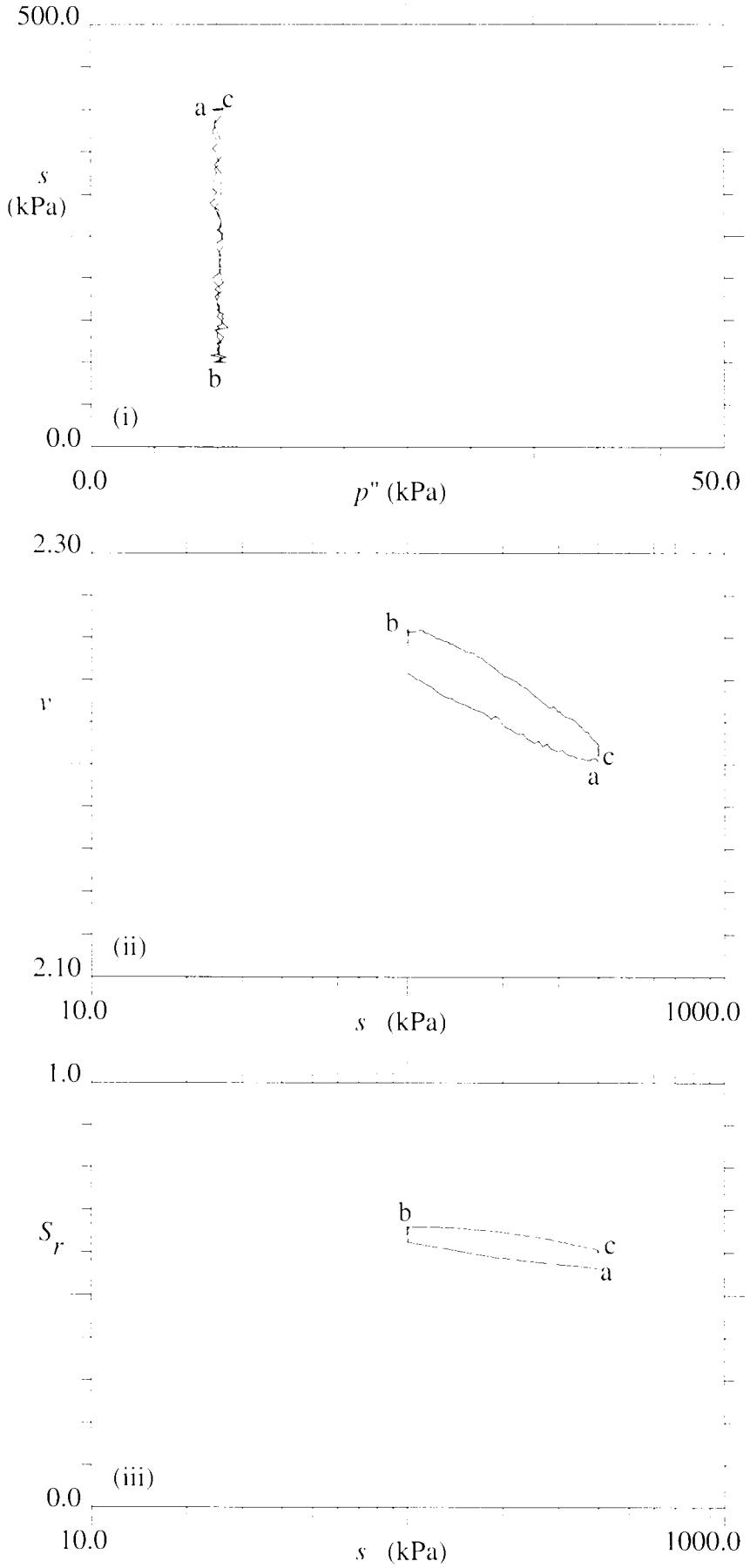

Figure 6.31 : Test 12 (Wetting/drying at p" = 10 kPa; kao sample; comp = 400 kPa)

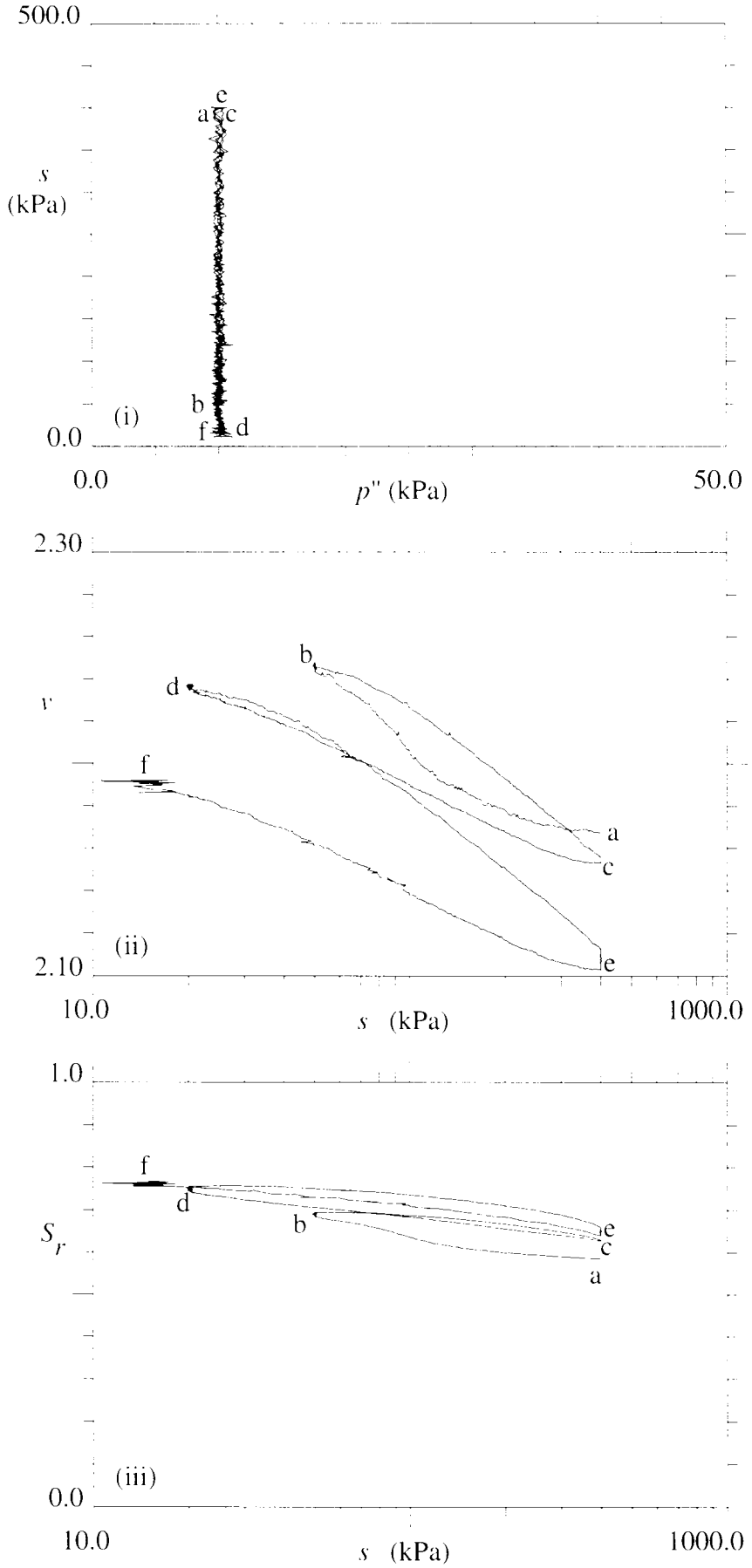

Figure 6.32 : Test 14 (Wetting/drying at p'' = 10 kPa; kao sample; comp = 400 kPa)

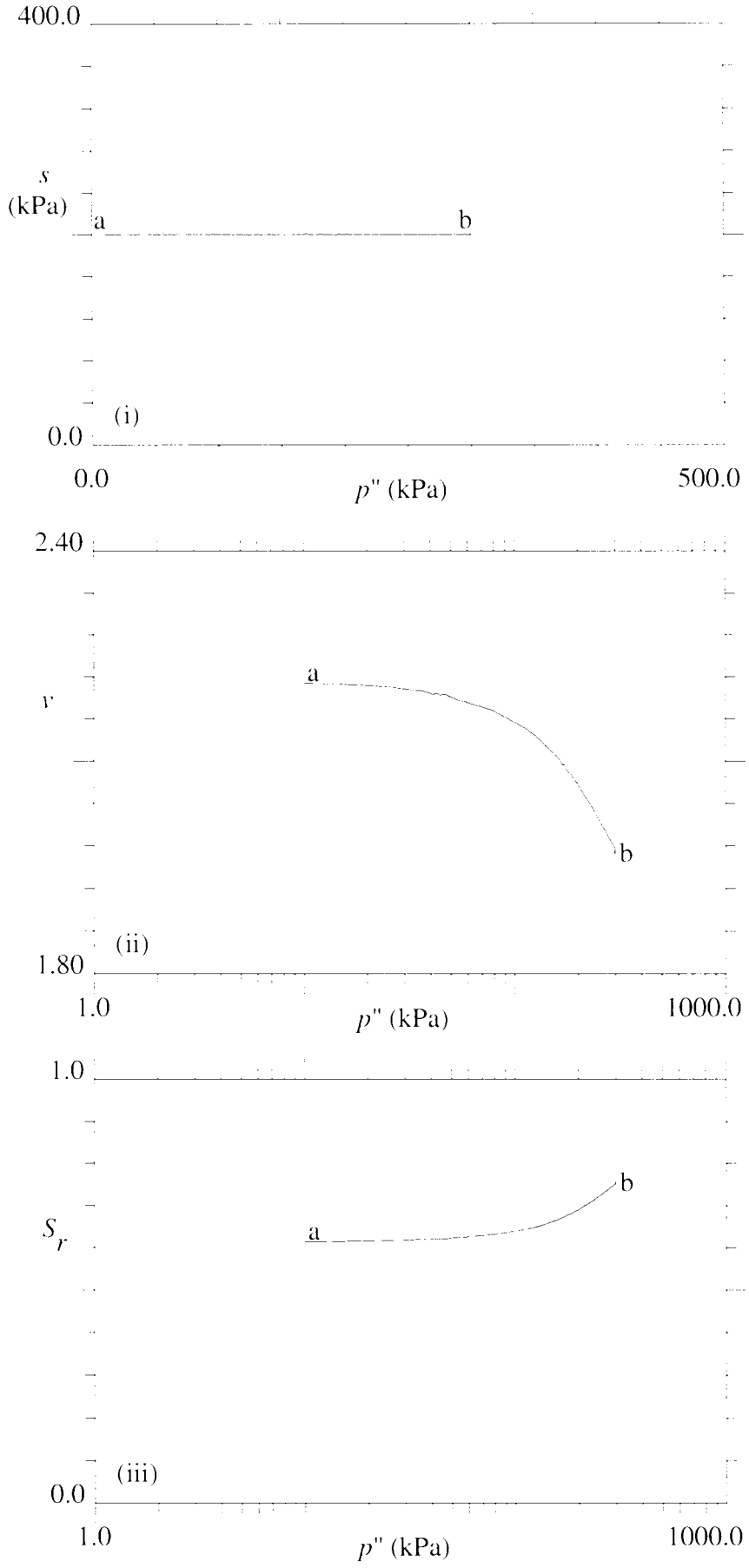

Figure 6.33 : Test 17 (Loading for kaolin sample at s = 200 kPa)

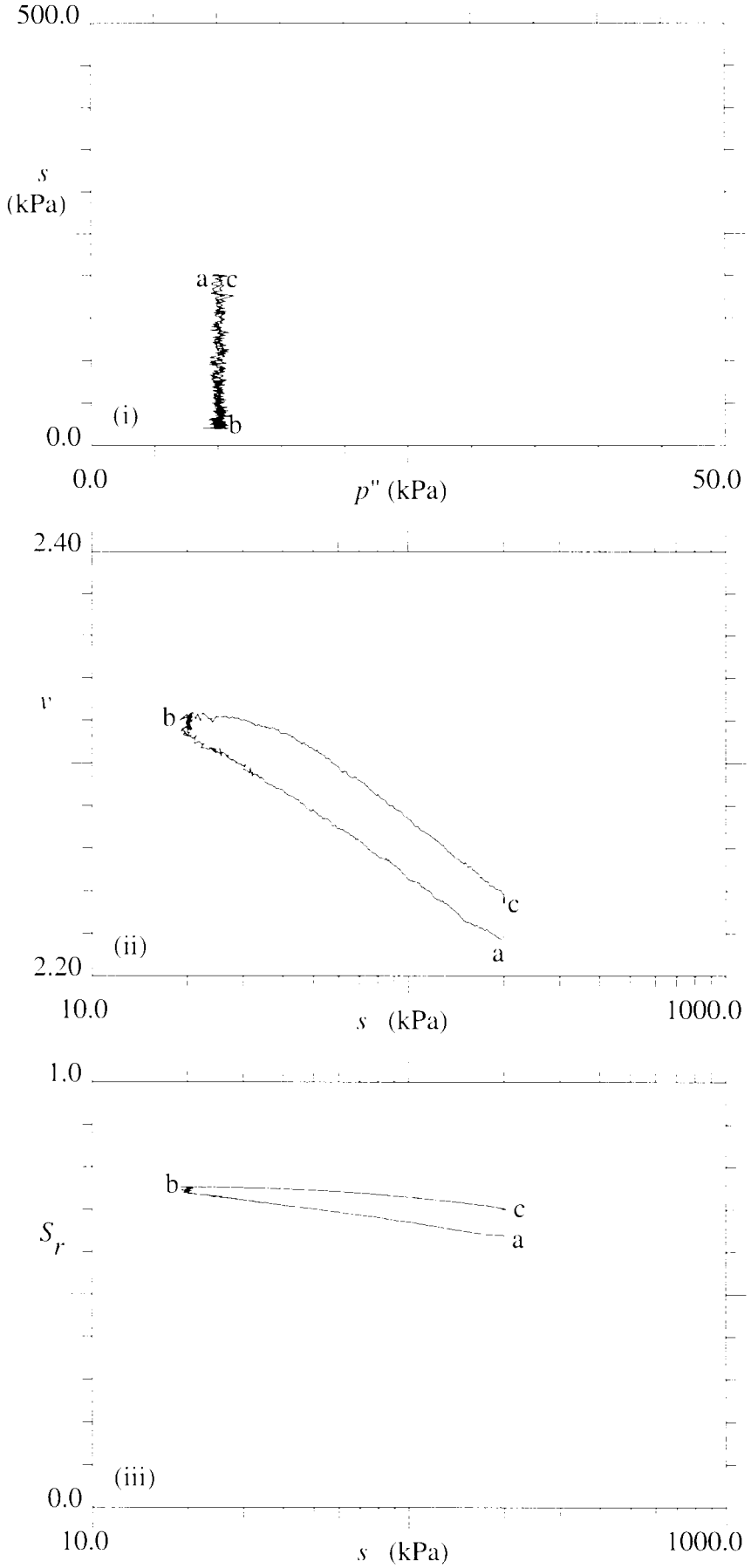

Figure 6.34 : Test 18 (Wetting/drying at p" = 10 kPa; kaolin sample; comp = 400 kPa)

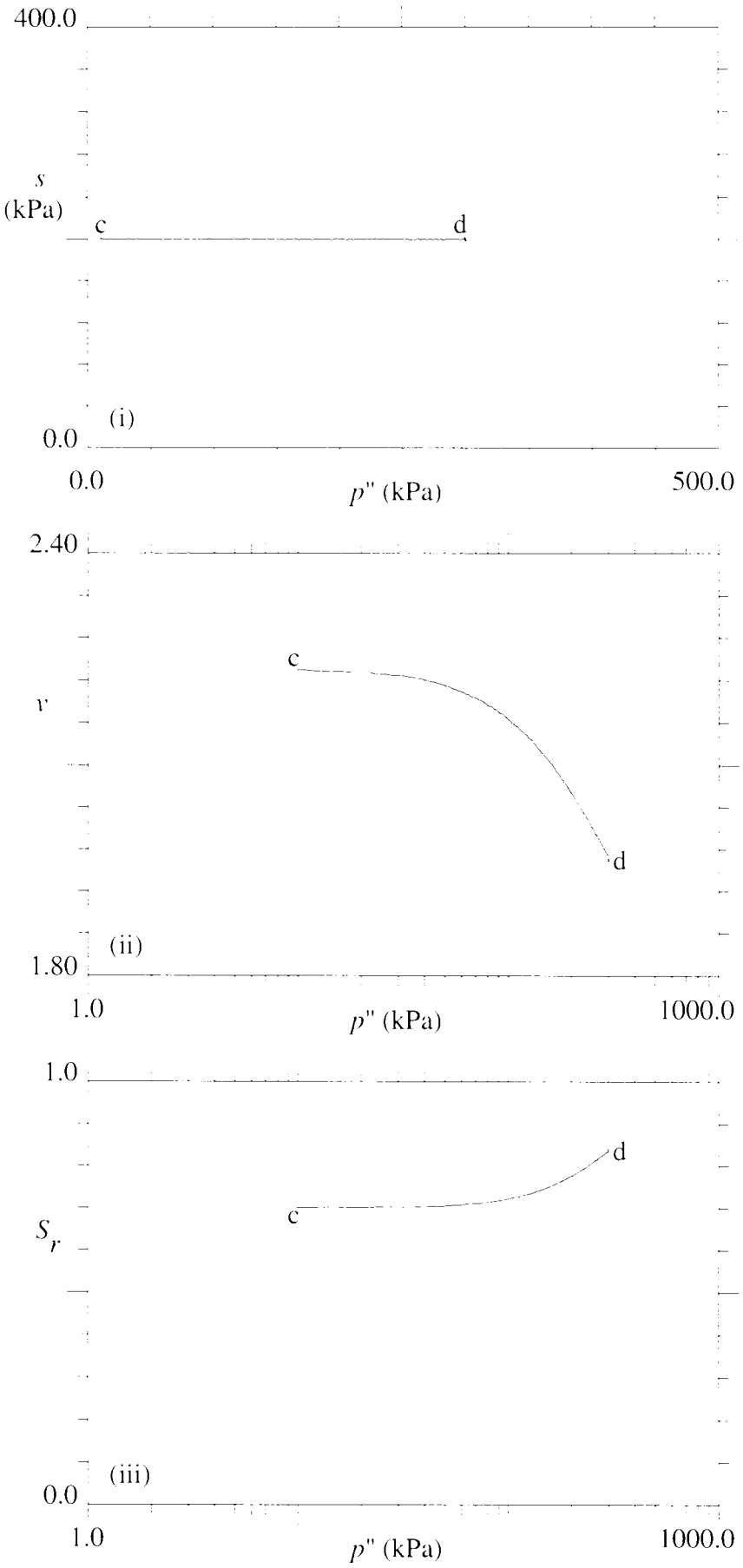

Figure 6.35 : Test 18 (Loading for kaolin sample at s = 200 kPa)

(i)

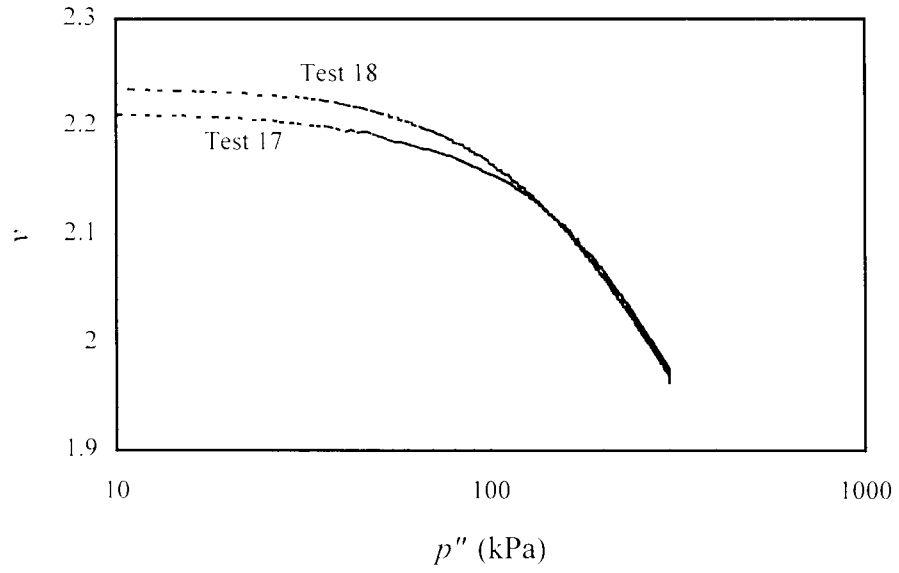

(ii)

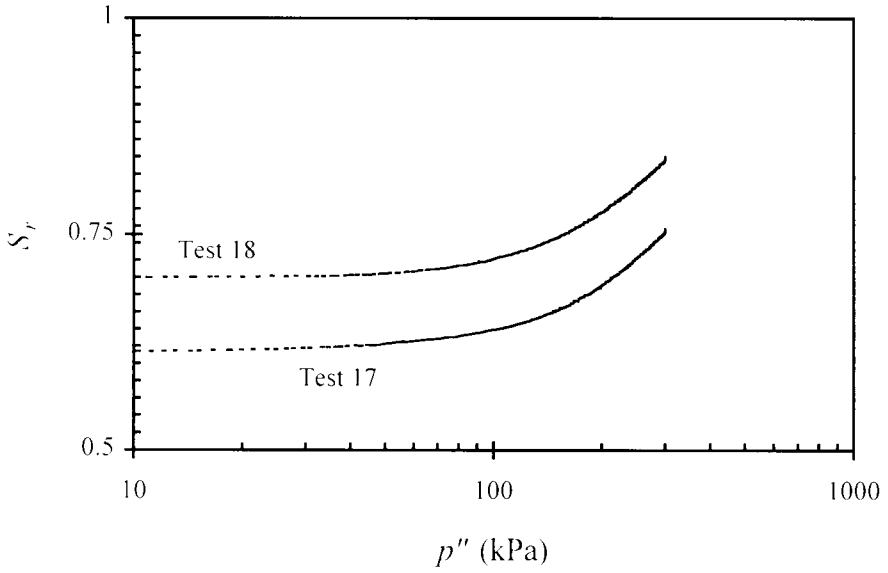

Figure 6.36 : Loading behaviour of kaolin samples prepared by compactoin under a pressure of 400 kPa

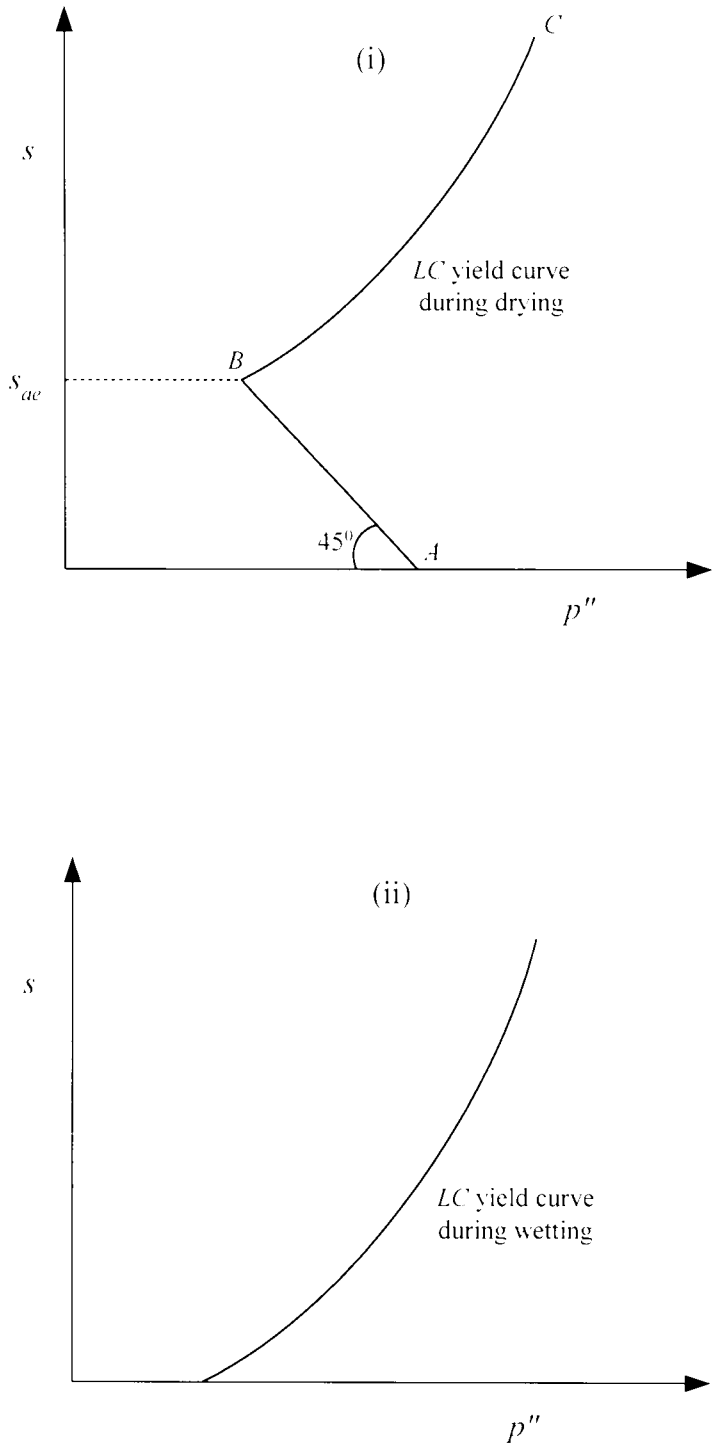

Figure 7.1 : Forms of *LC* yield curve during drying and wetting with p'' and s as two stress variables

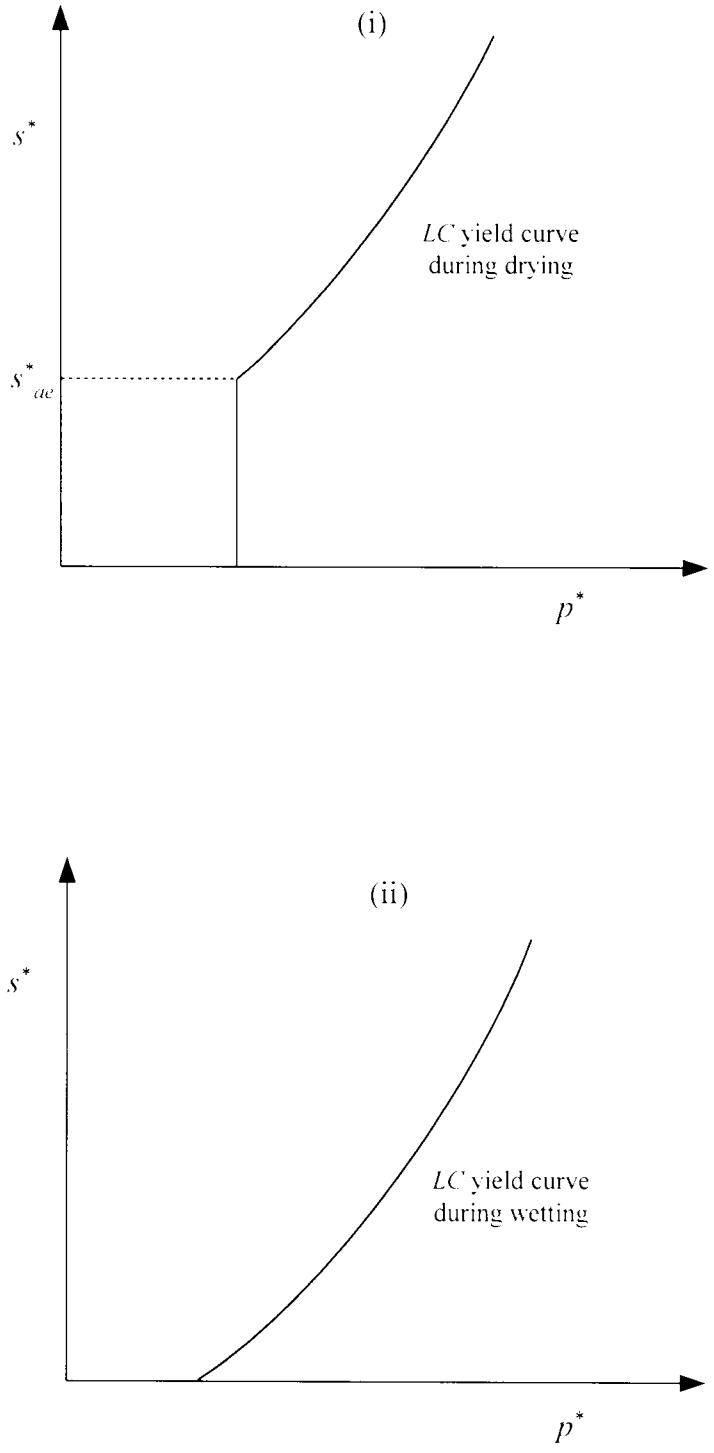

Figure 7.2 : Forms of LC yield curve during drying and wetting in terms of new stress variables p^* and s^*

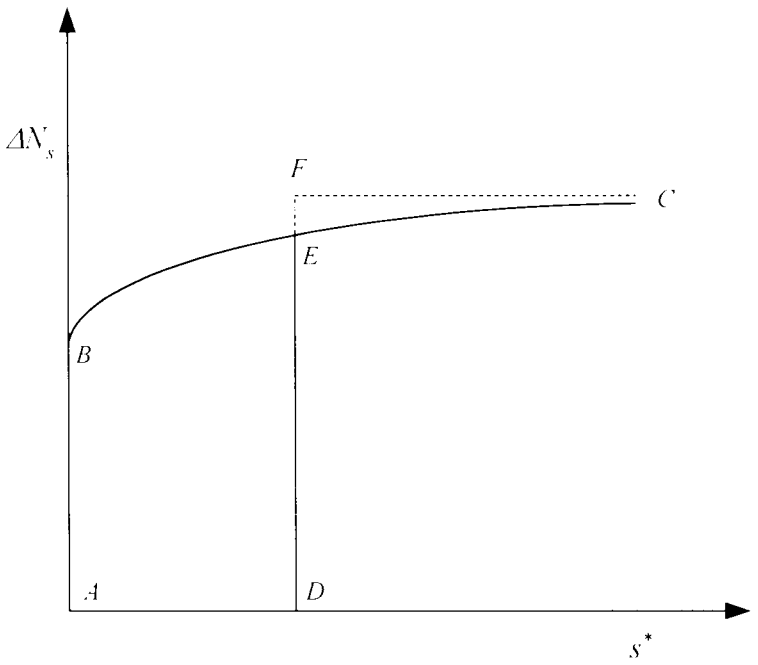

Figure 7.3 : Variation of additional inter-particle force due to suction in meniscus water (spherical particles)

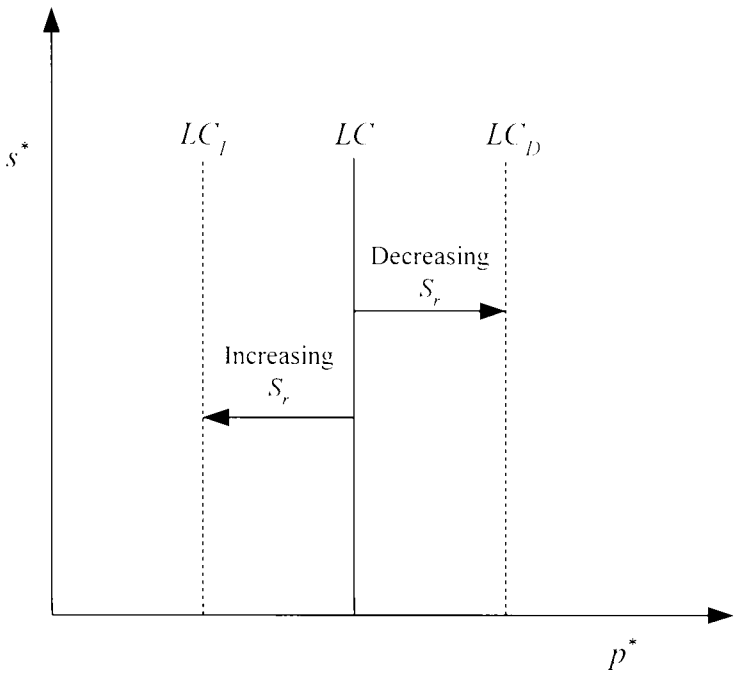

Figure 7.4 : Proposed form of LC yield curve in $s^* : p^*$ plane and movement of the LC yield curve as a function of variation of degree of saturation S_r

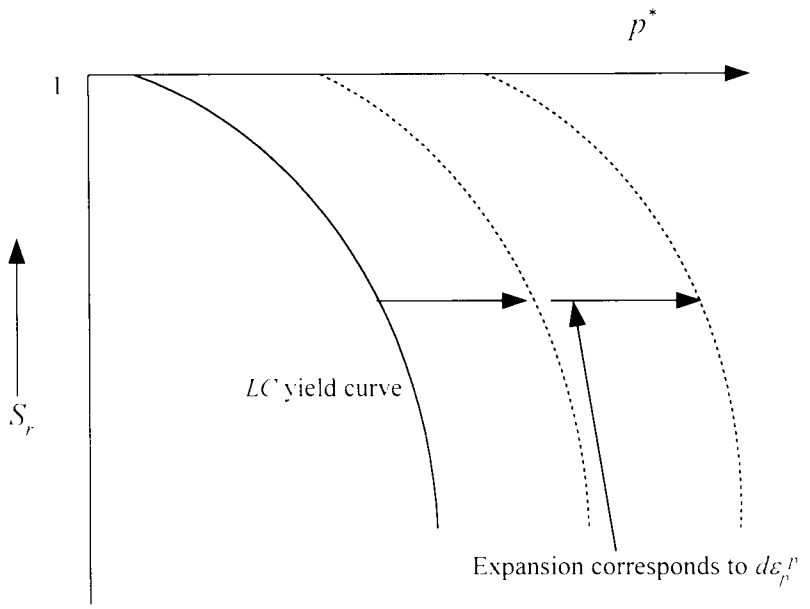

Figure 7.5 : LC yield curve in $S_r : p^*$ plane

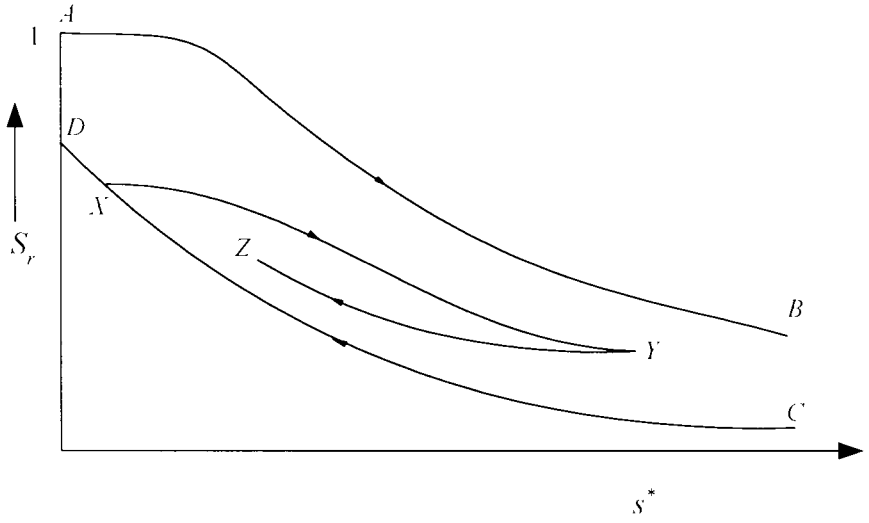

Figure 7.6 : Schematic representation of hysteretic soil-water characteristic curve in $S_r : s^*$ palne

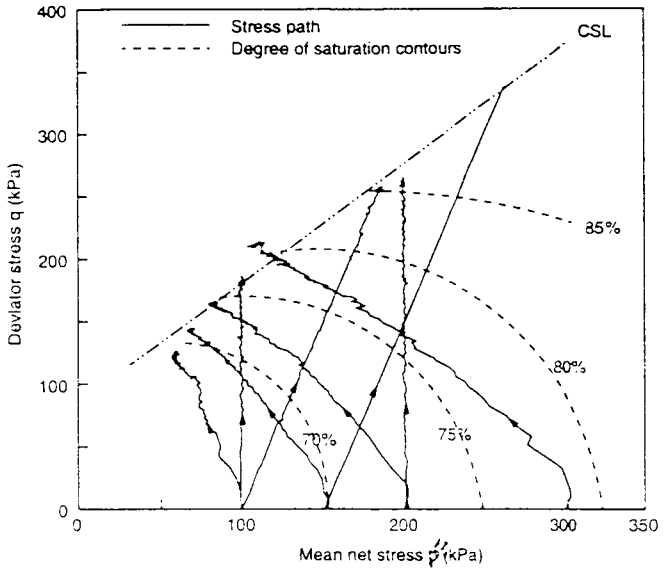

Figure 7.7 : Contours of degree of saturation from constant suction triaxial shear tests conducted on speswhite kaolin at s = 200 kPa (after Sivakumar (1993))

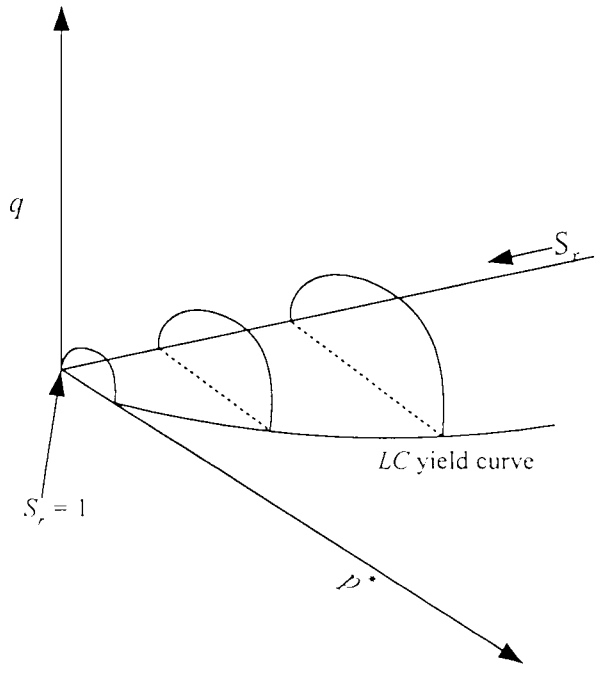

Figure 7.8 : Yield surface in $q : p^* : S_r$ space for triaxial stress condition

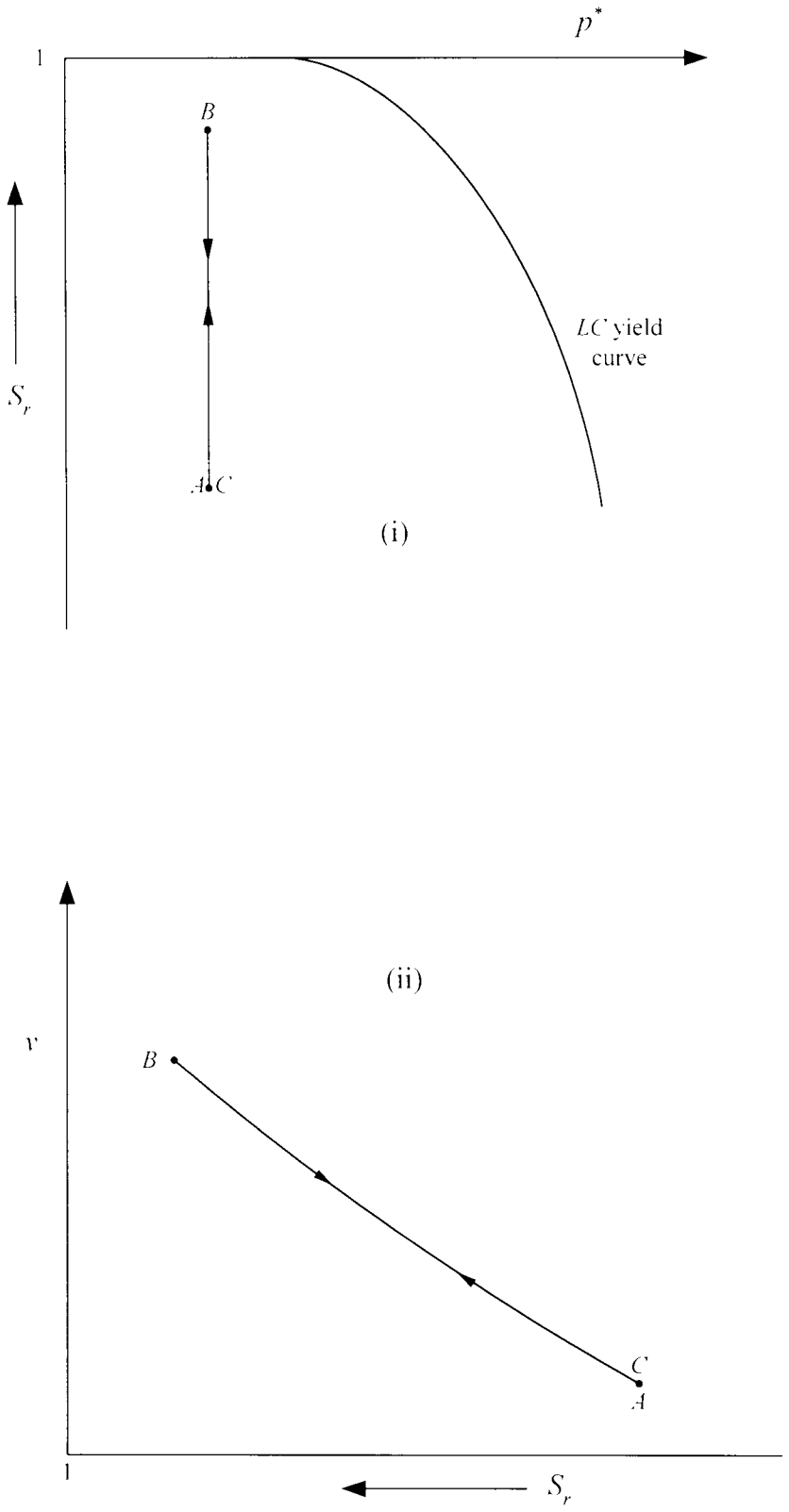

Figure 7.9 : Soil behaviour during a wetting/drying cycle at a constant value of p^*

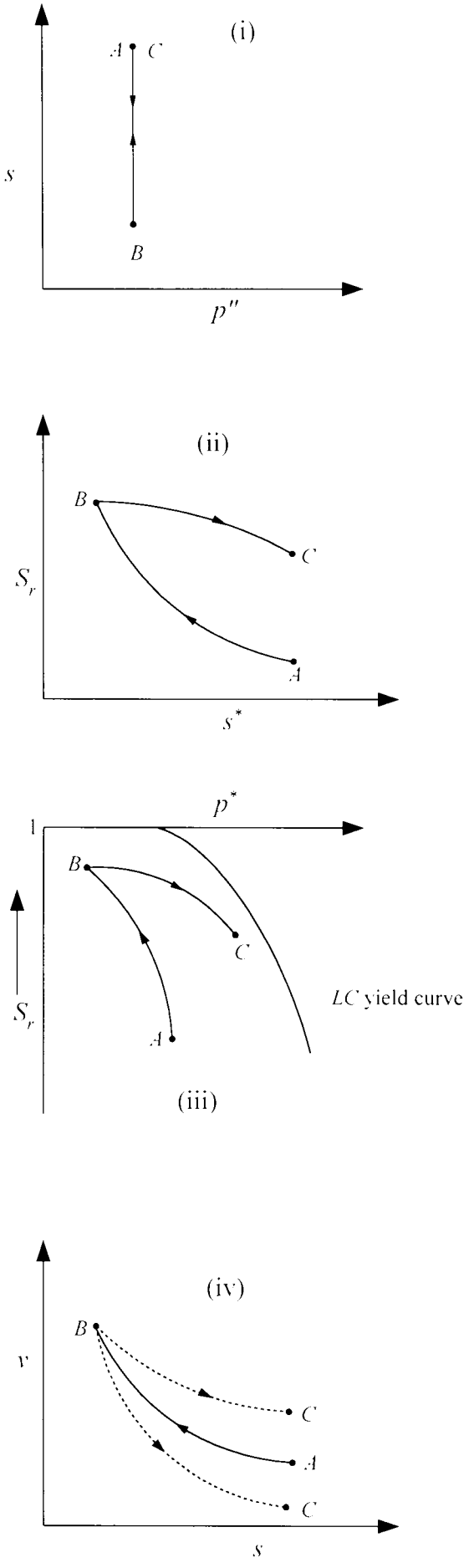

Figure 7.10 : Soil behaviour during a wetting/drying cycle at a constant value of p''

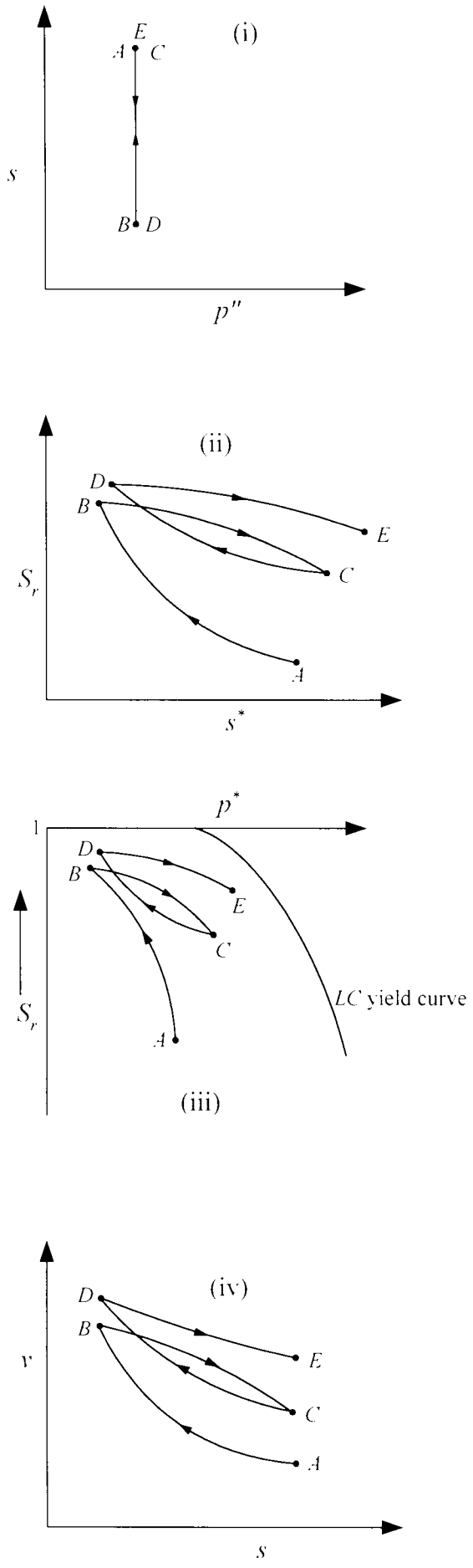

Figure 7.11 : Soil behaviour during multiple wetting/ drying cycles with test paths in $S_r : p^*$ plane remaining inside the *LC* yield curve.

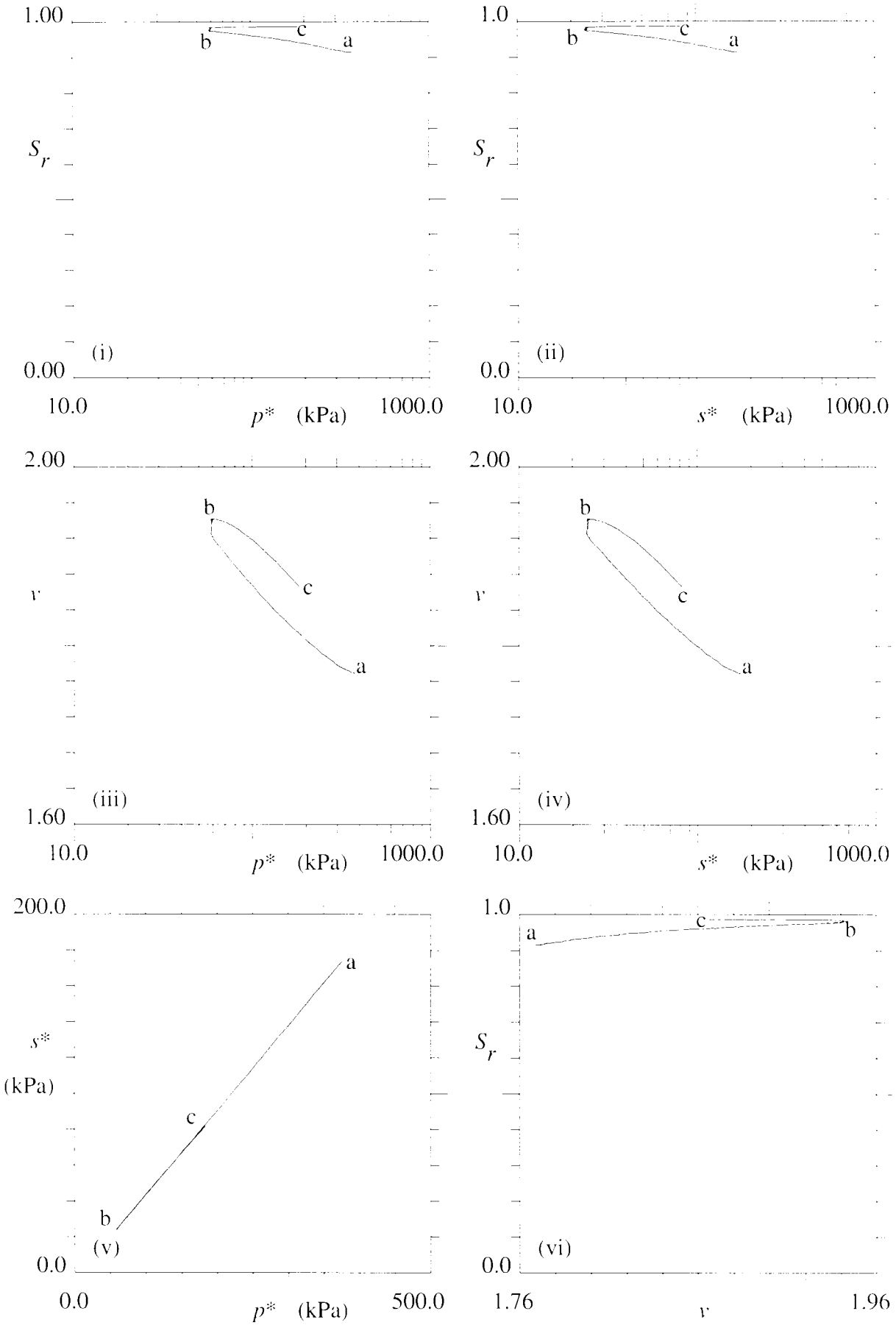

Figure 7.12 : Test 19 (Wetting/drying at p" = 10 kPa; bent/kao; comp = 3200 kPa)

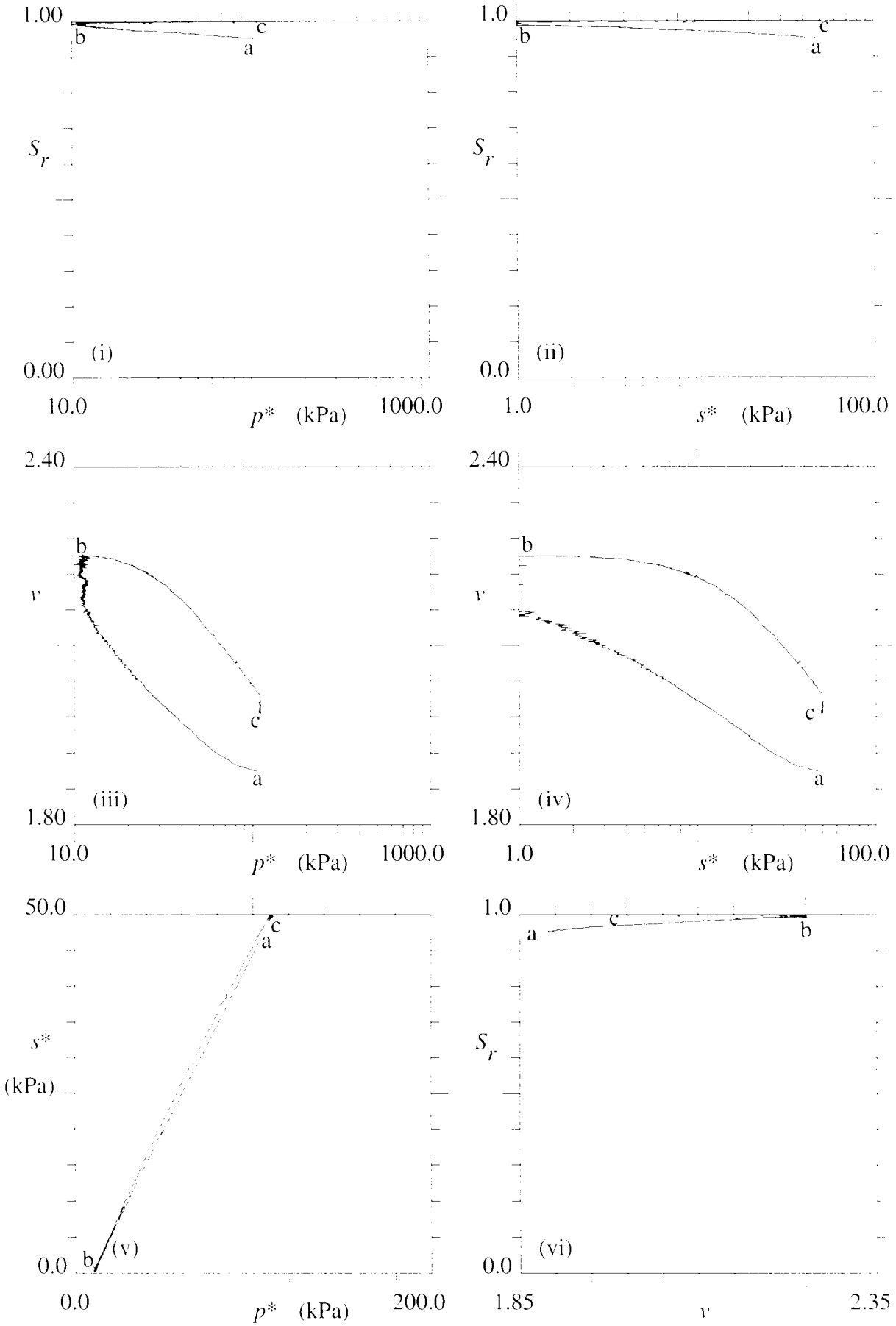

Figure 7.13 : Test 20 (Wetting/drying at p'' = 10 kPa; bent/kao; comp = 3200 kPa)

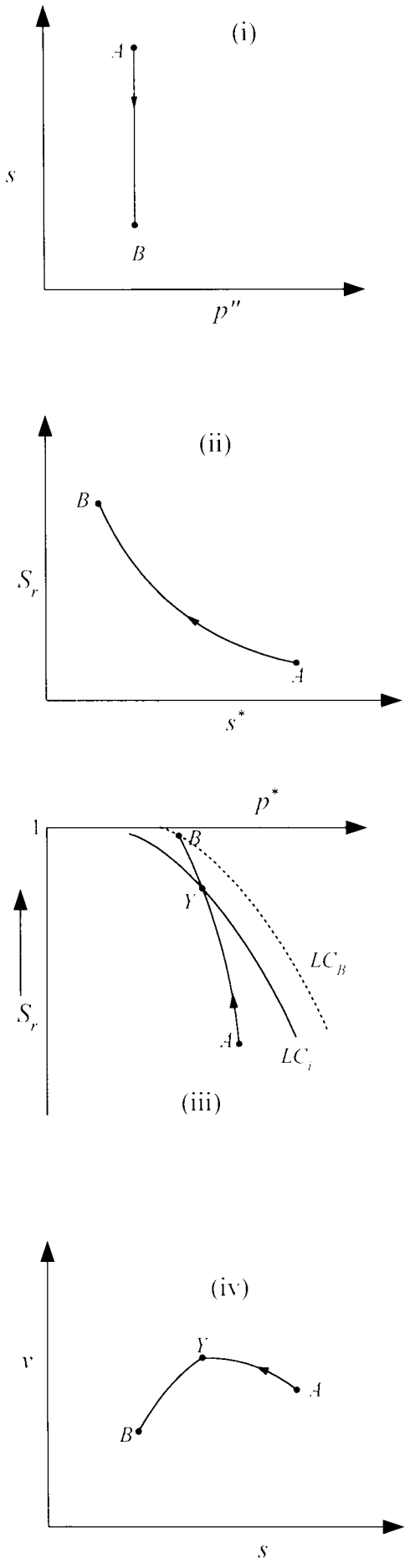

Figure 7.14 : Yielding during wetting

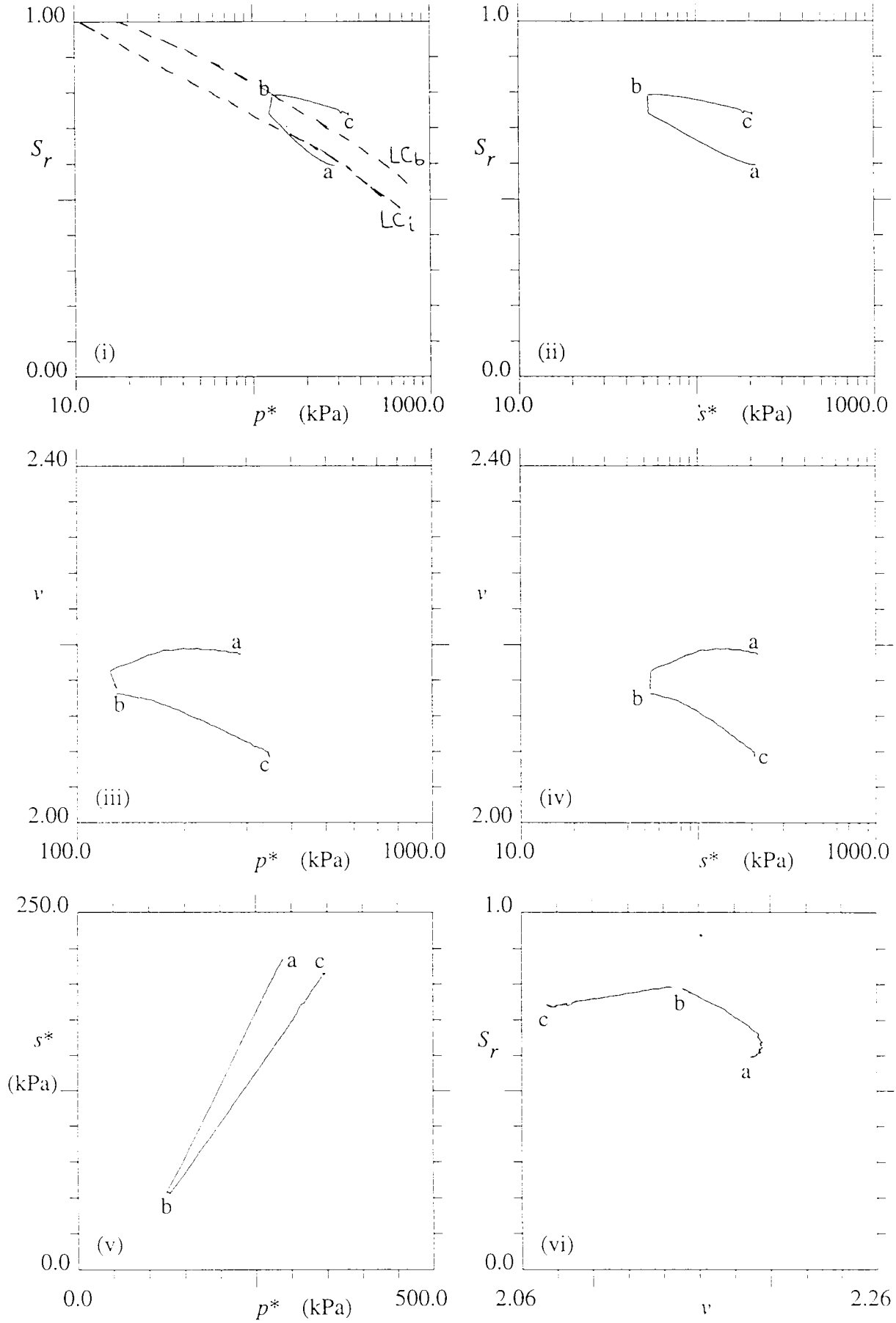

Figure 7.15 : Test 2 (Wetting/drying at p" = 50 kPa; bent/kao; comp = 400 kPa)

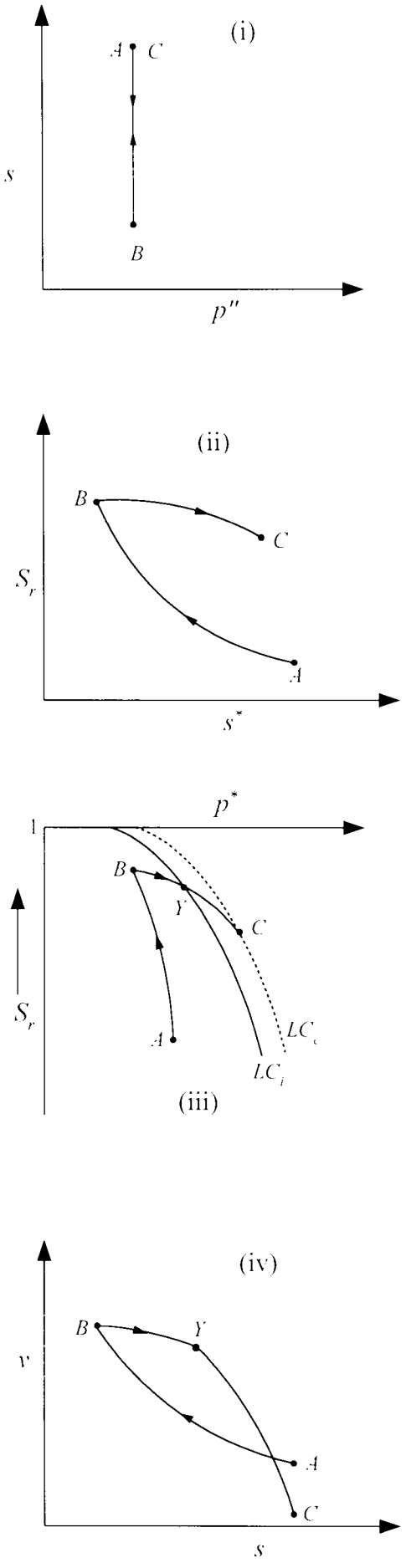

Figure 7.16 : Yielding during drying

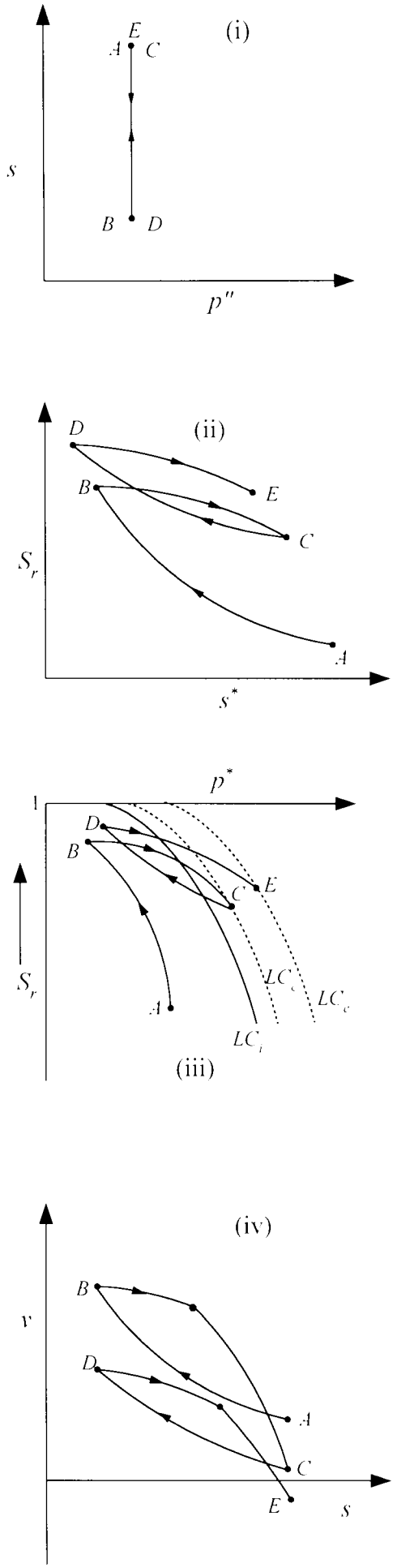

Figure 7.17 : Yielding during drying

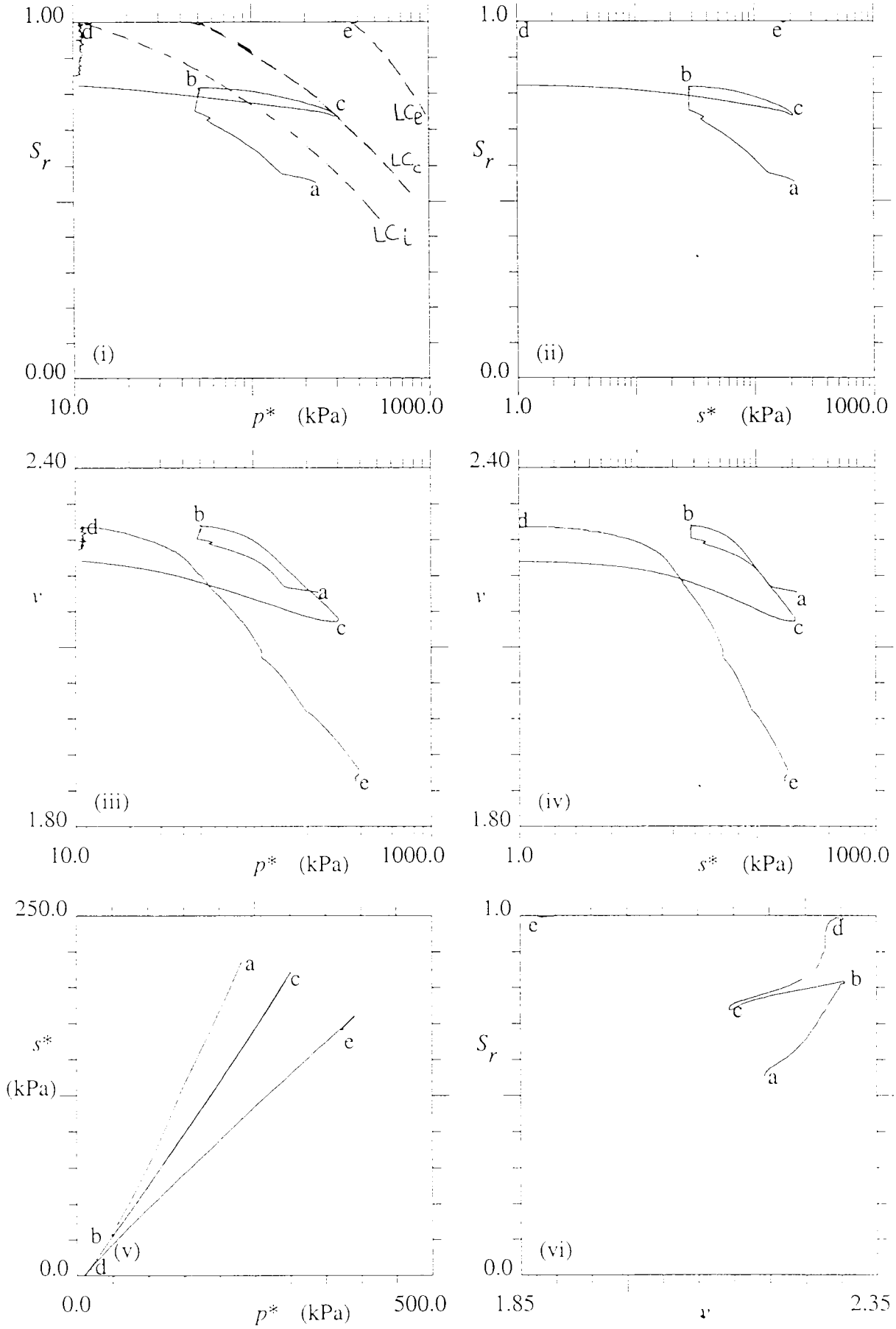

Figure 7.18 : Test 1 (Wetting/drying at p" = 10 kPa; bent/kao; comp = 400 kPa)

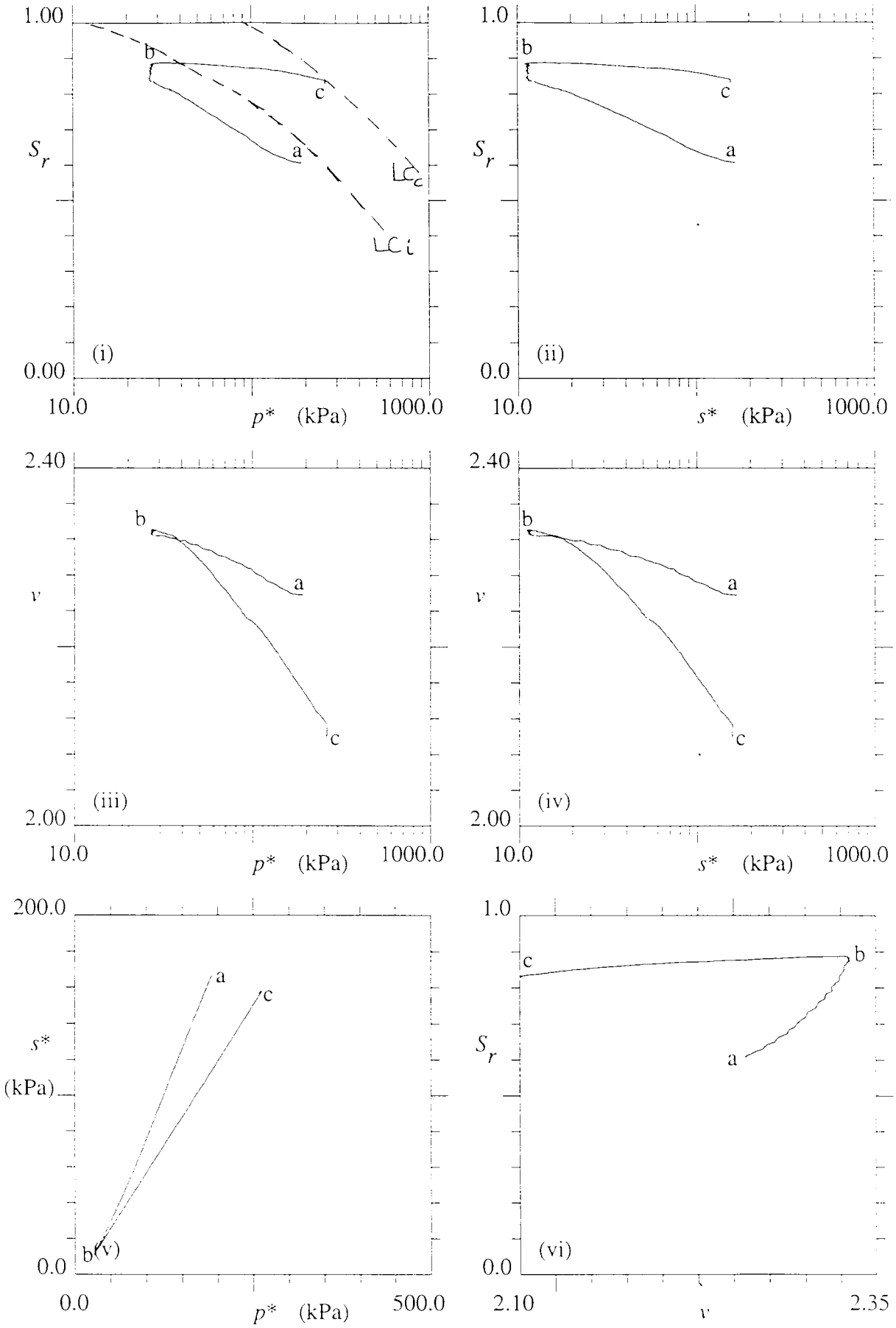

Figure 7.19 : Test 8 (Wetting/drying at p" = 10 kPa; bent/kao; comp = 400 kPa)

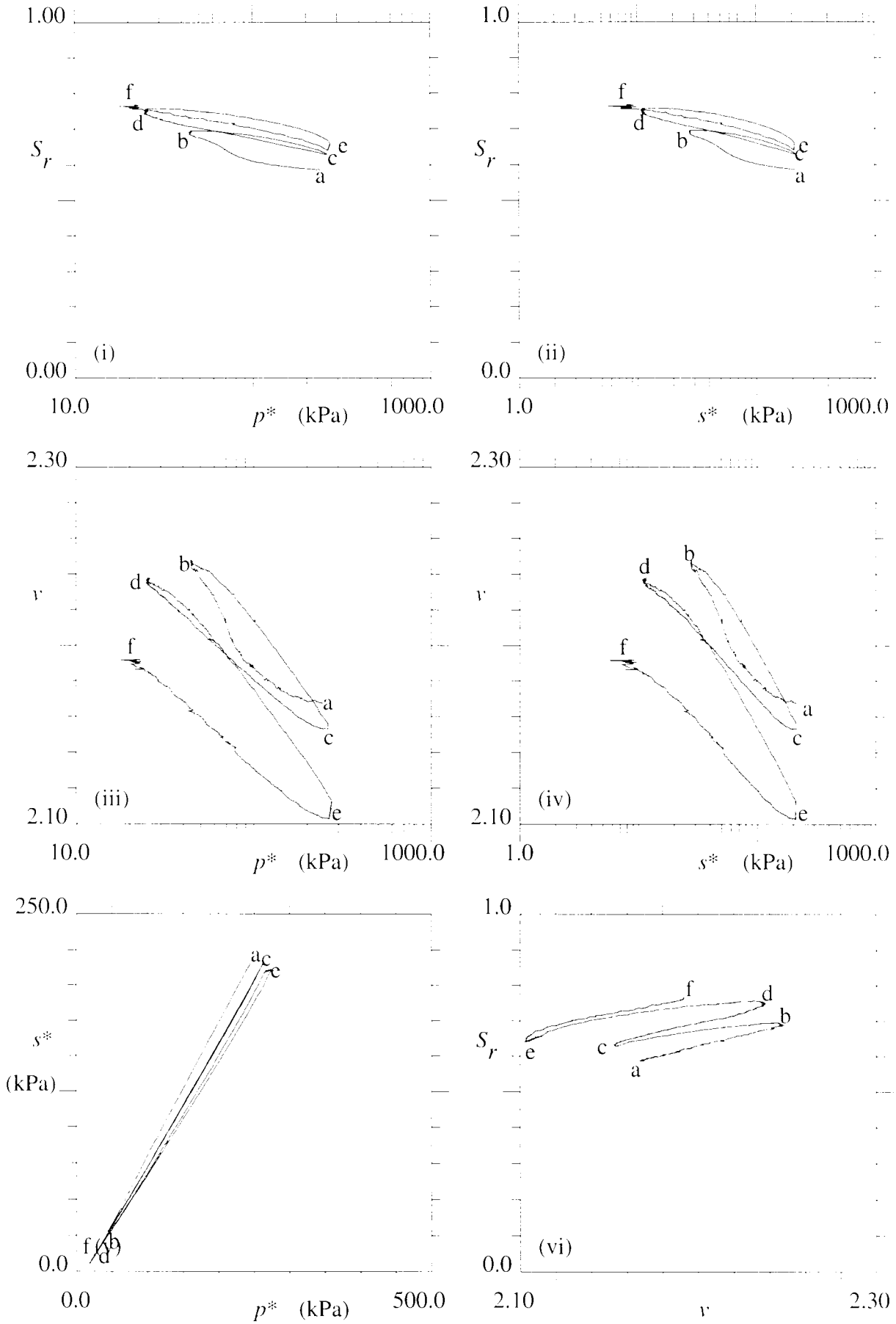

Figure 7.20 : Test 14 (Wetting/drying at p" = 10 kPa; kaolin sample; comp = 400 kPa)

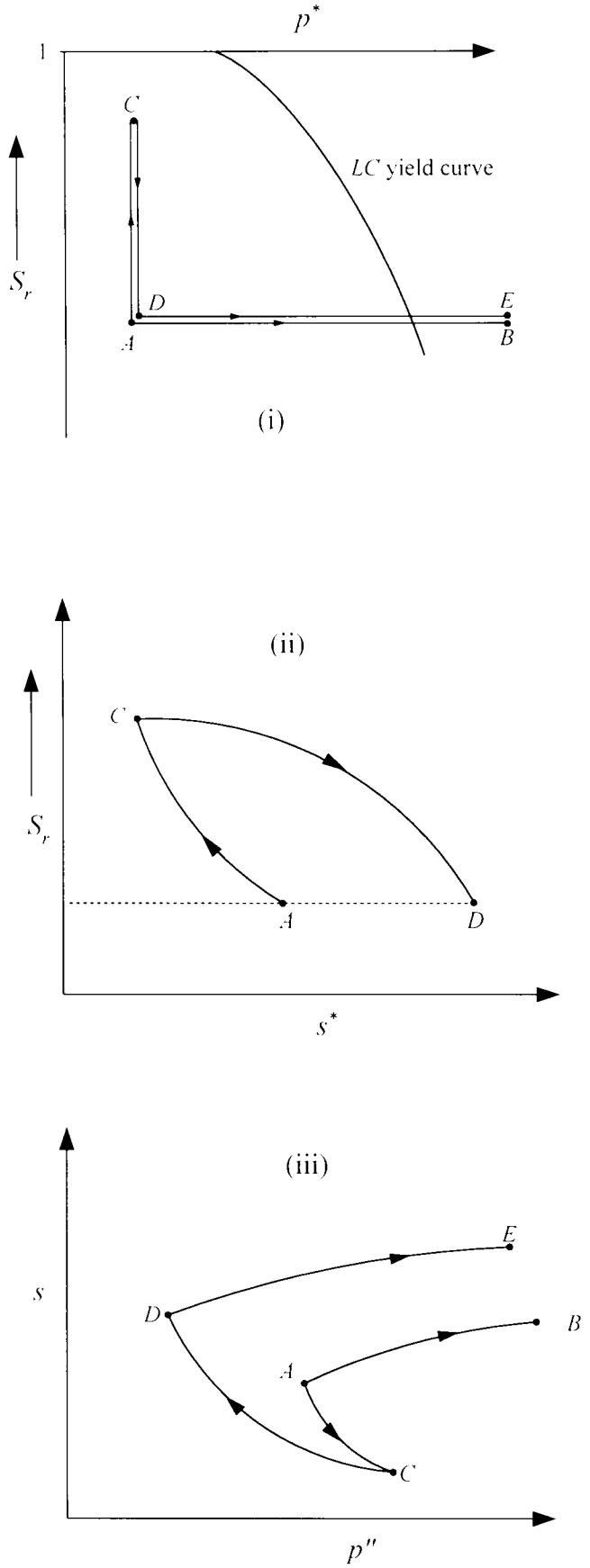

Figure 7.21 : Possible form of future laboratory test